OPTICAL PROPERTIES OF THIN FILMS AND OPAQUE SOLIDS.

By

Anoara Islam
B.Sc.(Calcutta), M.Sc.(Dacca).

A Thesis submitted for the Degree of
Doctor of Philosophy
in the Department of Physics
University of Adelaide.

JULY 1979.

C O N T E N T S

CONTENTS Continued..... PAGE

CONTENTS Continued..... PAGE

CONTENTS Continued.... PAGE

CONTENTS Continued....

PAGE

CONTENTS Continued....

SUMMARY

The work involved in this thesis is an account of the manner in which the optical reflectance and transmittance of thin films of Ge , and the reflectance of opaque films and polished specimens of metals such as Au, Ni, Co and Mo relate to their optical constants and hence their band structures.

Chapter 1 presents introductory theory on band gaps and electronic transitions in metals and semiconductors and a short review of various methods of determining their optical constants.

Chapter 2 gives a brief description of the experimental methods used.

The changes in the optical constants n and k of thin films of Ge as they are converted from the amorphous to the crystalline state have been determined for the spectral region between 0.62 to2.2 eV by the normal incidence reflectance and transmittance method and are discussed in Chapter 3. For the amorphous state of Ge an interpretation is made according to the Mott and Davis (1971) model of energy bands. A detailed study has been made of the effects on the optical constants of annealing amorphous films from 200 to 700°C and of preparing films at higher substrate temperatures (300 to 600°C). The energy gaps of both amorphous and polycrystalline films of Ge , and of amorphous films converted to the polycrystalline state by annealing, have been calculated from the relation $(EnK)^{\frac{1}{2}} = c(E - Eg)$.

In Chapter 4 a method is given for evaluating the optical constants of Ge within the region 1.8 to 15 eV by using Kramers-Kronig dispersion relations. For reflectances at high energies (above

10 or 15 eV), three similar extrapolation formulae have been investigated in attempts to improve extrapolation procedures by using additional parameters which are determined from the directly measured values of the optical constants within the region 1.8 to 4.0 eV .

Chapter 5 gives an introduction to the single and double layer formulae derived by Tomlin (1972, 1978) for determining the optical constants of metals. The effects of errors in the measurement of reflectances are considered.

Measurements of the optical constants of opaque Au films in the region 1.7 to 4.2 eV are presented in Chapter 6. The results are discussed and the features of the spectra due to interband transitions are identified.

The optical properties and interband transitions in the region 0.62 to 4.0 eV of the transition metals Ni, Co, and Mo are discussed in Chapter 7 and some tentative identifications of optical features are made. Polished specimens of Co and Ni have almost identical band structures and polished specimens of Mo and opaque Mo films have some similarities with Ni and Co .

Appendices contain a brief account of some preliminary observations of the optical properties of stearic acid films, and contain details of Kramers-Kronig calculations.

DECLARATION

All the theoretical and experimental work presented in this thesis was performed in the thin film laboratory of the Physics Department between February 1973 to July 1979. To the best of the author's knowledge and belief, this thesis contains no material which has been accepted for the award of any other degree or diploma in any University and no material previously published or written by another person except where due reference is made in the text.

Anoara Islam.

ACKNOWLEDGEMENTS

My grateful thanks are due to my supervisor Dr. S.G. Tomlin for suggesting the project and for his many helpful and critical discussions during the period of the work. I also acknowledge the help of Dr. E.H. Medlin as an interim supervisor.

The facilities of the Physics Department were enjoyed over the years during the Chairmanship of Professors J.H. Carver and J.R. Prescott and Dr. W.G. Elford.

I am greatly indebted to Mr. A.G. Ewart for his valuable technical support and for preparing the diagrams.

My sincere acknowledgements are due to:
The Defence Research Centre of Salisbury (D.R.C.S.) for the preparation of sputtered films and for polishing the metal specimens; Dr. K. Bartusek, Optical Centre and Mr. R. Miles, Waite Agricultural Research Institute for providing the electron microscope facilities; Mrs. P. Coe for typing the thesis.

It is a pleasure to acknowledge the award of a University of Adelaide Research Grant.

CHAPTER I

INTRODUCTION

1.1. Aim of the Project

A great deal of work has been done on the optical properties of crystalline Ge. In recent years experimental and theoretical investigations have been extended to liquid and non-crystalline materials. Many recent studies have been made on the structural and electronic properties of crystalline and amorphous forms of the same material in attempts to understand the effects of disorder. But the optical absorption edge remains a largely unresolved problem in amorphous Ge and Si. To quote from a recent paper by Moss and Alder (1973).

> " However, instead of settling the issues, many of the new results have been contradictory and have left observers with a feeling either that most of the experimental data reported are due to artifacts or that a wide variety of different forms of amorphous silicon and germanium exists...
>
> The band gap of amorphous Ge ranges between 0.5 eV and 1.1 eV; for Si, it is 0.8 eV, 1.6 eV, or 1.8 eV. The absorption edge is gradual, indicative of disorder-induced band tailing, is sharp even in as-deposited films, which is put forward in evidence against significant band tails, or is gradual in as-deposited films but sharp after annealing "

Clearly the problem of determining the optical constants of these materials (Ge and Si) is not straightforward. In our laboratory a careful study of Si has been carried out by Thutupalli (1976). In the present investigation a systematic study of the optical properties of Ge in both amorphous and polycrystalline form has been undertaken. In the following, we shall examine some of the

questions which are still open concerning the electronic band structure of Ge , for example :

(1) What is the value of the energy gap (or mobility gap) ?

(2) Does the gap persist in the disordered material as in ordered crystalline material ?

(3) If the gaps do persist in the presence of disorder, how do the gaps differ from those of the ordered material ?

(4) Does the energy gap change with annealing or with deposition temperature of the substrate ?

(5) To what extent can the crystalline band structure be used to describe the properties of amorphous material ?

An account will be given of the determination of the optical constants of Ge by means of the normal incidence reflectance-transmittance method, and the changes observed in them as amorphous material is converted to crystalline Ge by annealing, or as a result of deposition at higher temperatures. An attempt to interpret these results in terms of the Mott-Davis (1971) theory of amorphous materials will be given.

Another question has been raised by measurements on Ge extending into the absorbing region by means of the method of measuring reflectances from the specimen surface and the surface coated with a thin layer (Tomlin 1972). The question is to what extent such measurements might be used in conjunction with measurements of

reflectivity over a very wide range of wavelengths to improve the Kramers-Kronig method by increasing the reliability of the extrapolation procedures needed in that method. With this object in mind and the possible application of this method to metals a study has been made of some possible improvements in extrapolation formulae.

The third part of the work is concerned with an investigation of the above-mentioned method involving the measurement of two reflectances as applied to the determination of the optical constants of metals. This is a preliminary study of the applicability of the method when reflectances are high and is concerned mainly with the accuracy that might be achieved.

In comparison with semiconductors, less work has been done on metals though people started to use metallic films for various purposes long before semiconductors. Kohn (1966) comments " the field of the optical properties of metals has, during the last five years, become a quite impressive quantitative science. The experiments and analyses of the optical properties of Cu and Ag (Ehrenreich and Philipp, 1962), and Al(Ehrenreich *et al*, 1963) are good examples of this progress.... To my knowledge, these results are still rather mysterious and suggest that, at least in some metals, important modifications of our current ideas concerning their electronic structure may be required. "

It is interesting to note that six years later Abeles (1971) also makes similar comments, e.g. "The experimental results are still very often obtained with metallic films having an unknown or poorly known structure, and they are more subject to revision and modification in the near future."

From these comments it can be concluded that the confusion surrounding the optical properties of metals has arisen from variations in preparation conditions and methods. Moreover, one of the greatest difficulties with metals is the preparation of good surfaces and the effects of oxidation.

Of all metals, gold is probably the easiest to work with because it does not react with gases in the atmosphere. On the contrary transition metals which have partially filled d or f shells are much more difficult to work with than normal metals. I chose both gold (Au) and transition metals (Ni, Co and Mo) for the present work on the optical constants of metals using Tomlin's method (1972).

The purposes of the present investigations are :

(1) To supplement the work already carried out on amorphous and polycrystalline Ge in our laboratory.

(2) To attempt to improve the evaluation of optical constants by using Kramers-Kronig analysis of reflectance data.

(3) To extend the work to polished bulk metals and opaque metal films.

(4) To further examine the suitability of Tomlin's method of determining the optical constants of metals.

(5) To evaluate the optical constants of metal films by reflection measurements at normal incidence from both sides of the substrates on which they are deposited.

1.2 Optical Absorption

The optical properties of optically isotropic solids with which we shall be concerned are the behaviour of the refractive and

absorption indices as functions of wavelength or photon energy. The interaction between the solid and electromagnetic radiation may cause absorption of radiation through excitations of electrons between, or in case of metals within, energy bands. Measurement of the optical properties has proved to be a powerful tool for studying the energy spectrum of these excitations and therefore of the electronic band structures.

From Maxwell's equations, which are a set of partial differential equations which describe the space and time behaviour of electromagnetic field vectors, the wave equations for linear isotropic non-conducting media are

$$\left(\nabla^2 - \frac{1}{v^2}\frac{\partial^2}{\partial t^2}\right)\left\{\begin{matrix}\underline{E}\\ \underline{B}\end{matrix}\right. = 0 \qquad 1.2.1$$

where $\underline{E}$ and $\underline{B}$ are electric and magnetic field vectors. For infinite plane waves $\underline{E}$ and $\underline{B}$ are perpendicular to one another and to the direction of propagation, and the velocity of the wave within the medium is $v = \frac{c}{N}$ where N is the refractive index of the medium and c is the velocity of light in free space. Equation (1.2.1) are vector wave equations i.e. they are valid for each rectangular component of $\underline{E}$ and $\underline{B}$. Therefore the scalar wave equation

$$\nabla^2\psi - \frac{1}{v^2}\frac{\partial^2\psi}{\partial t^2} = 0 \qquad 1.2.2$$

is satisfied for $\psi = Ex, Ey, Ez, Bx, By, Bz$. Now we are interested in the plane wave solutions to the wave equation (1.2.2). The one-dimensional wave equation for propagation along the positive x-direction is

$$\frac{\partial^2\psi}{\partial x^2} - \frac{1}{v^2}\frac{\partial^2\psi}{\partial t^2} = 0 \qquad 1.2.3$$

The solution of the equation (1.1.3) is of the form

$$\psi = Ae^{\pm iw\left(\frac{Nx}{c} - t\right)} \qquad 1.1.4$$

where w = angular frequency = $2\pi\nu$, ν = frequency of vibration. If the medium is absorbing, it has a complex refractive index $N = n \pm ik$ where the real part n is the refractive index and k the absorption index. Here we shall use $N = n - ik$ except in the section on the Kramers-Kronig relations where it is more usual to use $N = n + ik$. Putting the value of N ($= n - ik$) in equation (1.1.4) we get

$$\psi = Ae^{-\frac{kwx}{c}} e^{iw\left(t - \frac{nx}{c}\right)} \qquad 1.1.5$$

The energy flow is given by the Poynting vector which is proportional to the product of the amplitude of the electric and magnetic vectors. As both terms contain $e^{-\frac{kwx}{c}}$, the attenuation is $e^{-\frac{2wkx}{c}}$ and the absorption coefficient

$$K = \frac{2wk}{c} = \frac{4\pi k}{\lambda} \qquad 1.1.6$$

where λ = wavelength in free space. The penetration depth of light is $\frac{1}{K} = \frac{\lambda}{4\pi k}$.

We can measure n, k experimentally for a wide range of wavelengths and K which is needed in discussion of the optical absorption formulae can be determined from k.

It is also convenient to express the optical constants of materials in terms of a complex dielectric constant ε, which can be defined as

$$\varepsilon = \varepsilon_1 + i\varepsilon_2 = N^2 = (n - ik)^2 \qquad 1.1.7$$

where $\varepsilon_1 = n^2 - k^2$ is the real part and $\varepsilon_2 = 2nk$ is the imaginary part of the dielectric constant.

1.3 Band Structure of Solids

The energies of electrons in crystal lattices are arranged in energy bands, separated by regions in energy for which no wave functions exist. The Bragg reflections at $\underline{k} = \pm n\pi/a$ of electron waves is the origin of energy gaps in a simple linear solid of lattice constant 'a' where n is an integer and $\underline{k}$ is the magnitude of the wave vector related to the wavelength λ by $\underline{k} = 2\pi/\lambda$. The low energy portions of the band structure are shown qualitatively in Figure (1.1a) for entirely free electrons and in Figure (1.1b) for electrons that are nearly free. In this latter case there is an energy gap at $\underline{k} = \pm \pi/a$ and other energy gaps occur for successive values of the integer n . The reflection at $\underline{k} = \pm \pi/a$ occurs because in the linear lattice, the wave reflected from one atom interferes constructively with the wave reflected from a nearest-neighbour atom. The region between $-\pi/a$ and π/a is the first Brillouin Zone of this lattice in wave vector space. The energy gap at the zone boundary for the Kronig-Penney potential is shown in Figure (1.1c) for $P = 3\pi/2$.

Such energy gaps are called band gaps or forbidden bands and may be defined as the distance between the highest maximum of the valence band and lowest minimum of the conduction band in wave vector space. The magnitude of this energy gap and the occupation of the available energy levels by the electrons determine whether the solid is a metal, semiconductor or insulator.

The crystal will be an insulator when the valence band is full, the conduction band above it is empty and the forbidden band is wide enough. The crystal will behave as a metal if the valence band is partly filled, and as a semiconductor if the valence band is full or

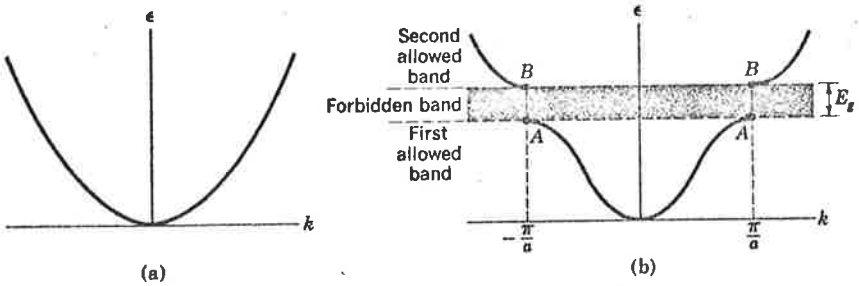

FIG.1·1 (a) Plot of energy ϵ versus wavevector k for a free electron. (b) Plot of energy versus wavevector for an electron in a monatomic linear lattice of lattice constant a. The energy gap E_g shown is associated with the first Bragg reflection at $k = \pm\pi/a$; other gaps are found at $\pm n\pi/a$, for integral values of n. (FROM KITTEL, 1976)

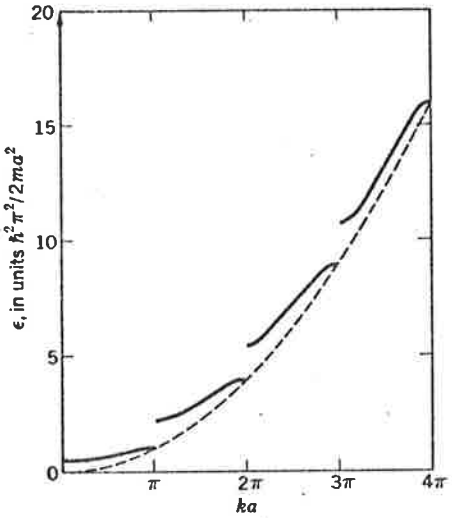

FIG.1·1(c) Plot of energy vs. wavenumber for the Kronig-Penney potential, with $P = 3\pi/2$. (After Sommerfeld and Bethe.)
(FROM KITTEL, 1976)

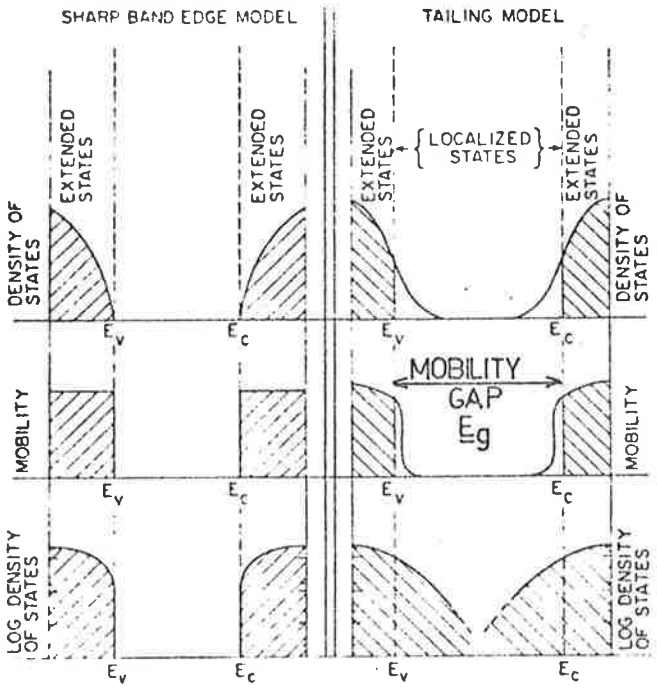

FIG.1·1(d) Two models for the electron structure of amorphous Ge and Si near the band edges.
(FROM SPICER et al, 1972)

almost full and the forbidden gap is small. The metal is a good conductor whose conductivity decreases with increasing temperature. In contrast to this the conductivities of semiconductors increase with increasing temperature. Conductivity not only depends on temperature but also on the size of the forbidden gap.

The best values of the band gaps are obtained by optical absorption measurements.

1.3.1 Optical interband transitions in semiconductors

One of the most important feature of the semiconductor is the transition of electrons from one electron band to another. The process is called interband transition.

Interband electronic transitions can be considered as direct or indirect according to whether or not the conduction or valence band extrema lie at the same point or different points in wave vector space.

(a) Direct transitions

In this process photons are absorbed by the crystal with the transition of an electron from the valence band to the conduction band without any change in the electron vector. This is shown in Figures 1.2(a) and 1.3(a) where only the vertical transitions between the two states which have the same value of the wave vector are allowed. The absorption coefficient $K(E)$ for a given photon energy E, is proportional to the transition probability P_{if} for the transition from the initial state to the final state, and to the density of electrons in the initial state N_i, and also to the density of available empty final states N_f, summed over all possible transitions between states with an energy difference equal to E (Smith 1961,

Pankove 1971). With the assumption that the band edges are parabolic one finds

$$K(E) \propto \Sigma P_{if} N_i N_f \qquad 1.3.1$$

$$\propto \frac{A}{n\hbar w} |P_{if}|^2 (E - Eg)^{\frac{1}{2}}$$

$$\text{or} \quad EnK \propto (E - Eg)^{\frac{1}{2}}$$

$$\text{or} \quad (EnK)^2 \propto (E - Eg) \qquad 1.3.2$$

where A is a constant, Eg is the band gap and n is the refractive index of the solid.

(b) Indirect transitions

Both photon and phonon are involved in indirect transitions. Direct and indirect gaps of crystals are shown in Figures 1.2(a), 1.3(a), 1.2(b) and 1.3(b). The transition probability is calculated first by considering that the electron makes a vertical transition to a state where the energy is not conserved, but momentum is conserved. Electron phonon scattering then takes place so that both energy and momentum are finally conserved. The threshold energy is slightly greater or less than the true band gap for the indirect transition process. This process may occur in two ways either by the absorption or emission of a phonon. For an indirect transition, (Smith 1961, Pankove 1971), again assuming parabolic band edges

$$\hbar wnK(E) \propto (E - Eg' \pm h\,\Omega)^2 \qquad 1.3.3$$

where Eg' is the indirect band gap and Ω is the frequency of vibration of the phonon, since $h\,\Omega$ is very small, then to a good approximation

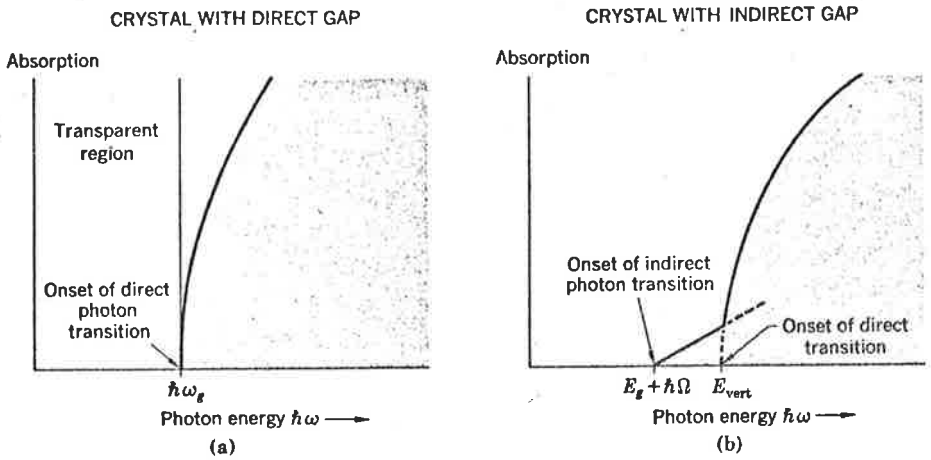

FIG. 1·2. Optical absorption in pure insulators at absolute zero. In (a) the threshold determines the energy gap as $E_g = \hbar\omega_g$. In (b) the optical absorption is weaker near the threshold: at $\hbar\omega = E_g + \hbar\Omega$ a photon is absorbed with the creation of three particles: a free electron, a free hole, and a phonon of energy $\hbar\Omega$. In (b) the energy E_{vert} marks the threshold for the creation of a free electron and a free hole, with no phonon involved. Such a transition is called vertical; it is similar to the direct transition in (a). These plots do not show absorption lines that sometimes are seen lying just to the low energy side of the threshold. Such lines are due to the creation of a bound electron-hole pair, called an exciton. (FROM KITTEL, 1976)

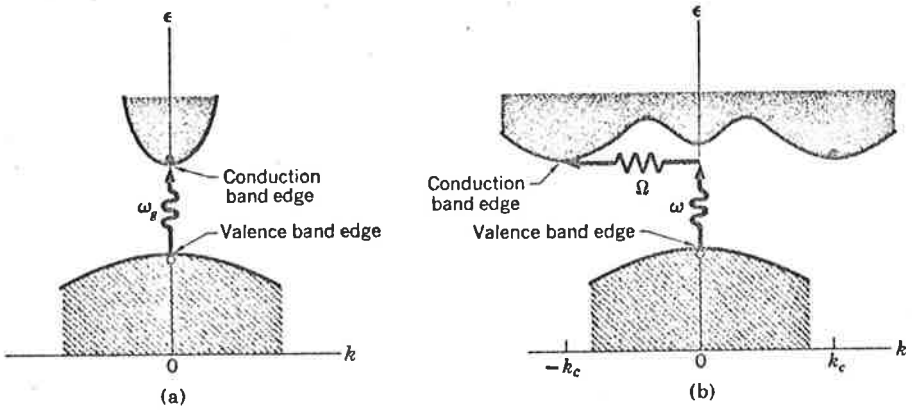

FIG. 1·3. In (a) the lowest point of the conduction band occurs at the same value of k as the highest point of the valence band. A direct optical transition is drawn vertically with no significant change of k, because the absorbed photon has a very small wavevector. The threshold frequency ω_g for absorption by the direct transition determines the energy gap $E_g = \hbar\omega_g$. The indirect transition in (b) involves both a photon and a phonon because the band edges of the conduction and valence bands are widely separated in k space. The threshold energy for the indirect process in (b) is greater than the true band gap. The absorption threshold for the indirect transition between the band edges is at $\hbar\omega = E_g + \hbar\Omega$, where Ω is the frequency of an emitted *phonon* of wavevector $\mathbf{K} \cong -\mathbf{k}_c$. At higher temperatures phonons are already present; if a phonon is absorbed along with a photon, the threshold energy is $\hbar\omega = E_g - \hbar\Omega$. *Note:* The figure shows only the threshold transitions. Transitions occur generally between almost all points of the two bands for which the wavevectors and energy can be conserved. (FROM KITTEL, 1976)

$$\hbar wnK(E) \propto (E - Eg')^2$$

$$\text{or} \quad (EnK)^{\frac{1}{2}} \propto (E - Eg') \qquad 1.3.4$$

from equation (1.3.2) and (1.3.4) the absorption in a crystal may be represented by

$$(E - Eg) \propto (EnK)^{\alpha} \qquad 1.3.5$$

where $\alpha = 2$ for direct transition, $\alpha = \frac{1}{2}$ for indirect transitions.

Thus it is possible to determine which kind of transition occurs and also the band gap energy from values of n and k by plotting $(EnK)^{\alpha}$ as a function of photon energy E for various α. Optical measurements offer the only possibility of distinguishing the types of transitions. The photon energy at which the optical absorption begins is called the absorption edge of the semiconductor. The energy band of most semiconductors consists of several sub-bands which may be separated by spin orbit interaction. The conduction and valence bands of germanium are shown in Figure (1.4) based on a combination of theoretical and experimental results. Within the range of our measurement we are primarily interested in the nature and density of electron states just near maxima and minima of the bands.

1.3.2 Amorphous semiconductors

So far we have considered only ideal crystals but now it is useful to discuss how the concepts appropriate to crystalline solids can be applied to disordered materials i.e. to amorphous materials. Solid phases of both amorphous and polycrystalline forms of Ge are semiconductors. Amorphous solids yield X-ray diffraction patterns similar to those of a microcrystalline powder. In amorphous solids it is believed that as a result of disorder the bands are modified by the formation of tails of states extending the bands into the gaps.

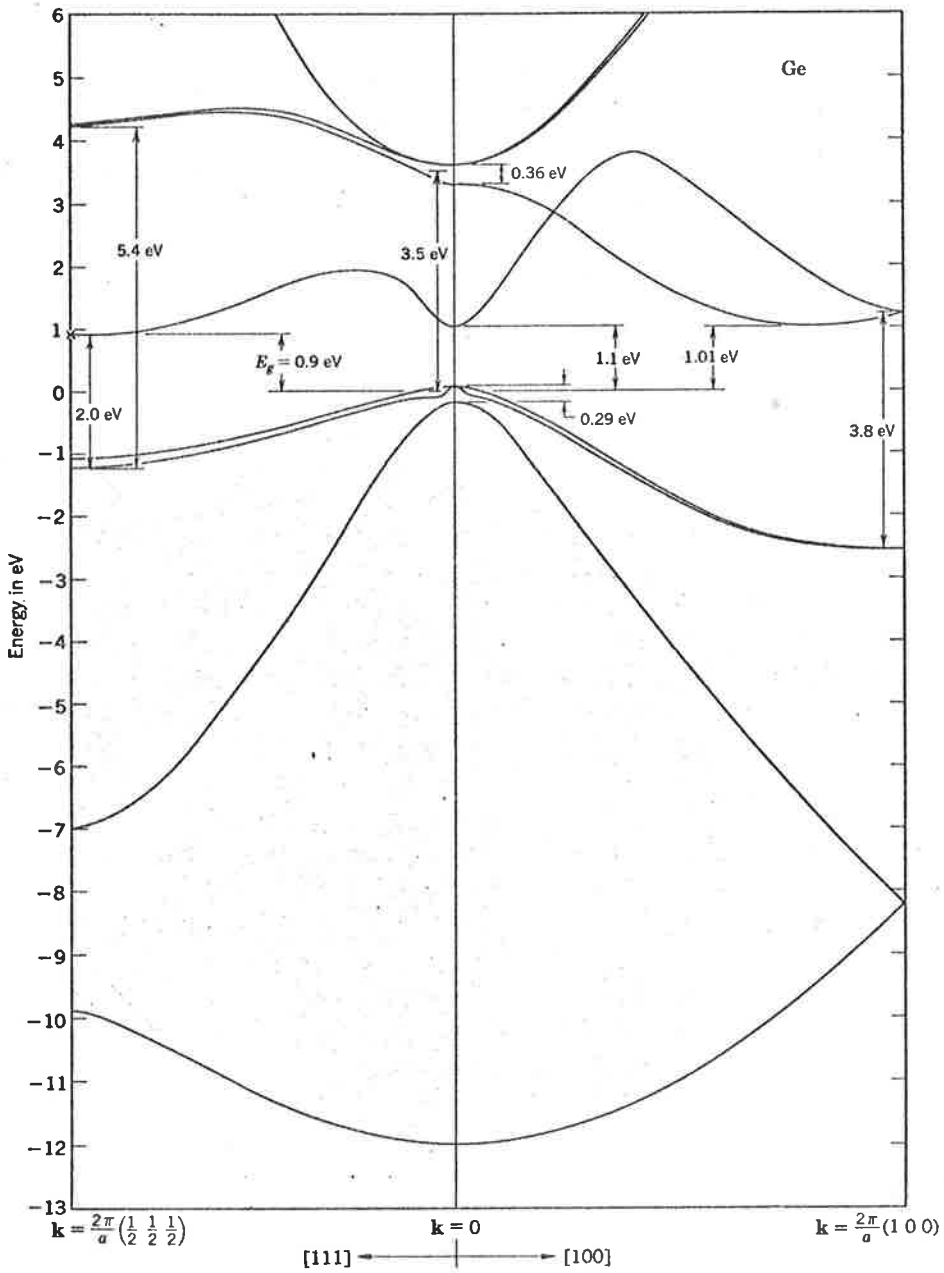

FIG. 1·4. Calculated band structure of germanium, after C. Y. Fong. The general features are in good agreement with experiment. The four valence bands are shown in gray. The fine structure of the valence band edge is caused by spin-orbit splitting. The energy gap is indirect; the conduction band edge is at the point $(2\pi/a)(\frac{1}{2}\frac{1}{2}\frac{1}{2})$. The constant energy surfaces around this point are ellipsoidal. (FROM KITTEL, 1976)

Here we shall use the model suggested by Mott and Davis (1971) as a general account of amorphous semiconductors which are considered to be homogeneous uniform materials. In amorphous semiconductors the energy gap Eg, as shown in Figure (1.1d), is the mobility gap between the bands of extended states i.e. a gap between mobility edges.

The relations between the energy gaps in amorphous and polycrystalline forms of a given material and the changes as one form is converted to the other are of fundamental interest. Again according to Davis (1973) " A general rule appears to be that, if the local atomic order is not appreciably altered in the amorphous phase, then the gaps of the two states are not appreciably different. "

This statement can also be verified from our experimental results for Ge (see Ge chapter). The "Tailing Model" for electron structure of amorphous Ge and Si near the band edges is shown in Figure (1.1d).

1.3.3 Optical intraband and interband transitions in free-electron metals

At energies well below the energy gap or fundamental gap, electronic absorption can occur through intraband transitions which are the transitions characteristic of a free-electron metal and therefore take place only in metals. Intraband transitions involve the excitation of electrons from below the Fermi surface to another state above it within the same band. No threshold energy is needed for such transitions. Nearly free-electron band structures for monovalent and multivalent metals are shown in Figures (1.5a) and (1.5b). According to Nilsson (1974) " The theory for intraband transitions is not yet satisfactory. The band structure is usually assumed to be simply free-electron-like with an effective mass. Thus the influence of distortions of the bands, such as band gaps, is not included..... Also, the accuracy of the experimental results is in many cases not clear. Because of the high

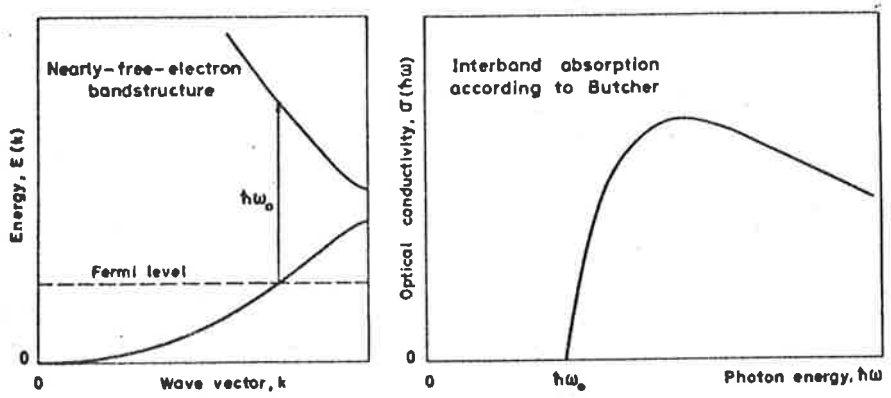

FIG. 1·5(a) A nearly-free-electron band structure for a monovalent metal and the corresponding optical conductivity according to Wilson and Butcher.
(From Nilsson, 1974)

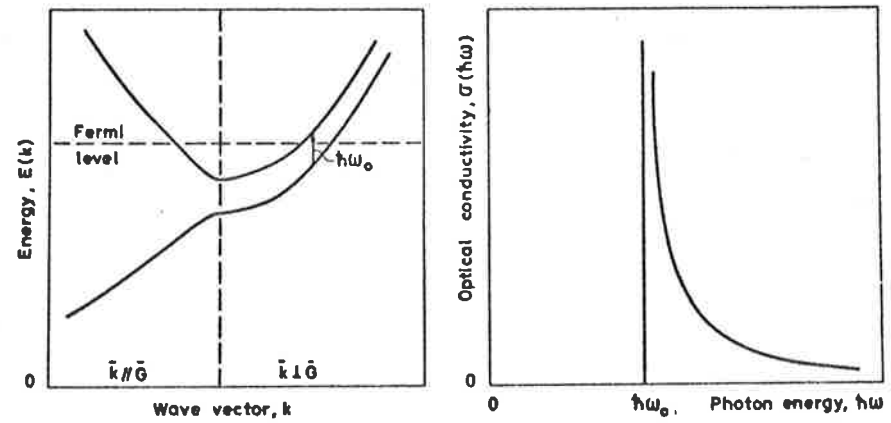

FIG. 1·5(b) A nearly-free-electron band structure for multivalent metal and the partial optical conductivity due to parallel band absorption according to Golovashkin and others.
(From Nilsson, 1974)

reflectance in the infrared region, where Drude absorption dominates, there has been difficulty in obtaining good results."

In principle metals are similar to semiconductors and may be considered as a limiting case of a highly degenerate semiconductor. Interband transitions set in at a minimum photon energy which is also one of the important characteristic of the electronic structure of the metals. The position of this minimum frequency is in the visible region for copper and gold. The low energy band structure of nickel observed at 0.25, 0.40 and 1.3 eV by Hanus *et al* (1968) using temperature modulated reflectance is shown in Figure (1.6). Here nickel films are assigned interband transitions with a band scheme in which the conduction band is lowered with respect to the d bands so that L_2' is below L_{32} in both the majority and minority spin bands. The broad structure at 1.3 eV was also observed by others, but the interpretation of the reversal of the two low-lying peaks was given by Zornberg (1970). The structure observed in the reflectance at low temperature at 0.4 eV disappears at room temperature. An optical feature around 1.25 eV is also observed in the present investigation of bulk, polished nickel and opaque metallic films of Ni (details in Chapter 7).

The main difference between a metal and a semiconductor is that no absorption takes place in a semiconductor until the absorption edge is passed whereas in metals the conduction or free electrons contribute a strong absorption in the infrared region, the magnitude of which decreases smoothly with increasing photon energy and is much less in the visible region.

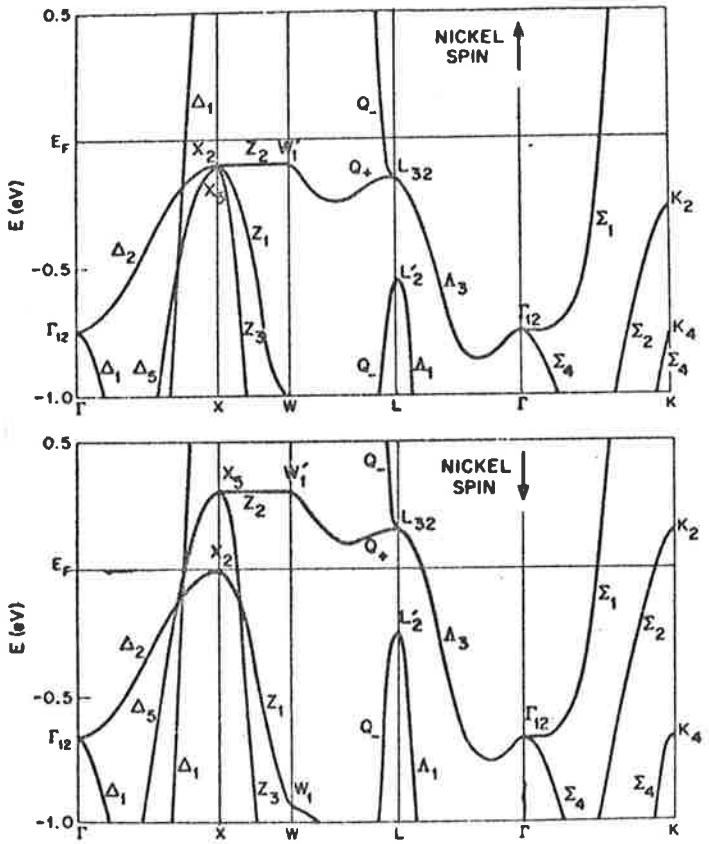

FIG.1·6 Energy band structure for Ni as proposed by J. Hanus, J. Feinleib, and W. J. Scouler, *J. Appl. Phys.* **39**, 1272 (1968).
(From Nilsson,1974)

1.4 Advantages of the Optical methods for the study of band structure

Besides optical measurements, there are several experimental techniques e.g. cyclotron resonance, de Haas-van Alphen effect, galvano metric and magneto - acoustic resonance which provide information about band structure. Although the accuracies of these experiments are very high the energy levels may be studied only within a few kT of the Fermi surface where k is Boltzmann's constant and T is absolute temperature. Ion neutralization spectroscopy and soft X-ray emission also provide information over a wide range, but they have not proved to be as useful as optical methods.

1.5 Thin films and bulk specimens

The investigation of the optical properties can be carried out either with bulk samples or with thin films. But the study of the bulk samples is restricted to reflection measurements which are often greatly dependent on the surface condition of the samples. One great advantage of using thin films is that one can measure reflection coefficients as well as transmission coefficients which are less dependent on the surface conditions.

Optical constants of thin films of metals show a marked dependence on thickness. According to Abeles (1972), " and their surface is as smooth as that of the substrate if they are not too thick. For instance, even when using opaque specimens, one prepares them a few thousand ångströms thick only. The principal defects which are found in the thinner films are grain boundaries, whereas the thicker ones contain mainly dislocations and stacking faults."

Since the transmittance of metallic films a few thousand ånström thick is of the order of one percent or less, the normal

incidence reflectance-transmittance method is suitable for determining the optical constants only of very thin films. But such films have optical properties different from those of bulk material. So for the comparison of the observed values of the optical constants with that of the bulk polished metal, thick opaque films must be used and then the only measurements that can be made are of reflectances.

Apart from the desire to measure the optical properties of thin and thick films as means of studying electronic band structure, the study of these properties is relevant to many practical applications such as in electronics, engineering, optics, bio-medical, nuclear and space science.

Among non-crystalline materials are liquid metals, semiconductors, simple and complex glasses and amorphous evaporated films. In recent years the optical properties of amorphous solids have become of considerable interest since simple and complex glasses of various kinds are essential materials for making different optical devices. Ge can be prepared in the amorphous state in thin layers. In important applications thin films of semiconductors are used in solar cells, photodetectors and in optical devices where they are used in anti-reflection coatings and as multilayer interference filters. Multilayers of semiconductors and opaque metallic films are used together in solar cells to enhance the absorption in the optical region concerned and are commonly called "dark mirror coatings" .

The optical properties of thin films of semiconductors and opaque metallic films are of importance both in fundamental and applied solid state research for advances in knowledge of their band structures and for numerous practical applications.

The following sections discuss briefly the various methods of determining the optical constants of solids as well as the method used in the present investigation for the determination of the optical properties of amorphous and crystalline Ge , of opaque films and bulk samples of Au, Co, Ni and Mo , and of multilayer organic films of stearic acid $(CH_3(CH_2)_{16}COOH)$.

1.6 Various methods of determining the optical constants of thin films

There exist several methods for determining the optical constants of thin films either absorbing or transparent, supported on transparent or absorbing substrates.

(a) Transparent films

If a transparent film ($k = 0$) is deposited on a transparent substrate ($k_1 = 0$) , the refractive index and thickness can be determined either independently or as a product without any difficulty by using any of the experimental techniques developed by Vasicek (1947), Fochs (1950), Hartman (1954), Schulz (1954) and Abelès (1958). The simplest method is due to Abelès. It gained wide popularity because of its sensitivity, accuracy and simplicity both experimentally and theoretically.

1.6.1 Abelès Method

For films whose optical thickness lies in the neighbourhood of odd multiples of a quarter of a wavelength, Abelès described a simple method for measuring the refractive index of the film or the substrate on which it is to be deposited. Generally this method requires only a spectro — meter with a scale which may be read to one minute of arc. Experimentally one coats a part of the substrate with the film whose refractive index is desired and then determines the angle of incidence

ϕ_A , for which reflectances from both parts of the surface are equal. According to him n_1 , the film index and n_2 , that of the medium from which the light is incident (generally air) is related to the angle of incidence ϕ_A by the formula $\phi_A = \arctan n_1/n_2$. So any particular film of suitable thickness satisfies this condition only for one angle of incidence provided the difference between substrate and film is not too large. (Abelès suggests $|n_1 - n_2| \nmid 0.3$, an accuracy of $\pm .002$ in refractive index is attainable). The result is independent of film thickness and also completely independent of the refractive index of the substrate.

For isotropic homogeneous transparent films the conclusion one may draw from a review of the literature is that if the refractive index alone is required Abelès' Brewster angle measurement is convenient whereas if the refractive index as well as the thickness of the film is required then Fochs' (1950) interferometer method is to be preferred when the film thickness is sufficiently great.

(b) Absorbing films

Some of the most commonly employed techniques used to determine the optical constants and thickness of thin absorbing films deposited either on a transparent or an absorbing substrate are briefly described below :

1.6.2 Polarimetric Method (Ellipsometer)

This method requires the measurement of the ratio of the amplitudes of the two components of plane polarised light after reflection from a film when the light is incident at an angle ϕ , and also the relative phase difference Δ between these components. The

experimental apparatus used to measure Δ and ϕ is called an ellipsometer. The ellipticity of the reflected beam can be analysed by any of the standard methods. In most cases the direction of vibration of the plan polarised light is inclined at 45° to the plane of incidence. It enables the simultaneous determination of n, k and d (thickness). Since all the measurements are taken at non-normal incidence, the effects of optical anisotropy on the optical constants are of great concern. The phase difference Δ in particular is very sensitive to surface films. For example 30Å to 40Å thick oxide films which generally form on metal surfaces cause Δ to change by several degrees as shown by Burge and Bennet (1964). This method can give excellent results provided the correctors for any surface film are properly made, and it may be applied to both transparent and absorbing films. The optical constants of absorbing films which are thick enough to be opaque can also be determined by making ellipsometric measurements on a single sample.

1.6.3 Schopper's Method (Combined method)

In principle Schopper's method (1951 , 1952) is a combination of polarimetric and normal incidence spectrophotometric methods. It involves the simultaneous measurement of the amplitude and phase change of light reflected from each side of the film $(R_1^{\frac{1}{2}}, R_2^{\frac{1}{2}}, \phi_1, \phi_2)$ and transmitted by the film $(T^{\frac{1}{2}}, \phi_3)$. Of the six quantities to be measured three intensities (R_1, R_2, T) can be measured accurately, but the determination of three phase shift parameters (ϕ_1, ϕ_2, ϕ_3) is more difficult. Moreover the phase change ϕ_3 on transmission is generally very small, and therefore difficult to measure, for film thicknesses less than 1000Å. Most of the other methods require only a maximum of four measurements whereas this method requires six. The calculations involved

in this method are tedious and very time consuming.

1.6.4 Spectrophotometry at oblique incidence

Generally the optical properties of a film can be derived from a pair of reflectance measurements using either linearly polarised radiation or unpolarised radiation at two different angles of incidence. A large variety of intensity methods with oblique incidence exist. Two reflectance measurements may be selected in a number of ways. The sensitivities of all these methods have been examined by Humphreys-Owen (1961) who concluded that even in the low absorbing region all these methods suffer from an apparent decrease in sensitivity as the absorption in the film decreases. No method is exceptionally better than the other. Only a few percent accuracy is obtained in most of these cases.

1.6.5 Spectrophotometry at normal incidence

Murmann (1933, 1936) first used the well known technique which requires the measurements of reflectances (R_1 and R_2) from each side of the film on a transparent substrate. In this method the thickness of the film is to be determined independently. In addition to the reflectances on both sides of the film, the transmittance (T) through the film is also measured by Male (1950). This method does not require an independent determination of the film thickness but yields optical constants and film thickness in terms of the measured reflectances and transmittances. Apart from "heavy" computing and extensive graphical procedures the method has disadvantages in the low absorbing region when the values of reflectances from each side of the film are nearly equal. This results in an ill defined point of intersection of two curves in the calculation of the optical constants.

There are several methods which derive the optical constants from the measured reflectance (R) and transmittance (T) at normal incidence.

A method using the exact relations with modified expressions (Tomlin, 1968) for $\left(\frac{1+R}{T}\right)$ and $\left(\frac{1-R}{T}\right)$ has been used successfully by Denton (1972), Khawaja (1975) and Thutupalli (1976) in their studies of the optical properties of Ge, CdS, ZnS, CdSe and Si.

Except for the fact that it requires measurements over a wide spectral range and cannot be used for very thin films (< 500Å) without an accurage knowledge of the film thickness, it has the following advantages :

1. Exact mathematical formulae used in this method are fairly simple and less time consuming for computing when compared with the other methods.

2. The dispersion curve obtained is such that the problem of distinguishing the correct solutions from the others may be solved easily.

3. Surface conditions may be allowed for by treating the surface of the film as an additional layer.

4. Since the method yields the values of refractive indices, absorption indices and the film thickness simultaneously, it has advantages over the other normal incidence methods which require independent determination of film thickness.

5. Because it is a normal incidence method the results are least affected by any possible anisotropy of the film.

6. A single film with smooth surfaces has only one value for the film thickness (d) for an acceptable continuous dispersion curve (Denton 1972).

A continuous dispersion curve is not obtained if there are irregularities on the surface of the film such as an oxide layer or granular structure. In this case considering the surface inhomogenity equivalent to a separate layer one may use reflectance and transmittance formulae for a double layer to obtain an acceptable continuous dispersion curve.

All phase change measurements which may be made by several methods are experimentally difficult. The results obtained by the polarimetric method and by spectrophotometry at oblique incidence are prone to inaccuracies due to surface conditions and anisotropy of the films. Spectrophotometry at normal incidence is probably the most common method for optical measurement on thin films of semiconductors and metals. This method is used in the present investigation for determining the optical constants of amorphous and polycrystalline Ge .

1.7 Principal Methods for determining the optical constants of bulk materials

For transparent material (for which the value of the extinction coefficient becomes zero) the refractive index can be determined without any difficulty by simply measuring either the transmittance or the reflectance at normal incidence on a suitably polished uniform slab of the material. If the material can be obtained in the form of a prism, the refractive index n, can also be determined by measuring A , the angle of the prism and Dm, the angle of minimum deviation. The refractive index is given by

$$n = \sin\left(\frac{A + Dm}{2}\right) / \sin A/2$$

This is one of the most accurate techniques for determining the refractive index of a transparent material. But absorbing materials are characterised by a complex refractive index (N) , in which there are two optical constants (n, k) which must be evaluated from two independent measurements. As Heavens (1955) comments " The study of absorbing materials, and especially those in which the absorption is large (e.g. metals in the visible and infrared) presents a much more difficult problem" . This will be discussed in detail in Chapter 5.

Some possible methods which can be used to determine the optical constants of an absorbing bulk material are described below:-

1.7.1 Reflectivity measurements at normal or oblique incidence

A common method of determining the optical constants of an absorbing bulk material involves measurement of its reflectivity at different angles of incidence. Bulk materials must be optically polished very carefully for getting accurate results. Evaporated metal films a few thousand angstroms thick may be regarded as optically equivalent to bulk samples. So for determining the optical constants of opaque solids deposited on a transparent substrate, the only method open to the investigator entails the examination of the light reflected from both sides of the specimen at normal or oblique incidence. All these measurements depend on surface conditions.

1.7.2 The Kramers-Kronig Relation

A method based on the Kramers-Kronig theory has been very useful for evaluating the optical constants of bulk absorbing materials from normal incidence reflectance measurements taken over a wide spectral range. It is particularly convenient for highly reflecting materials.

The reflectivity at normal incidence (R) can be expressed in terms of r , the amplitude reflectivity by

$$R(\omega) = r(\omega)\, r^*(\omega) \qquad 1.7.1$$

where ω is the frequency. For normal incidence the amplitude reflectivity $r(\omega)$ is given in terms of the complex index of refraction $(n + ik)$ by

$$r(\omega) = \rho e^{i\theta(\omega)} = \frac{n + ik - 1}{n + ik + 1} \qquad 1.7.2$$

where $R = \rho^2$ i.e. $\rho = R^{\frac{1}{2}}$ and θ is the phase angle. Then the Kramers-Kronig relation (see for example, Stern 1963) may be written as

$$\theta(\omega_0) = \frac{\omega_0}{\pi} \int_0^\infty \frac{\ell n\, R(\omega) - \ell n\, R(\omega_0)}{\omega_0^2 - \omega^2}\, d\omega \qquad 1.7.3$$

Because the experimental data are always available for a limited range, it is necessary to extrapolate the reflectance curve throughout the whole region of the spectrum in order to evaluate $\theta(\omega_0)$. The optical constants can be evaluated from $\theta(\omega_0)$ and R by the relations

$$n = (1-R)/(1 + R - 2\sqrt{R} \cos \theta) \qquad 1.7.4$$

$$k = 2 \sin \theta \sqrt{R} / (1 + R - 2\sqrt{R} \cos \theta) \qquad 1.7.5$$

If the amplitude reflectivity $r(\omega)$ is given in terms of the complex index of refraction $(n - ik)$, instead of $(n + ik)$, then the sign of $\theta(\omega_0)$ in equation (1.7.3) will be changed. The evaluation of the integrand in equation (1.7.3) is carried out numerically. A special case arises when $\omega = \omega_0$. Then the value of the integrand is the average value at the grid point just preceding and just following. Details will be given in Chapter 4 . It will be convenient to express θ

in terms of energy as follows

$$\theta(E_0) = \frac{E_0}{\pi} \int_0^{\infty} \frac{\ell n\, R(E) - \ell n\, R(E_0)}{E_0^2 - E^2} dE \qquad 1.7.6$$

Within the range of experimental measurement the phase shift contribution of the equation (1.7.6) can be calculated numerically by applying any of the standard formulae, such as Simpson's rule, or the Newton-Coates method. Extrapolation of reflectance outside the range of experimental measurement must be done with great care. At the low energy region, the reflectivities of metals approach unity whereas for non-metals the reflectance can be extrapolated with sufficient accuracy from the experimental data. In the high energy region the extrapolation is much more difficult for both metals and non-metals and may cause large errors in phase calculations.

1.7.3 The Vincent-Geisse method

Vincent-Geisse (1964) developed a method for evaluating the optical constants of an absorbing solid by means of a thin transparent layer of constant refractive index deposited on that solid. This method involves the measurements of reflectances at normal incidence before and after the deposition of the films. It has been applied only to measurements in the infrared region where the conditions of deposition of suitable thin films could be met easily. This method fails in the visible and U-V regions because it is difficult to find a suitable dielectric of constant refractive index in these two regions. To overcome this difficulty, Vincent-Geisse *et al* (1967) proposed another method for determining the optical constants of absorbing solids within the region of strong absorption. This modified technique requires three measurements which are as follows:-

(i) Reflectance (R) from the bare specimen.

(ii) Reflectance (R_1) from the specimen coated with a thin transparent layer.

(iii) Reflectance (R_2) from the specimen coated with a layer of the same material, but of exactly twice the thickness of the first layer.

Theoretically this method satisfies all requirements for the determination of optical constants and has the advantage of normal incidence measurements. But practically it is very difficult to deposit a second transparent layer of exactly twice the thickness of that of the first layer.

1.7.4 Tomlin's method

To overcome the practical difficulties associated with the method discussed above without sacrificing the advantage of normal incidence reflectance measurements, Tomlin (1972) developed a method of finding the optical constants of highly absorbing solid materials. His method requires the measurement of reflectances from the surface of the specimen itself and from an area of the specimen coated with a thin transparent layer of known optical constants. This method has been used successfully by Khawaja(1975a) and Thutupalli (1976). In the present investigation the possibility of applying this method to metals has been studied and is discussed in detail in Section (5.2) of Chapter 5.

CHAPTER 2

EXPERIMENTAL METHODS

2.1 The Spectrophotometer

In the present investigation the measurement of reflectances (R) and (R_1) and transmittance (T) with light incident normally on either the air or the substrate side of the films were performed by using the spectrophotometer shown in Figure (2.1). Since the construction and operational features of the system were described by Denton (1972), only a brief outline will be given here.

Figure (2.2) shows the optical path from the monochromator, through the mechanical chopper on to the specimen and then to the detector. An illustration of the method of measuring the reflectance (R) and transmittance (T) from the specimen is given in Figure (2.3). It should be pointed out here that the errors in R and T due to the angle of incidence of about 5° are negligible.

2.2 Light Source and Monochromator

A 100-watt quartz iodide lamp powered by a 12V D.C. regulated supply was used in the spectral range 2000 to 500 nm, and a Philips deuterium lamp, type 126138, operating on D.C. according to the circuit supplied by the maker, was used in the spectral range 500 to 250 nm.

A Carl-Leiss double prism monochromator with interchangeable prisms was used as the incident radiation selector. Flint glass and fused quartz prisms were used for dispersing the light in the spectral ranges 2000 to 500 nm and 500 to 250 nm respectively. The quartz prism alone

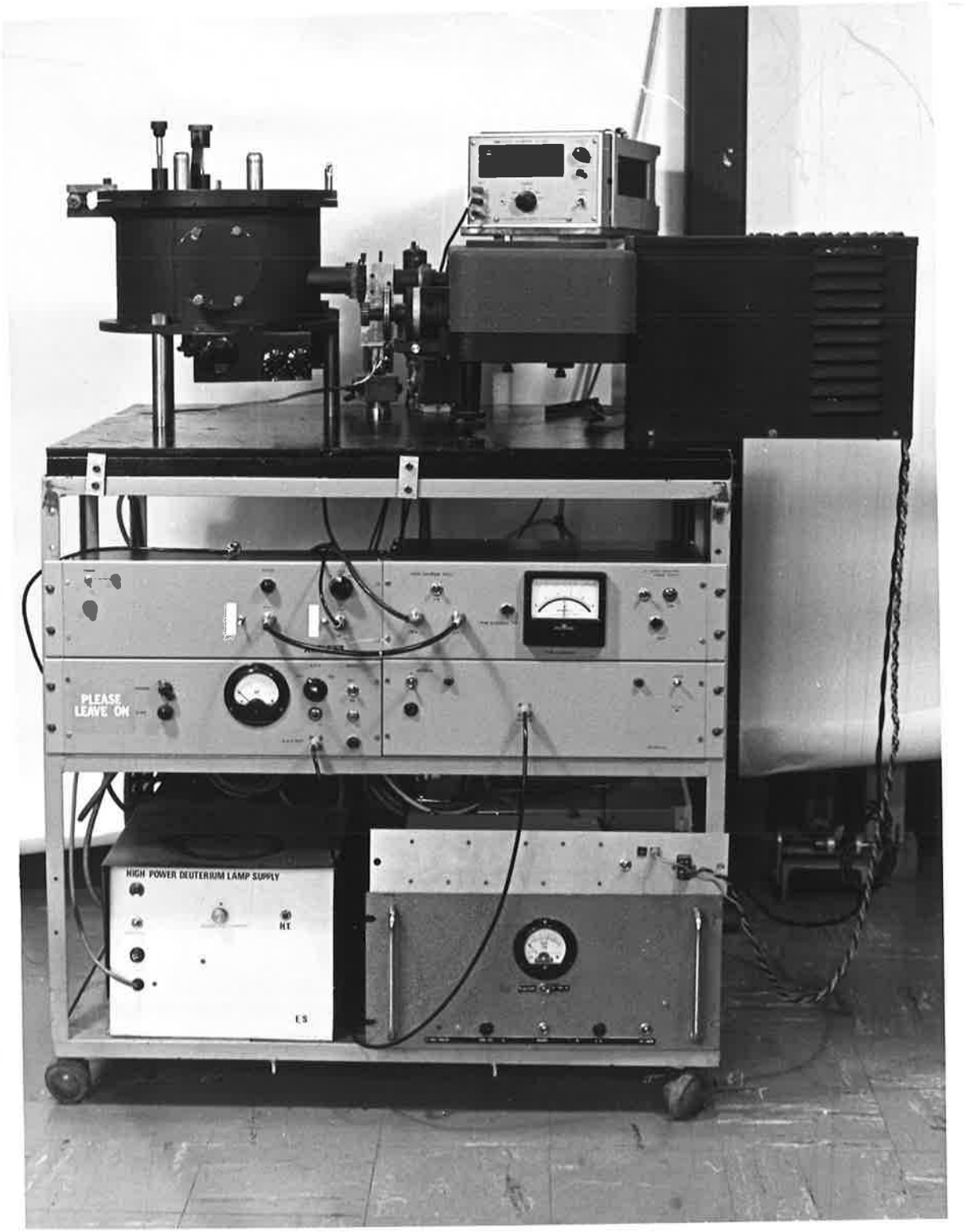

Fig.2·1

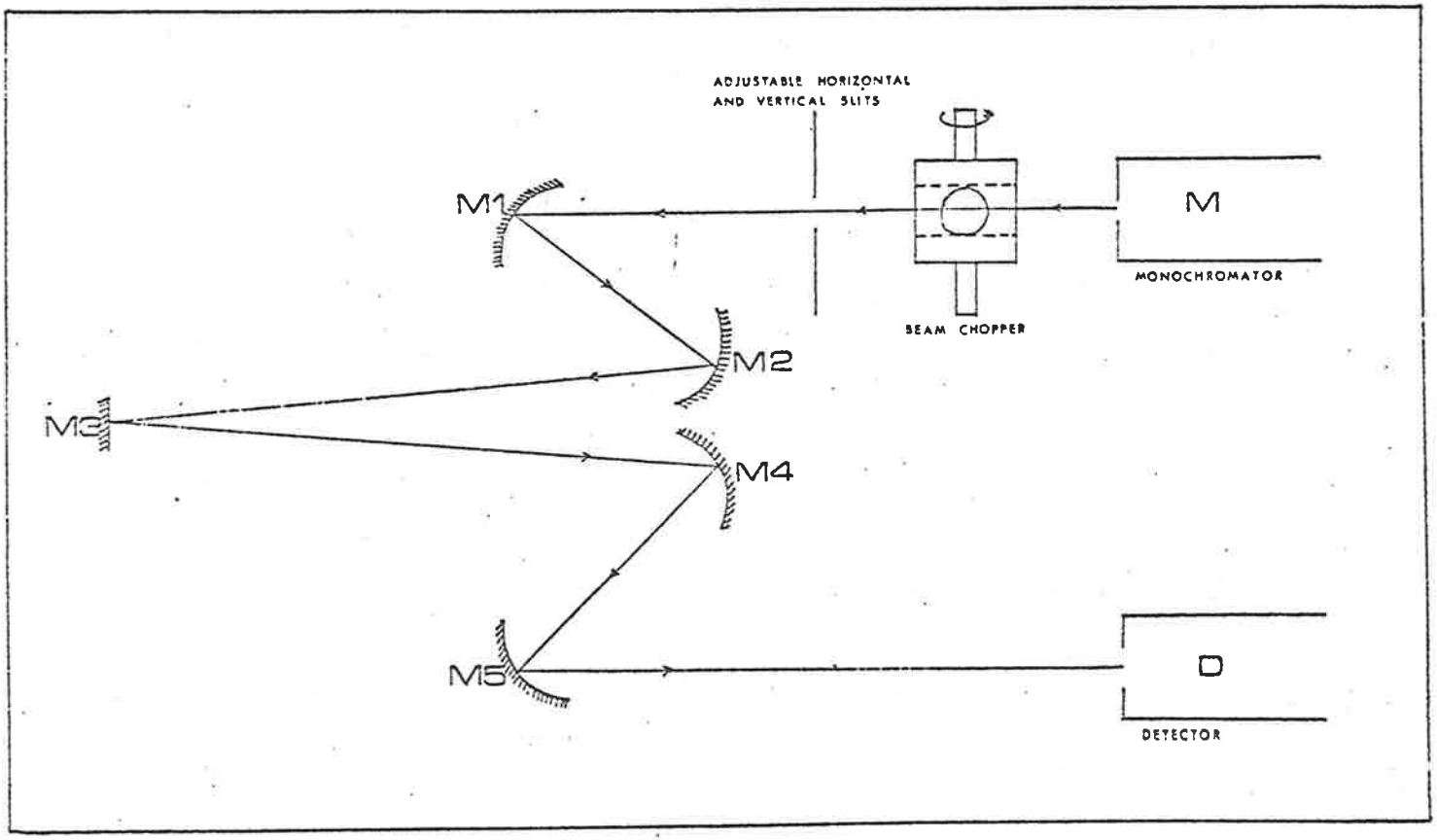

DIAGRAM OF THE OPTICAL SYSTEM

Figure 2.2

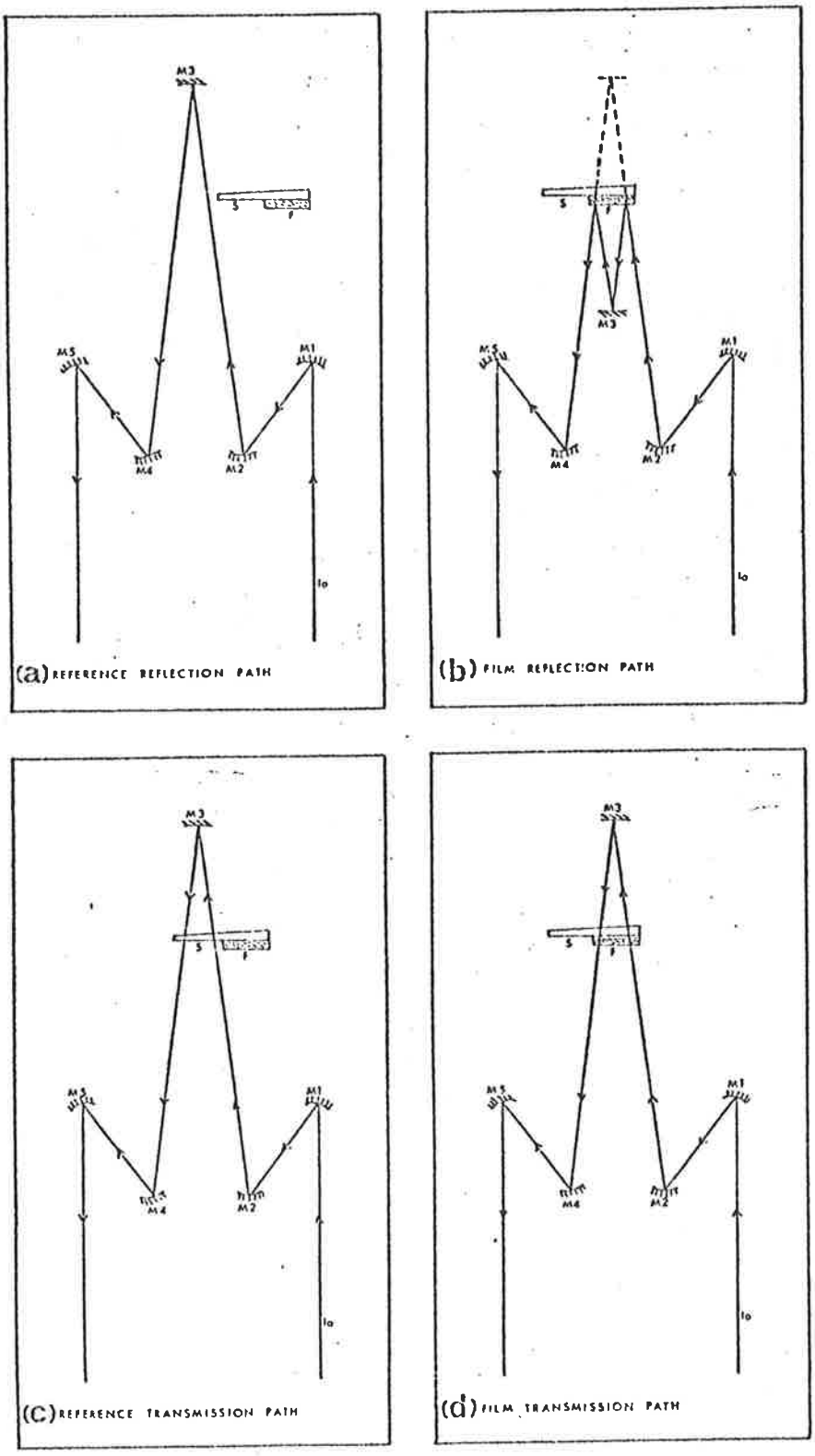
M3
S
M5
M1
M4
M2
Io
(a) REFERENCE REFLECTION PATH
(b) FILM REFLECTION PATH
(c) REFERENCE TRANSMISSION PATH
(d) FILM TRANSMISSION PATH

Figure 2.3

could be used in the entire spectral range from 2000 to 250 nm, but for achieving a better accuracy in the wavelength selection, the flint glass prism was used because it has higher dispersive power in the infrared and visible regions than quartz. Standard sources such as the Philips low pressure Hg, high pressure Hg, He, Na and Cd lamps whose emission spectra are accurately known were used to calibrate the monochromator.

2.3 Detectors

Three different types of detectors were needed. A lead sulphide cell, a silicon-photodiode and a Philips IP28 photomultiplier were used to cover the spectral ranges 2000 to 900 nm, 1000 to 450 nm and 500 to 250 nm respectively. For some spectral ranges, measurements were taken with each of two different detectors. These measurements have two advantages. Firstly, the accuracy of the values obtained by individual detectors could be determined and, secondly, the uniformity of the films could be checked. For instance, at a particular wavelength two detectors had different sensitivities necessitating input signals of different intensities which were controlled by adjusting the width of the slits of the monochromator. This altered the cross-sectional area of the beam falling on the specimen. If there existed any variations in film thickness across the area of the film under investigation this resulted in variations in the measured reflectance and transmittance values obtained. In the case of uniform films it was observed that the measurements taken by each detector in the region of overlap were in good agreement.

2.4 Amplifier

The output from the detector was fed into a high input

impedance amplifier. The circuit diagram is shown in Figure (2.4). To achieve high input impedance at unity gain the input stage incorporates a dual gate MOSFET. The input stage was built in a separate shielded box and was followed by a stable double stage A.C. amplifier with three amplification ranges, X10, X100 and X1000. A filter resonant at the chopper frequency was followed by a rectifier giving a smoothed D.C. voltage which was displayed on a digital voltmeter. The amplifier gain was linear and the calibration accurate to 0.1%.

2.5 Substrate materials and preparations

Thin film specimens were prepared by deposition on optically flat quartz wedges. These wedges measured 6.5 x 4.0 cm and were cut in half to form thick and thin wedges. The evaporated film was deposited on the thicker half whereas the thinner one was used as a reference when measuring transmittances. The wedge angle of 3° was selected so that the internal reflection from the rear surface of the substrate which would result in multiple reflections, would be deviated and not enter the detector. This angle was sufficiently small that the transmittance across the face of the substrate was given sufficiently accurately by the transmittance formula for normal incidence.

Careful cleaning of the substrate prior to deposition of the film is essential for obtaining satisfactory films. For this purpose there exists a variety of procedures, of which the following was found to be satisfactory and straightforward. The substrates were first cleaned with Analar acetone and then held in warm chromic acid till the acid formed an even layer over the substrate. The acid was then

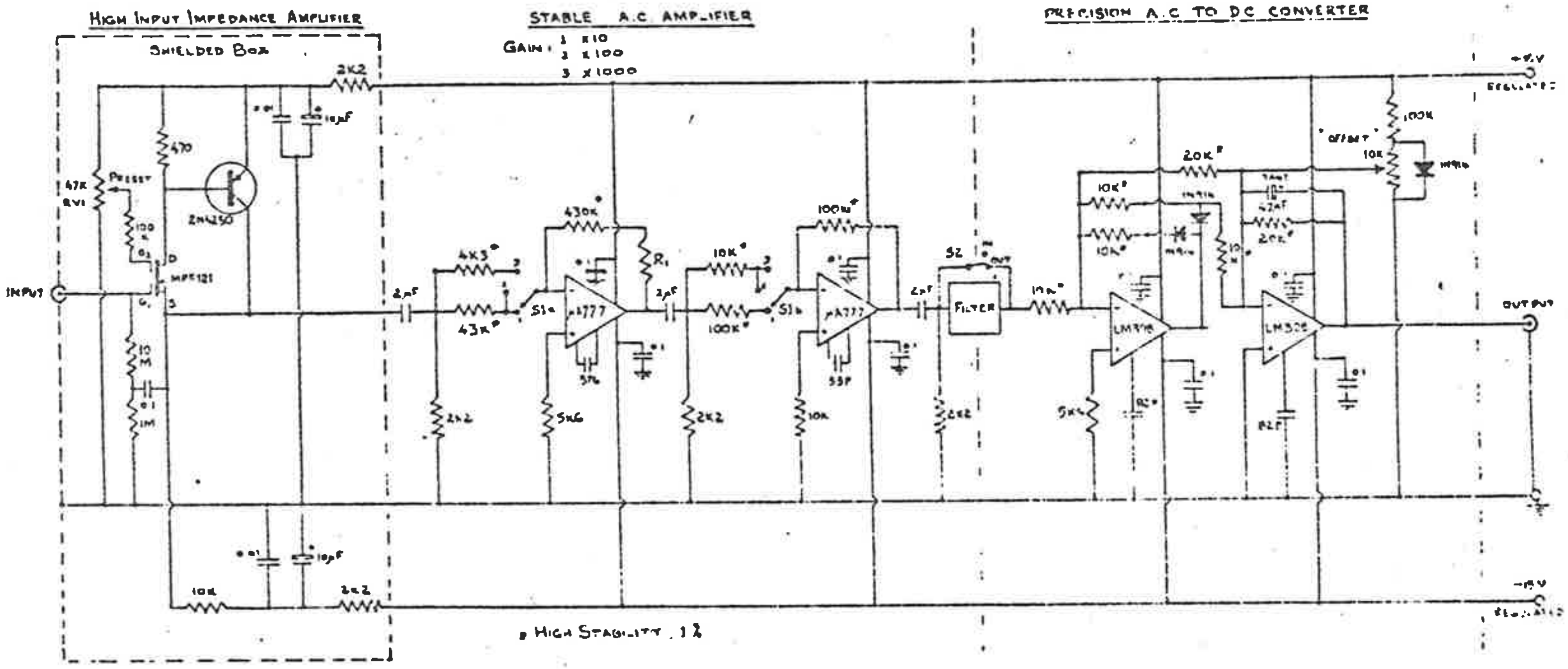

HIGH INPUT IMPEDANCE AMPLIFIER
SHIELDED BOX
STABLE A.C AMPLIFIER
GAIN: 1 x10
2 x100
3 x1000
PRECISION A.C TO DC CONVERTER
INPUT
OUTPUT
FILTER
* HIGH STABILITY 1%

Fig.2·4

removed by washing the substrate in a continuous flow of double distilled water and immediately dried under a stream of clean dry air. Finally the substrates were placed in a vacuum chamber and ion bombarded for about five minutes. All polished specimens of metals were cleaned by washing in isopropyl alcohol.

2.6 Film deposition technology

The thin films of stearic acid were deposited on quartz wedges by evaporation in a vacuum of the order of 10^{-6} Torr using an alumina crucible which was heated by a uniformly wound tungsten coil.

The thin films of Ge, and opaque Ni films, were deposited by using an electron beam evaporation source. A photograph of the vacuum system incorporating the electron beam evaporation source is shown in Figure (2.5). The vacuum system employed a diffusion pump with a speed of 400 litres/sec with a cryotrap to minimize backstreaming of oil vapour. The rate of evaporation was precisely controlled and monitored by a quartz crystal film thickness monitor and evaporation control unit. The distance between the source and the substrate was about 250 mm. The ultimate vacuum attainable by the vacuum system was 5×10^{-6} Torr and the pressure during the evaporation was approximately 10^{-5} Torr.

Thin films of Ta_2O_5 and opaque films of Ni, Mo and Au were prepared by D.R.C. Laboratories, Salisbury, South Australia, by the method of sputtering and the apparatus used was an MRC Type 8620 sputtering module.

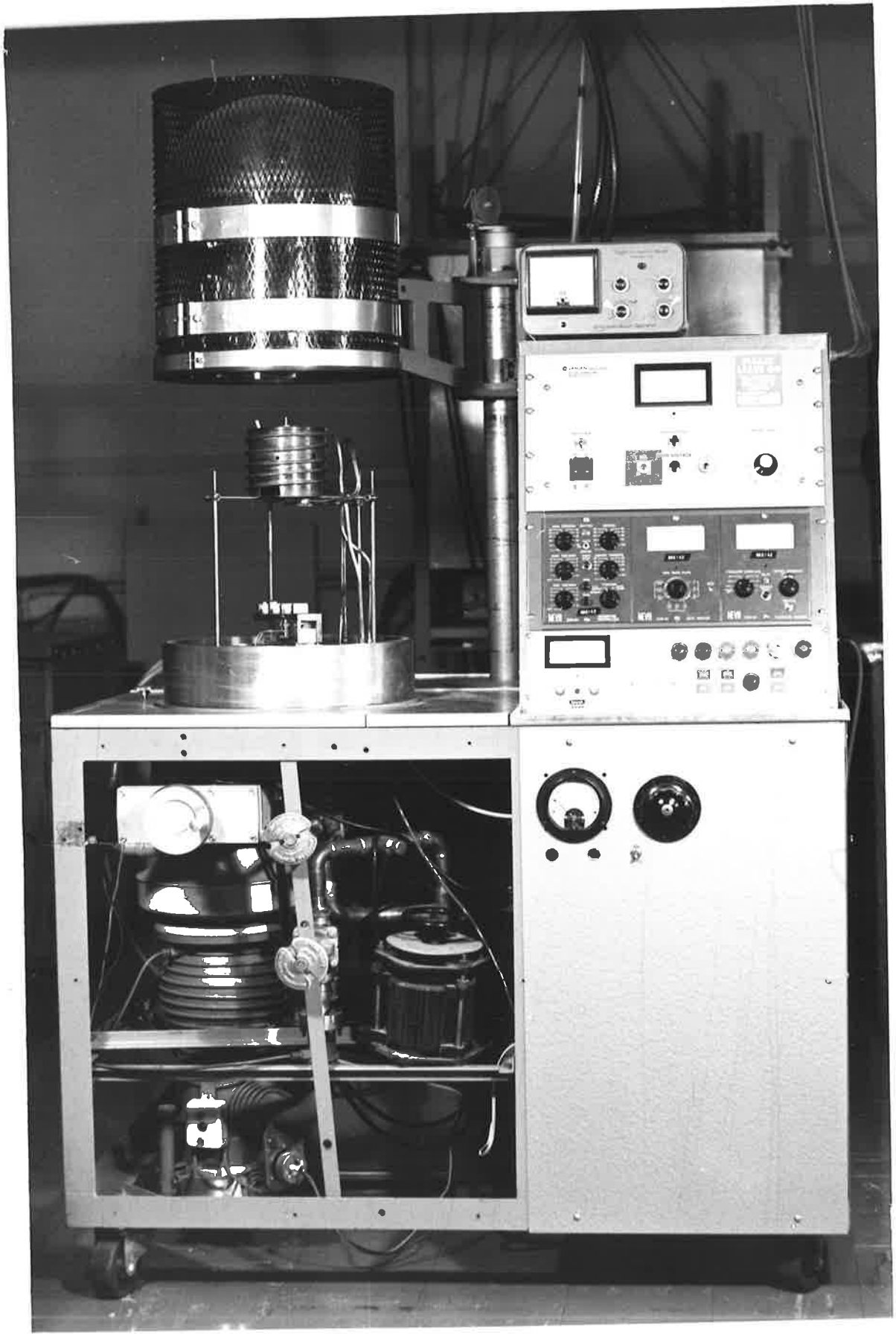

Fig.2·5

2.7 Substrate heating system

The substrate temperature which governs many properties of the deposited layer is very significant because, with increasing substrate temperature, a marked increase in crystallite size was noted. For deposition and annealing of Ge films ranging from amorphous to highly polycrystalline, it was essential to maintain the substrate temperatures in the range from room temperature to 700° C during the evaporation or annealing.

The substrate was suspended by a cradle, made of Mo wire, inside a furnace. The furnace consisted of a spiral heater made of Ta strip enclosed in a water cooled jacket to prevent thermal radiation heating the bell jar. To measure the substrate temperature a chromel-alumel thermocouple was attached to the substrate surface by a Mo clip. Before the deposition of the films the substrates were soaked at the required temperature for 2 hours in order to ensure a uniform temperature across the substrate.

2.8 Electron-microscopy and X-ray diffraction techniques

In the present investigation the crystalline nature of the films was determined by the standard X-ray powder diffraction technique.

Examination of the surface topography of all the films either thin or opaque was carried out by using a Siemens auto-scanning electron microscope, and with either a Philips EM 300 electron microscope or J.E.O.L. JEM100CX transmission electron microscope using a replica technique (Bradely 1965) as follows.

First the surface of the specimen was coated with a solution to form a plastic replica. This was then removed from the specimen

and the replica coated with an evaporated carbon film. The plastic was then dissolved away to leave a carbon replica which was shadowed with palladium.

CHAPTER 3

OPTICAL PROPERTIES OF AMORPHOUS AND CRYSTALLINE GERMANIUM

3.1 Introduction

The electronic and optical properties of amorphous and crystalline Ge films depend on the film structures which again depend on deposition parameters. Many recent experiments (Brust 1964, Ghosh 1966, Potter 1966, Clark 1967, Tauc 1969, Davis and Shaw 1970, Brodsky *et al* 1970, Spicer and Donovan 1970, Fischer 1971, Polk 1971, Theye 1971, Bauer and Galeener 1972, Spicer *et al* 1972, Connell and Paul 1972, Fischer and Donovan 1972, Blum and Feldman 1976, Halder *et al* 1977) have been concerned with the structure and temperature dependence of the optical and electronic properties of amorphous and crystalline Ge and on the amorphous to crystalline transition.

The band gap values of amorphous and crystalline Ge determined from the optical absorption data differ notoriously according to the method of preparation and subsequent treatment. There is still disagreement about the existence of distinct localized and extended electronic states in amorphous Ge. Thus while most writers (Clark 1967, Tauc 1969, Brodsky and Title 1969, Theye 1971) agree that the optical properties are affected by annealing, Fischer and Donovan (1972) oppose the idea of the existence of localized states in the band and Spicer and Donovan (1970) concluded from their photoemission experiments that "we find no evidence for either band 'tailing' or extremely large numbers of states in the forbidden region". Discussions of the optical absorption in amorphous Ge have been given by Mott and Davis (1971) and Tauc and Menthe (1972); although different assumptions were made, both

investigations led to the same expression for the optical absorption. This has been used as a basis for the latter analysis of experimental data.

Experiments done by Tomlin *et al* (1976) and in the present study of amorphous and crystalline Ge showed clearly the changes in optical properties due to annealing when the absorption data are analysed in terms of the Mott and Davis (1971) model. At higher substrate temperatures of 350 to 500°C, or on annealing at temperatures of 450 to 700°C Ge films become progressively more crystalline. The band gaps of polycrystalline films also change as the degree of crystallinity increases.

3.2 Experimental

Thin films of Ge were prepared in a vacuum of 10^{-5} Torr by evaporation from a conical tungsten basket on to carefully cleaned quartz substrates (Section 2.5) maintained at temperatures in the range from 20 to 500°C. Above the source a magnetically operated shutter was used to shield the substrate during outgassing of the Ge prior to deposition at the rate of 20 to 40 nm per minute. Films of thickness from 60 to 200 nm were used for analysis of the absorption data in the photon energy range of 0.62 to 2.2 eV. A pair of such films was made each time. After the completion of evaporation the specimens were allowed to cool to room temperature and then dry nitrogen was let into the system.

For studying the effects of annealing on optical properties, the annealing (from 300 to 700°C) was carried out in the vacuum system used for preparing the films (Section 2.6). After making the optical measurements on a pair of films deposited at room temperature, both of them were annealed simultaneously at successively higher temperatures

from 300 to 700°C, each time for three hours, and optical measurements were repeated at room temperature after each heat treatment. The same process was repeated for a number of pairs of films.

The structure of the films used in the present investigation was examined with a Siemen's auto-scanning electron microscope (SEM) and by standard X-ray diffraction techniques. For the later technique, the materials used were deposited on quartz substrates, scraped off and put into thin walled polythene capillary tubes. The surface topography of films was examined by electron microscopy using a carbon replica technique (Section 2.8).

It is not possible to examine the same film at each of the annealing temperatures by X-ray diffraction or transmission electron microscopy, because the film is destroyed during surface replication or scraping off for X-ray diffraction. The film is examined only after the completion of the whole annealing cycle. At least three or four thick films were needed to obtain sufficient materials to fill the desired length of thin walled polythene capillary tube for X-ray diffraction technique, because the quantity of material in each film was very small.

Direct examination of the film can only be made by the scanning electron microscope (SEM) which gives only the surface structure of the film within the limit of resolution 7.0 to 7.5 nm , depending upon the contrast.

3.3 Mathematical formulae used in determining the optical constants of Ge films

The optical constants of all Ge films either amorphous or polycrystalline were derived from the measured normal incidence reflectance (R) and transmittance (Tm) using the following single

layer formulae (Tomlin 1968), for a single absorbing layer on a transparent substrate :

$$\frac{1+R}{Tm} = \frac{1}{(n_0+n_2)^2\,(n_1^2+k_1^2)}\,[\,(n_0^2+n_1^2+k_1^2)\,\{\,(n_1^2+n_2^2+k_1^2)\,x$$

$$\cosh 2\alpha_1 + 2n_1n_2\sinh 2\alpha_1\} + (n_0^2-n_1^2-k_1^2)\,x$$

$$\{\,(n_1^2-n_2^2+k_1^2)\cos 2\gamma_1 - 2n_2\,k_1\sin 2\gamma_1\,\}\,] \qquad 3.3.1$$

$$\frac{1-R}{Tm} = \frac{2n_0}{(n_0+n_2)^2\,(n_1^2+k_1^2)}\,[\,n_1\,\{(n_1^2+n_2^2+k_1^2)\sinh 2\alpha_1$$

$$+ 2n_1n_2\cosh 2\alpha_1\} + k_1\,\{(n_1^2-n_2^2+k_1^2)\sin 2\gamma_1$$

$$+ 2n_2\,k_1\cos 2\gamma_1\,\}\,] \qquad 3.3.2$$

where $(n_1 - ik_1)$ is the complex refractive index of the film of thickness d_1 deposited on a transparent substrate of refractive index n_2. λ is the wavelength, n_0 is the refractive index of air, $\alpha_1 = \frac{2\pi\,k_1\,d_1}{\lambda_1}$ and $\gamma_1 = \frac{2\pi\,n_1\,d_1}{\lambda_1}$.

The procedures applied in solving the above equations for n and k were basically the same as those used by Denton *et al* (1972). An approximate idea of the value of film thickness is essential at the beginning, but this could be easily derived from either a transmittance or reflectance curve (Figure 3.1) using the relation $d = \frac{\lambda_1\,\lambda_2}{4n_1(\lambda_1-\lambda_2)}$

where λ_1 and λ_2 are the wavelengths at the consecutive turning points in the non-absorbing region and n_1 is the long wavelength refractive index. This calculated (approximate) value of the film thickness was then adjusted until a closed and continuous dispersion curve (Figures 3.2 and 3.3) could be obtained. In these and subsequent figures the error bars shown are those for extreme systematic errors and are discussed in the Addendum, page 113A.

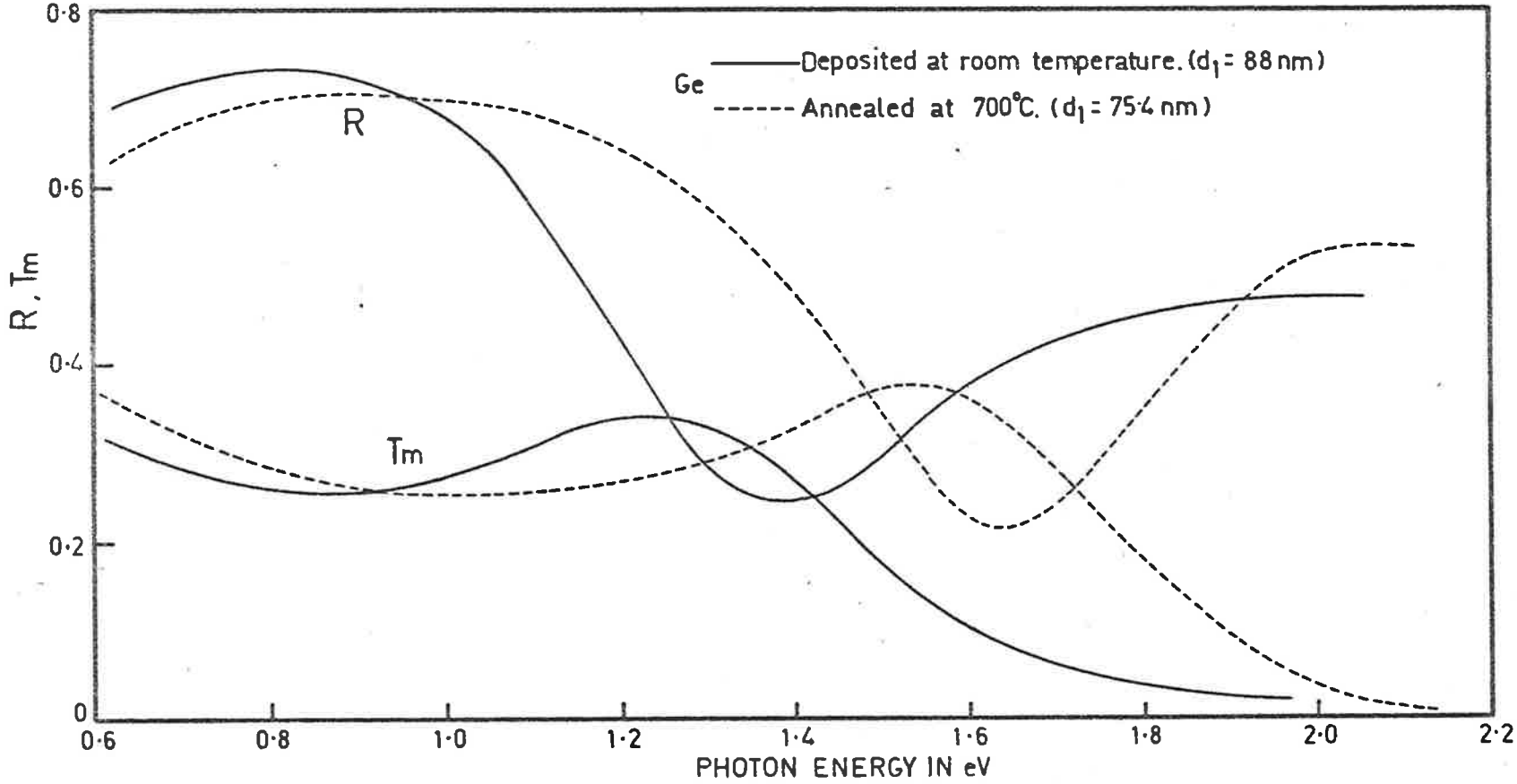
Ge
Deposited at room temperature. (d_1 = 88 nm)
Annealed at 700°C. (d_1 = 75·4 nm)
R
Tm
R, Tm
0·8
0·6
0·4
0·2
0
0·6
0·8
1·0
1·2
1·4
1·6
1·8
2·0
2·2
PHOTON ENERGY IN eV

Fig. 3.1

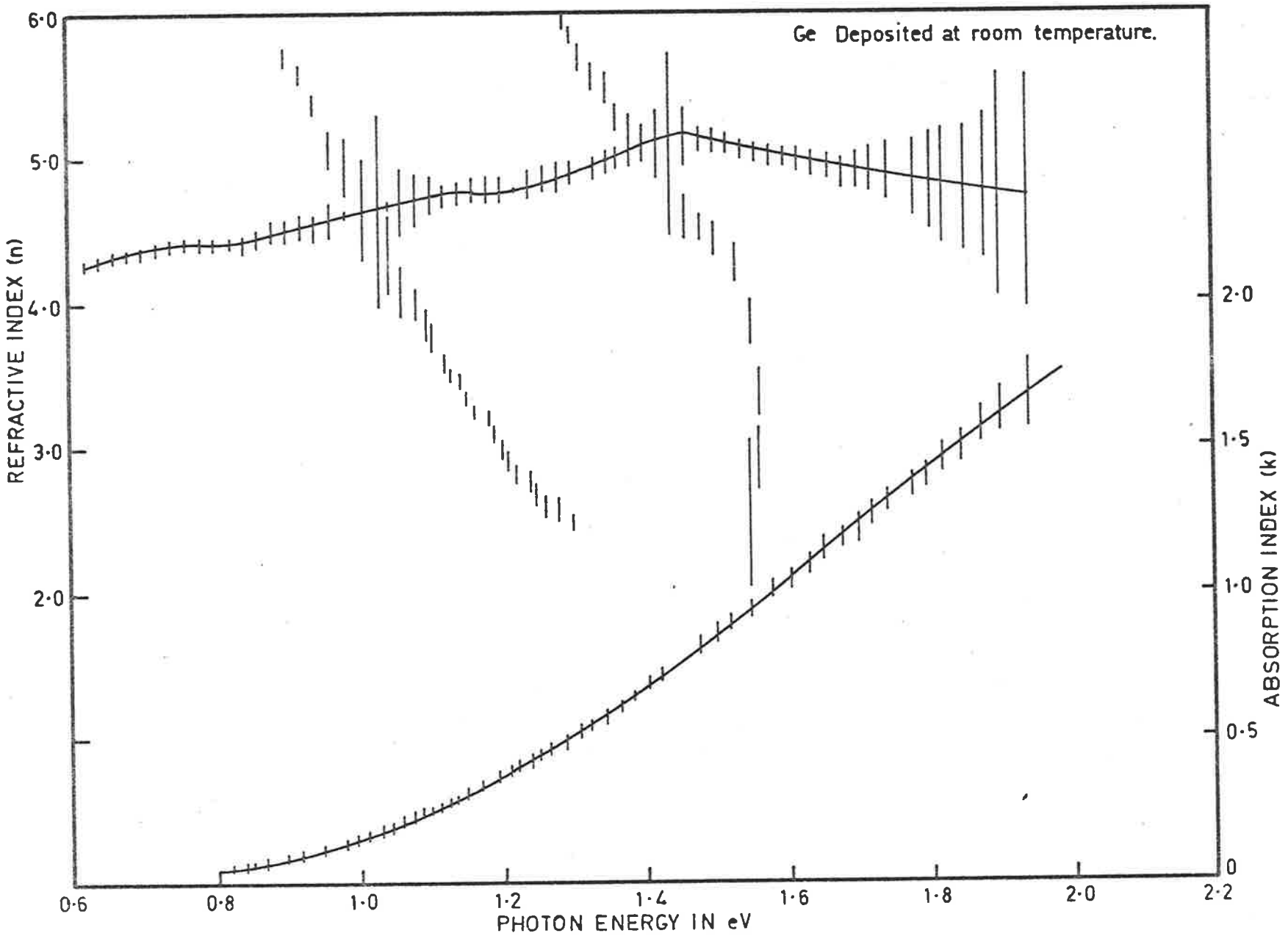
Ge Deposited at room temperature.
REFRACTIVE INDEX (n)
ABSORPTION INDEX (k)
PHOTON ENERGY IN eV
6·0
5·0
4·0
3·0
2·0
2·0
1·5
1·0
0·5
0
0·6
0·8
1·0
1·2
1·4
1·6
1·8
2·0
2·2

Fig. 3.2

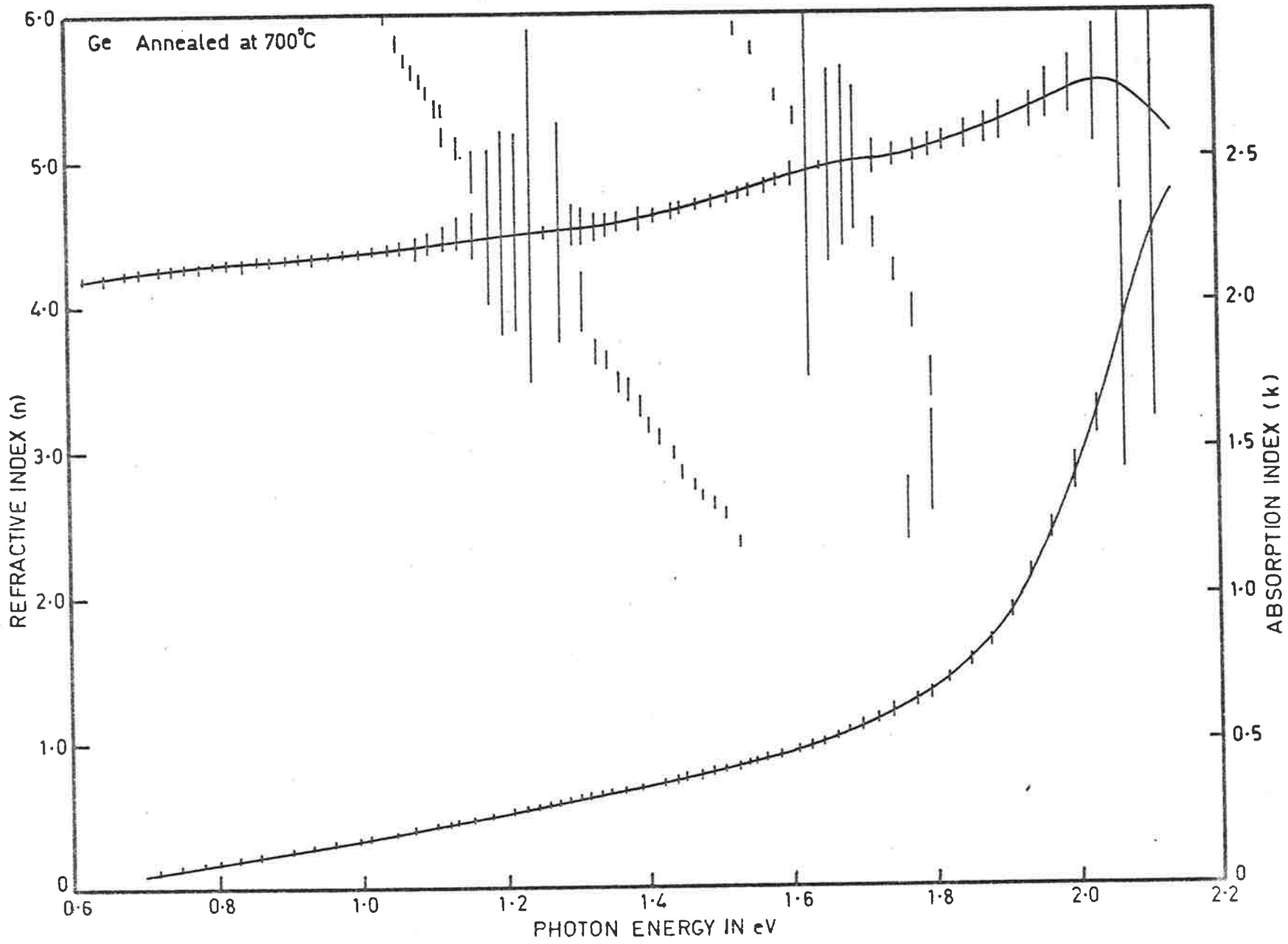
Ge Annealed at 700°C
REFRACTIVE INDEX (n)
ABSORPTION INDEX (k)
PHOTON ENERGY IN eV
6·0
5·0
4·0
3·0
2·0
1·0
0
2·5
2·0
1·5
1·0
0·5
0
0·6
0·8
1·0
1·2
1·4
1·6
1·8
2·0
2·2

Fig.3.3

Earlier studies (Khawaja 1975a) at room temperature indicated that a surface layer of the order of 0.5 to 1.0 nm formed on the surface of Ge exposed to the atmosphere. In the range of our measurement 0.62 to 2.2 eV such layers if formed would reduce the measured reflectivity by about 0.001 which is less than the accuracy of our reflectance and transmittance measurements. So the presence of such an oxide layer may be ignored. This was verified by computations for a double layer i.e. a single absorbing layer and an oxide layer. Proper closure of dispersion curves using the single layer formulae was achieved which supports this conclusion, for this would not have been possible if the postulated oxide layer had an appreciable effect on reflectances or transmittances.

3.4 Density and thickness of Ge films

The densities of Ge films were determined from masses measured with a Mettler M microbalance, and thicknesses obtained from the optical measurements. It was observed that the density of the Ge film deposited at room temperature was uniformly 10 to 15% less than that of the crystalline value. For films deposited above 450°C or annealed above 550°C, the density was within 4 to 7% of the bulk crystalline value. Thicknesses obtained from the optical measurements after each annealing were plotted against annealing temperature (Figure 3.10). It is observed that the thickness does not change much when annealed up to 200°C but after that, the thickness of the annealed film decreases approximately by 25Å, i.e. a decrease of 3%, after each annealing up to 700°C and altogether a 12% decrease in thickness was observed during the transition from the amorphous to the

fully crystalline state. Density measurements showed corresponding increases in density of about 10 to 15% indicating that the change in thickness was not due to loss of material but to structural changes. In our laboratory Thutupalli (1976) measured the density of Si films using a Mettler M microbalance. He observed a 20 to 25% increase in density during the amorphous to crystalline transition.

3.5 Surface microstructure of Ge films

Ge films deposited at room temperature and annealed up to 400°C are amorphous and have smooth surfaces. This was revealed by the study of electron diffraction patterns and electron transmission micrographs (Denton 1972, Khawaja 1975a, Tomlin *et al* 1976). From Figures 3.4 and 3.5A it is clear that the optical constants of pure amorphous films (curves 1 and 2 of Figures 3.4 and 3.5A) are different from those of mixed amorphous and crystalline composition (curves 3 and 4 of Figure 3.4 and curve 3 of Figure 3.5A), and from fully crystalline films (curve 5 of Figure 3.4). When the curves of optical constants shown in Figures (3.4 and (3.5A) are compared with those of Figure (3.5B) for single crystal Ge (Potter 1966) it is observed that films annealed at 500 to 700°C, or deposited at 300 to 500°C, show a close resemblance to the curves (a) and (b) in Figure (3.5B).

Ge films deposited at 300 to 400°C and annealed at 300 to 700°C did not show any structure when examined with the scanning electron microscope which means that if there were any roughness it was less than 7.0 nm which is the resolving power of the instrument under ideal conditions.

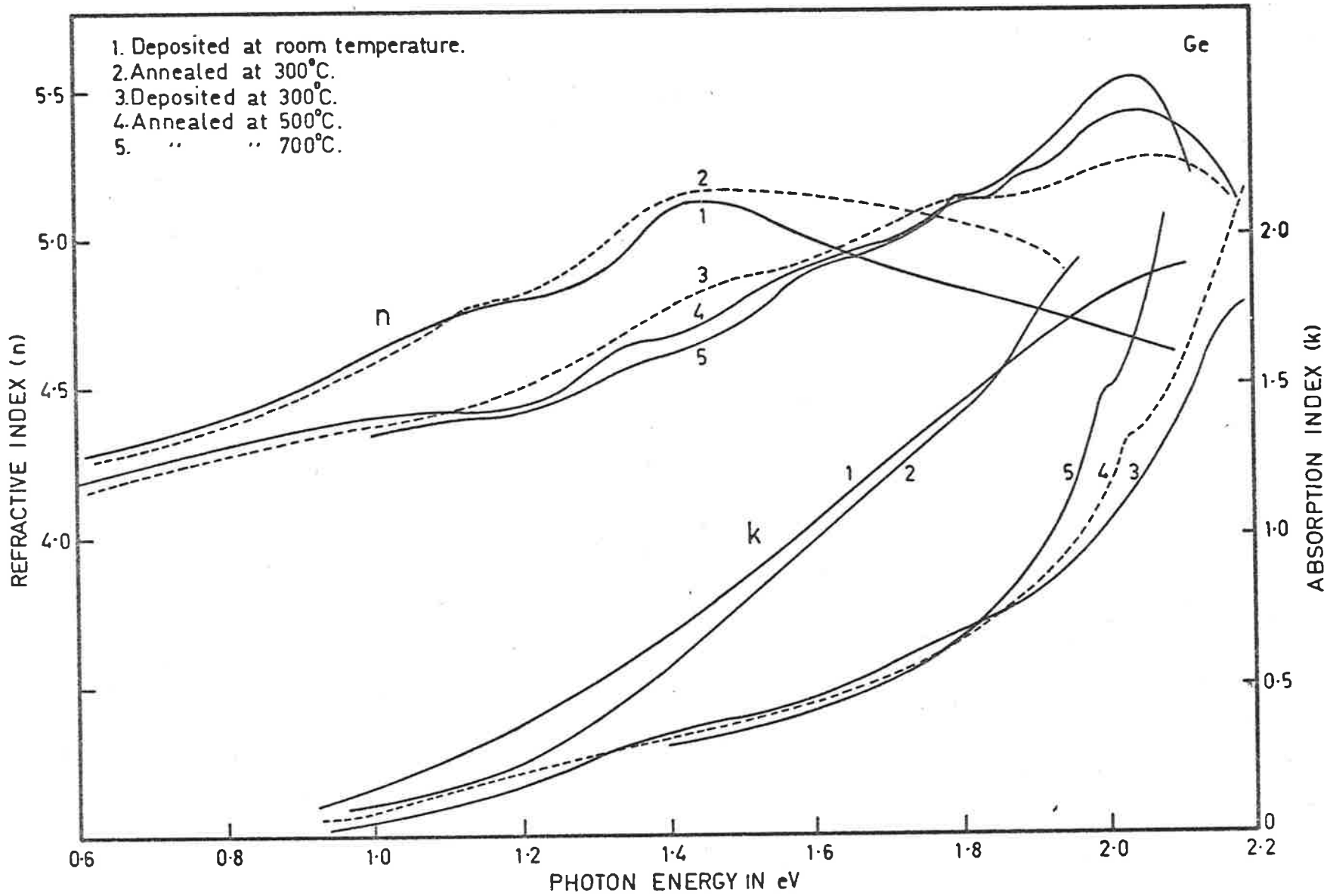
1. Deposited at room temperature.
2. Annealed at 300°C.
3. Deposited at 300°C.
4. Annealed at 500°C.
5. " " 700°C.
Ge
n
k
REFRACTIVE INDEX (n)
ABSORPTION INDEX (k)
PHOTON ENERGY IN eV
5·5
5·0
4·5
4·0
2·0
1·5
1·0
0·5
0
0·6
0·8
1·0
1·2
1·4
1·6
1·8
2·0
2·2

Fig.3.4

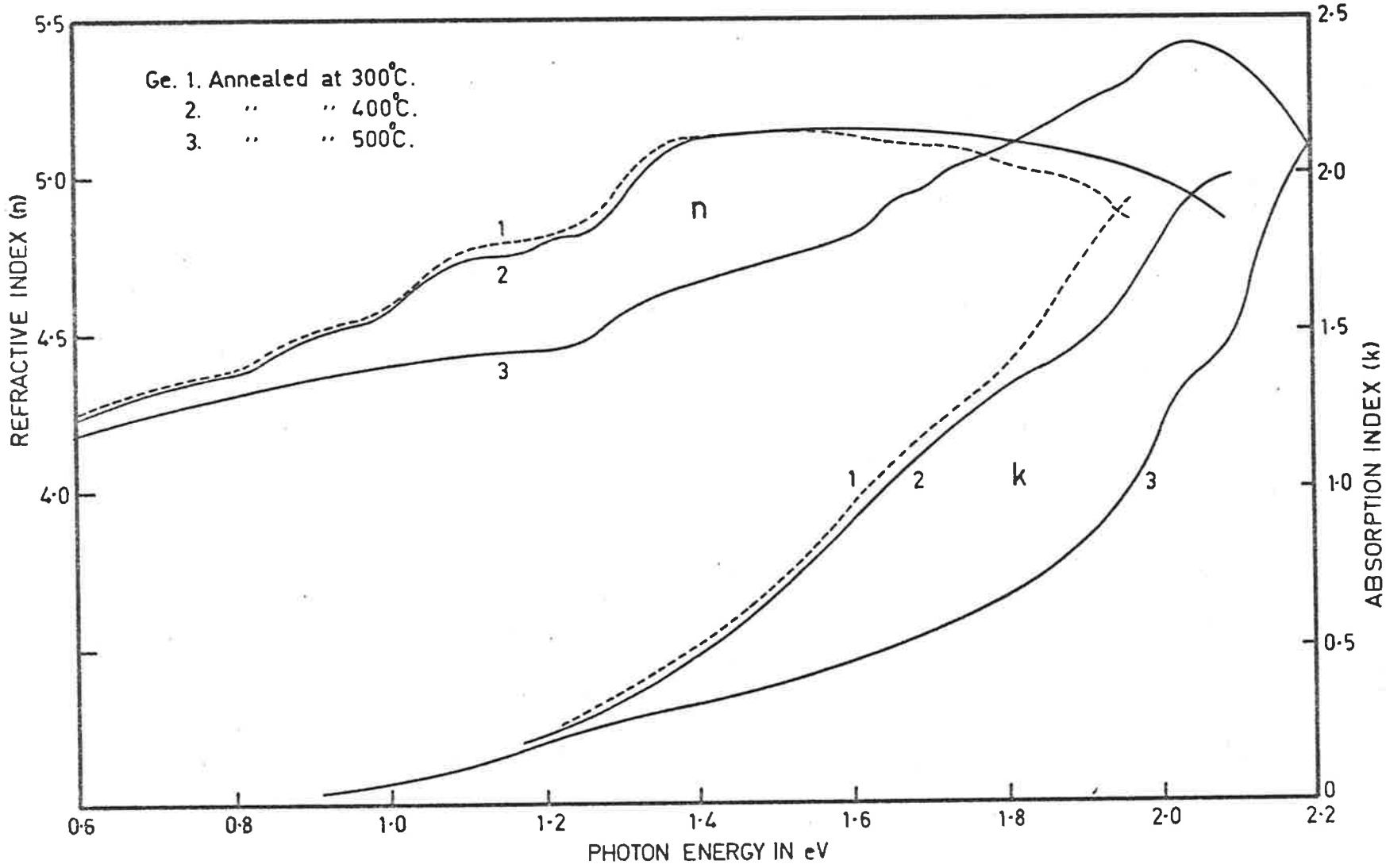
Ge. 1. Annealed at 300°C.
2. " " 400°C.
3. " " 500°C.
n
k
1
2
3
REFRACTIVE INDEX (n)
ABSORPTION INDEX (k)
PHOTON ENERGY IN eV
5·5
5·0
4·5
4·0
2·5
2·0
1·5
1·0
0·5
0
0·6
0·8
1·0
1·2
1·4
1·6
1·8
2·0
2·2

Fig. 3.5A

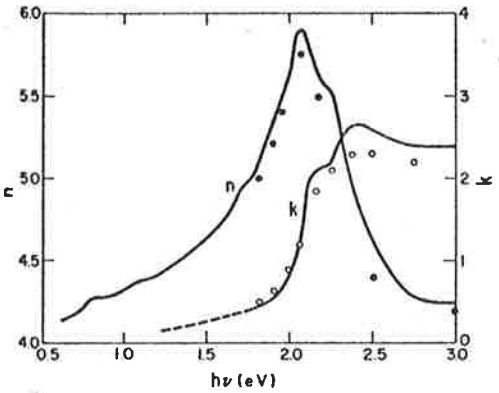

(a) The refractive index constants for Ge at 300°K.

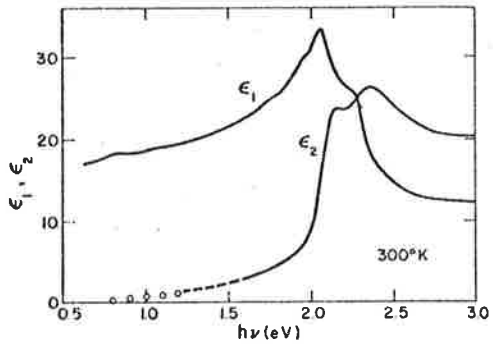

(b) The optical dielectric constants for electro-polished germanium at 300°K.

from Potter (1966)

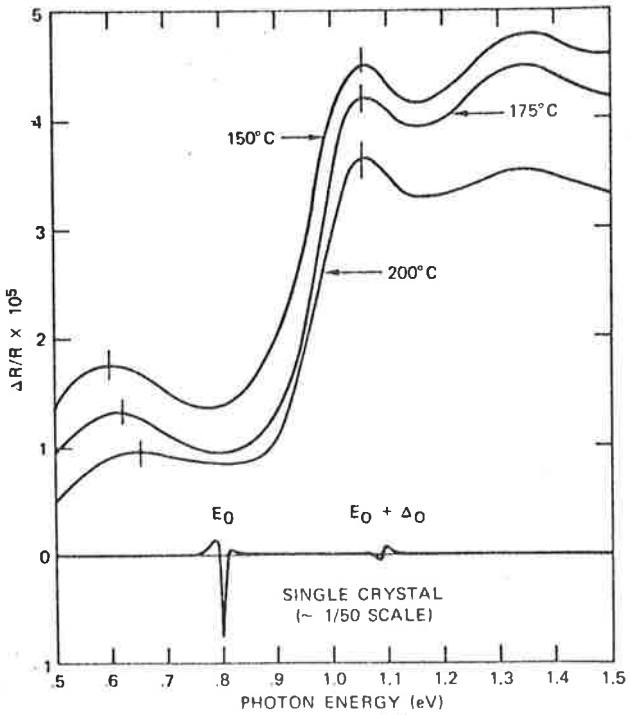

(c) ER spectra of the original samples grown at 150, 175, and 200°C; all are nominally 2400Å thick. A typical crystalline Ge spectrum is shown for comparison.

from Fischer (1971)

Fig. 3·5B

When examined with the transmission electron microscope using the carbon replica technique it was found that Ge films deposited at 300°C, or annealed at 700°C had crystalline particles of dimension 1.5 to 2.0 nm (Figure 3.a) and 4.0 to 4.5 nm (Figure 3.d) respectively.* An electron micrograph of a Ge film annealed at 700°C obtained with the scanning electron microscope is shown in Figure (3.c) The practical limits of resolution of the J.E.O.L. JEM100CX and Philips EM300 transmission electron microscopes are 0.4 and 0.5 nm respectively.

Films deposited at 500°C when examined with the scanning electron microscope showed surface roughness of 7.0 to 7.5 nm (Figure 3.b) and X-ray diffraction analysis showed that they are crystalline. Film deposited at 600°C showed a colour different from the other films of Ge . This might have been due to contamination and for this reason no optical measurements were made with this film and no further films were made at deposition temperature above 500°C.

From the above discussion it is seen that Ge films deposited at room temperature and annealed up to 400°C were amorphous, and those deposited at 500°C were highly crystalline.

Deposition at temperatures below 500°C or annealing at temperatures above 400°C produced partially crystalline films. The absorption of such a film may be expected to be a linear combination of the absorption of the amorphous and crystalline components and be given by

$$K(E) = \frac{x\,Ka(E) + y\,Kc(E)}{x + y} \qquad 3.5.1$$

* These figures were obtained by counting the number of particles in several areas of the micrographs (Jarrett and Ward 1976)

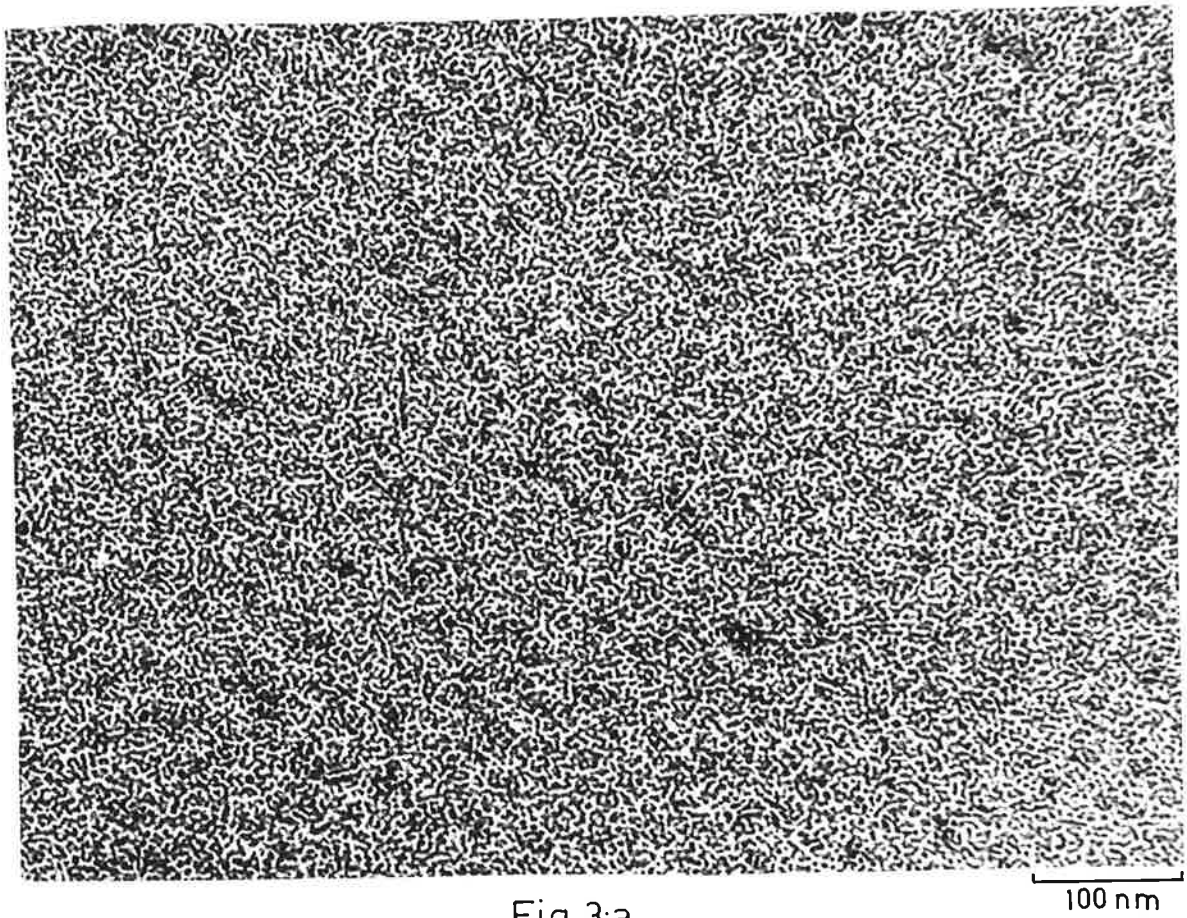

Fig.3·a

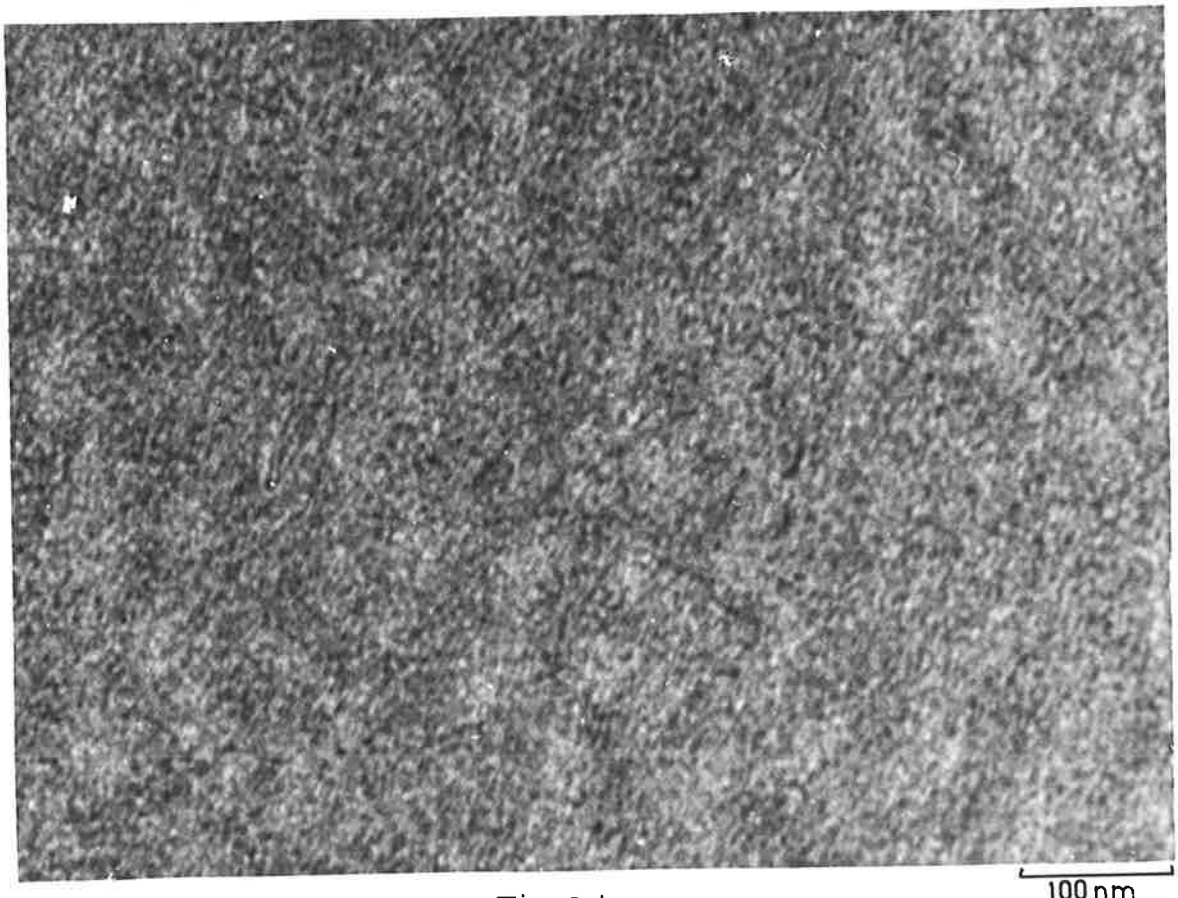

Fig.3·b

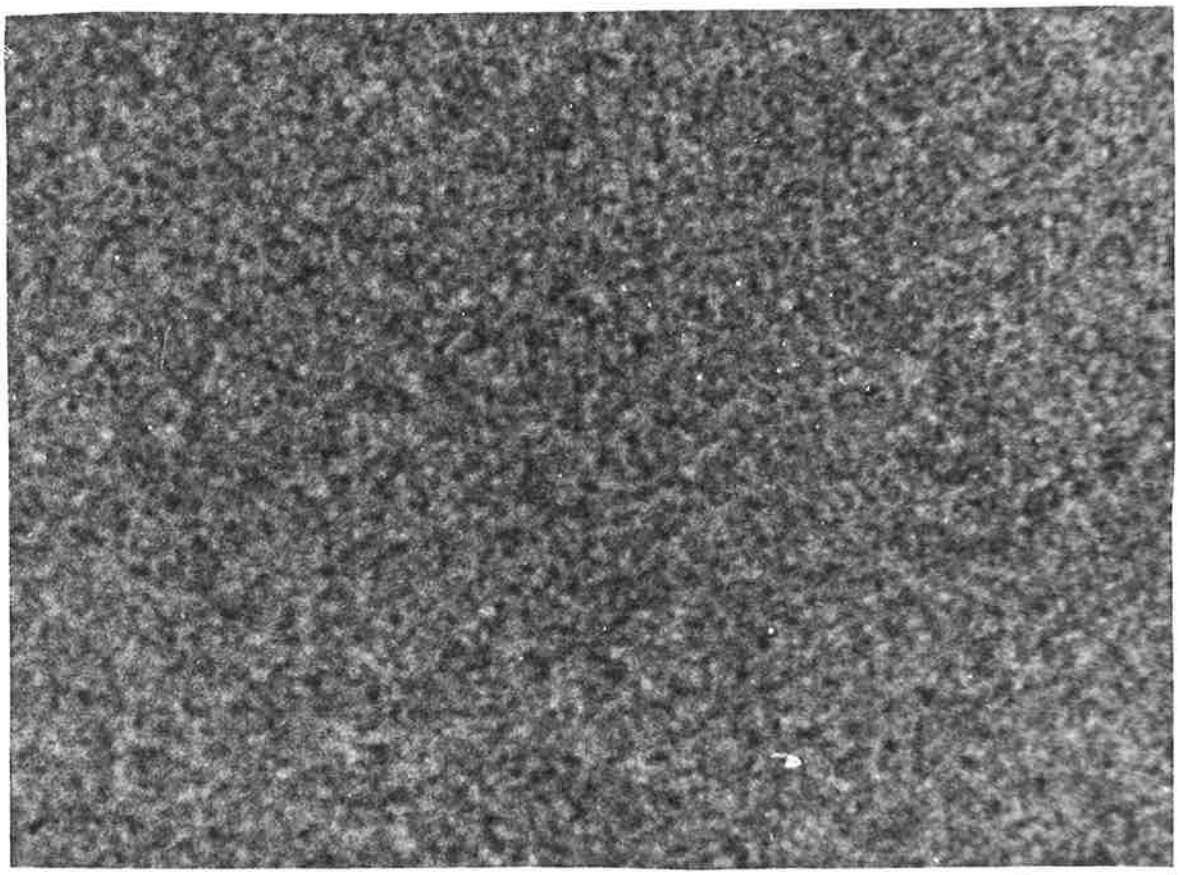

Fig. 3·c

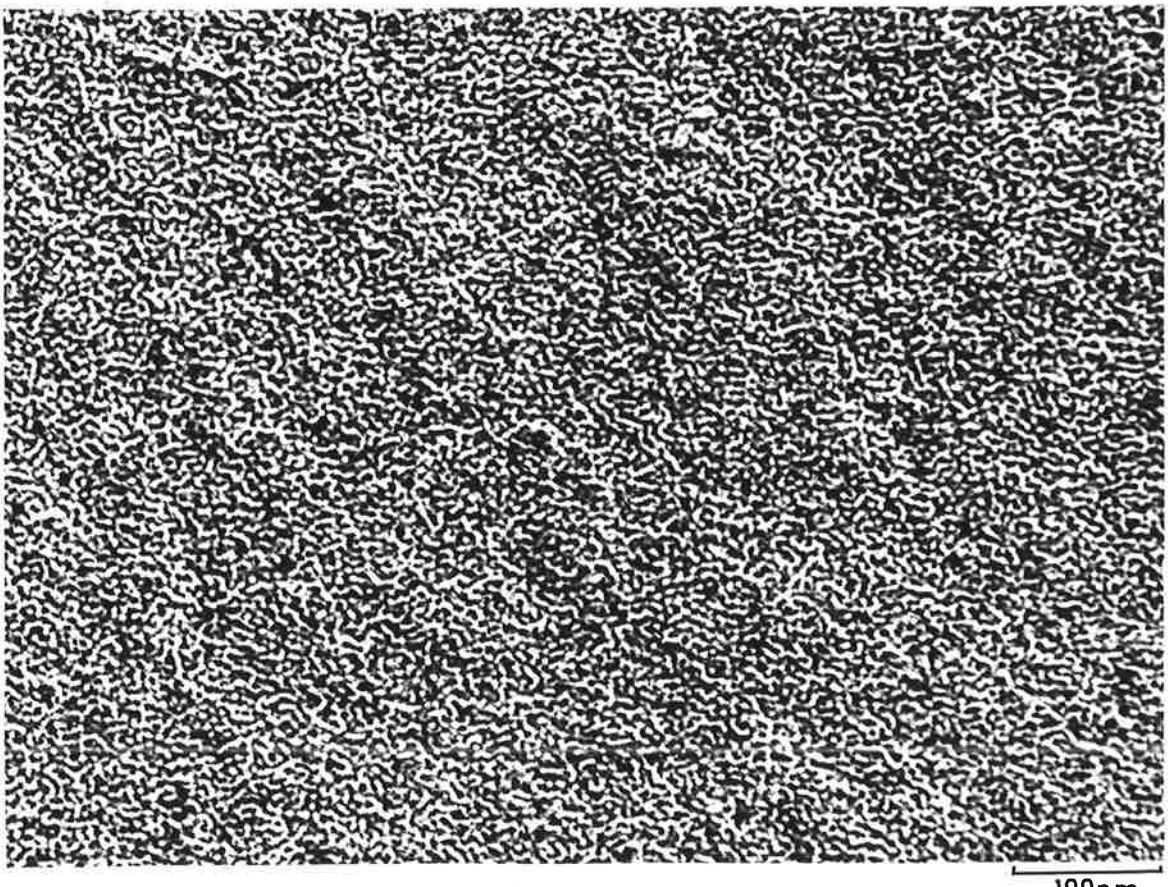

Fig. 3·d

where K(E), Ka(E) and Kc(E) are the absorption coefficients of partially crystalline, amorphous and crystalline Ge films respectively at any particular energy E, and x and y are the proportions of the amorphous and crystalline material in the film. From experimentally determined values of K(E), Ka(E) and Kc(E), the proportions x and y may be found by using a Least Squares curve fitting procedure (Table 3.1). The cross marks shown in the continuous absorption index curve of Figure (3.7) are the theoretical points calculated with the optimum values of x and y for a Ge film deposited at 400°C.

TABLE 3.1

Deposition temperature	Amorphous phase x%	Crystalline phase y%
300°C	88	12
400°C	40	60
Annealed at 500°C	50	50

The results presented in Table 3.1 show that Ge films annealed at 500°C or deposited at 300 to 400°C were partially crystalline. Those annealed at 600 and 700°C were fully crystalline. Blum and Feldman (1976) in their study of crystallization of amorphous Ge films observed that the absorption coefficients for the amorphous phase were about double those of the crystalline phase. They measured the optical transmission near 0.65 μm where the absorption constant is most

sensitive to phase tranformation. From the writer's data the ratio was found to be 1.83 to 2.35 for films deposited at 500°C, 1.75 to 2.27 and 1.79 to 2.28 for films annealed at 600°C and 700°C respectively, the absorption measurements being made in the range 0.63 to 1.0 μm.

For crystalline materials the following well known relations hold for direct and indirect transitions respectively,

$$(EnK)^{\frac{1}{2}} = C_1 (E - Eg_d) \qquad 3.5.2$$

$$(EnK)^{2} = C_2 (E - Eg_i) \qquad 3.5.3$$

where Eg_d and Eg_i are the direct and indirect energy gap values, n is the refractive index, $K = \frac{4\pi k}{\lambda}$ is the absorption coefficient, C_1 and C_2 are constants, and phonon energy is neglected for indirect transitions. These equations may be used to determine the band gaps (Spicer *et al* 1972, Denton and Tomlin 1972, Khawaja and Tomlin 1975, Thutupalli and Tomlin 1976). In the case of amorphous films or mixed amorphous and crystalline films, there is no strong theoretical justification for using such formulae but experimentally they are found to apply, and the characteristic energies Eg which may, or may not, be true energy gaps, can be found.

In this way energy gaps of Ge films annealed at 600°C, or deposited at 500°C, were found to be 0.69 and 0.65 eV respectively (Tables 3.3 and 3.4 of Sections 3.7 and 3.8 respectively). The values of these energy gaps are very close to that of crystalline Ge , 0.67 eV (Kittel 1976). The fundamental energy gap of crystalline Ge films formed by annealing at 700°C was found to be 0.57 eV.

Theye (1971) also showed that partially crystalline films would give values of refractive index intermediate between those of the

limiting amorphous and fully crystalline states depending on the proportions of amorphous and crystalline phases. From Figures 3.4, 3.5A, 3.6 and 3.7, it is observed that the refractive index of all partially polycrystalline films lies between the refractive index curve for amorphous films annealed at the temperature of 400°C and that of the crystalline Ge films. Moreover from the energy gap data (Tables 3.3 and 3.4 of Sections 3.7 and 3.8 respectively) it will be observed that the values of the first energy gap E_{g1} of all partially crystalline Ge films lay between the first energy gap of fully crystalline Ge and of amorphous Ge films annealed at 400°C.

From the above discussion a classification of the nature of Ge films in accordance with the deposition and annealing temperatures and surface microstructures may be presented as follows:

TABLE 3.2

Type of film	Temperature of substrate	Surface microstructure of the film	Nature of film
1	Deposited at room temperature to 200°C or Annealed up to 400°C	<1.0 nm	Amorphous
2	Deposited at 300°C	1.5 to 2.0 nm	Mostly Amorphous
	Deposited at 400°C or Annealed at 500°C	5.0 to 5.5 nm 2.5 to 3.0 nm	Partially Crystalline
3	Deposited at 500°C or Annealed at 600 to 700°C	7.0 to 7.5 nm 3.5 to 4.5 nm	Fully Crystalline

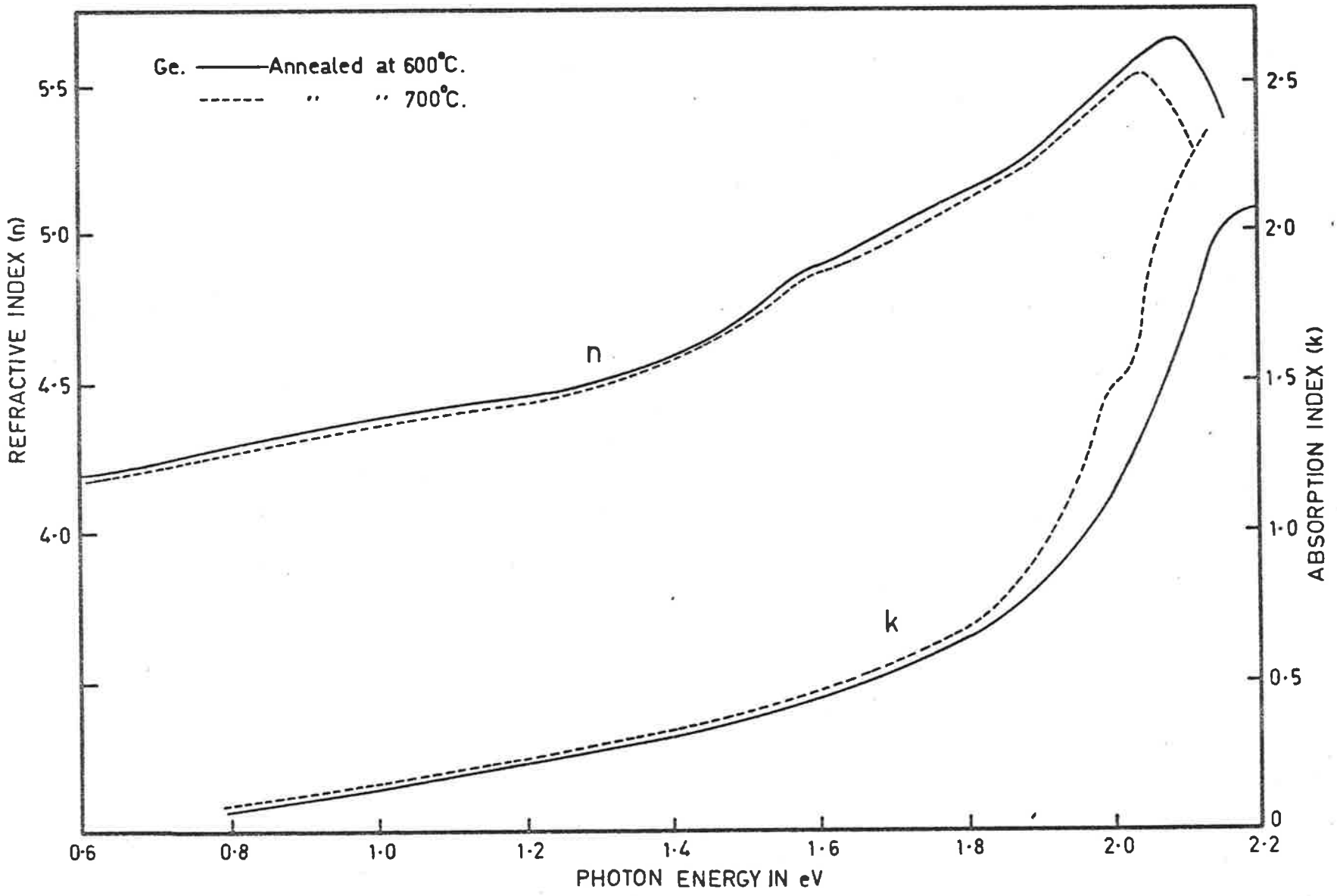
Ge. ——Annealed at 600°C.
------ " " 700°C.
n
k
REFRACTIVE INDEX (n)
ABSORPTION INDEX (k)
PHOTON ENERGY IN eV
5·5
5·0
4·5
4·0
2·5
2·0
1·5
1·0
0·5
0
0·6
0·8
1·0
1·2
1·4
1·6
1·8
2·0
2·2

Fig. 3.6

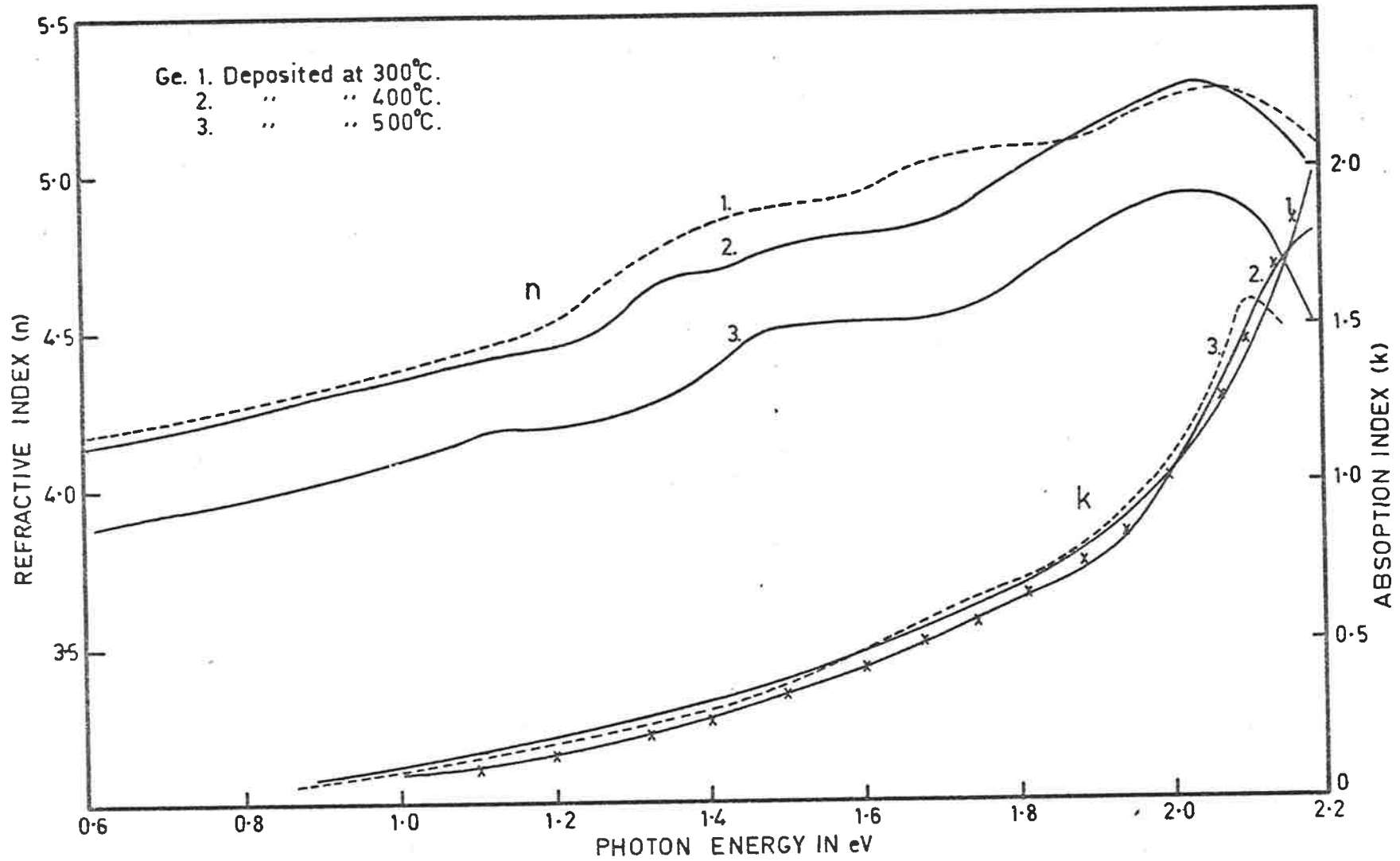
Ge. 1. Deposited at 300°C.
2. " " 400°C.
3. " " 500°C.
n
k
1.
2.
3.
REFRACTIVE INDEX (n)
ABSOPTION INDEX (k)
PHOTON ENERGY IN eV
5·5
5·0
4·5
4·0
3·5
2·0
1·5
1·0
0·5
0
0·6
0·8
1·0
1·2
1·4
1·6
1·8
2·0
2·2

Fig.3.7

These findings agree with those of Tauc (1969) who found some layers when annealed at 250°C remained amorphous, but had different optical properties, and that annealing at 450°C converted the layers into the polycrystalline state whose optical properties were essentially those of the crystal. The present results also agree with Piller *et al* (1969) who observed the transition of Ge films from polycrystalline to amorphous in the range 100 to 500°C. They reported that no crystal symmetry could be detected below 225 to 250°C but was well defined above 300°C substrate temperature. Our results are also similar to those of Spicer and Donovan (1970) who observed structural details of Ge films associated with the amorphous to crystalline transformation by photoemission technique. Recently Bauer and Galeener (1972) suggested that changes with increasing substrate temperature were due to gradual elimination of highly anisotropic voids for $Ts \leq 160°C$, and to gradual film crystallization for $Ts \geq 200°C$ where Ts is the substrate temperature. The present observations on film structure show that Ge films start to crystallize for $300°C > Ts > 200°C$ which agrees quite well with Fischer (1971), (Figure 3. 5B) who observed the electro-reflectance spectra of Ge films prepared with Ts = 150, 175 and 200°C were those of amorphous material. All the structural observations interpreted by Rudee (1972) showed that amorphous Ge and Si consist of particles of about 15Å in diameter which is close to our measurements of surface roughness of less than 1.0 nm for amorphous Ge films.

Theye (1971) studied the influence of annealing on the optical, electrical and structural properties of thin amorphous Ge films. She found that they remained amorphous until $T_A \simeq 400°C$

and after annealing at 500°C for 15 minutes, the films were entirely recrystalized. This agrees with the present work except that we find annealing at 600°C necessary to produce a completely polycrystalline film. According to Tauc (1969) one model of amorphous Ge pictures is composed of small particles with linear dimensions of the order of 10Å and another model is considered as homogeneous. Recently Halder *et al* (1977) reported that a study of X-ray photoelectron spectra of Ge films deposited at room temperature and a pressure of 10^{-6} Torr showed them to be a mixture of amorphous and polycrystalline materials. They concluded that Ge films prepared in this way are thermodynamically metastable during preparation but that a small amount of phase transition could give some polycrystallinity which at times is hard to detect. Their statement is not very definite and does not refute the general conclusions that Ge films made at room temperature may be regarded as completely amorphous. In general it may be concluded that the present observations on the structure of Ge films are in good agreement with other reports.

3.6 Optical constants of Ge films in the region 0.62 to 2.2 eV

The results of determinations of n and k, the refractive and absorption indices are shown in Figures 3.2 to 3.5A, 3.6 and 3.7 for films ranging from the amorphous through the partially crystalline to the almost completely crystallized state.

Each curve represents the averaged results for a number of specimens of each particular kind of film and covers an energy range of about 0.62 to 2.2 eV. The upper limit to the measurements by the reflectance-transmittance method is determined by absorption in the specimen but the range is quite adequate for discussing the absorption and deriving the values of energy gaps, which is the immediate object.

Measurements on amorphous and crystalline Ge to higher energies have been made by other methods such as Tomlin's method (1968), K-K dispersion relations (see Chapter 4).

The values of refractive and absorption indices are independent of thickness. The observed variations in optical constants from film to film at any particular substrate temperature and photon energy are within 1.0 to 1.5% of the individual values.

Like polycrystalline films of II-IV compounds, polycrystalline films of Ge have rough surfaces with a surface roughness dimension of the order of 3.5 to 7.5 nm. Since the dimension of the roughness is less than 10.0 nm proper closure of dispersion curves can be achieved using the single layer formulae of Section 3.3, especially as the measurements are limited to the relatively long wavelength region from 0.62 to 2.2 eV. Small errors due to roughness lie well within the average error of the optical constants. For Si films Thutupalli (1976) considered a double layer when the order of roughness was 15 to 25 nm.

Curve (3) of Figure (3.8A) shows the plot of $\varepsilon_2 = 2nk$ against energy for a Ge film deposited at 500°C. There is a sharp peak at 2.12 eV and an indication of another peak at about 2.2 eV in agreement with the ε_2 curve for single crystal Ge (Tomlin *et al* 1976, Figure 3.8B) which shows two well-resolved peaks at 2.1 and 2.3 eV. The ε_2 curve for Ge films prepared and measured at room temperature and after annealing at 300°C, Curve (1) of Figure (3.8A) shows only a flat maximum, characteristic of amorphous films. The ε_2 curves for Ge films annealed at 600° and 700°C, Figure (3.9) do not suggest the occurrence of the 2.1, 2.3 eV doublet of the single crystal Ge but only the single peak of polycrystalline

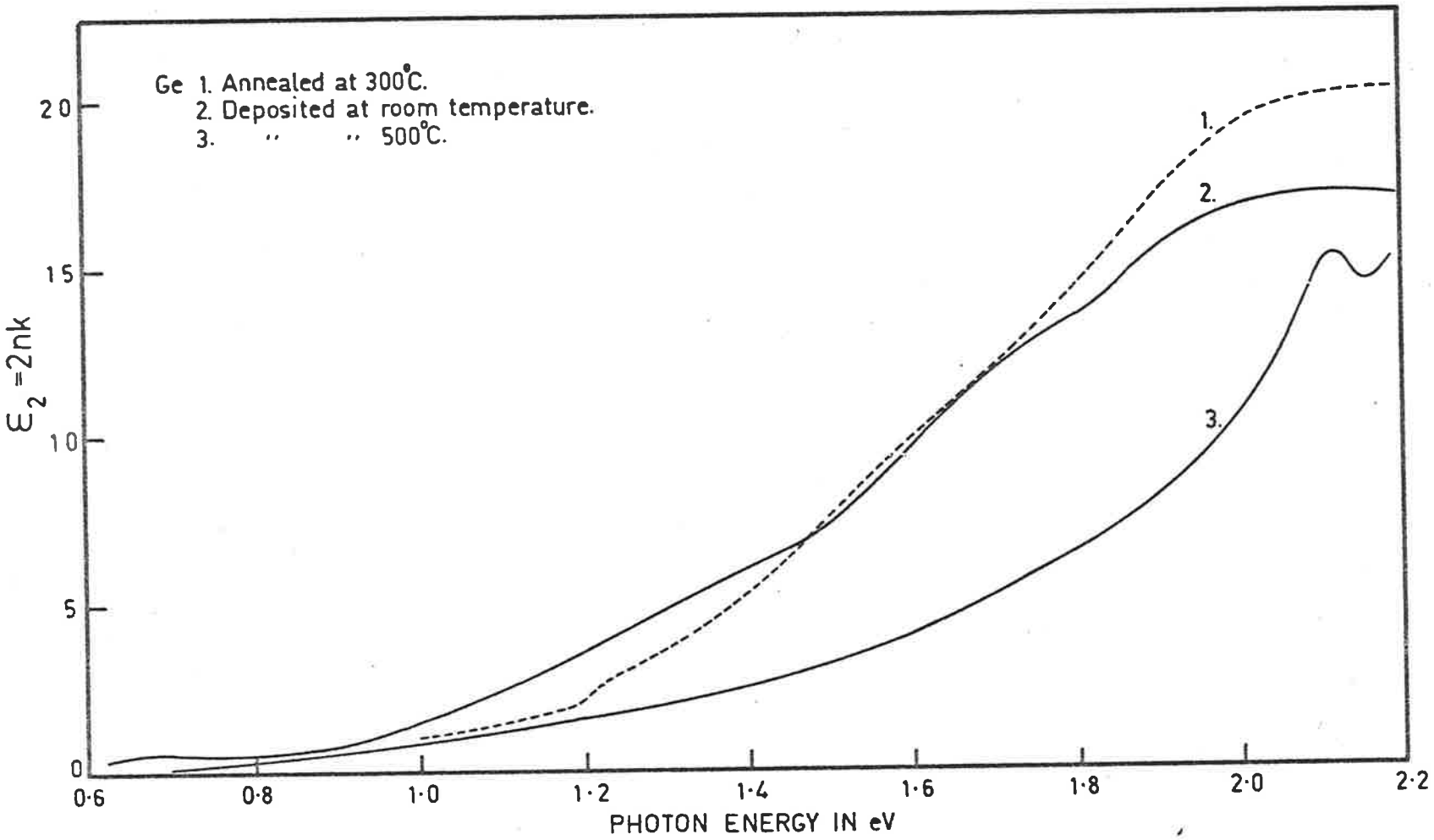
Ge 1. Annealed at 300°C.
2. Deposited at room temperature.
3. " " 500°C.
1.
2.
3.
$\varepsilon_2 = 2nk$
20
15
10
5
0
0·6
0·8
1·0
1·2
1·4
1·6
1·8
2·0
2·2
PHOTON ENERGY IN eV

Fig. 3·8A

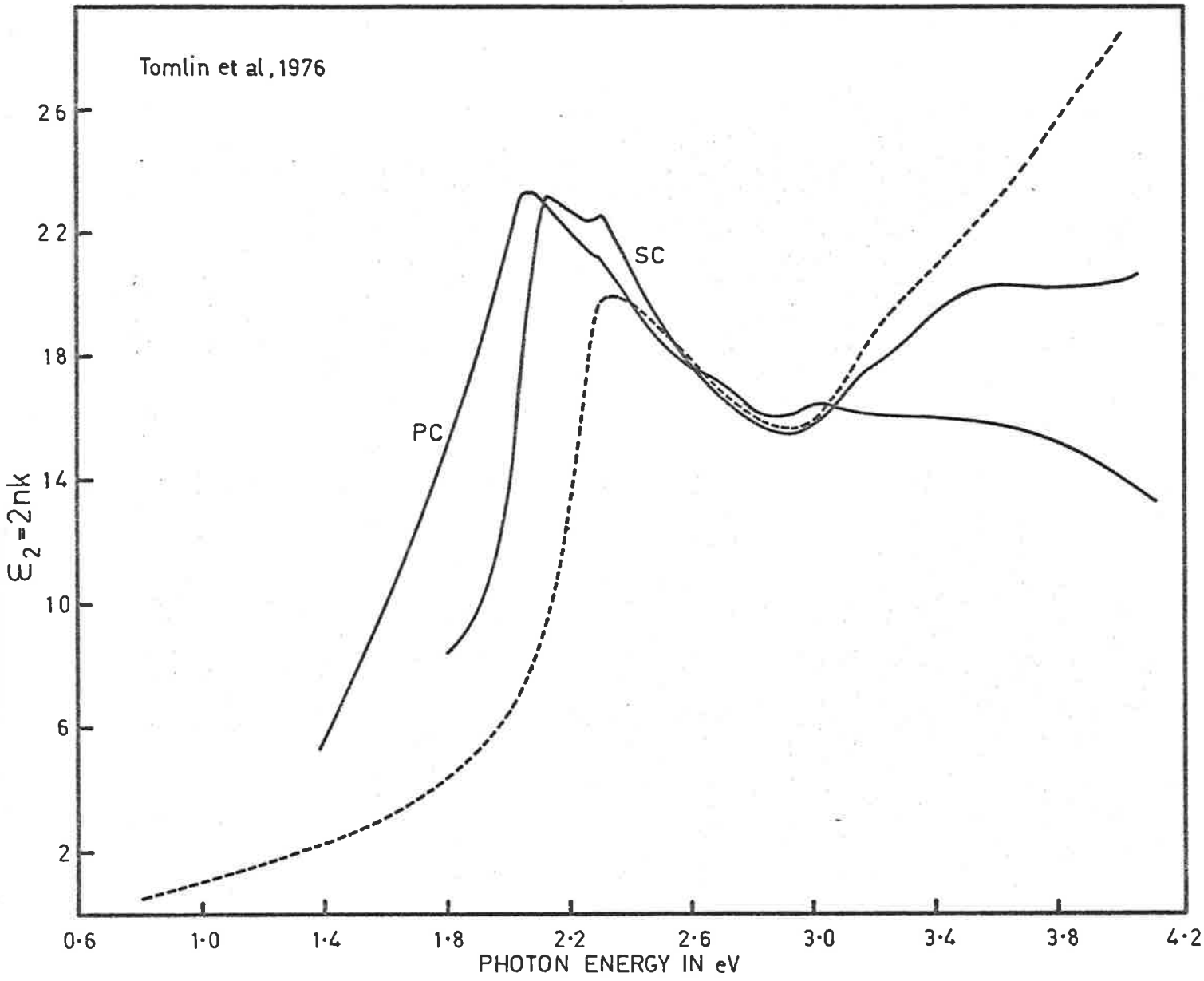
Tomlin et al, 1976
PC
SC
$\varepsilon_2 = 2nk$
26
22
18
14
10
6
2
0·6
1·0
1·4
1·8
2·2
2·6
3·0
3·4
3·8
4·2
PHOTON ENERGY IN eV

Fig. 3·8B

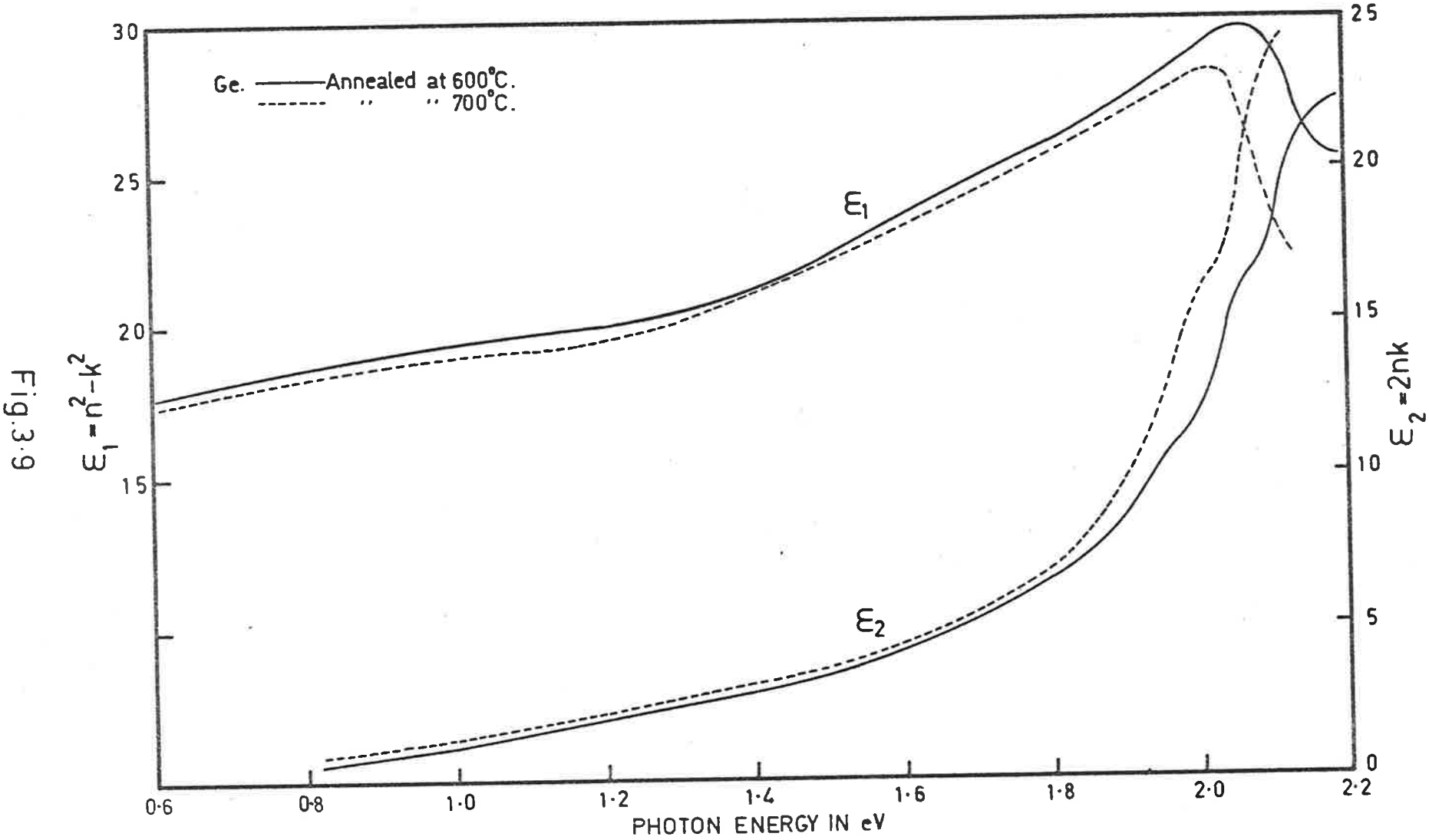
Ge. ——Annealed at 600°C.
------- " " 700°C.
ε_1
ε_2
$\varepsilon_1 = n^2 - k^2$
$\varepsilon_2 = 2nk$
30
25
20
15
25
20
15
10
5
0
0·6
0·8
1·0
1·2
1·4
1·6
1·8
2·0
2·2
PHOTON ENERGY IN eV

Fig.3.9

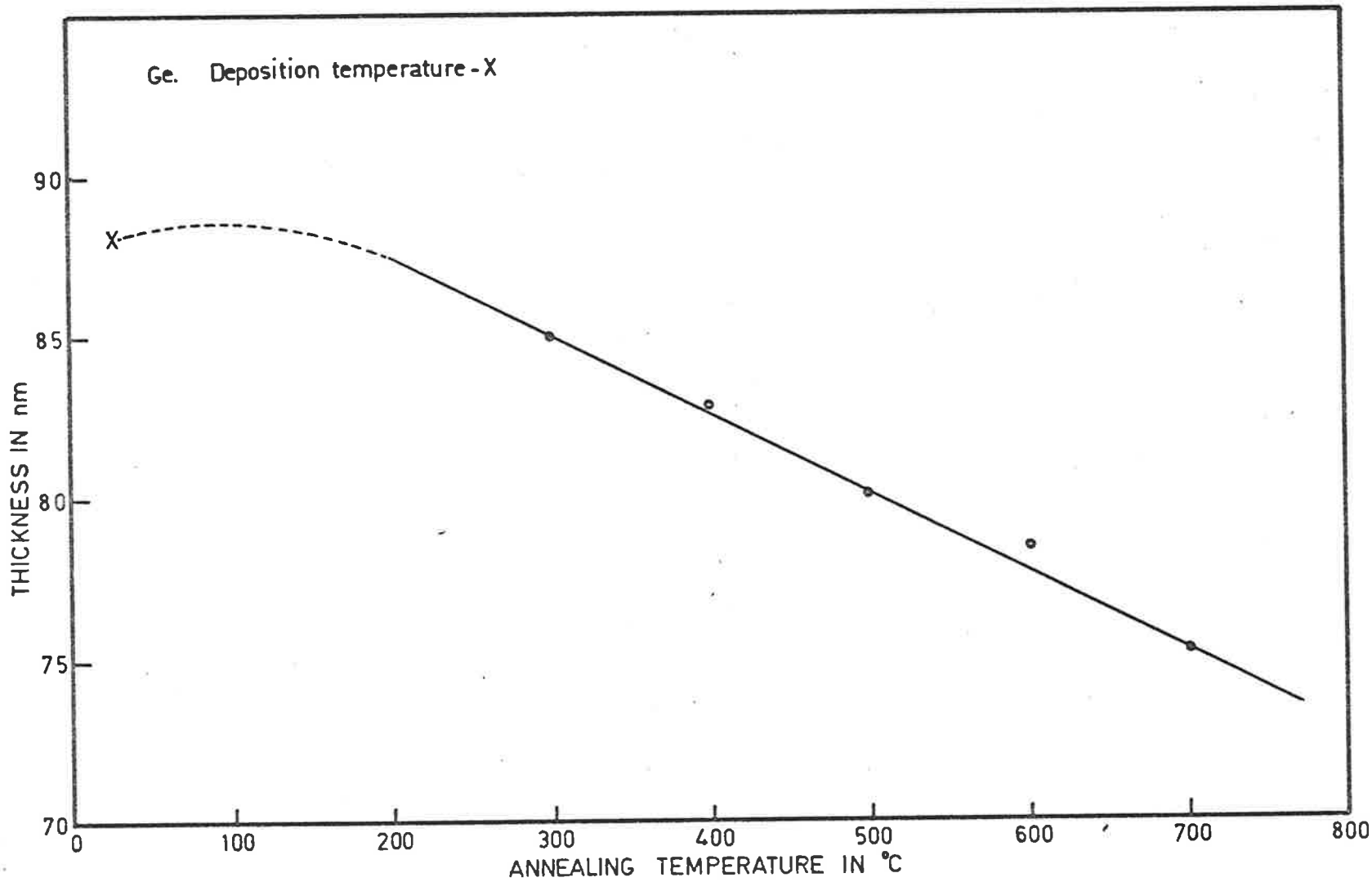
Ge. Deposition temperature - X
X
90
85
80
75
70
THICKNESS IN nm
0
100
200
300
400
500
600
700
800
ANNEALING TEMPERATURE IN °C

Fig.3.10

material at about 2.1 eV, Figure (3.8B). The ε_2 curve for Potter's (1966), Figure (3.5B), obtained for electro-polished intrinsic Ge also does not show any sharp well-resolved peaks like single crystal Ge (Tomlin *et al* 1976). It seems that films deposited at 500°C or annealed at 600 or 700°C have ε_2 curves characteristic of crystalline material. Films deposited at 500°C or annealed at 600°C have fundamental energy gaps of 0.69 and 0.65 eV respectively in agreement with other measurements on polycrystalline films as mentioned before in Section 3.5. The energy gap for the Ge film annealed at 700°C is found to be 0.57 eV which is close to the value of 0.60 eV, the theoretical prediction made by Brust (1964) due to the transition Γ_2' to Γ_{25}'.

3.7. Amorphous Ge films

3.7.1 Absorption processes in amorphous Ge films

Our main interest is the study of the fundamental absorption near the band edges. Here we shall use the Mott and Davis (1971) model of amorphous semiconductors which states that there is an isotropic density of states distribution which has localized wave function for the states at the top and bottom of a valence and conduction band whereas the remaining states have extended wave functions. These authors also assumed that the valence and conduction bands in amorphous materials have tails of localized states due to defects in structure or imperfections in the films. This model is shown in Figure (3.11A). Above the energy E_C and below E_V the wave functions are extended as in ideal crystals, but in the ranges E_A to E_C and E_B to E_V the wave functions are localized. The quantity E_C-E_V defines a mobility gap. The dotted portion indicates additional localized states in un-annealed material which tail off gradually depending upon the conditions of

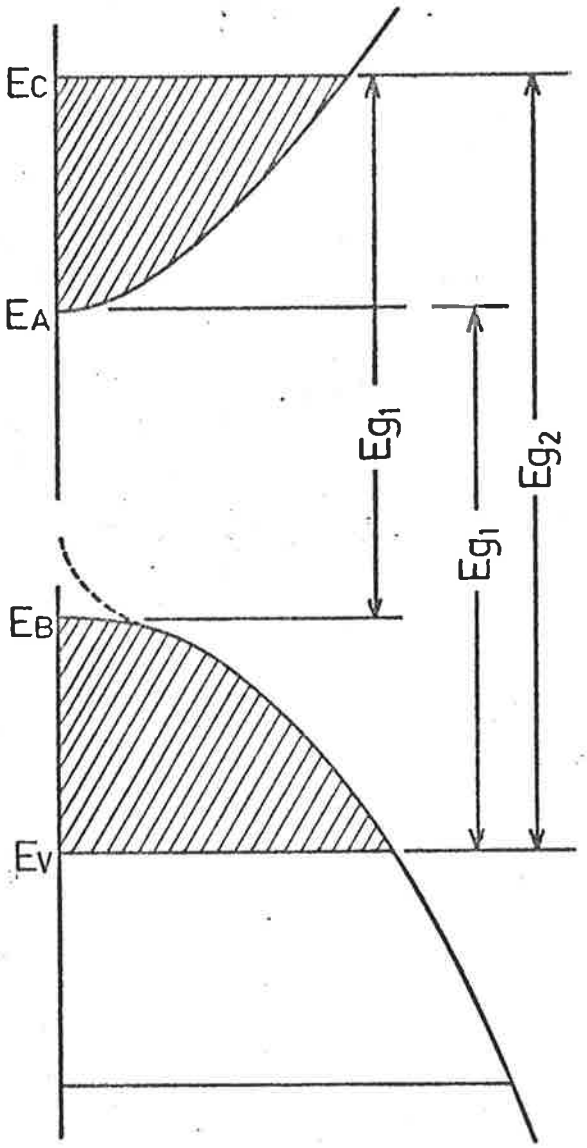

Mott and Davis (1971) Model of amorphous semiconductor showing our assignment of the characteristic energies E_{g_1} and E_{g_2}

Fig.3·11A

preparation of the films. Brodsky and Title's (1969) electron spin resonance experiments with Ge thin films and Tauc's (1969) and Theye's (1971) experiments on the effects of annealing on thin Ge films suggested the existence of tailing of the energy levels at the band edges.

It should be mentioned here that the band tailing is shown in Figure (3.11A) as an appendage of the valence band only, but the existence of such a tail to the conduction band is not excluded.

It is assumed that optical transitions can occur between two extended states and between localized and extended states but with less probability. Transitions between localized states are too improbable to contribute appreciably to optical absorption and transitions between valence and conduction band tails are forbidden (Sak 1972).

The absorption near the absorption edge has been found empirically to follow the relation (3.5.2) as explained in Section (3.5) and a number of experimental results for a variety of amorphous materials lead to plausible values of Eg (Mott and Davis 1971). There is little theoretical justification for applying this formula to amorphous materials, though it has been derived by Mott and Davis, who assumed that the density of states function near the band edges varies linearly with the energy. Tauc and Menthe (1972) made the different assumption that the density of states at the band edges are linear functions of the square root of energy and that the transitions between localized states should be included and obtained a similar result.

3.7.2 Determination of band gaps and discussion .

The plot of $(EnK)^{\frac{1}{2}}$ against energy E is given in Figure

(3.11B) which is derived from the absorption data averaged for four Ge films deposited at room temperature. The linear portion of the curve at low energies indicates a gap of 0.72 eV which is similar to that observed by Denton and Tomlin (1972). Below this energy there exists some absorption but it is very low and does not satisfy the equation (3.5.2) and according to Donovan *et al* (1970) cuts off sharply at 0.6 eV . This low energy absorption is attributed to transitions from the tails of the valence band to the extended conduction band states as shown in Figure (3.19). This minimum energy gap may be expected to depend upon preparation conditions so that different workers get different values. This energy gap of 0.72 eV is identified with the intervals E_C-E_B and E_A-E_V of Figure (3.19) and the absorption above this energy with transitions $\ell \leftrightarrows e$ (i.e. from localized to extended states and vice versa) which are assumed to satisfy the relation (3.5.2). For determining other energy gaps the analysis of the $(EnK)^{\frac{1}{2}}$ curves of Figure (3.11B) was carried further using the procedure described by Khawaja and Tomlin (1975) and successfully used by Thutupalli and Tomlin (1976) in their study of crystalline films of CdTe, ZnTe, ZnSe, Si and Ge and amorphous Si and Ge . This analysis illustrated in Figure (3.11B) gives four energy gaps which are at 0.72, 1.02, 1.34 and 1.64 eV with corresponding values of the constant C of 8.71, 13.27, 17.32 and 19.62×10^3 $eV^{-\frac{1}{2}} m^{-\frac{1}{2}}$ respectively. In the figure the inset shows the extensions of the plot beyond 1.6 eV.

The mobility gap of 1.02 eV i.e. the gap between the extended states is in good agreement with the observed activation energy for electrical conductivity of 0.55 eV (Mott and Davis 1971). It is also close to the Figure of 1.06 eV determined by Fischer (1971) from

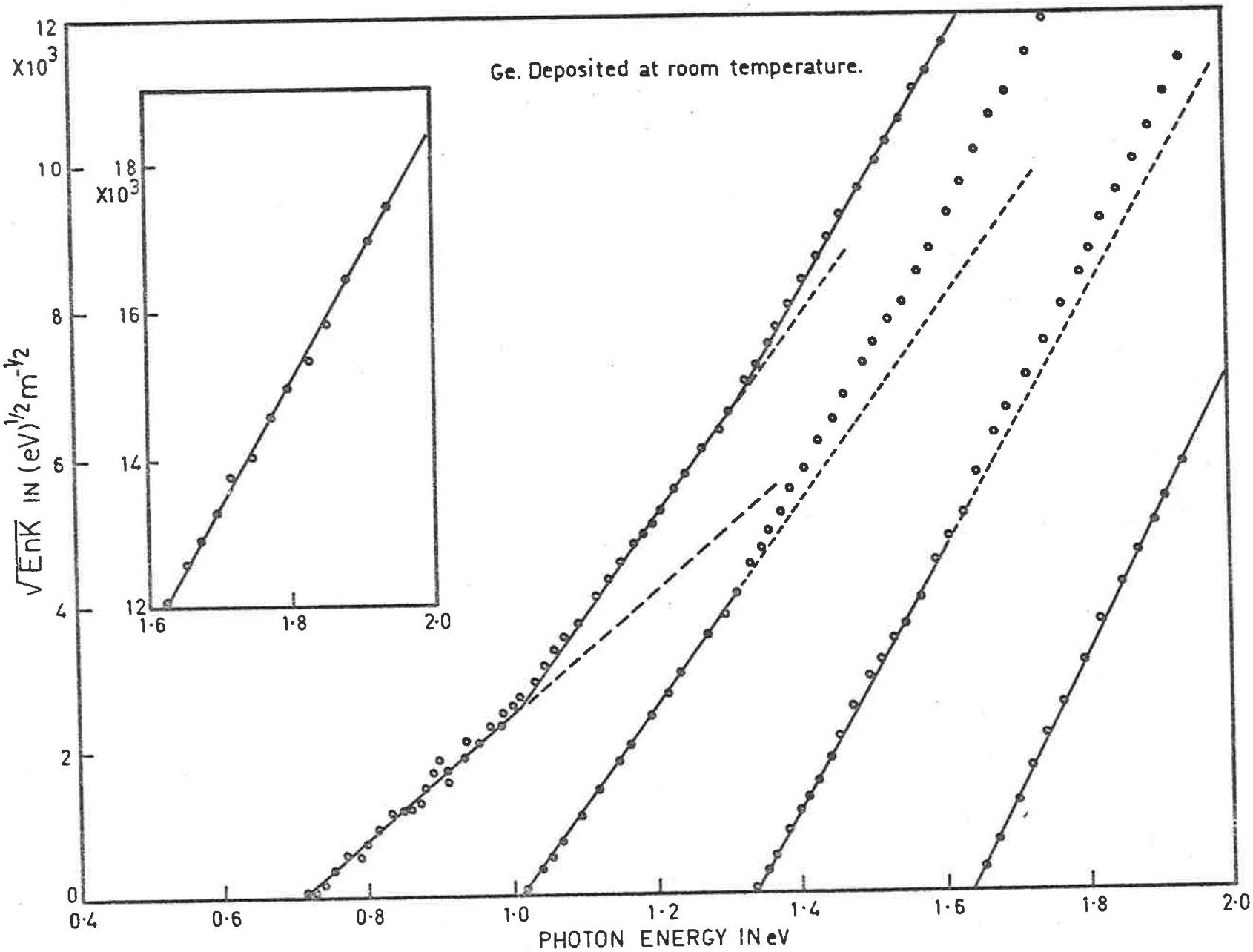
Ge. Deposited at room temperature.
12
X10^3
10
8
6
4
2
0
√EnK IN (eV)^½ m^-½
18
X10^3
16
14
12
1·6
1·8
2·0
0·4
0·6
0·8
1·0
1·2
1·4
1·6
1·8
2·0
PHOTON ENERGY IN eV

Fig.3.11B

electroreflectance spectra of amorphous Ge films prepared at substrate temperatures of 150, 175 and 200°C (Figure 3.5B) and also near to the values in the range 0.9 to 1.1 eV determined by Piller *et al* (1969) for electroreflectance spectra of disordered Ge films. The third energy gap of 1.34 eV is very close to the peak at 1.35 eV given in Figure (3.5B) and also similar to the value 1.34 eV obtained by Tomlin *et al* (1976). We attribute this energy gap to a spin orbit splitting of the valence band amounting to 0.32 eV. Tomlin *et al* (1976) also found a fourth gap of 1.60 eV and the writer finds a gap of 1.64 eV . This may possibly arise from the spin orbit splitting of extended conductance band states but it is doubtful if the analysis can be properly pushed to such high energies.

A similar analysis of the data of Figure (3.12) for Ge films annealed at 300°C gives five energy gaps which occur at 0.84, 1.01, 1.32, 1.62 and 1.92 eV with corresponding constants C of 7.14, 14.44, 17.50, 20.10 and 21.05 x 10^3 $eV^{-\frac{1}{2}}$ $m^{-\frac{1}{2}}$ respectively. In this figure the inset shows the extension of the plot beyond 1.62 eV.

The appearance of the gaps at 1.62 and 1.92 eV does not seem to accord with the Mott-Davis theory. If there are real gaps at these energies it may be that the theory is an oversimplication, but it may be that the kind of analysis used here is unjustified at these energies. Moreover it may be noted that crystalline films show a gap of 1.82 to 1.92 eV (Table 3.4 , Section 3.8) attributable probably to the transition $L_1 \rightarrow L_3' + \Delta So$. If this analysis is justified (Figure 3.19) it indicates a narrowing of the bands of localized states from 0.30 to 0.17 eV as a result of annealing, but the mobility gap 1.01 eV

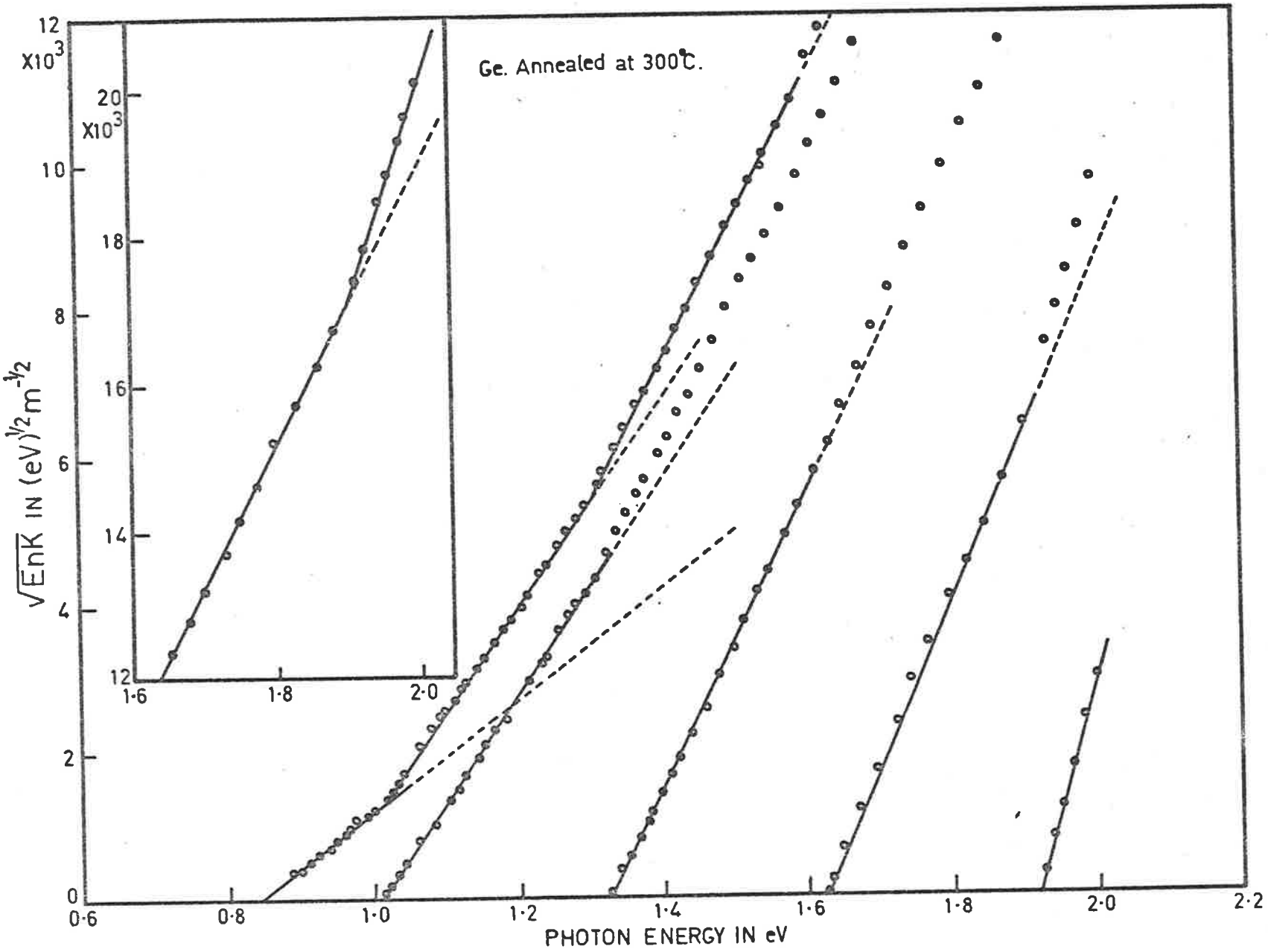
Ge. Annealed at 300°C.
$\sqrt{EnK}$ IN $(eV)^{1/2}m^{-1/2}$
X10³
PHOTON ENERGY IN eV
0·6
0·8
1·0
1·2
1·4
1·6
1·8
2·0
2·2
0
2
4
6
8
10
12
14
16
18
20
1·6
1·8
2·0

Fig. 3·12

remains unaltered. The gap of 0.31 eV agrees quite well with the spin orbit splitting, and should be a more reliable figure than that of 0.43 eV found by Tomlin *et al* (1976) from fewer observations.

Amorphous Ge films annealed at 400°C also give five energy gaps which occur at 0.84, 1.11, 1.31, 1.62 and less certainly at 1.98 eV with corresponding values of C, 8.69, 13.76, 18.04, 20.50 and 23.56 x 10^3 $eV^{-\frac{1}{2}}$ $m^{-\frac{1}{2}}$ respectively. The first gap and the mobility gap are increased due to further annealing but the third and fourth gaps remain unaltered. The comparatively large change in the first gap from 0.72 to 0.84 as a result of annealing at 400°C is attributed to the elimination of layer imperfections, which give rise to band tailing, and the approach to an ideal amorphous state which may not be reached before crystallization begins. The values of energy gaps for all amorphous Ge films, and for Ge films deposited at 300°C , are given in Table 3.3.

TABLE 3.3

Energy gap in eV	Amorphous Films			Film deposited at 300°C. Mostly amorphous (88% amorphous and 12% crystalline)
	film deposited at room temp.	Film deposited at room temp. and subsequently annealed at		
		300°C	400°C	
Eg_1 →	0.72	0.84	0.84	0.83
Eg_2 →	1.02	1.01	1.11	0.98
Eg_3 →	1.34	1.32	1.31	1.32
Eg_4 →	1.64	1.62	1.62	1.62
Eg_5 →		1.92	1.98	1.91
Eg_6 →				2.12

3.8 Polycrystalline Ge films

3.8.1 Absorption processes in polycrystalline Ge films

As explained in Chapter I, Section (1.3.1), if the electronic energy levels are assumed to be parabolic, the absorption coefficient for crystalline material follows the relations (3.5.2) and (3.5.3) for direct and indirect transitions respectively.

The energy gaps of all Ge films (un-annealed, annealed films and films deposited at higher substrate temperatures) have been determined by using the equation (3.5.2).

This is a common procedure for analyzing the optical absorption data though not universally accepted. Eg defines a gap which may be a true gap in the density of states of crystalline materials, but which may be only a parameter in an empirical relationship in the case of amorphous materials.

3.8.2 Determination of band gaps and discussion

Figure (3.13) shows the plot of $(EnK)^{\frac{1}{2}}$ against energy E for Ge films deposited at 300°C (Table 3.3). This plot gives five energy gaps of 0.83, 0.98, 1.32, 1.62 and 1.91 eV with corresponding values for C of 6.92, 9.17, 12.75, 14.77 and 27.47 x 10^3 $eV^{-\frac{1}{2}}$ $m^{-\frac{1}{2}}$ respectively and the possibility of another peak at 2.12 eV. In this figure the inset shows the extension of the plot beyond 1.88 eV. These energy gaps are close to those of the annealed (at 300°C) amorphous Ge films, supporting the conclusion that Ge films deposited at 300°C are almost entirely amorphous (see Tables 3.2, 3.3 and 3.4 and Figures 3.11B and 3.12). The energy gaps of 0.83, 1.31, 1.60, 1.91 and 2.12 eV for partially crystalline Ge films deposited at 400°C are associated with the transitions $\Gamma_2' \rightarrow \Gamma_{25}'$, $\Gamma_2' \rightarrow \Gamma_{25}' + \Delta S_o$, $L_1 \rightarrow L_3'$, $L_1 \rightarrow L_3' + \Delta S_o$ and $\Lambda_1 \rightarrow \Lambda_3$ respectively where ΔS_o represents the spin orbit splitting. The corresponding values of C are

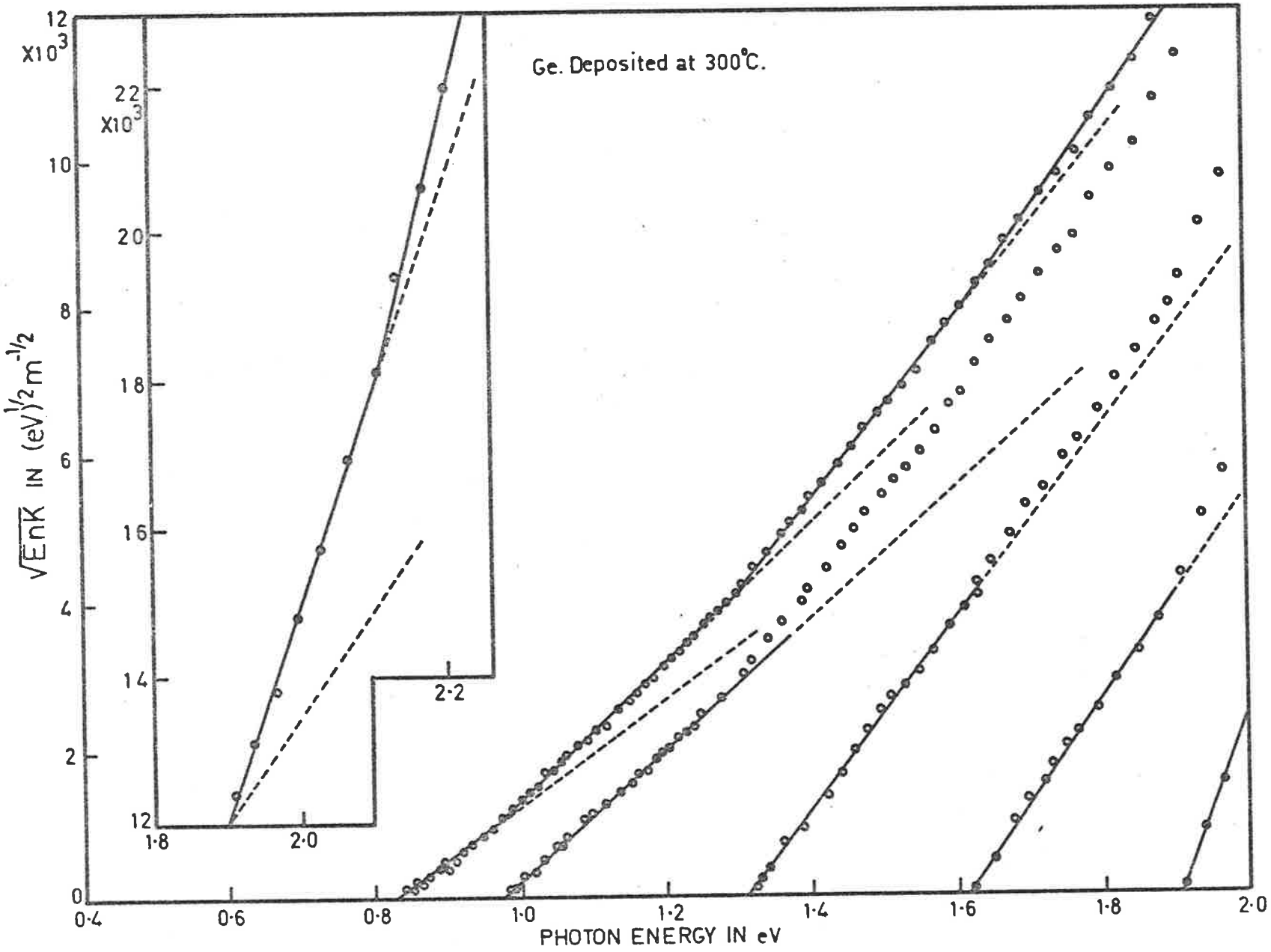
Ge. Deposited at 300°C.
$\sqrt{EnK}$ IN $(eV)^{1/2}m^{-1/2}$
X10^3
PHOTON ENERGY IN eV
0·4
0·6
0·8
1·0
1·2
1·4
1·6
1·8
2·0
2·2

Fig.3.13

8.85, 10.91, 14.28, 30.78 and 37.32 x 10^3 $eV^{-\frac{1}{2}}$ $m^{-\frac{1}{2}}$. The first gap is in good agreement with the value of 0.80 for crystalline Ge according to Braunstein *et al* (1958), Zwerdling and Lax (1956), Potter (1966), Cardona (1961). The third, fourth and fifth gap also agree with Potter, Figure (3.5B) whose values are 1.74 (300° K), 1.84 (120° K) for the $L_1 \rightarrow L_3'$ transition, 1.94 (300° K), 2.04 (120° K) for $L_1 \rightarrow L_3' + \Delta S_o$ transition, and 2.13 eV (300° K), 2.22 eV (120° K) for the $\Lambda_1 \rightarrow \Lambda_3$ transition (Tables 3.4 and 3.5) where ΔS_o = 0.29 eV (Seraphin and Hess 1965). Similar analysis for partially crystalline Ge film deposited at room temperature and annealed at 500° C (Figure 3.14) gives five energy gaps 0.78, 1.29, 1.60, 1.88 and 1.99 eV which are associated with the same transitions suggested for Ge films deposited at 400° C . The corresponding values of C are 8.63, 10.58, 15.50, 33.85 and 37.32 x 10^3 $eV^{-\frac{1}{2}}$ $m^{-\frac{1}{2}}$. The plot of $(EnK)^{\frac{1}{2}}$ against energy E (Figure 3.16) gives four energy gaps 0.69, 1.30, 1.57 and 1.92 eV for crystalline Ge films deposited at 500° C which are associated with the transitions, $\Gamma_2' \rightarrow \Gamma_{25}'$, $\Gamma_2' \rightarrow \Gamma_{25}' + \Delta S_o$, $L_1 \rightarrow L_3'$ and $L_1 \rightarrow L_3' + \Delta S_o$ respectively. The corresponding values of C are 6.62, 9.33, 16.32 and 29.04 x 10^3 $eV^{-\frac{1}{2}}$ $m^{-\frac{1}{2}}$. In this figure the inset shows the extension of the plot beyond 1.9 eV. Another energy gap at 2.10 eV is observed in the ε_2 curve for Ge films deposited at 500° C which is probably due to transition $\Lambda_1 \rightarrow \Lambda_3$. The value of the first energy gap is in good agreement with the value of 0.67 eV (300° K) and 0.6367 to 0.6913 eV (291° K) according to Kittel (1976) and McFarlane *et al* (1957) respectively. The first energy gap (0.6367 to 0.6913eV)is due to the transition $L_1 \rightarrow \Gamma_{25}'$ according to McFarlane *et al* but according to Brust (1964) who calculated the theoretical band structures of Ge , the gap due to the transition

$\Gamma_2' \rightarrow \Gamma_{25}'$ is 0.60 eV , and according to Bassani (1957), the value is 0.80 eV due to the same transition. see Table (3.5). Thus there seems to be some evidence in favour of the transition $\Gamma_2' \rightarrow \Gamma_{25}'$ being responsible for the fundamental band gap.

Similar analysis for crystalline Ge films annealed at 600°C gives six energy gaps of 0.65, 1.31, 1.55, 1.86, 2.01 and 2.12 eV which are associated with the transitions $\Gamma_2' \rightarrow \Gamma_{25}'$, $\Gamma_2' \rightarrow \Gamma_{25}' + \Delta S_o$, $L_1 \rightarrow L_3'$, $L_1 \rightarrow L_3' + \Delta S_o$, $L_1 \rightarrow L_3' + 2\Delta S_o$ and $\Lambda_1 \rightarrow \Lambda_3$ respectively. The corresponding values of C are 6.87, 8.69, 13.76, 29.04, 37.32 and 46.52 x 10^3 $eV^{-\frac{1}{2}} m^{-\frac{1}{2}}$. The energy gaps (Figure 3.15) of 0.57, 1.18, 1.52, 1.82, 1.93 and 2.06 eV for crystalline Ge films annealed at 700°C are also associated with the same transitions. The corresponding values of C, 6.49, 8.39, 14.83, 34.87, 43.31, and 45.65 x 10^3 $eV^{-\frac{1}{2}} m^{-\frac{1}{2}}$. In this figure the inset shows extension of the plot beyond 1.85 eV.

From the above discussion it appears that all partially crystalline and fully crystalline Ge films have energy gaps in the ranges (Table 3.4) E_1 = 0.57 to 0.83 eV, E_2 = 1.18 to 1.31 eV, E_3 = 1.52 to 1.60 eV, E_4 = 1.82 to 1.92 eV, E_5 = 1.93 to 2.12 eV and E_6 = 2.06 to 2.13 eV. They are probably due to transitions $\Gamma_2' \rightarrow \Gamma_{25}'$, $\Gamma_2' \rightarrow \Gamma_{25}' + \Delta S_o$, $L_1 \rightarrow L_3'$, $L_1 \rightarrow L_3' + \Delta S_o$, $L_1 \rightarrow L_3' + 2\Delta S_o$ and $\Lambda_1 \rightarrow \Lambda_3$. However there is still some controversy as to whether the fundamental energy gap corresponds to $L_1 \rightarrow \Gamma_{25}'$ or $\Gamma_2' \rightarrow \Gamma_{25}'$.

Depending on the degree of crystallinity the ε_2 curves of predominantly crystalline Ge show peaks around 2.1 eV and give an indication of another beyond 2.15 eV see Section (3.6). Two prominent

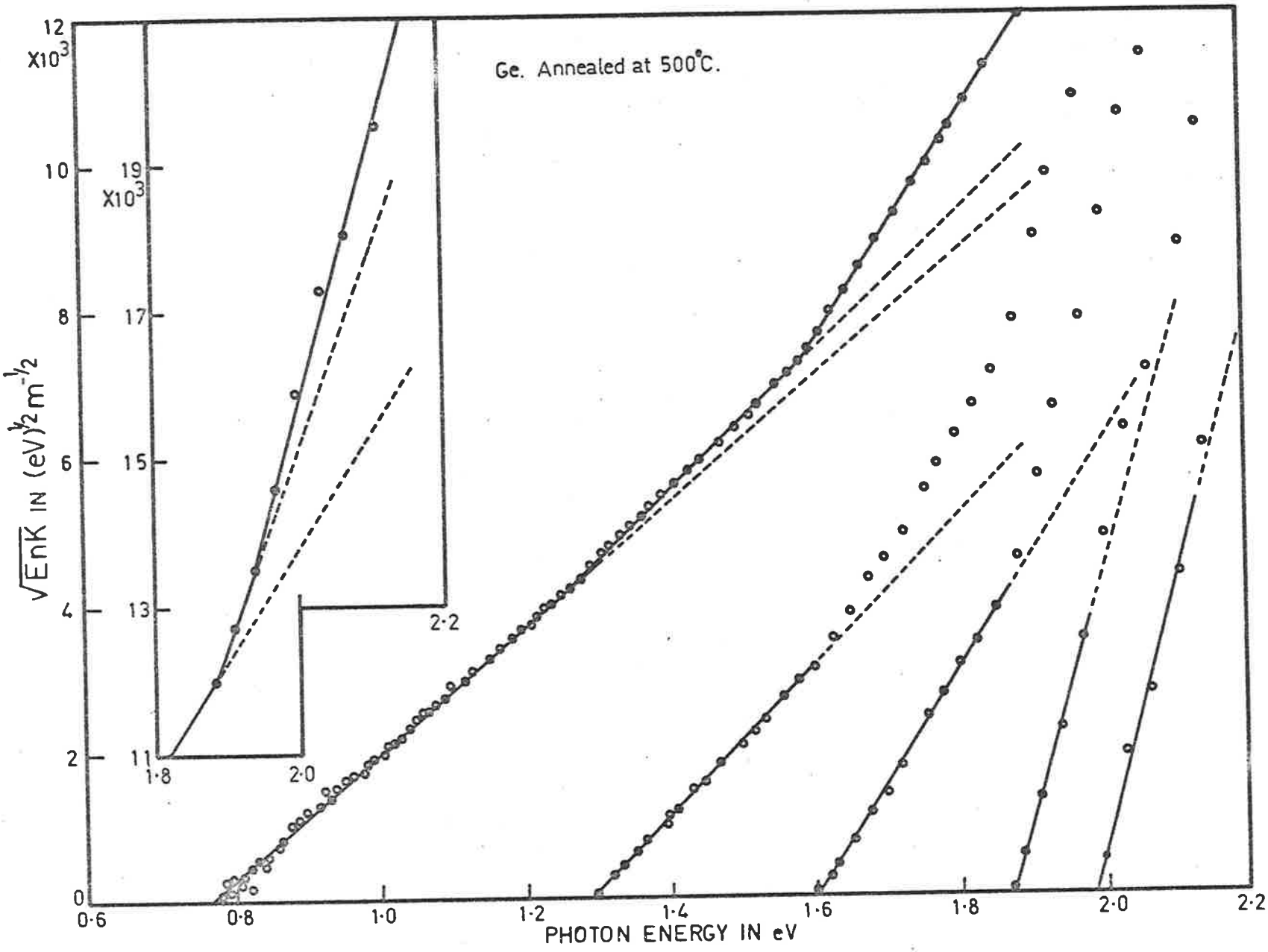
Ge. Annealed at 500°C.
12
X10^3
10
8
6
4
2
0
19
X10^3
17
15
13
11
1·8
2·0
2·2
√EnK IN (eV)^½m^-½
0·6
0·8
1·0
1·2
1·4
1·6
1·8
2·0
2·2
PHOTON ENERGY IN eV

Fig. 3·14

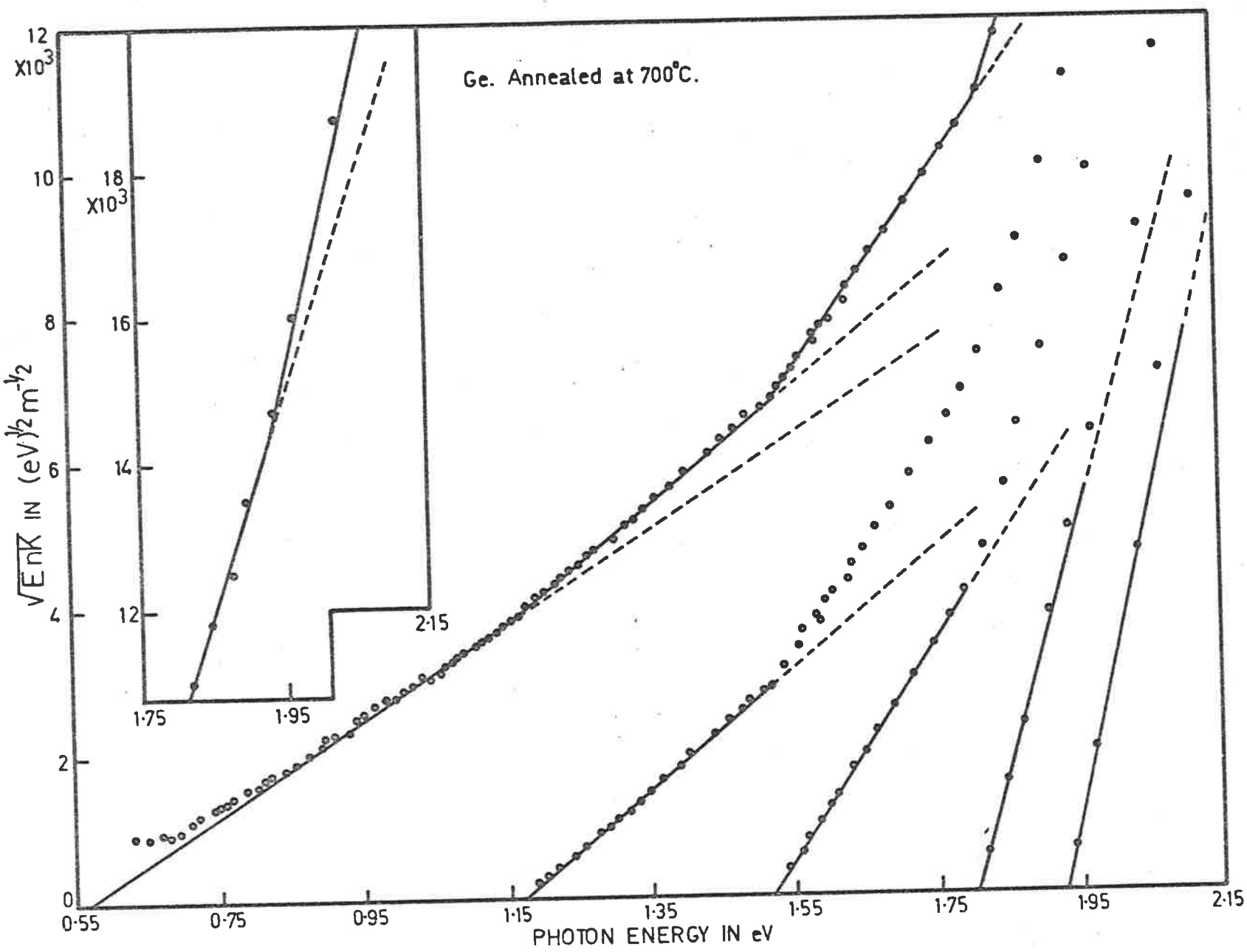
Ge. Annealed at 700°C.
12
X10^3
10
8
6
4
2
0
18
X10^3
16
14
12
2·15
1·75
1·95
√EnK IN (eV)^½ m^-½
0·55
0·75
0·95
1·15
1·35
1·55
1·75
1·95
2·15
PHOTON ENERGY IN eV

Fig.3.15

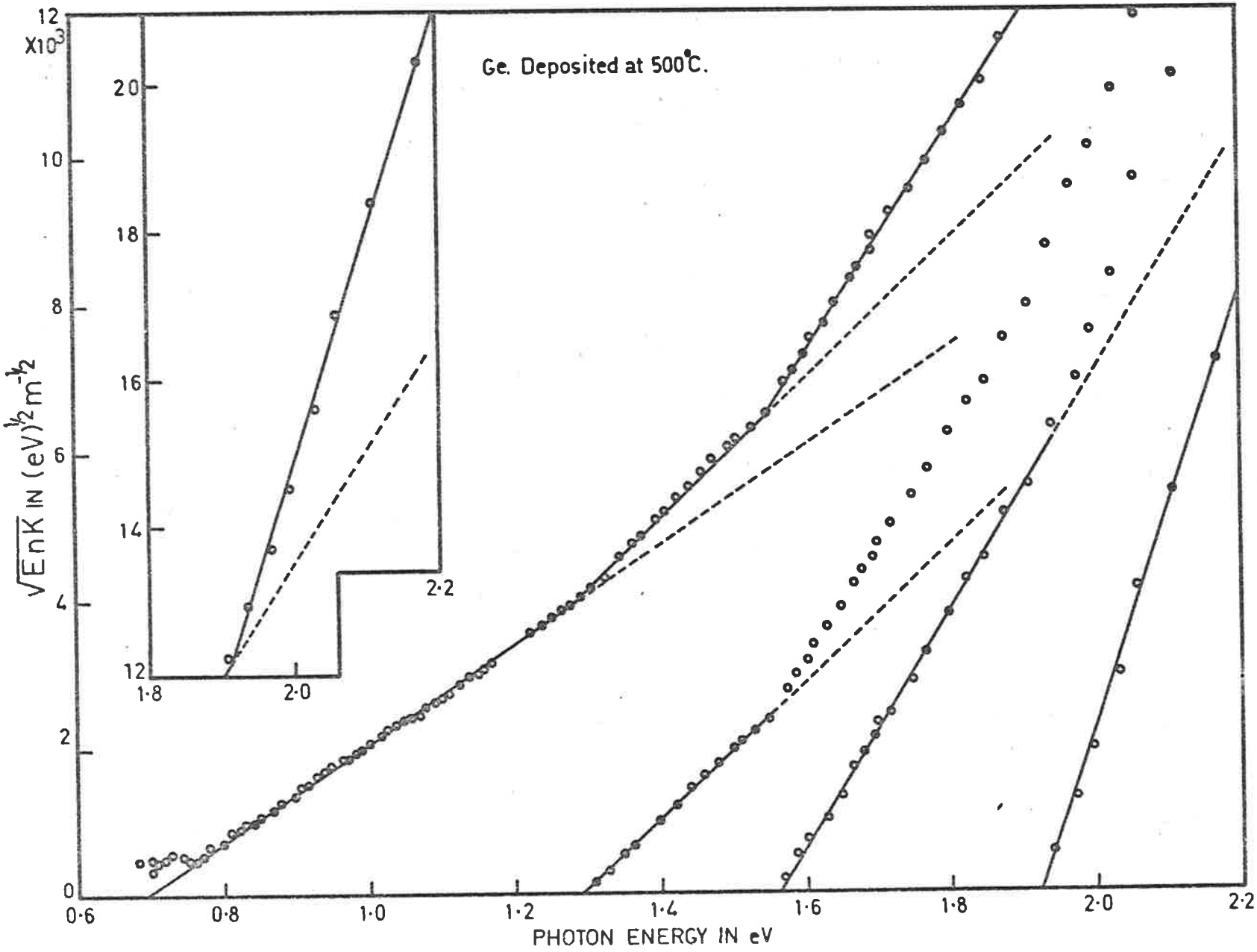
Ge. Deposited at 500°C.
$\sqrt{EnK}$ IN $(eV)^{\frac{1}{2}}m^{-\frac{1}{2}}$
X10^3
PHOTON ENERGY IN eV
0·6
0·8
1·0
1·2
1·4
1·6
1·8
2·0
2·2
1·8
2·0
2·2

Fig. 3.16

TABLE 3.4

Energy Gap in eV	Partially and fully crystalline Ge films				
	Film deposited at		Film deposited at room temperature and subsequently annealed at		
	400°C (partially cryst.)	500°C (fully cryst.)			
			500°C (partially cryst.)	600°C (fully cryst.)	700°C (fully cryst.)
Eg_1 →	0.83	0.69	0.78	0.65	0.57
Eg_2 →	1.31	1.30	1.29	1.31	1.18
Eg_3 →	1.60	1.57	1.60	1.55	1.52
Eg_4 →	1.91	1.92	1.88	1.86	1.82
Eg_5 →	2.12	2.10	1.99	2.01	1.93
Eg_6 →			2.13	2.12	2.06

TABLE 3.5

AUTHOR	Transition assignment for crystalline Ge in eV						
	$L_1 \rightarrow \Gamma_{25}'$	$\Gamma_2' \rightarrow \Gamma_{25}'$	$\Gamma_2' \rightarrow \Gamma_{25}' + \Delta S_o$	$L_1 \rightarrow L_3'$	$L_1 \rightarrow L_3' + \Delta S_o$	$\Lambda_1 \rightarrow \Lambda_3$	$\Lambda_1 \rightarrow \Lambda_3 + \Delta S_o$
Bassani 1957 (Theoretical)		0.80		2.0			
Brust 1964 (Theoretical)		0.60		1.8			
Dash and Newman 1955 (single crystal)	0.62 (300° K) 0.72 (77° K)	0.81 (300° K) 0.88 (77° K)					
Zwerdling and Lax 1956 (single crystal)		0.80					
McFarlane *et al* 1957 (single crystal)	0.6367-0.6913 (291° K) 0.7063-0.7614 (77° K) 0.7686-0.7485 (4.2° K)						
Braunstein *et al* 1958 (single crystal)		0.80					

/Continued....

TABLE 3.5 (continued)

Author	Transition assignment for crystalline Ge in eV.						
	$L_1 \rightarrow \Gamma_{25}'$	$\Gamma_2' \rightarrow \Gamma_{25}'$	$\Gamma_2' \rightarrow \Gamma_{25}' + \Delta S_o$	$L_1 \rightarrow L_3'$	$L_1 \rightarrow L_3' + \Delta S_o$	$\Lambda_1 \rightarrow \Lambda_3$	$\Lambda_1 \rightarrow \Lambda_3 + \Delta S_o$
Potter 1966 (single crystal)		0.80±0.02 (300° K) 0.88±0.02 (120° K)	1.09±0.02 (300° K) 1.20±0.02 (120° K)	1.74±0.02 (300° K) 1.84±0.02 (120° K)	1.94±0.02 (300° K) 2.04±0.02 (120° K)	2.13±0.02 (300° K) 2.22±0.02 (120° K)	2.32±0.02 (300° K) 2.41±0.02 (120° K)
Ghosh 1966 (single crystal)				e_1 2.15	$e_1 + \Delta_1$ 2.35	E_1 2.22	$E_1 + \Delta_1$ 2.42
Batz 1966 (single crystal)				1.97	-	2.18	2.36

energy gaps at 2.1 and 2.3 eV have been observed in all normal incidence reflectance measurements (see Chapter 4) since they were first seen by Tauc (1962). Initially they were attributed to direct transitions from the L point at the edge of the Brillouin zone with a valence band splitting of between 0.18 to 0.20 eV. But detailed band structure calculations by Brust *et al* (1962) and Brust (1964) indicated that the transitions at this energy occur in the Λ direction and not at the edge of the zone. These two peaks in the form of a doublet are due to transitions $\Lambda_1 \rightarrow \Lambda_3$, $\Lambda_1 \rightarrow \Lambda_3 + \Delta S_o$. The first peak which varies from 2.06 to 2.13 eV due to transition $\Lambda_1 \rightarrow \Lambda_3$ is observed in all fully or partially crystalline Ge films but the position of the second peak is beyond the range of the present method of measurement. All the results for partially crystalline and fully crystalline films are given in Table (3.4).

3.9 Dependence of energy gaps on deposition and annealing temperatures

Figures (3.17 and (3.18) show how the energy gaps Eg_1 , Eg_2 , Eg_3 and Eg_4 measured at room temperature vary with the substrate temperature at which the film was deposited, and as a result of successive annealings of initially amorphous films deposited at room temperature. As the temperature increases the gap widths increase to a maximum and then decrease to values corresponding to those of purely crystalline films.

Following Brodsky and Title (1969), Theye (1971), Tomlin *et al* (1976), the form of these curves is interpreted as follows. On annealing an amorphous film formed at room temperature it is supposed that structural imperfections which produce a tail of energy states

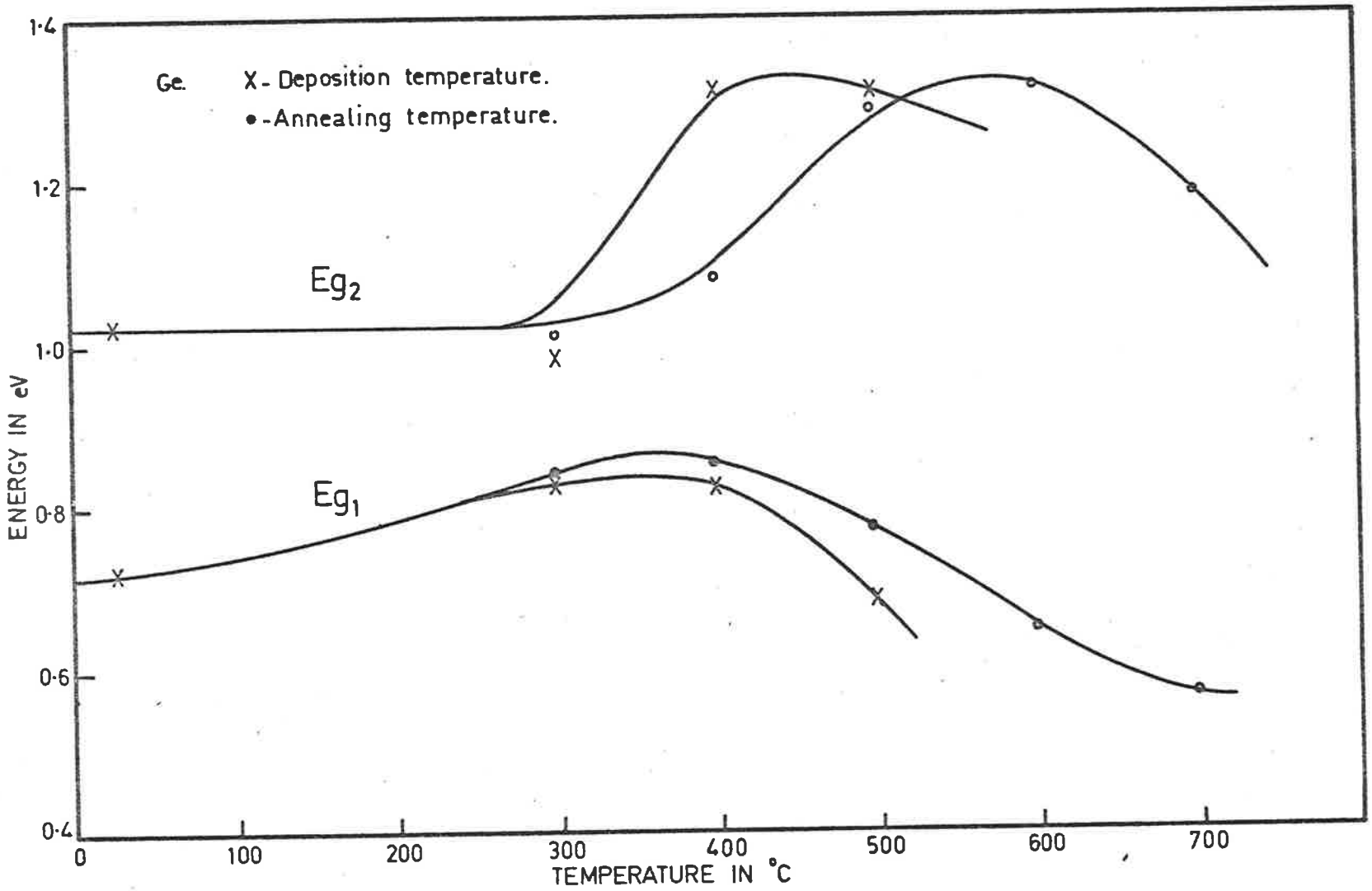
Ge.
X - Deposition temperature.
• - Annealing temperature.
Eg_2
Eg_1
ENERGY IN eV
1·4
1·2
1·0
0·8
0·6
0·4
0
100
200
300
400
500
600
700
TEMPERATURE IN °C

Fig.3.17

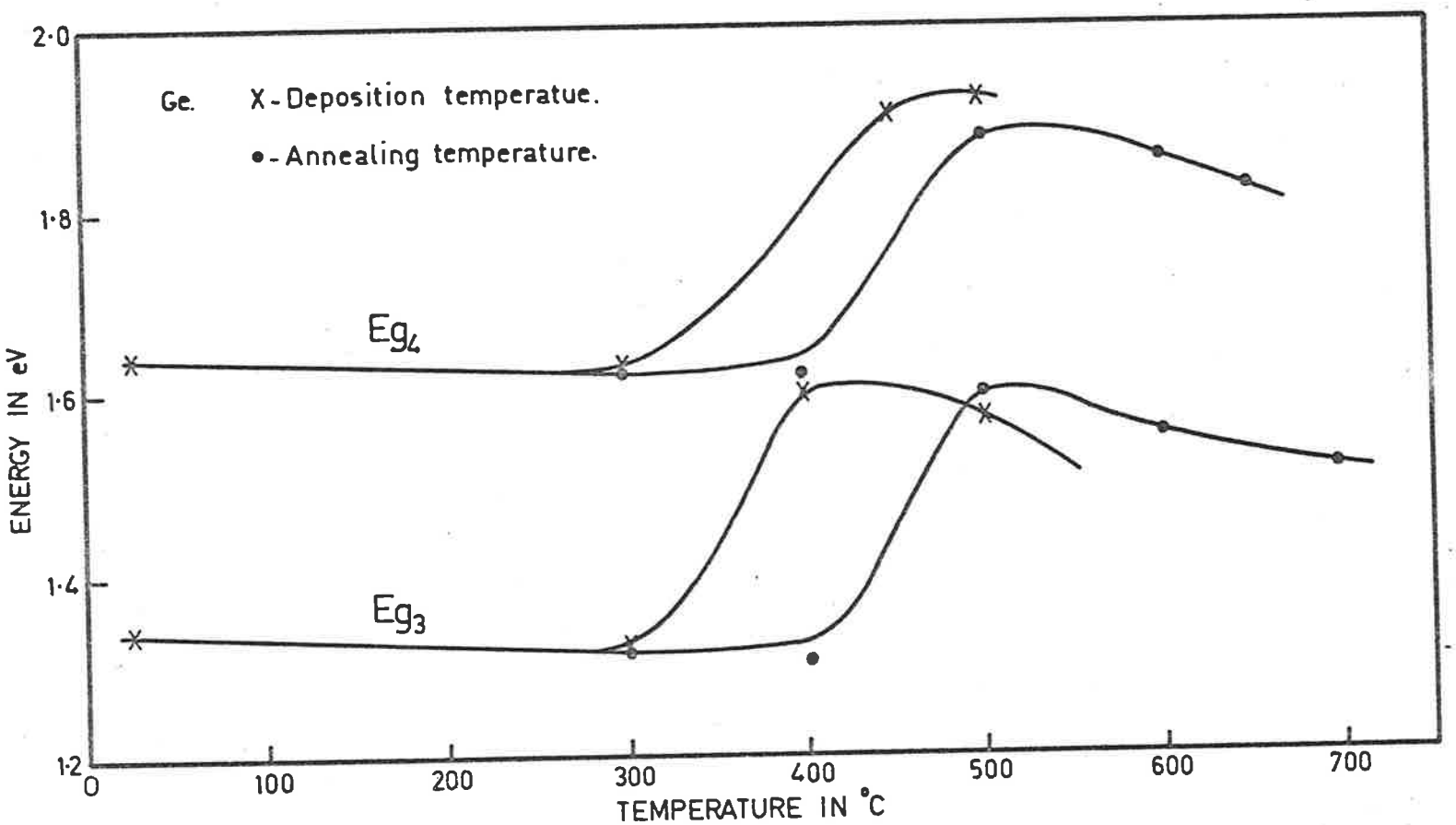
Ge.
X - Deposition temperatue.
• - Annealing temperature.
Eg4
Eg3
ENERGY IN eV
2·0
1·8
1·6
1·4
1·2
0
100
200
300
400
500
600
700
TEMPERATURE IN °C

Fig.3.18

extending into the forbidden band (see Figure 3.19) are removed, and that an ideal, or nearly ideal amorphous film is formed which begins to crystallize on annealing at about 450°C. Further annealing at higher temperatures results in films with increasing crystalline content until at 600°C almost wholly crystalline films result. The film thicknesses obtained from the optical measurements shown as a function of annealing temperature in Figure (3.10) reflect the change from the amorphous to the crystalline state.

3.10 Conclusions

(1) Ge films annealed at 300°C are amorphous. Any crystallites present are of dimensions less than 1.0 nm . Energy gaps or characteristic energies occur at 0.84, 1.01, 1.32, 1.62 and 1.92 eV (Figure 3.12). Ge films deposited at 300°C are largely amorphous but contain crystallites of dimensions 1.5 to 2.0 nm . Energy gaps occur at 0.83, 0.98, 1.32, 1.62, 1.91 and 2.12 eV. (Figure 3.13). The similarity of these two sets of energy gaps suggests the degree of crystallinity is not appreciably different.

(2) The energy gaps are approximately the same as those occurring in the corresponding crystalline phase. Ge films annealed at 400°C have some energy gaps at 1.31, 1.62 and 1.98 eV (amorphous) and on annealing at 500°C which produces a large proportion of crystalline material, some of the energy gaps are at 1.29, 1.60 and 1.99 eV. This conclusion is almost identical with that of Davis and Shaw (1970) who found that the electrical and thermal energy gaps of amorphous materials are approximately the same as those occurring in the corresponding crystalline phase (where this exists). Generally, amorphous specimens show a broadening of features in their optical absorption spectra as compared to crystalline material (Figures 3.8A, 3.8B and 3.9). The ϵ_2

E (eV)
UNANNEALED AMORPHOUS Ge
Ec
EA
ED
EB
Ev
0·30
0·60
0·72
1·02
1·34
0·30
0·32
SPIN ORBIT SPLITTING
N(E)

E (eV)
AMORPHOUS Ge ANNEALED AT 300°C
0·17
0·84
0·84
1·01
1·32
0·17
0·31
N(E)

Fig. 3·19

curves of fully crystalline Ge films annealed at 600° and 700°C (3.5 to 4.5 nm) do not show sharp peaks (Figure 3.6) like those of single crystal Ge (Figure 3.8B) suggesting that crystallization of such films may not be complete. On the other hand the ϵ_2 curve of fully crystalline Ge films (7.0 to 7.5 nm) deposited at 500°C shows these peaks (Figure 3.8A).

(3) Generally, amorphous films are homogeneous and have smooth surfaces (< 1.0 nm) whereas polycrystalline films (4.0 to 7.5 nm) have much rougher surfaces.

(4) The density of amorphous films is less than that of the corresponding crystalline films. In the case of annealed films it is observed that (Figure 3.10) the thickness of the annealed film decreases by 12% during the amorphous to fully crystalline transition.

(5) The refractive indices and band gap values of all partially crystalline films lie between the refractive indices and band gap values of the limiting amorphous and fully crystalline films as described in Section (3.6).

(6) The change in optical properties of films deposited at successively higher temperatures, or annealed at successively higher temperatures can be understood in terms of a model which assumes that a film prepared at room temperature is amorphous but contains imperfections such as voids. By annealing at 300°C , or deposition at 250°C the film becomes a more nearly ideal amorphous film, but at higher temperatures crystallization begins, so that films vary from amorphous, through mixed amorphous and crystalline composition, to the wholly polycrystalline state. It is only for such polycrystalline films

that the band gaps deduced have precise meanings. For amorphous films and films of mixed composition, the energy gaps, or characteristic energies, cannot be related with the same assurance to electron band structures, although for amorphous films the energy gaps find a plausible interpretation in the Mott-Davis theory.

CHAPTER 4

DETERMINATION OF THE OPTICAL CONSTANTS OF GE IN THE REGION 1.8 TO 15 eV USING THE KRAMERS-KRONIG DISPERSION RELATIONS

A method is given for evaluating the optical constants of Ge by using the Kramers-Kronig dispersion relations. For reflectances at high energies (above 10 or 15 eV) three similar extrapolation formulae have been investigated in attempts to improve the extrapolation procedure by using additional parameters in the extrapolation formulae. The additional parameters used have been fixed by using directly measured values of the optical constants within the region 1.8 to 4.0 eV.

The reflection data of Philipp* and Ehrenreich (1963) for crystalline Ge have been used. Present results are compared with those of Philipp and Ehrenreich which were obtained by a different extrapolation method.

Amorphous Ge films deposited at room temperature have also been investigated by this method.

4.1 Introduction

Great attention has recently been paid to the reflection spectra of the materials as a means of studying the band structure in the region where extremely high absorption makes optical transmission methods impossible. The method which has been receiving increased attention uses the Kramers-Kronig dispersion relations (1963) which permit the evaluation of optical constants, and hence a number of associated

* The reflectance data used in this extrapolation were kindly provided by Dr H. R. Philipp, General Electric Research Laboratory, Schenectady, New York.

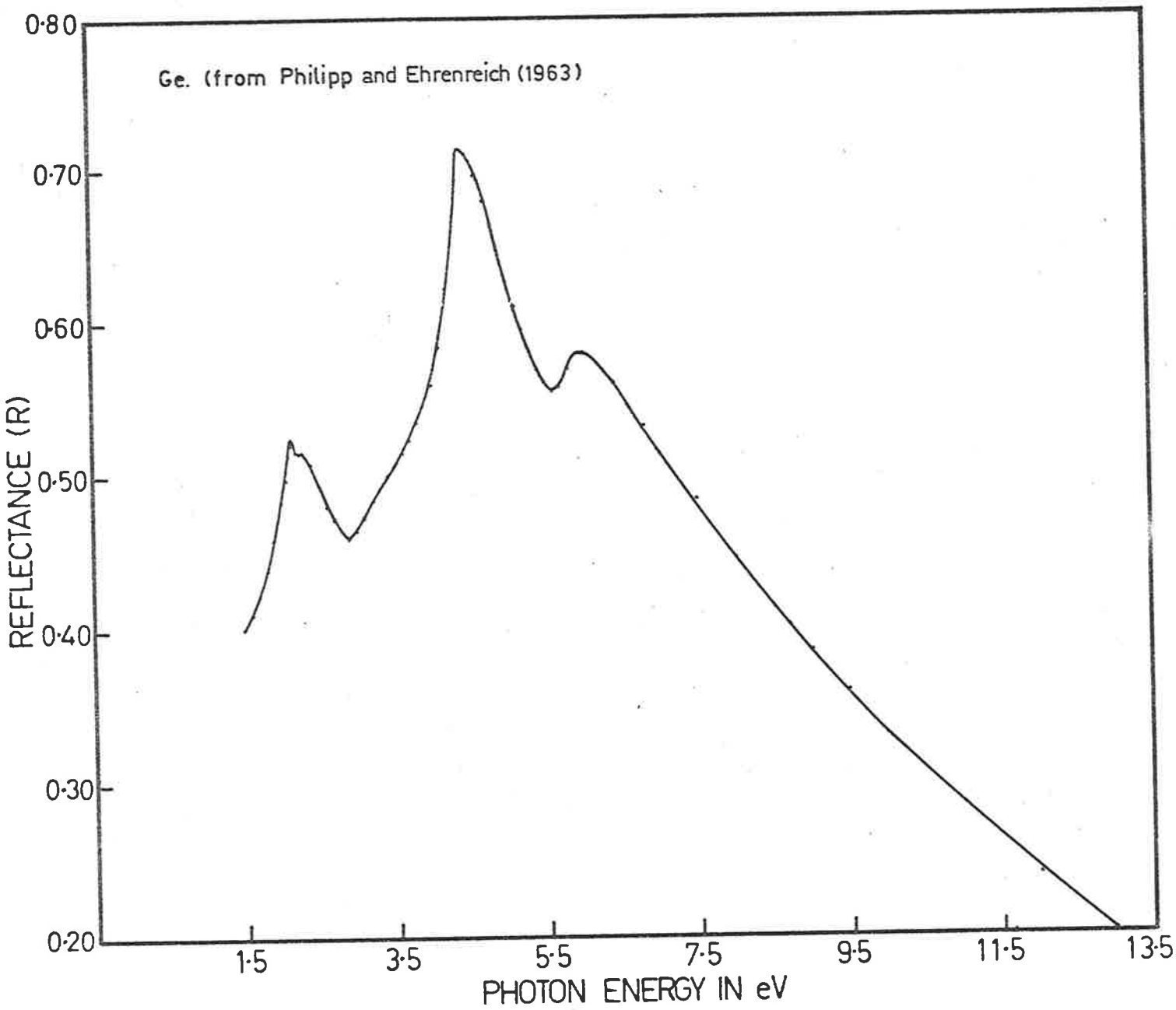
Ge. (from Philipp and Ehrenreich (1963)
0·80
0·70
0·60
0·50
0·40
0·30
0·20
REFLECTANCE (R)
1·5
3·5
5·5
7·5
9·5
11·5
13·5
PHOTON ENERGY IN eV

Fig. 4.1

dielectric parameters, from the normal incidence reflectance data. This procedure was first used by Robinson (1952) in the infrared region and by Jahoda (1957) and Philipp and Taft (1959), in the ultraviolet. Roessler (1965) used this method to evaluate the optical constants from normal incidence reflectance data and also from reflectance data measured at an angle of $45°$. Recently Wooten (1972) described in detail extrapolation procedures for the calculation of reflectances beyond 40 eV using extrapolation formula $R(\omega) = R_{ef} \left(\frac{\omega_{ef}}{\omega} \right)^s$ where ω_{ef} is the frequency of the last measured reflectance value R_{ef} and s is a parameter.

4.2 Kramers-Kronig dispersion relations

From Section (1.7.2) of Chapter I, the phase shift dispersion relation which applies to the reflectivity of solids at normal incidence is

$$\theta(E_0) = \frac{E_0}{\pi} \int_0^\infty \frac{\ell n\, R(E) - \ell n\, R(E_0)}{E_0^2 - E^2} dE \qquad 4.2.1$$

where $R(E)$ and $R(E_0)$ are the reflectances of the material at energies E and E_0. Measurements made over a finite range say E_1 to E_2 need extrapolation from $E_1 \to 0$ and from $E_2 \to \infty$.

The extrapolation from $0 \to E_1$ is over a relatively small range beyond the range of the reflectivity measurements. For semiconductors the absorption index k is nearly equal to zero in this range and the refractive index n can be extrapolated graphically and from this extrapolation R can then be calculated. For metals the reflectance R approaches unity at zero frequency.

Then for the range $E_2 \to \infty$, we must assume some extrapolation formulae which must give a curve continuous with the measured reflectance

curve, i.e. at the join the functions $R(E)$ and $R'(E)$ must be continuous. This condition will fix two parameters of the assumed extrapolation formula. Since it is possible to measure n and k over the optical range (1.8 to 4.0 eV) directly, it is proposed to try to improve the extrapolation procedure by putting additional parameters into the extrapolation formula and fixing them by using n and k values obtained by direct measurements. $\theta(E_0)$ which we have to calculate is given by

$$\theta(E_0) = \theta_1(E_0) + \theta_2(E_0) + \theta_3(E_0) \qquad 4.2.2$$

where $\theta_1(E_0)$ is the contribution of the integral from 0 to E_1,

$\theta_2(E_0)$ is the contribution of the integral from E_1 to E_2,

$\theta_3(E_0)$ is the contribution of the integral from E_2 to ∞.

$$\theta_2(E_0) = \frac{E_0}{\pi} \int_{E_1}^{E_2} \frac{\ell n\, R(E) - \ell n\, R(E_0)}{E_0^2 - E^2}\, dE \qquad 4.2.3$$

which is calculated from the experimental values of $R(E)$ and $R(E_0)$ using numerical integration.

$\theta_1(E_0)$ makes a small contribution to $\theta(E_0)$ and can be dealt with as already explained. $\theta_3(E_0)$ makes a large contribution and the extrapolation needs to be as accurate as possible. If we assume for the reflectance an extrapolation formula containing adjustable parameters we may proceed as follows.

From directly measured n and k at values of E_0 find values of $\theta_{exp}(E_0)$ in a suitable energy range. Then since

$$\theta_3(E_0) = \theta_{exp}(E_0) - \theta_1(E_0) - \theta_2(E_0) \qquad 4.2.4$$

We have a means of finding values of the parameters occurring in $\theta_3(E_0)$.

4.3 Extrapolation formulae with additional parameters

Three similar formulae have been investigated.

Extrapolation formula I

A convenient extrapolation formula in the range $E_2 < E < \infty$ is of the form i.e.

$$\ln R/R_2 = [\, a_0 + a_1 (1 - E_2/E) + a_2 (1 - E_2/E)^2 + \text{-----} \,] \ln E_2/E \qquad 4.3.1$$

where the a's are parameters. This gives

$$R = R_2 \quad \text{at} \quad E = E_2 \qquad 4.3.2$$

and continuity if the experimental R' at $E = E_2$ equals the slope of the extrapolation curve at that point, i.e.

$$\frac{d}{dE} \left(\ln \frac{R}{R_2}\right)_{E=E_2} = R'(\text{exp}) = -\frac{a_0}{E_2} \qquad 4.3.3$$

Thus a_0 is found directly from the continuity requirement.

At large E, (4.3.1) reduces to

$$\ln R/R_2 = (a_0 + a_1 + a_2 \text{ ----}) \ln E_2/E$$

$$\text{or} \quad R/R_2 = (E_2/E)^{(a_0 + a_1 + a_2 \text{ ---- })} \qquad 4.3.4$$

which gives the form of the reflectance curve at high energy.

From equation (4.2.1) we know that

$$\theta_3(E_0) = \frac{E_0}{\pi} \int_{E_2}^{\infty} \frac{\ln R(E) - \ln R(E_0)}{E_0^2 - E^2} \, dE$$

For simplicity we write

$$\theta_3(E_0) = \frac{E_0}{\pi} \int_{E_2}^{\infty} \frac{\ell n\ R - \ell n\ R_0}{E_0^2 - E^2}\, dE$$

$$= \frac{E_0}{\pi} \int_{E_2}^{\infty} \frac{\ell n\ R/R_2 - \ell n\ R_0/R_2}{E_0^2 - E^2}\, dE$$

$$= \frac{E_0}{\pi} \int_{E_2}^{\infty} \frac{\ell n\ R_0/R_2}{E^2 - E_0^2}\, dE - \frac{E_0}{\pi} \int_{E_2}^{\infty} \frac{\ell n\ R/R_2}{E^2 - E_0^2}\, dE \qquad 4.3.5$$

Now using the extrapolation formula we get

$$\theta_3(E_0) = \frac{1}{2\pi}\ \ell n\ R_0/R_2\ \ \ell n \frac{(E_2 + E_0)}{(E_2 - E_0)} - \frac{E_0}{\pi} \int_{E_2}^{\infty} \frac{\ell n\ E_2/E\ \Sigma\ a_n\ (1 - E_2/E)^n}{E^2\ (1 - (E_0/E)^2)}\, dE$$

$$\text{or}\quad \theta_3(E_0) = X - a_0\, I_0 - \sum_{n=1} a_n I_n \qquad 4.3.6$$

$$\text{where}\quad X = \frac{1}{2\pi}\ \ell n\ R_0/R_2\ \ \ell n \frac{(E_2 + E_0)}{(E_2 - E_0)}$$

$$I_n = \frac{E_0}{\pi} \int_{E_2}^{\infty} \frac{(1 - E_2/E)^n\ \ell n\ E_2/E}{E^2\,(1 - E_0^2/E^2)}\, dE$$

$$= -\frac{1}{\pi} \sum_{m=o} Amn\ (E_0/E_2)^{2m+1}$$

$$\text{and}\quad Amn = \frac{1}{(2m+1)^2} - \frac{n}{(2m+2)^2} + \frac{n(n-1)}{\lfloor 2(2m+3)^2} + \text{-------}(-)^n\ \frac{1}{(n+2m+1)^2}$$

$$I_0 = -\frac{1}{\pi} \sum_{m=o} \frac{1}{(2m+1)^2}\ (E_0/E_2)^{2m+1}$$

Now putting this value of $\theta_3(E_0)$ in equation (4.2.4),

$$\theta_{exp} = \theta_1(E_0) + \theta_2(E_0) + X - a_0 I_0 - \sum_{n=1} a_n I_n$$

$$\text{or}\quad -\sum_{n=1} a_n I_n = \theta_{exp} - \{\ \theta_1(E_0) + \theta_2(E_0) + X - a_0 I_0\ \}$$

4.3.7

From the equation (4.3.7) we can find directly the additional parameters other than a_0 since $\theta_1(E_0)$, $\theta_2(E_0)$ and $\theta_{exp}(E_0)$ can be evaluated from experimental results for suitably chosen values of E_0.

After fixing the values of additional parameters and putting these values back in equation (4.3.7) we get the required values of θ, viz.

$$\theta_{cal} = \theta_1(E_0) + \theta_2(E_0) + X - a_0 I_0 - \sum_{n=1} a_n I_n \qquad 4.3.8$$

To determine the parameters one may either evaluate $\theta_{exp}(E_0)$ at a sufficient number of points and solve the resulting set of simultaneous equations for the a's, or fix them by means of a Least Squares method in which the a's are fixed by the requirement that $\sum_p (\theta_{exp} - \theta_{cal})^2$ should be a minimum. Applying this latter procedure we then minimise

$$\sum_p [\theta_{pexp} - f(E_{0_p}) + a_1 I_1(E_{0_p}) + a_2 I_2(E_{0_p}) + \text{----}]^2 \qquad 4.3.9$$

where $\theta_1 + \theta_2 + X - a_0 I_0 = f$

p is the number of reference points and E_{0_p} is the pth reference point . Now after performing partial differentiation on (4.3.9) with respect to the a's we get

$$\sum_p \{\theta_{p\,exp} - f(E_{0_p}) + a_1 I_1(E_{0_p}) + a_2 I_2(E_{0_p}) + \text{---} \} I_1(E_{0_p}) = 0 \qquad 4.3.10$$

and

$$\sum_{p} \{\theta_{pexp} - f(E_{0_p}) + a_1 I_1(E_{0_p}) + a_2 I_2(E_{0_p}) + \text{---} \} I_2(E_{0_p})$$

----------etc., respectively. 4.3.11

There is one such equation for each 'a' , but any number of reference points can be chosen. After solving equations (4.3.10) and (4.3.11) ------etc., we get the values of the a's, putting these calculated values of the a's back in equation (4.3.8) we get the different values of θ_{cal} corresponding to different E_0's. From θ_{cal} and R the corresponding values of n and k can be calculated from the equations

$$n = \frac{1 - R}{1 + R - 2\sqrt{R}\cos\theta_{cal}} \qquad 4.3.12$$

$$k = \frac{2\sin\theta_{cal}\sqrt{R}}{1 + R - 2\sqrt{R}\cos\theta_{cal}} \qquad 4.3.13$$

Extrapolation formula II

$$R/R_2 = e^{-[a_1(1 - E_2/E) + a_2(1 - E_2/E)^2 + \text{----}]} \qquad 4.3.14$$

and consequently

$$\ell n\, R/R_2 = -a_1(1 - E_2/E) - a_2(1 - E_2/E)^2 - a_3(1 - E_2/E)^3 \text{ -----} \qquad 4.3.15$$

The equation (4.3.14) gives $R = R_2$ at $E = E_2$ and for continuity

$$R'(exp) = -\frac{a_1}{E_2} \qquad 4.3.16$$

The value of a_1 in equation (4.3.15) is exactly the same as that of a_0 in extrapolation formula I.

At large E, $R/R_2 = e^{-(a_1 + a_2 + a_3 + \text{----})}$ 4.3.17

$$\theta_3 = \frac{E_0}{\pi} \int_{E_2}^{\infty} \frac{\ell n\ R/R_0}{E_0^2 - E^2}\, dE$$

$$= -\frac{E_0}{\pi} \int_{E_2}^{\infty} \frac{\ell n R/R_2 + \ell n\ R_2/R_0}{E^2 - E_0^2}\, dE$$

$$= \frac{E_0}{\pi} \int_{E_2}^{\infty} \frac{\ell n\ R_0/R_2}{E^2 - E_0^2}\, dE - \frac{E_0}{\pi} \int_{E_2}^{\infty} \frac{\ell n\ R/R_2}{E^2 - E_0^2}\, dE$$

$$= X + \frac{E_0}{\pi} \int_{E_2}^{\infty} \frac{\Sigma a_n\ (1 - E_2/E)^n}{E^2 - E_0^2}\, dE$$

$$= X + \sum_{n=1} a_n I_n \qquad 4.3.18$$

where $$I_n = \frac{E_0}{\pi} \int_{E_2}^{\infty} \frac{(1 - E_2/E)^n}{(E^2 - E_0^2)}\, dE$$

$$= \frac{1}{\pi} \sum_{m=1} \frac{\lfloor n \quad \lfloor 2m - 2}{\lfloor 2m + n - 1} (E_0/E_2)^{2m-1} \qquad 4.3.19$$

and $$\theta_{cal} = \theta_1 + \theta_2 + X + a_1 I_1 + \sum_{n=2} a_n I_n \qquad 4.3.20$$

where X is same as that of extrapolation formula I. Using the same Least Squares method as with formula I, we get

$$\sum_p [\ \{\theta_{pexp} - f(E_{0_p})\ \} - a_2 I_2(E_{0_p}) - a_3 I_3(E_{0_p})\ ]\ x\ I_2(E_{0_p}) = 0 \qquad 4.3.21$$

and $$\sum_p [\ \{\theta_{pexp} - f(E_{0_p})\ \} - a_2 I_2(E_{0_p}) - a_3 I_3(E_{0_p})\ ]\ x\ I_3(E_{0_p}) = 0 \qquad 4.3.22$$

------etc., respectively.

where $(\theta_1 + \theta_2 + X + a_1 I_1) = f$ and equations (4.3.21) and (4.3.22) ------ etc., give the values of the a's. n and k may then be found as before.

Extrapolation formula III

$$R/R_2 = (E_2/E)^4 \; e^{-[\, a_1(1 - E_2/E) + a_2(1 - E_2/E)^2 + \text{-------} \,]} \qquad 4.3.23$$

and consequently $\ell n\, R/R_2 = 4\, \ell n\, E_2/E - \sum_{n=1} a_n (1 - E_2/E)^n$ 4.3.24

Equation (4.3.24) gives $R = R_2$ at $E = E_2$. 4.3.25

For continuity, $R'(exp) = \dfrac{-(a_1+4)}{E_2}$ 4.3.26

At large E, (4.3.23) reduces to

$$R/R_2 = e^{-(a_1 + a_2 + a_3 + \text{-----})(E_2/E)^4} \qquad 4.3.27$$

This may be regarded as more acceptable behaviour than that of the other formulae.

$$\theta_3 = X - \frac{E_0}{\pi} \int_{E_2}^{\infty} \frac{\ell n\, R/R_2}{E^2 - E_0^2}\, dE$$

$$= X - \frac{4E_0}{\pi} \int_{E_2}^{\infty} \frac{\ell n\, E_2/E}{E^2 - E_0^2}\, dE$$

$$+ \frac{E_0}{\pi} \int_{E_2}^{\infty} \frac{\Sigma a_n\, (1 - E_2/E)^n}{E^2 - E_0^2}\, dE$$

$$= X - 4I_0 + \sum_{n=1} a_n I_n \qquad 4.3.28$$

where X and I_0 are as for the extrapolation formula I and the I_n's for n=1, 2 ---- etc., are as for the extrapolation formula II

i.e. $$I_0 = \frac{-1}{\pi} \sum_{m=o} \frac{1}{(2m+1)^2} (E_0/E_2)^{2m+1}$$

and $$I_n = \frac{1}{\pi} \sum_{m=1} \frac{\lfloor n \quad \lfloor 2m-2}{\lfloor 2m+n-1} (E_0/E_2)^{2m-1} \qquad 4.3.29$$

$$\theta_3 = X - 4I_0 + a_1 I_1 + \sum_{n=2} a_n I_n \qquad 4.3.30$$

$$\theta_{cal} = \theta_1 + \theta_2 + X - 4I_0 + a_1 I_1 + \sum_{n=2} a_n I_n$$

$$= f + \sum_{n=2} a_n I_n \qquad 4.3.31$$

where $f = \theta_1 + \theta_2 + X - 4I_0 + a_1 I_1$

Determination of the a's and finally of n and k proceeds as before.

4.4 Discussion of the extrapolation formulae

The values of θ shown in Figure (4.4) were calculated by using the extrapolation formula III for two and three arbitrary parameters by using the Least Squares method as well as the direct method of fitting the theoretical curve to two or three points of the experimental curve covering the range 1.8 to 4.0 eV.

For extrapolation formulae II and III the equations for curve fitting at two reference points are, as explained in Section (4.3) of the form

$$a_2 I_{21} + a_3 I_{31} = f_1 \qquad 4.4.1$$

$$a_2 I_{22} + a_3 I_{32} = f_2 \qquad 4.4.2$$

where $$I_{np} = \frac{1}{\pi} \sum_{m=1} \frac{\lfloor n \quad \lfloor 2m-2}{\lfloor 2m+n-1} (E_0/E_2)_p^{2m-1}$$

$$= \frac{1}{\pi} \sum_{m=1} Anm \, (x_p)^{2m-1} \qquad 4.4.3$$

and $x_p = (E_0/E_2)_p = E_{0p}/E_2$ where E_{0p} is the pth reference point. From the equations (4.4.1) and (4.4.2) the values of a_2 and a_3 are of the form

$$a_2 = \frac{f_1 I_{32} - f_2 I_{31}}{I_{21} I_{32} - I_{22} I_{31}} \qquad 4.4.4$$

and

$$a_3 = \frac{f_2 I_{21} - f_1 I_{22}}{I_{21} I_{32} - I_{31} I_{22}} \qquad 4.4.5$$

From equation (4.4.3)

$$I_{21} = \frac{2}{\pi}\left[\frac{1}{1.2.3} x_1 + \frac{1}{3.4.5} x_1^3 + \frac{1}{5.6.7} x_1^5 \text{ --- }\right]$$

$$= \alpha_1 x_1 + \alpha_2 x_1^3 + \alpha_3 x_1^5 + \text{----} \qquad 4.4.6$$

where $\alpha_1 = \frac{2}{\pi}\frac{1}{1.2.3}$, $\alpha_2 = \frac{2}{\pi}\frac{1}{3.4.5}$, $\alpha_3 = \frac{2}{\pi}\frac{1}{5.6.7}$

$$I_{31} = \frac{6}{\pi}\left(\frac{1}{1.2.3.4} x_1 + \frac{1}{3.4.5.6} x_1^3 + \frac{1}{5.6.7.8} x_1^5 + \text{---}\right)$$

$$= 3(\tfrac{1}{4}\alpha_1 x_1 + 1/6\ \alpha_2 x_1^3 + 1/8\ \alpha_3 x_1^5 + \text{---}) \qquad 4.4.7$$

Similarly the values of I_{32} and I_{22} can be determined from the equation (4.4.3). Now putting the values of I_{21}, I_{22}, I_{31}, I_{32} in equations (4.4.4) and (4.4.5) and neglecting the higher powers of x_1^3, x_2^3, x_1^5, x_2^5 (being very small), the approximate values of a_2 and a_3 are of the form

$$a_2 = \frac{3/4\ (f_1 x_2 - f_2 x_1)}{x_1 x_2 (x_1^2 - x_2^2)\tfrac{1}{4}\alpha_2} \qquad 4.4.8$$

and

$$a_3 = \frac{-\ (f_1 x_2 - f_2 x_1)}{x_1 x_2 (x_1^2 - x_2^2)\tfrac{1}{4}\alpha_2} \qquad 4.4.9$$

which are of the order of x^{-3} and the ratio of

$$a_3/a_2 = -4/3 = -1.333 \qquad 4.4.10$$

In a similar way it can be proved that if the extrapolation formula I is used the values of the corresponding parameters a_1 and a_2 are also of the order of x^{-3}.

Similarly solving the three simultaneous equations for three arbitrary parameters viz.

$$a_2 I_{21} + a_3 I_{31} + a_4 I_{41} = f_1 \qquad 4.4.11$$

$$a_2 I_{22} + a_3 I_{32} + a_4 I_{42} = f_2 \qquad 4.4.12$$

$$a_2 I_{23} + a_3 I_{33} + a_4 I_{43} = f_3 \qquad 4.4.13$$

it can be proved that the values of all the a's are of the order of x^{-5} i.e. $(E_0/E_2)^{-5}$.

Thus for the two arbitrary parameters, the a's are of the order of $(E_0/E_2)^{-3}$ and, for three parameters, the a's are of the order of $(E_0/E_2)^{-5}$, and so on for four, five or more parameters. If E_2 is much larger inclusion of more parameters makes them numerically very large.

A similar situation arises if the Least Squares method is used either for extrapolation formula I, II or III (see Appendix B).

In the present investigation the reference points of 1.8, 2.25, 2.4, 2.8 and 3.6 eV were chosen after examination of the ε_2 versus energy curve determined from direct measurements.

The direct method with E_2 = 10 eV and curve fitting at the single point E_0 = 3.6 eV gave a_1= - 2.0048 and a_2 = - 0.7140. With two reference points at E_0 = 1.8 and 3.6 eV, the result was a_1= -2.0048, a_2 = - 509.6 and a_3 = 681.6.

The values of a's depend of course upon the choice of reference points. The Least Squares method employing four reference points (1.8, 2.25, 2.4 and 3.6 eV) for E_2=15 eV with two parameters gave $a_1 = -0.948$, $a_2 = -0.2169$, and with three parameters gave $a_1 = -0.948$, $a_2 = -1143.4$ and $a_3 = 1526.5$. Figures (4.3) and (4.4) show the resulting θ, E_0 curves for these various extrapolations.

The extrapolation formulae are such that in principle one can use as many a's as one likes, but the values of the R's are correct at best to three significant figures and this limits the accuracy with which the a's may be calculated. When more higher order terms are used the a's become larger and the exponent in the extrapolation formulae involves the difference of very large numbers which can be found only with very limited accuracy. It is therefore impossible to include more than two or three terms in the approximation unless E_0 can be chosen near to E_2. This applies whether the curve fitting method or the Least Squares method is used.

In case of the direct method of curve fitting at one or two points, the resulting values of the a's depend very much upon the choice of reference points, but with the Least Squares method, the choice of reference points appears to be much less critical and for this reason this method is to be preferred.

The difficulty with the proposed method is that so far the direct measurement of n and k is possible to about 4 eV whereas the experimental measurement of reflectivity can be carried out to 10 eV

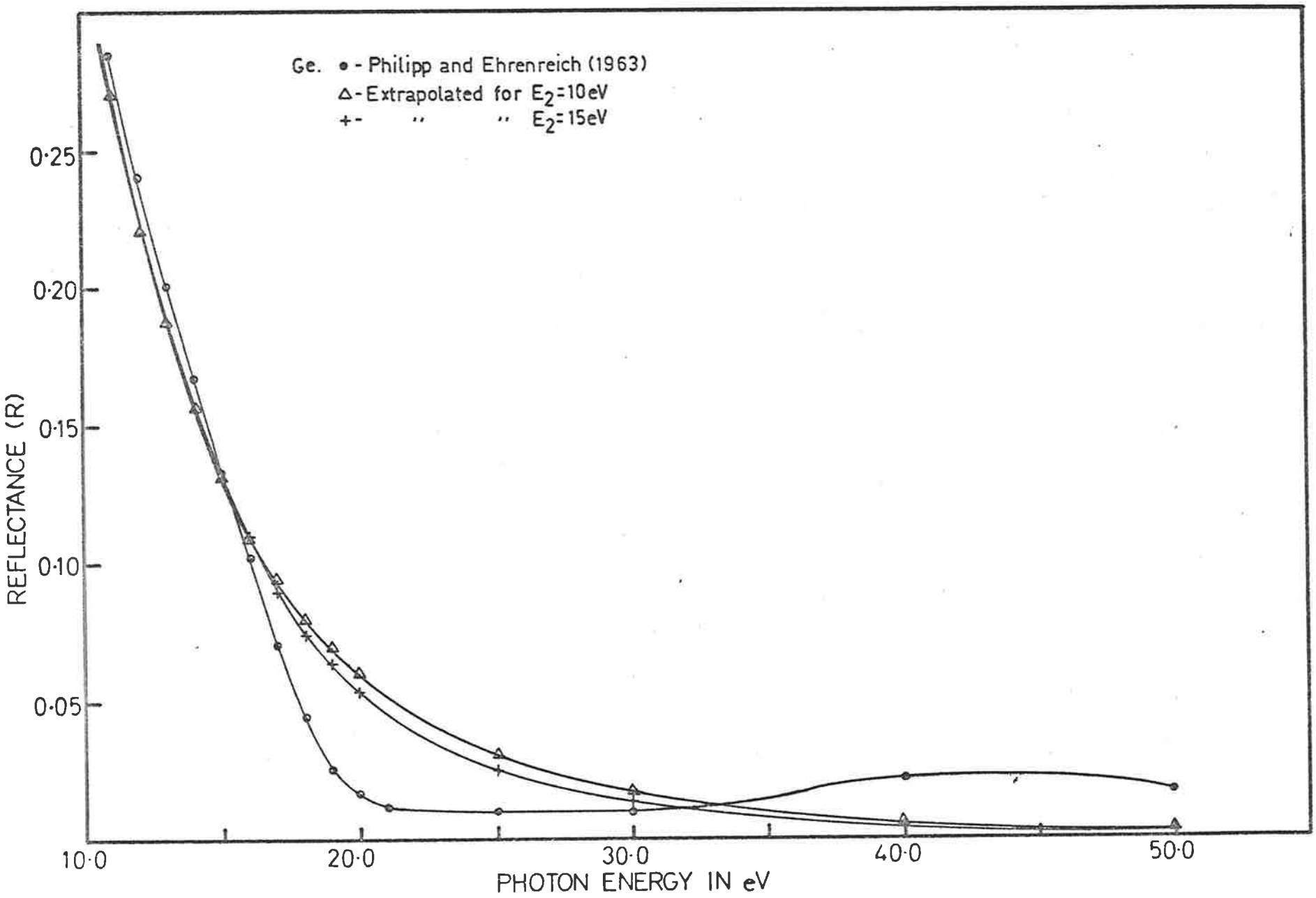
Ge. • - Philipp and Ehrenreich (1963)
△ - Extrapolated for E_2=10eV
+ - " " E_2=15eV
0·25
0·20
0·15
0·10
0·05
REFLECTANCE (R)
10·0
20·0
30·0
40·0
50·0
PHOTON ENERGY IN eV

Fig. 4.2

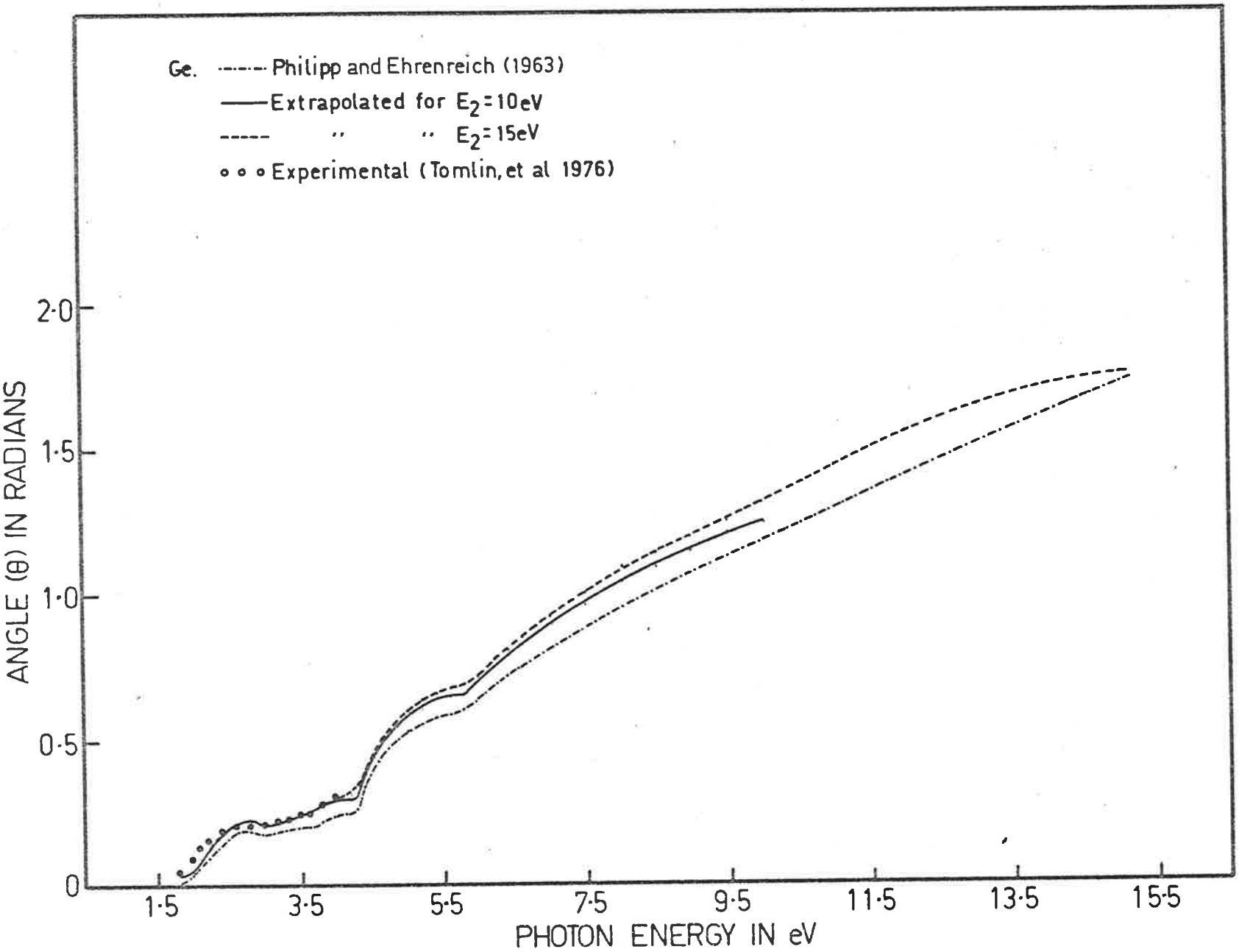
Ge. ----- Philipp and Ehrenreich (1963)
——Extrapolated for E_2=10eV
----- " " E_2=15eV
o o o Experimental (Tomlin, et al 1976)
ANGLE (θ) IN RADIANS
2·0
1·5
1·0
0·5
0
1·5
3·5
5·5
7·5
9·5
11·5
13·5
15·5
PHOTON ENERGY IN eV

Fig. 4.3

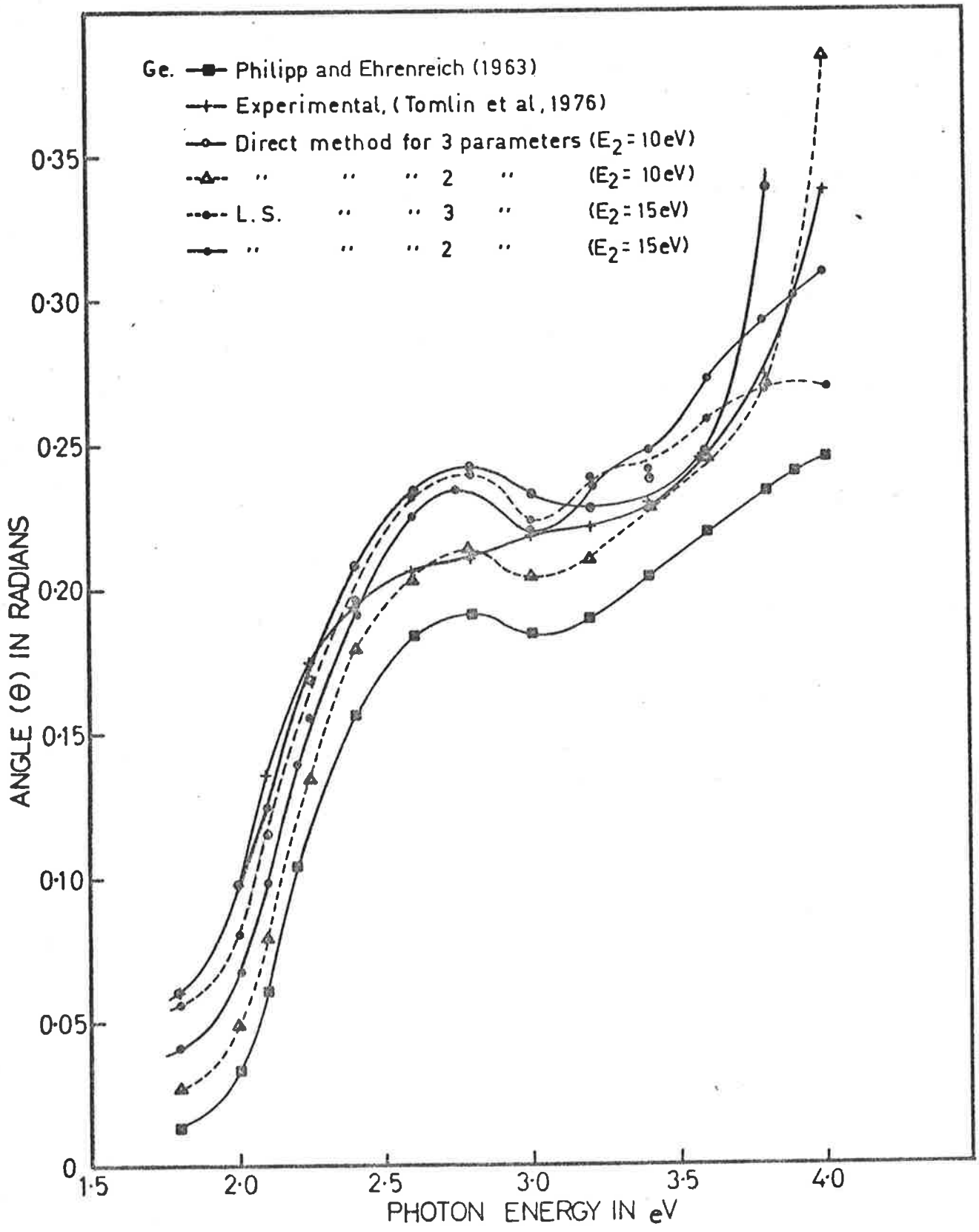
Ge. Philipp and Ehrenreich (1963)
Experimental, (Tomlin et al, 1976)
Direct method for 3 parameters (E_2 = 10eV)
" " " 2 " (E_2 = 10eV)
L.S. " " 3 " (E_2 = 15eV)
" " " 2 " (E_2 = 15eV)
ANGLE (θ) IN RADIANS
0·35
0·30
0·25
0·20
0·15
0·10
0·05
0
1·5
2·0
2·5
3·0
3·5
4·0
PHOTON ENERGY IN eV

Fig. 4·4

or even higher energies and the extrapolation is needed beyond this range i.e. beyond $E_2 = 10$ eV . But as has been shown, the values of the a's increase rapidly with higher powers of (E_2/E_0) as the number of constants is increased. Since very large values of the a's which can be relied on to only three significant figures lead to large errors in the extrapolation formulae, good results can be expected only if E_2 is not too much greater than E_0 . This is made clear by the results computed for $E_2 = 10$ and 15 eV (Figure 4.8) which show that the extrapolated values of optical constants for $E_2 = 10$ eV ($a_1 = -2.0048$ and $a_2 = -0.2597$) are closer to the extrapolated values of Philipp than for $E_2 = 15$ eV ($a_1 = -0.9480$ and $a_2 = -0.2169$), see Appendix B and Figure (4.9).

It should be emphasized that, in this consideration of the extrapolation procedures, direct experimental measurements of n and k were made on different specimens from those used for reflectance measurements of Philipp. Clearly all measurements should be made on the same specimens but I have not been able to do this. If this could be done satisfactorily, it would be expected that the use of the proposed extrapolation procedures should be an improvement on the rather crude methods that have been commonly used, the more so if a substantial improvement in the accuracy of measuring reflectances and transmittances could be effected.

4.5 Results and conclusions

The results of various computations are given in detail in Appendix B . The values of the parameters of the extrapolation formulae, calculated for crystalline Ge using the experimental results of

Tomlin *et al* (1976) in the range 1.8 to 4.0 eV together with the experimental data of Philipp and Ehrenreich (1963), may be tabulated in Table (4.1) as follows.

TABLE 4.1

Method		E_2 in eV	Extrapolation Formula I	Extrapolation Formula II	Extrapolation Formula III
Least Squares Method with four reference points	at E_0 = 1.8, 2.25, 2.4 and 3.6 eV	10	a_0= 1.9952 a_1= 1.0791	a_1= 1.9952 a_2= 5.7151	a_1= - 2.0048 a_2= - 0.2597
		15	a_0= 3.0521 a_1= 0.5334	a_1= 3.0521 a_2= 5.3690	a_1= - 0.9480 a_2= - 0.2169
		15			a_1= - 0.9480 a_2= - 1143.4 a_3= 1526.5
Curve Fitting	at E_0 = 3.6 eV	10			a_1= - 2.0048 a_2= - 0.7140
	at E_0 = 1.8 and 3.6 eV	10			a_1= - 2.0048 a_2= - 509.6 a_3= 681.6

Using these results the extrapolated reflectance curves of Figure (4.2) were obtained and are plotted together with the reflectances of Philipp and Ehrenreich (1963, Figure 4.1).

The optical constants obtained by the K-K method using one of those extrapolations are shown in Figures (4.5), (4.6), (4.8) and (4.9)

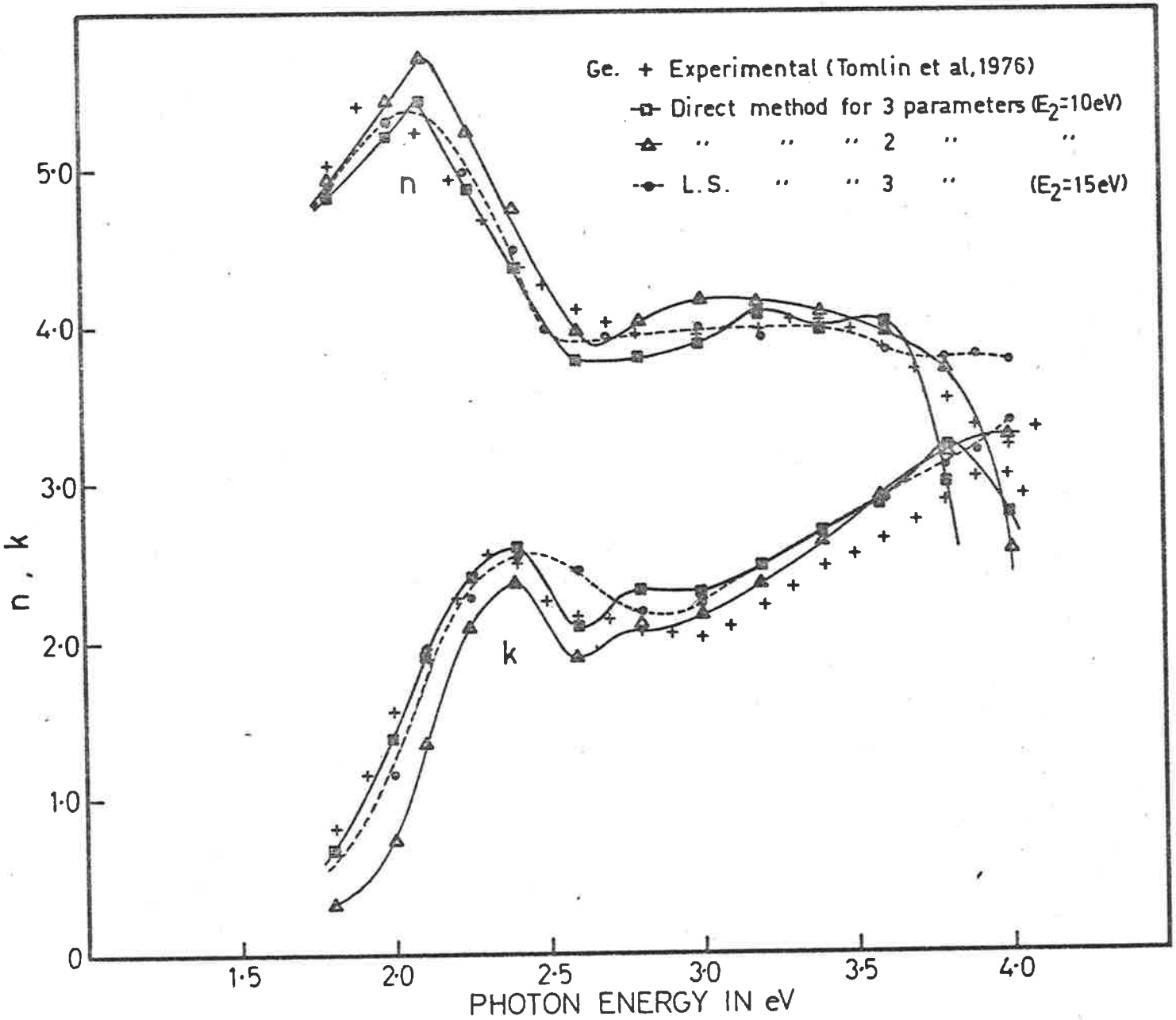
Ge. + Experimental (Tomlin et al, 1976)
Direct method for 3 parameters (E_2=10eV)
" " " 2 " "
L.S. " " 3 " (E_2=15eV)
n
k
n , k
5·0
4·0
3·0
2·0
1·0
0
1·5
2·0
2·5
3·0
3·5
4·0
PHOTON ENERGY IN eV

Fig.4.5

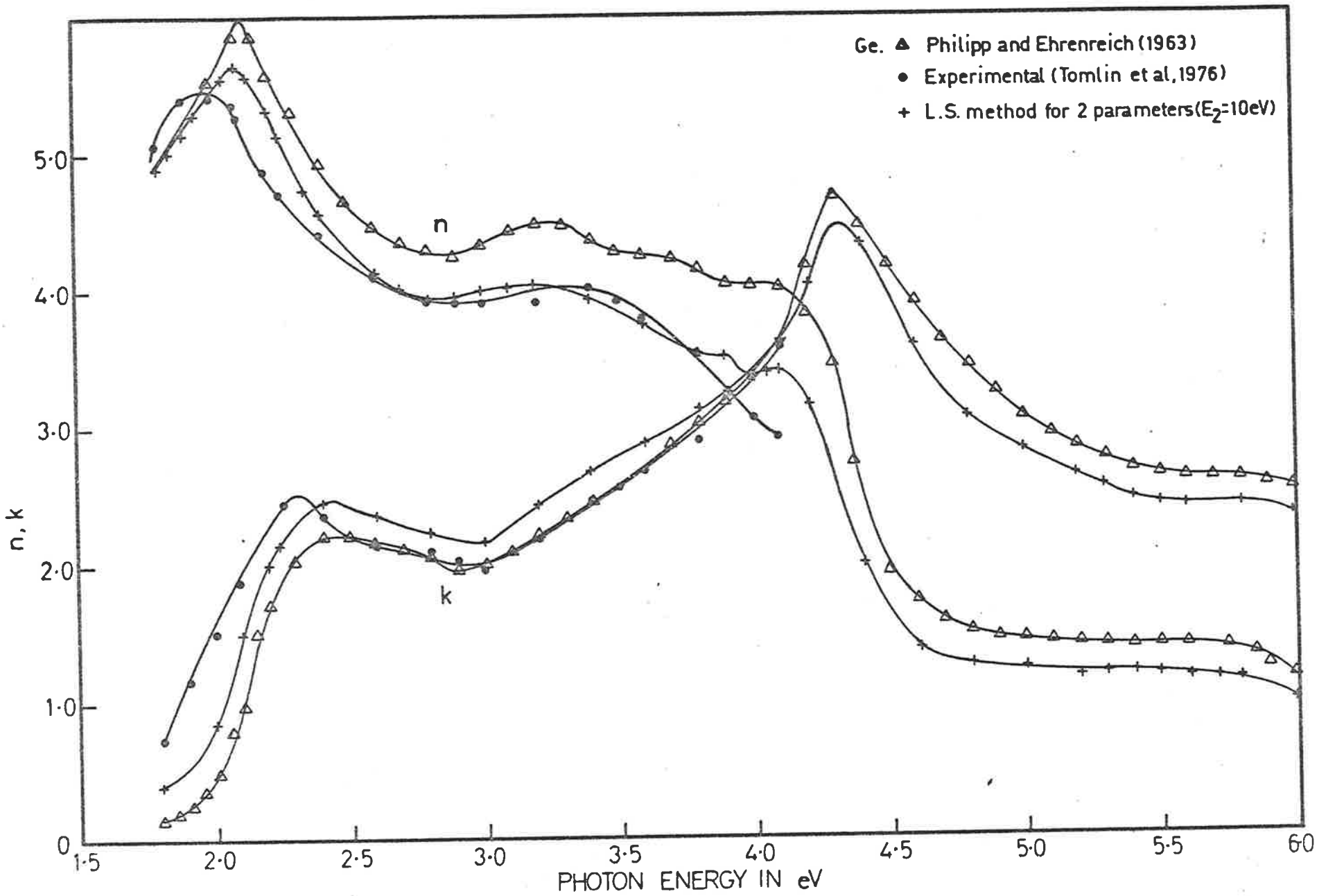
Ge. ▲ Philipp and Ehrenreich (1963)
● Experimental (Tomlin et al, 1976)
+ L.S. method for 2 parameters(E_2=10eV)
n
k
n, k
PHOTON ENERGY IN eV
0
1·0
2·0
3·0
4·0
5·0
1·5
2·0
2·5
3·0
3·5
4·0
4·5
5·0
5·5
6·0

Fig. 4.6

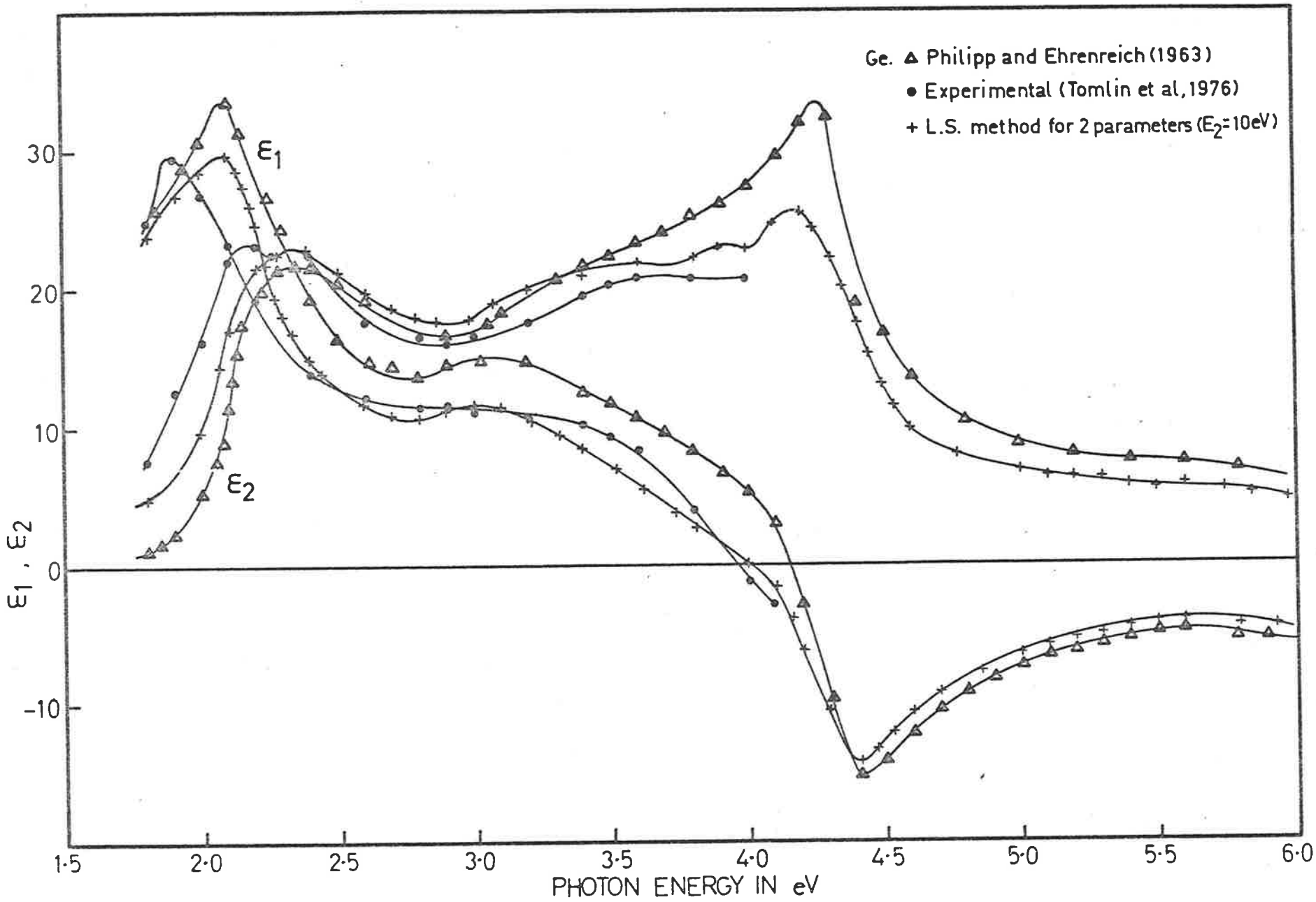
Ge. △ Philipp and Ehrenreich (1963)
● Experimental (Tomlin et al, 1976)
+ L.S. method for 2 parameters (E_2=10eV)
ε_1
ε_2
30
20
10
0
-10
ε_1 , ε_2
1·5
2·0
2·5
3·0
3·5
4·0
4·5
5·0
5·5
6·0
PHOTON ENERGY IN eV

Fig. 4.7

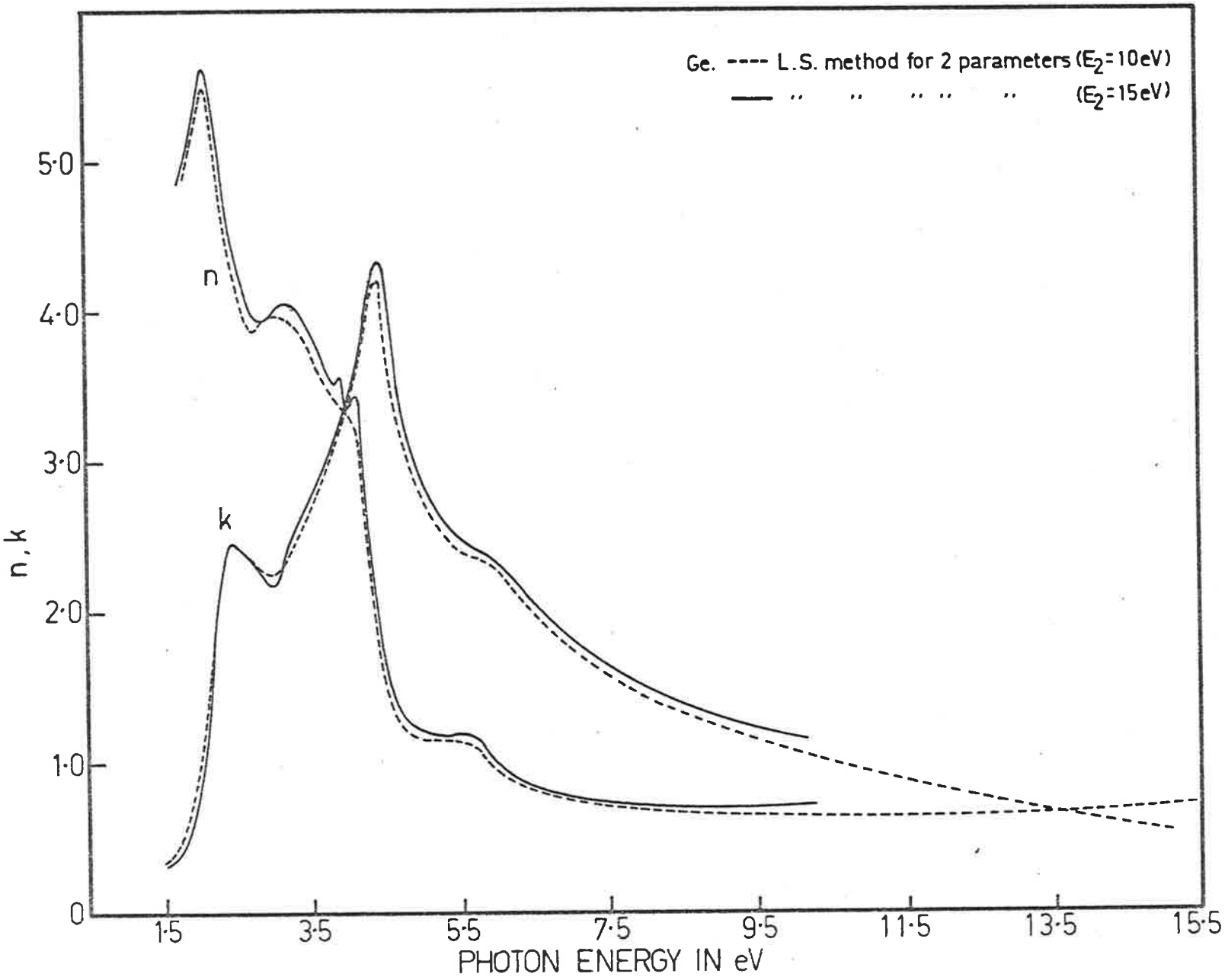
Ge. ---- L.S. method for 2 parameters (E_2=10eV)
—— ,, ,, ,, ,, ,, (E_2=15eV)
n
k
n, k
5·0
4·0
3·0
2·0
1·0
0
1·5
3·5
5·5
7·5
9·5
11·5
13·5
15·5
PHOTON ENERGY IN eV

Fig. 4.8

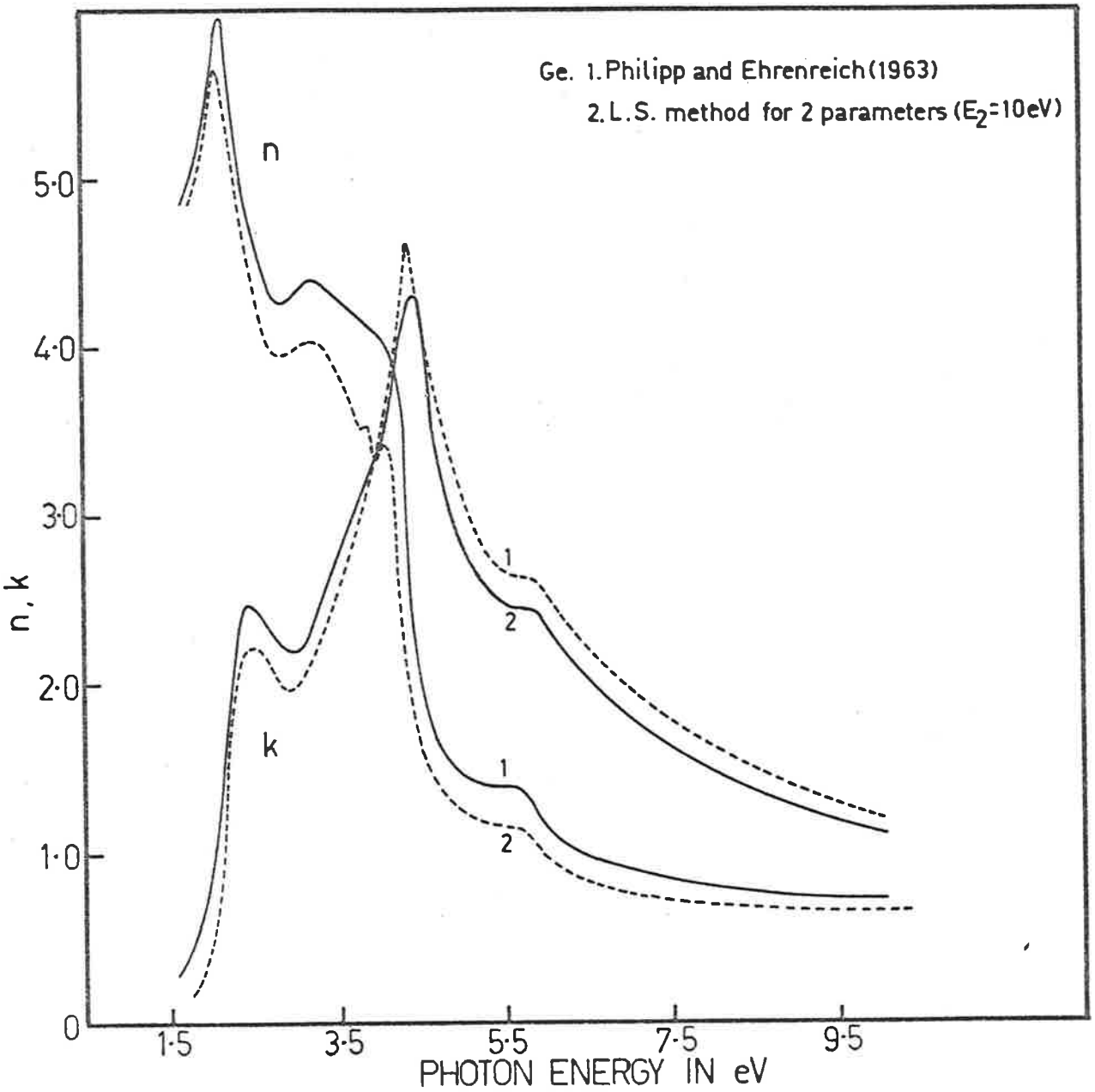
Ge. 1. Philipp and Ehrenreich (1963)
2. L.S. method for 2 parameters (E_2=10eV)
n
k
1
2
1
2
n, k
5·0
4·0
3·0
2·0
1·0
0
1·5
3·5
5·5
7·5
9·5
PHOTON ENERGY IN eV

Fig. 4.9

together with the results of Philipp and Ehrenreich (1963). Figure (4.7) shows the corresponding curves for ε_1 and ε_2, the real and imaginary parts of the complex dielectric constant, and includes the results of direct measurements in the range 1.8 to 4.0 eV. These latter results give an ε_2 curve with a doublet structure having components at 2.15 and 2.35 eV with a minor peak at 3.65 eV, but do not extend as far as the conspicuous maximum of the K-K curves at 6.0 eV.

Instead of the doublet nature of the $\Lambda_1 \rightarrow \Lambda_3$ transition (For details see Chapter 3), a single peak appears at 2.35 eV due to the transition $\Lambda_1 \rightarrow \Lambda_3 + \Delta S_o$, both in the extrapolated as well as Philipp and Ehrenreich's (1963) curves, but the peak corresponding to the transition $\Lambda_1 \rightarrow \Lambda_3$ appears in the real part of the dielectric constant ε_1 where ΔS_o represents the effect of spin orbit interaction. Using the new extrapolation procedures, the resulting curves show evidence of more detailed structures. The peaks at 3.55, 3.95 and 4.2 eV may be attributed to the transitions $\Gamma_{15} \rightarrow \Gamma_{25}'$, $X_1 \rightarrow X_4$, $\Sigma_1 \rightarrow \Sigma_4$ (Abeles 1972). Philipp and Ehrenreich's results from K-K analysis do not show all of these features but only a single peak at 4.27 eV.

Unfortunately a very firm conclusion about the value of the new method cannot be reached because we have no results for reflectivity measurements over a wide range of energies for the same specimens as were used for the direct measurements of n and k. Therefore it has not yet been possible to make a thorough assessment of the new extrapolations but it may be claimed that they show at least some slight advantages and are worthy of further study.

CHAPTER 5

DETERMINATION OF THE OPTICAL CONSTANTS OF OPAQUE SOLIDS (OR FILMS) OR ABSORBING MATERIALS

5.1 Introduction

In the previous chapter direct measurements of the optical constants of Ge in the absorbing region which had been made by Tomlin's method (1972) were used as a basis for improving the extrapolation procedures required in the application of the Kramers-Kronig relations. The remainder of this thesis will be concerned with a preliminary study of the application of this method of direct measurement to metals over the photon energy range of 0.62 to 4.0 eV (for Au 1.7 to 4.2 eV). A normal incidence method for this energy range alone would be valuable but has the added interest that might be helpful in applying the Kramers-Kronig method over a much wider range. Here some further discussion of the method will be given with an extension to the case where light is incident from the substrate side and passes through a thin transparent layer before falling on the opaque specimen. This requires consideration of the general case of light incident from air on to three layers each with optical constants of the form $n - ik$. From this general case the formulae applicable when light is incident through a substrate can be obtained, and also the case if the absorption in the applied transparent layer may be considered. The corresponding formulae for a specimen which may be treated as a single layer are also obtained by putting the appropriate film thickness equal to zero. (see Appendix C).

5.2 Equations for single layer absorbing films

The reflectance of a bulk specimen or opaque film which does not transmit is given by

$$R = \frac{(n_2 - n_0)^2 + k_2^2}{(n_2 + n_0)^2 + k_2^2} \qquad 5.2.1$$

where n_0 is the refractive index of air and $n_2 - ik_2$ is the complex refractive index of the bulk specimen or opaque film. If a transparent layer of thickness d_1 and refractive index n_1 is deposited on this specimen the resulting reflectance R_1 may be derived from the single layer formulae of Tomlin (1968). From these expressions one finds

$$\frac{1 + R_1}{1 - R_1} = \frac{1}{4n_0 n_1^2 n_2} [(n_0^2 + n_1^2)(n_1^2 + n_2^2 + k_2^2) + (n_0^2 - n_1^2) \{ (n_1^2 - n_2^2 - k_2^2) \cos 2\gamma_1 + 2n_1 k_2 \sin 2\gamma_1 \}] \qquad 5.2.2$$

where $\gamma_1 = 2\pi n_1 d_1/\lambda$ and λ is the wavelength.

The equation (5.2.1) can be written as

$$\{ n_2 - n_0 \frac{(1 + R)}{(1 - R)} \}^2 + k_2^2 = \frac{4n_0^2 R}{(1 - R)^2} \qquad 5.2.3$$

which is a circle in the n_2, k_2 plane with centre $n_0(1 + R)/(1 - R)$, 0 and radius $\frac{2 n_0 \sqrt{R}}{(1 - R)}$.

Equations (5.2.2) and (5.2.3) give

$$k_2 = \frac{n_1^2 + n_0^2}{2n_1} \tan\gamma_1 + \frac{2n_0}{n_1 (n_1^2 - n_0^2)} \frac{1}{\sin 2\gamma_1} x \{ \frac{(1 + R)}{(1 - R)} (n_1^2 \cos^2\gamma_1 + n_0^2 \sin^2 \gamma_1) - n_1^2 \frac{(1 + R_1)}{(1 - R_1)} \} n_2 \qquad 5.2.4$$

this equation (5.2.4) is a straight line in the n_2, k_2 plane.

Now equation (5.2.3) can be written as

$$k_2^2 = 2n_2 \frac{(1 + R)}{(1 - R)} - (n_2^2 + 1) \qquad 5.2.5$$

or $$k_2 = \pm \{ 2n_2 \frac{(1 + R)}{(1 - R)} - (n_2^2 + 1) \}^{\frac{1}{2}} \qquad 5.2.6$$

Equation (5.2.6) shows that for a given value of n_2 and R, k_2 has two values which are equal in magnitude but differ in sign only. The positive values of k_2 are acceptable but the negative values of k_2 must be considered in order to obtain the complete solutions of the simultaneous equations. Khawaja (1975a) solved the equations for n_2 and k_2 by calculating the values of the right-hand side of the equation (5.2.2) for given values of n_2 and the corresponding values of k_2 obtained from equation (5.2.4) and comparing with the known values of $\frac{(1 + R_1)}{(1 - R_1)}$. This iterative method (for details see Khawaja 1975a) of computing solutions is unnecessary and has been replaced by the following simpler method.

By substituting the values of k_2 given by equation (5.2.4) in equation (5.2.3) one obtains a quadratic equation in n_2. Although this has complicated coefficients it is easily solved numerically to give n_2 and consequently the values of k_2. This method of solving the quadratic equation for n_2 and k_2 is very direct and straightforward and less time consuming than the iterative method.

In order to carry out the solutions for n_2 and k_2 the film thickness must be known. A good estimate of the thickness d_1 is obtained from the equation (5.2.2) utilizing the following conditions.

Condition I

$R = R_1$ when

$$\gamma_1 = P\pi - \tan^{-1}\left|\frac{2\, n_1 k_2}{(n_1^2 - n_2^2 - k_2^2)}\right|$$

where p is an integer.

Condition II

if $\gamma_1 = P\pi$, then $R = R_1$

Condition III

R_1 has a maximum, when

$$\gamma_1 = P\pi - \frac{1}{2}\tan^{-1}\left|\frac{2\, n_1 k_2}{(n_1^2 - n_2^2 - k_2^2)}\right|$$

Condition II gives a straightforward way of determining the approximate value of d_1, because it involves only the known optical constant of the overlying layer.

We next consider the case where the transparent film is first deposited on a transparent substrate and the metal is evaporated on to the film. The light is then incident through the substrate. See Figure 5.1. (on following page). The reflectance R from the opaque specimen, when there is no transparent film, and when the light is incident from the substrate side, whose refractive index is n_3 , is given by

$$R = \frac{(n_2 - n_3)^2 + k_2^2}{(n_2 + n_3)^2 + k_2^2} \qquad 5.2.7$$

where n_2 and k_2 refer to the metal. The reflectance R_1 from a similar metal film when it is deposited on a transparent layer of refractive index n_1 and illuminated through the substrate is given by an obvious modification of equation (5.2.2) :-

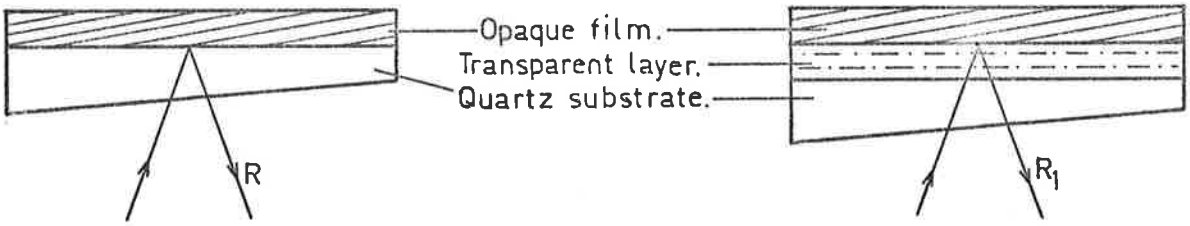

FIG. 5.1

$$\frac{1 + R_1}{1 - R_1} = \frac{1}{4n_3 n_1^2 n_2} \left[(n_3^2 + n_1^2)(n_1^2 + n_2^2 + k_2^2) + (n_3^2 - n_1^2) \{ (n_1^2 - n_2^2 - k_2^2) \cos 2\gamma_1 + 2n_1 k_2 \sin 2\gamma_1 \} \right] \qquad 5.2.8$$

Again from equations (5.2.7) and (5.2.8) a quadratic equation for n_2 may be obtained and solved directly to give numerical values for n_2 and k_2 .

5.3 Equations for a double layer on an opaque specimen

Consider first a film with optical constants n_2, k_2 on a substrate with constants n_3, k_3 . The normal incidence reflectance R_1 and the transmittance T_1 into the substrate are given by (Tomlin 1968).

$$\frac{1 + R_1}{T_1} = \frac{1}{4n_0 n_3 (n_2^2 + k_2^2)} \phi_1 \qquad 5.3.1$$

$$\frac{1 - R_1}{T_1} = \frac{1}{2n_3 (n_2^2 + k_2^2)} \phi_2 \qquad 5.3.2$$

n_0 is the refractive index of the non-absorbing medium (here air) from which the light is incident and

$$\phi_1 = (n_0^2 + n_2^2 + k_2^2)\{(n_2^2 + n_3^2 + k_2^2 + k_3^2)\cos h2\alpha_2 + 2(n_2n_3 + k_2k_3)\sin h2\alpha_2 + (n_0^2 - n_2^2 - k_2^2)\{(n_2^2 - n_3^2 + k_2^2 - k_3^2)\cos 2\gamma_2 + 2(n_2k_3 - n_3k_2)\sin 2\gamma_2\} \quad 5.3.3$$

and

$$\phi_2 = n_2[(n_2^2 + n_3^2 + k_2^2 + k_3^2)\sin h2\alpha_2 + 2(n_2n_3 + k_2k_3)\cos h2\alpha_2] + k_2[(n_2^2 - n_3^2 + k_2^2 - k_3^2)\sin 2\gamma_2 - 2(n_2k_3 - n_3k_2)\cos 2\gamma_2]$$

where $\gamma_2 = \frac{2\pi n_2 d_2}{\lambda}$ and $\alpha_2 = \frac{2\pi k_2 d_2}{\lambda}$ 5.3.4.

and d_2 is the film thickness.

Now from the equations (5.3.1) and (5.3.2) we get

$$\phi_1 - 2n_0 \frac{(1 + R_1)}{(1 - R_1)} \phi_2 = 0 \quad 5.3.5$$

If another transparent layer of refractive index n_1 (k_1=0) and thickness d_1 is deposited on the top of the layer defined by n_2,k_2 and d_2, then R_2, the reflectance for the double layer on the substrate is given by the equation (Tomlin 1972).

$$2n_0 \frac{(1 + R_2)}{(1 - R_2)} = \frac{(n_0^2 + n_1^2) F_1 + (n_0^2 - n_1^2) F_2}{n_1 G_1} \quad 5.3.6$$

where $G_1 = 4n_1 \phi_2$ 5.3.7

$$\phi_2 = n_2C + k_2D \quad 5.3.8$$

$$\phi_1 = (n_0^2 + n_2^2 + k_2^2) A + (n_0^2 - n_2^2 - k_2^2) B \quad 5.3.9$$

$$\frac{1}{2}F_1 = (n_1^2 + n_2^2 + k_2^2)\,A + (n_1^2 - n_2^2 - k_2^2)\,B \qquad 5.3.10$$

$$\frac{1}{2}F_2 = [\,(n_1^2 - n_2^2 - k_2^2)\,A + (n_1^2 + n_2^2 + k_2^2)\,B\,]\cos 2\gamma_1 - 2n_1\,(n_2D - k_2C)\sin 2\gamma_1 \qquad 5.3.11$$

$$A = (n_3^2 + k_3^2)\cos h\,2\alpha_2 + 2\,(n_2n_3 + k_2k_3)\sin h\,2\alpha_2 + (n_2^2 + k_2^2)\cos h\,2\alpha_2 \qquad 5.3.12$$

$$B = -(n_3^2 + k_3^2)\cos 2\gamma_2 - 2\,(k_2n_3 - n_2k_3)\sin 2\gamma_2 + (n_2^2 + k_2^2)\cos 2\gamma_2 \qquad 5.3.13$$

$$C = (n_3^2 + k_3^2)\sin h2\alpha_2 + 2\,(n_2n_3 + k_2k_3)\cos h\,2\alpha_2 + (n_2^2 + k_2^2)\sin h\,2\alpha_2 \qquad 5.3.14$$

$$D = -(n_3^2 + k_3^2)\sin 2\gamma_2 + 2\,(k_2n_3 - n_2k_3)\cos 2\gamma_2 + (n_2^2 + k_2^2)\sin 2\gamma_2 \qquad 5.3.15$$

Equation (5.3.6) may be written

$$(n_0^2 + n_1^2)\,F_1 + (n_0^2 - n_1^2)\,F_2 - 8\,n_0n_1^2\,\frac{1 + R_2}{1 - R_2}\,\phi_2 = 0 \qquad 5.3.16$$

Equation (5.3.5) becomes, on substituting for ϕ_1 and ϕ_2,

$$(n_3^2 + k_3^2)\,P_1 + 2n_3Q_1 + 2\,S_1k_3 + U_1 = 0$$

$$\text{or} \quad (n_3^2 + k_3^2) + \frac{2Q_1}{P_1}\,n_3 + 2\,\frac{S_1}{P_1}\,k_3 + \frac{U_1}{P_1} = 0 \qquad 5.3.17$$

and similarly equation (5.3.16) becomes

$$(n_3^2 + k_3^2) + \frac{2Q_2}{P_2}\,n_3 + \frac{2\,S_2}{P_2}\,k_3 + \frac{2\,S_2}{P_2}\,k_3 + \frac{U_2}{P_2} = 0 \qquad 5.3.18$$

where

$$P_1 = [\,(n_0^2 + n_2^2 + k_2^2)\cosh 2\alpha_2 - (n_0^2 - n_2^2 - k_2^2)\cos 2\gamma_2 - 2n_0\,\frac{(1 + R_1)}{(1 - R_1)}\,(n_2 \sinh 2\alpha_2 - k_2 \sin 2\gamma_2)\,]$$

$$Q_1 = \{\,(n_0^2 + n_2^2 + k_2^2)\, n_2 \sinh 2\alpha_2 - (n_0^2 - n_2^2 - k_2^2)\, k_2 \sin 2\gamma_2 - 2n_0\,\frac{(1 + R_1)}{(1 - R_1)}\,(n_2^2 \cosh 2\alpha_2 + k_2^2 \cos 2\gamma_2)\,\}$$

$$S_1 = [\,(n_0^2 + n_2^2 + k_2^2)\, k_2 \sinh 2\alpha_2 + (n_0^2 - n_2^2 - k_2^2)\, n_2 \sin 2\gamma_2 - 2n_0\,\frac{(1 + R_1)}{(1 - R_1)}\,(n_2k_2 \cosh 2\alpha_2 - n_2k_2 \cos 2\gamma_2)\,]$$

$$U_1 = (n_2^2 + k_2^2)\{\,(n_0^2 + n_2^2 + k_2^2)\cosh 2\alpha_2 + (n_0^2 - n_2^2 - k_2^2) \times \cos 2\gamma_2 - 2n_0\,\frac{(1 + R_1)}{(1 - R_1)}\,(n_2 \sinh 2\alpha_2 + k_2 \sin 2\gamma_2)\,\}$$

$$P_2 = P \cosh 2\alpha_2 - Q \cos 2\gamma_2 + S \sinh 2\alpha_2 + U \sin 2\gamma_2$$

$$Q_2 = P\, n_2 \sinh 2\alpha_2 - Q\, k_2 \sin 2\gamma_2 + S\, n_2 \cosh 2\alpha_2 - U\, k_2 \cos 2\gamma_2$$

$$S_2 = P\, k_2 \sinh 2\alpha_2 + Q\, n_2 \sin 2\gamma_2 + S\, k_2 \cosh 2\alpha_2 + U\, n_2 \cos 2\gamma_2$$

$$U_2 = (n_2^2 + k_2^2)\,(P \cosh 2\alpha_2 + Q \cos 2\gamma_2 + S \sinh 2\alpha_2 - U \sin 2\gamma_2)$$

where

$$P = (n_0^2 + n_1^2)\,(n_1^2 + n_2^2 + k_2^2) + (n_0^2 - n_1^2) \times (n_1^2 - n_2^2 - k_2^2) \cos 2\gamma_2$$

$$Q = (n_0^2 + n_1^2)\,(n_1^2 - n_2^2 - k_2^2) + (n_0^2 - n_1^2) \times (n_1^2 + n_2^2 + k_2^2) \cos 2\gamma_1$$

$$S = 2 n_1 k_2 (n_0^2 - n_1^2) \sin 2\gamma_1 - 4 n_0 n_1^2 n_2 \frac{(1 + R_2)}{(1 - R_2)}$$

$$U = 2 n_1 n_2 (n_0^2 - n_1^2) \sin 2\gamma_1 + 4 n_0 n_1^2 k_2 \frac{(1 + R_2)}{(1 - R_2)}$$

Note that these quantities P, Q, S, U, P_1, Q_1, S_1, U_1, P_2, Q_2, S_2, and U_2 do not involve the constants n_3 and k_3.

Now from equations (5.3.17) and (5.3.18) we find

$$(n_3^2 + k_3^2) + \frac{2Q_1}{P_1} n_3 + \frac{2S_1}{P_1} k_3 + \frac{U_1}{P_1} = 0 \qquad 5.3.19$$

and

$$2\left(\frac{Q_1}{P_1} - \frac{Q_2}{P_2}\right) n_3 + 2\left(\frac{S_1}{P_1} - \frac{S_2}{P_2}\right) k_3 + \left(\frac{U_1}{P_1} - \frac{U_2}{P_2}\right) = 0 \qquad 5.3.20$$

The first of these equations is quadratic in n_3 and k_3 and the second is a linear equation. Again we have a graphical solution represented by a straight line and a circle as for the single layer equations.

From equation (5.3.20) we get

$$k_3 = \frac{(Q_1/P_1 - Q_2/P_2)}{(S_2/P_2 - S_1/P_1)} n_3 + \frac{1}{2} \frac{(U_1/P_1 - U_2/P_2)}{(S_2/P_2 - S_1/P_1)}$$

i.e. $$k_3 = Z n_3 + F \qquad 5.3.21$$

where $$Z = \frac{Q_1/P_1 - Q_2/P_2}{S_2/P_2 - S_1/P_1} \qquad 5.3.22$$

and $$F = \frac{1}{2} \frac{U_1/P_1 - U_2/P_2}{S_2/P_2 - S_1/P_1} \qquad 5.3.23$$

Substituting the values of k_3 in the equation (5.3.19) gives

$$n_3^2 (1 + Z^2) + 2 \left(\frac{S_1}{P_1} Z + ZF + Q_1/P_1\right) n_3 + \left(\frac{U_1}{P_1} + \frac{2S_1}{P_1} F + F^2\right) = 0 \qquad 5.3.24$$

The coefficients in this simple quadratic equation can be easily computed from the formulae given above and the equations may then be solved for n_3 and k_3. It is necessary to have a value for the thickness d_1 of the applied film. This can be obtained from the condition that $R_1 = R_2$ when $\gamma_1 = p\pi$.

The equations for the double layer reduce to those for a single layer when $d_2 = 0$, as shown in Appendix C.

5.4 Solutions for hypothetical opaque specimens

Two hypothetical specimens approximately representing Mo and Ni are considered here to illustrate the nature of the solutions of equations (5.2.1) and (5.2.2.) for metals.

5.4.1 Molybdenum

The optical data of Waldron and Juenker (1964) for clean Mo in the wavelength region 248 to 570 nm were used to find approximate expressions for n and k. A Least Squares procedure was used to fit the data with equations of the form

$$k_2 = a + b\lambda + c\lambda^2 \qquad 5.4.1$$

$$n_2 = a^1 + b^1\lambda + c^1\lambda^2 \qquad 5.4.2$$

where a, b, c, a^1, b^1 and c^1 are 5.124, -6.676×10^{-4}, 6.829×10^{-8}, -3.431, 2.743×10^{-3} and -2.588×10^{-7} respectively.

n_2 and k_2 are the refractive and absorption indices at wavelength λ (in angstrom unit). From these values of complex refractive index $n_2 - ik_2$ of this hypothetical specimen (Figure 5.2) reflectances R and R_1 were calculated (Figure 5.3) using Tomlin's (1972) single layer

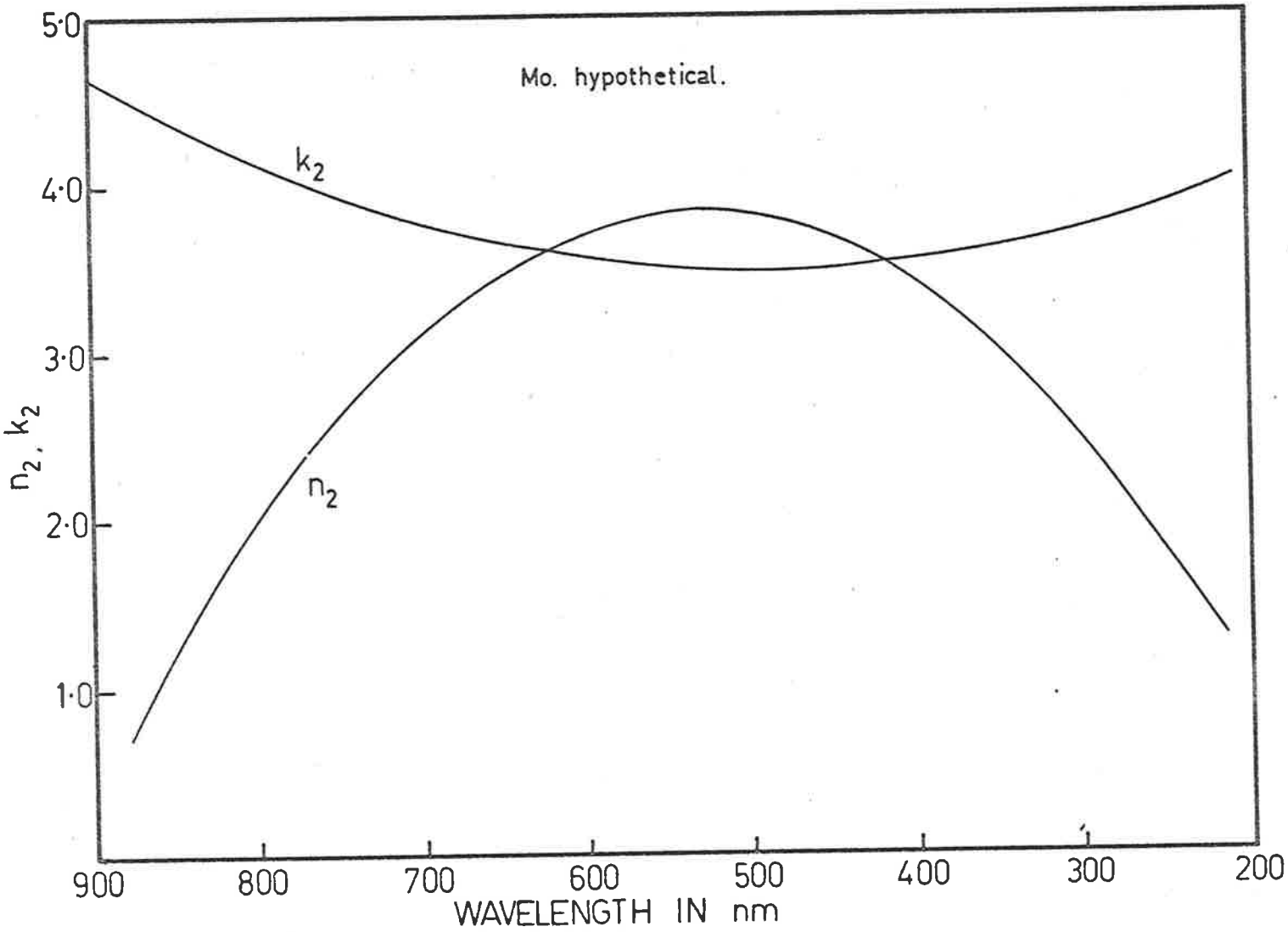
Mo. hypothetical.
k_2
n_2
5·0
4·0
3·0
2·0
1·0
n_2, k_2
900
800
700
600
500
400
300
200
WAVELENGTH IN nm

Fig.5.2

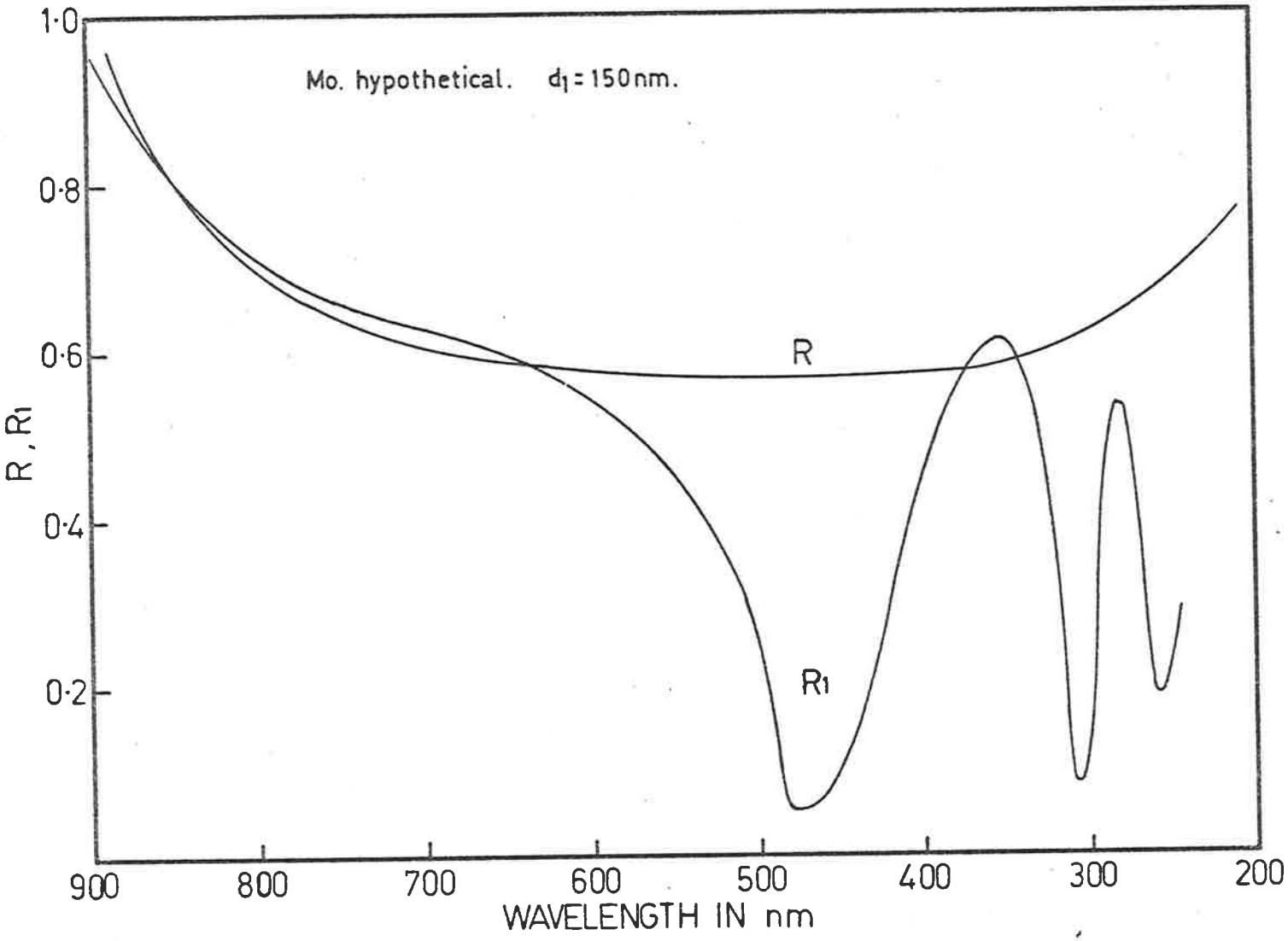
Mo. hypothetical. $d_1 = 150$nm.
R
R_1
1·0
0·8
0·6
0·4
0·2
R , R_1
900
800
700
600
500
400
300
200
WAVELENGTH IN nm

Fig. 5.3

formulae for a thin transparent layer of Ta_2O_5 of thickness 150 nm whose complex refractive index $n_1 - ik_1$ was known. Now using these calculated values of R and R_1 the equations for the optical constants n_2 and k_2 of the hypothetical specimens were solved (Figure 5.4) in order to find the nature of the two possible solutions. It is clear from Figure (5.4) that the correct dispersion curve is reproduced and the unwanted solutions give a quite different curve with a number of maxima and minima. Maxima in the false dispersion curve appear at the positions corresponding to the minima in the R_1 curve. If the reflectances are calculated at an interval of 50Å as in Figure (5.4) it is found that at certain intersections of R and R_1 where γ is a multiple of π, some solutions may be missing because of rounding-off of errors in the computer. This is also the case at the first minimum of R_1. The behaviour of the solutions for metals is very similar to that for semiconductors in the absorbing region (see Tomlin *et al* 1976).

5.4.2 Nickel

Similar calculations were carried out for a specimen with $n_2 = 3.0$ and $k_2 = 5.6 \times 10^{-2} \times \lambda^{\frac{1}{2}}$ which roughly represents the behaviour of Ni in the region 2000 to 300 nm. The calculated values of R and R_1 for this model (d_1 = 125 nm) are shown in Figure (5.5) and the nature of the solution is shown in Figure (5.6). The results are very similar to those for the hypothetical Mo example.

5.5 Effects of errors in the thickness of the semitransparent overlying layer

If the thickness of the film is underestimated there is a strong effect on the solutions for n_2 and k_2, which was shown as

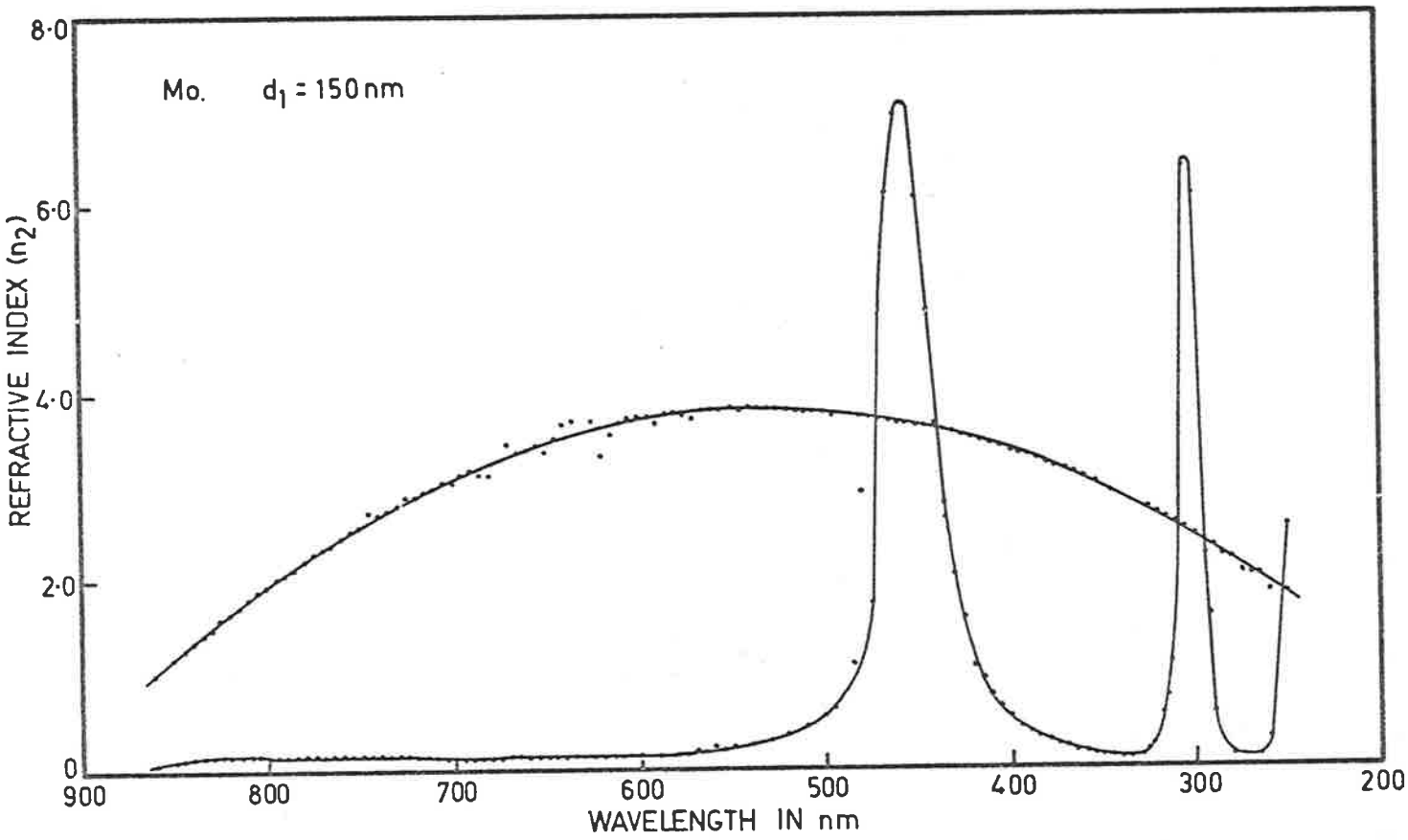
Mo. d_1 = 150 nm
REFRACTIVE INDEX (n_2)
8·0
6·0
4·0
2·0
0
900
800
700
600
500
400
300
200
WAVELENGTH IN nm

Fig. 5.4

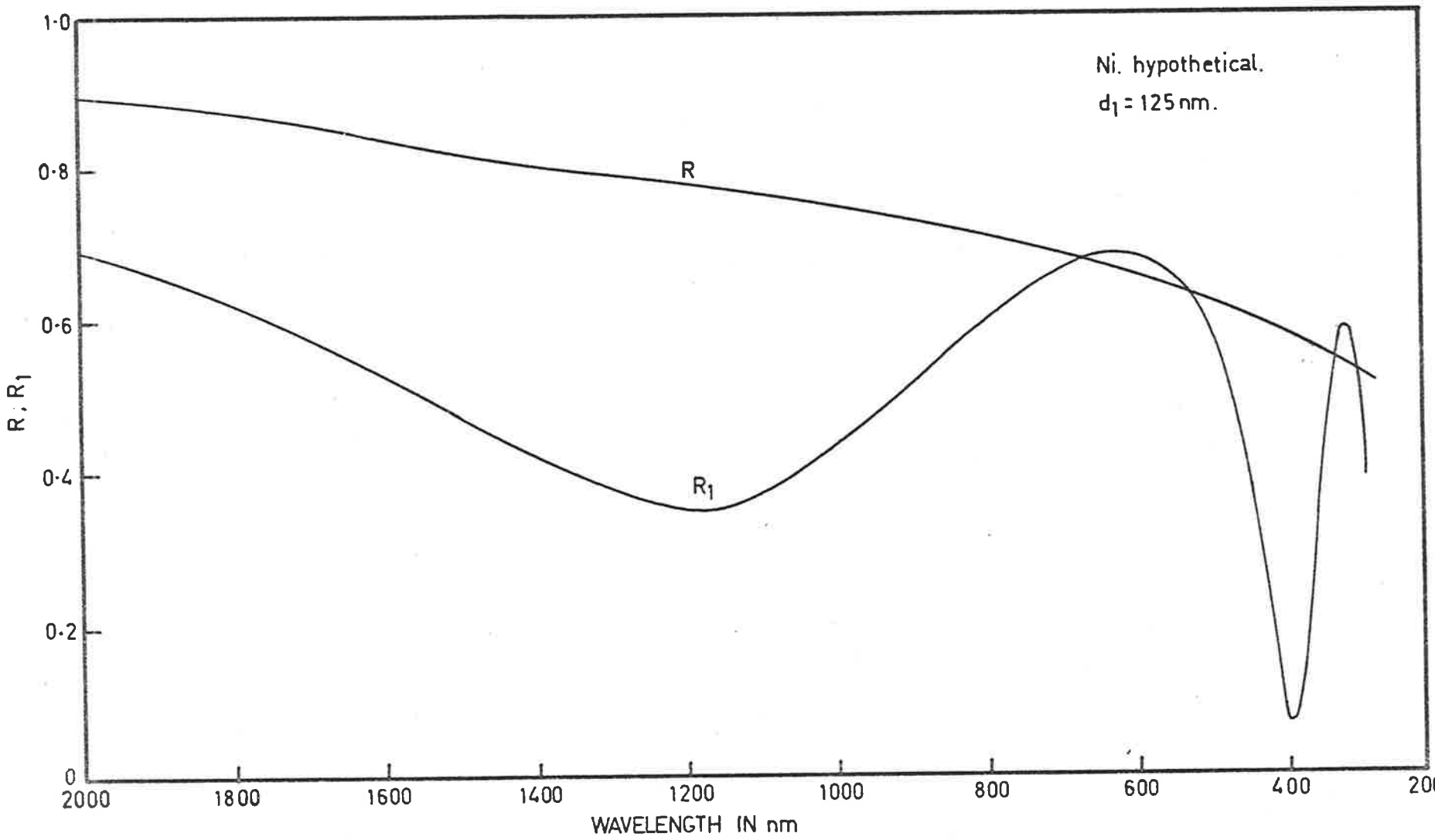
Ni. hypothetical.
d_1 = 125 nm.
R
R_1
R ; R_1
1·0
0·8
0·6
0·4
0·2
0
2000
1800
1600
1400
1200
1000
800
600
400
200
WAVELENGTH IN nm

Fig. 5.5

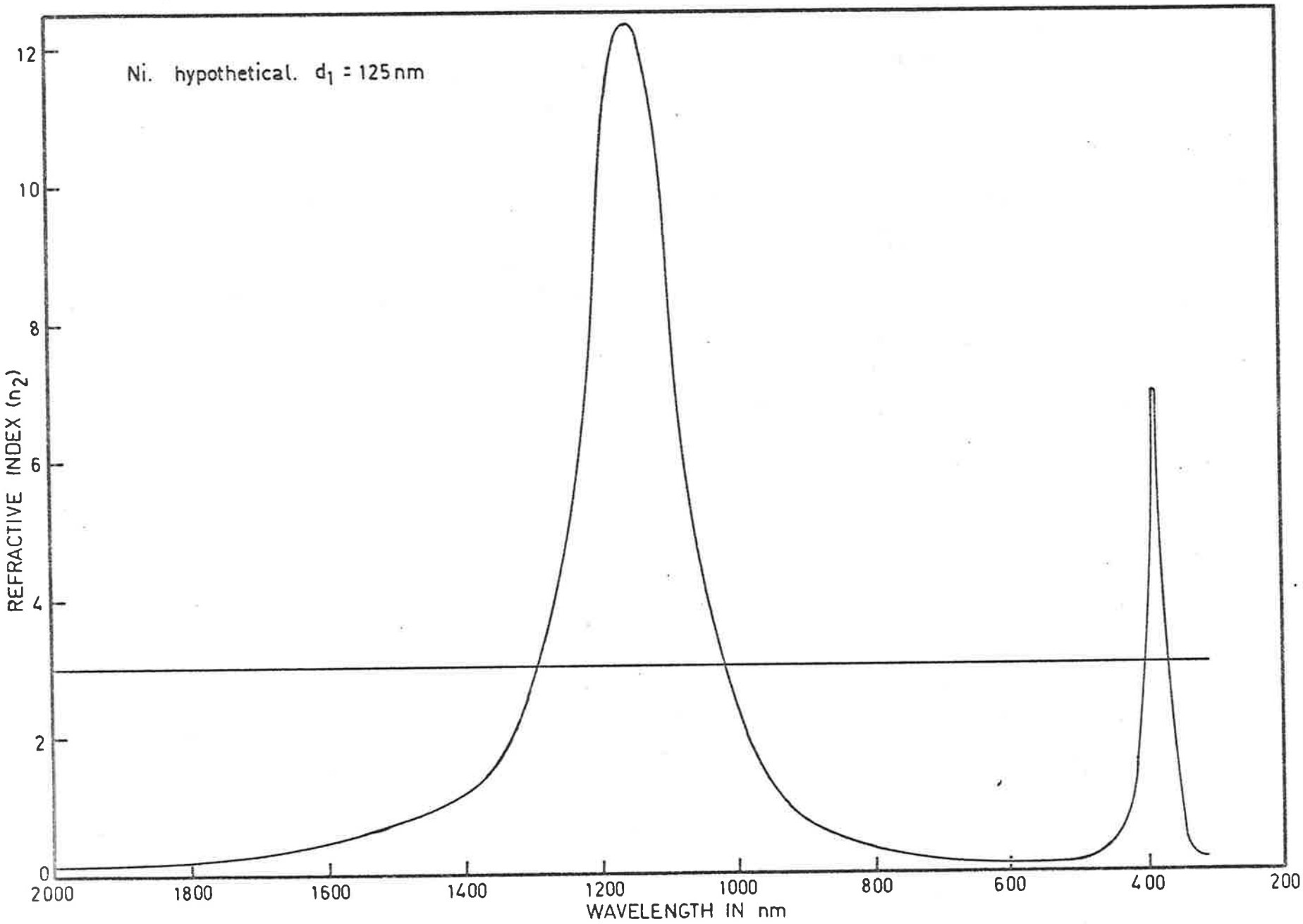
Ni. hypothetical. d_1 = 125 nm
REFRACTIVE INDEX (n_2)
0
2
4
6
8
10
12
2000
1800
1600
1400
1200
1000
800
600
400
200
WAVELENGTH IN nm

Fig. 5.6

follows.

Using the calculated reflectances R and R_1 for the Mo model which are shown in Figure (5.3), n_2 and k_2 were calculated when the film thickness was changed from the correct value of 150 nm to 149 (Figure 5.7) and 151 nm (Figure 5.8). In both cases the true dispersion curve breaks up into sections which join up with the wrong solutions. The resulting patterns are distinctly different for under and over estimation of thickness. Thus, when solutions for n_2 are obtained from experimental data it is quite clear whether the value assumed for the film thickness is too great or too small. The thickness may then be adjusted until a continuous dispersion curve results.

Further calculations were carried out with similar results for the Ni model. The effects of underestimating the film thickness by 3.0 nm are shown in Figure (5.9) and of overestimating it by 3.0 nm are shown in Figure (5.10). In both examples the maxima in the curves appear at the wavelengths which corresponds to the minima of R_1 and the intersections of the R and R_1 curves.

From Figures(5.4) and(5.6 to 5.10) it may be concluded that the acceptable continuous dispersion curve could not be obtained unless the errors in film thickness was less than 0.7%.

5.6 Effects of errors in R and R_1 on optical constants

The effects of systematic errors in the reflectances can be studied in the same way as systematic errors in the thickness of the Ta_2O_5 film.

For the hypothetical Ni specimen solutions for n_2 were calculated using the correct thickness (d_1 = 125 nm) but with

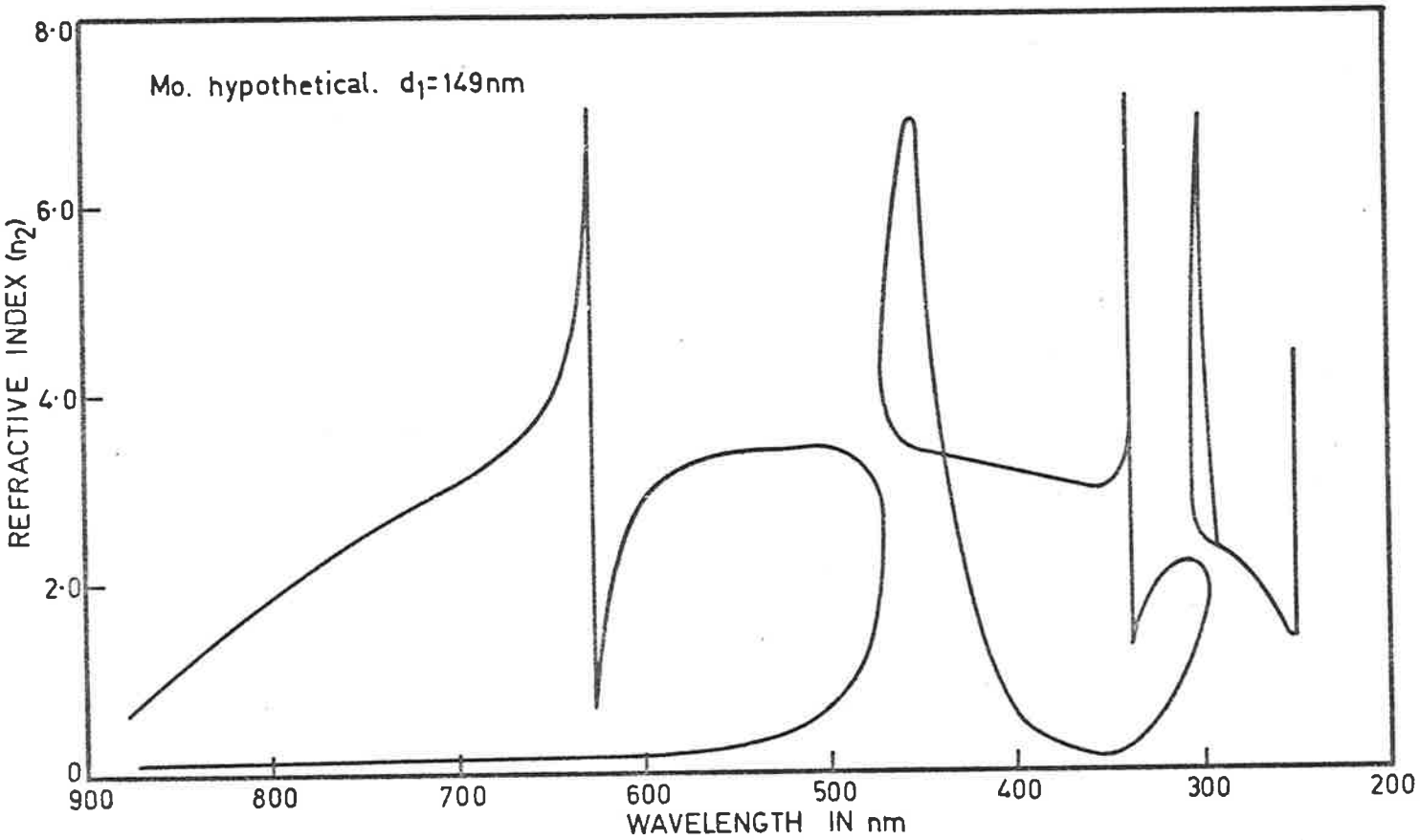
Mo. hypothetical. d_1=149nm
REFRACTIVE INDEX (n_2)
8·0
6·0
4·0
2·0
0
900
800
700
600
500
400
300
200
WAVELENGTH IN nm

Fig.5.7

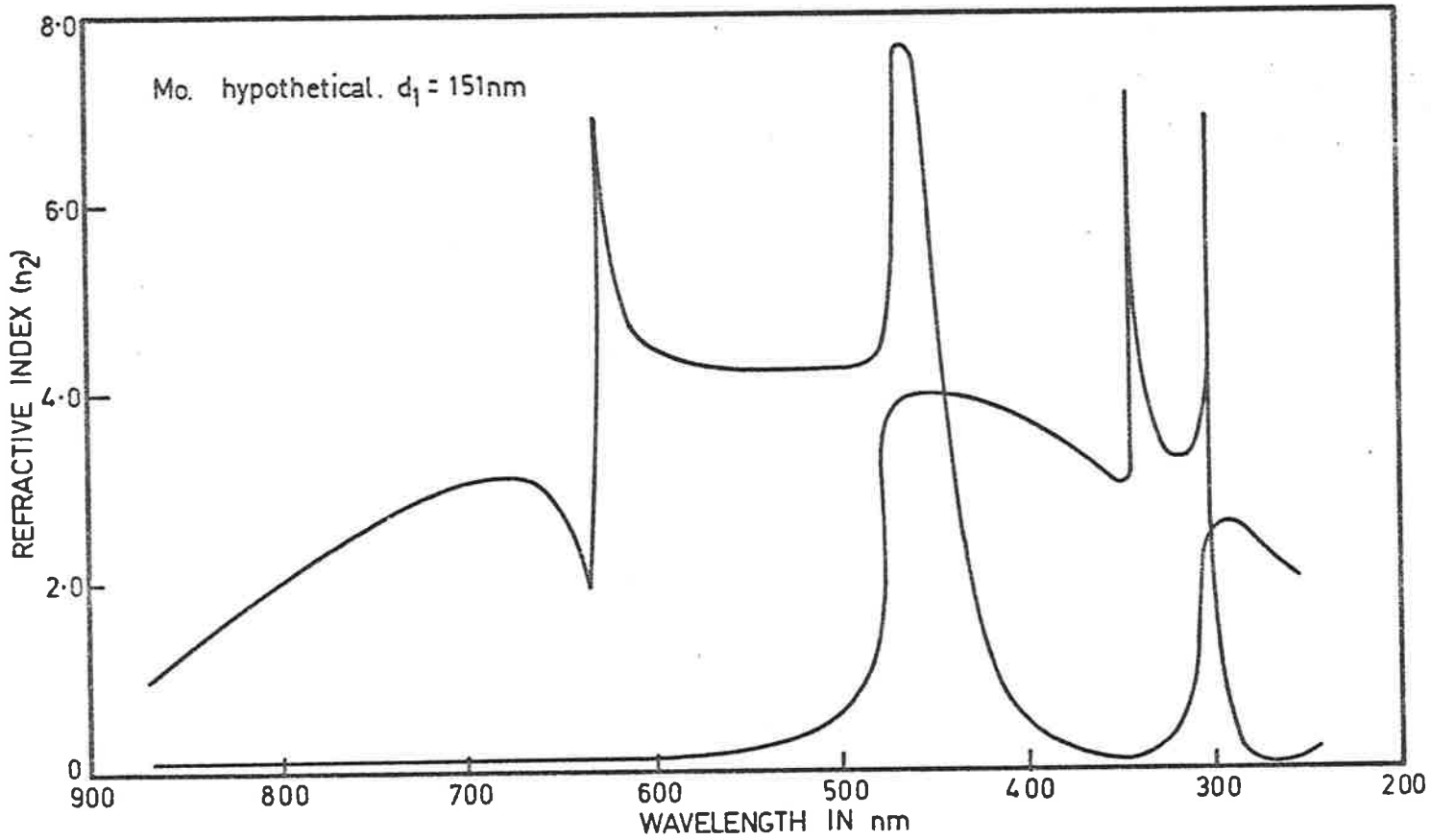
Mo. hypothetical. d_1 = 151nm
REFRACTIVE INDEX (n_2)
8·0
6·0
4·0
2·0
0
900
800
700
600
500
400
300
200
WAVELENGTH IN nm

Fig. 5.8

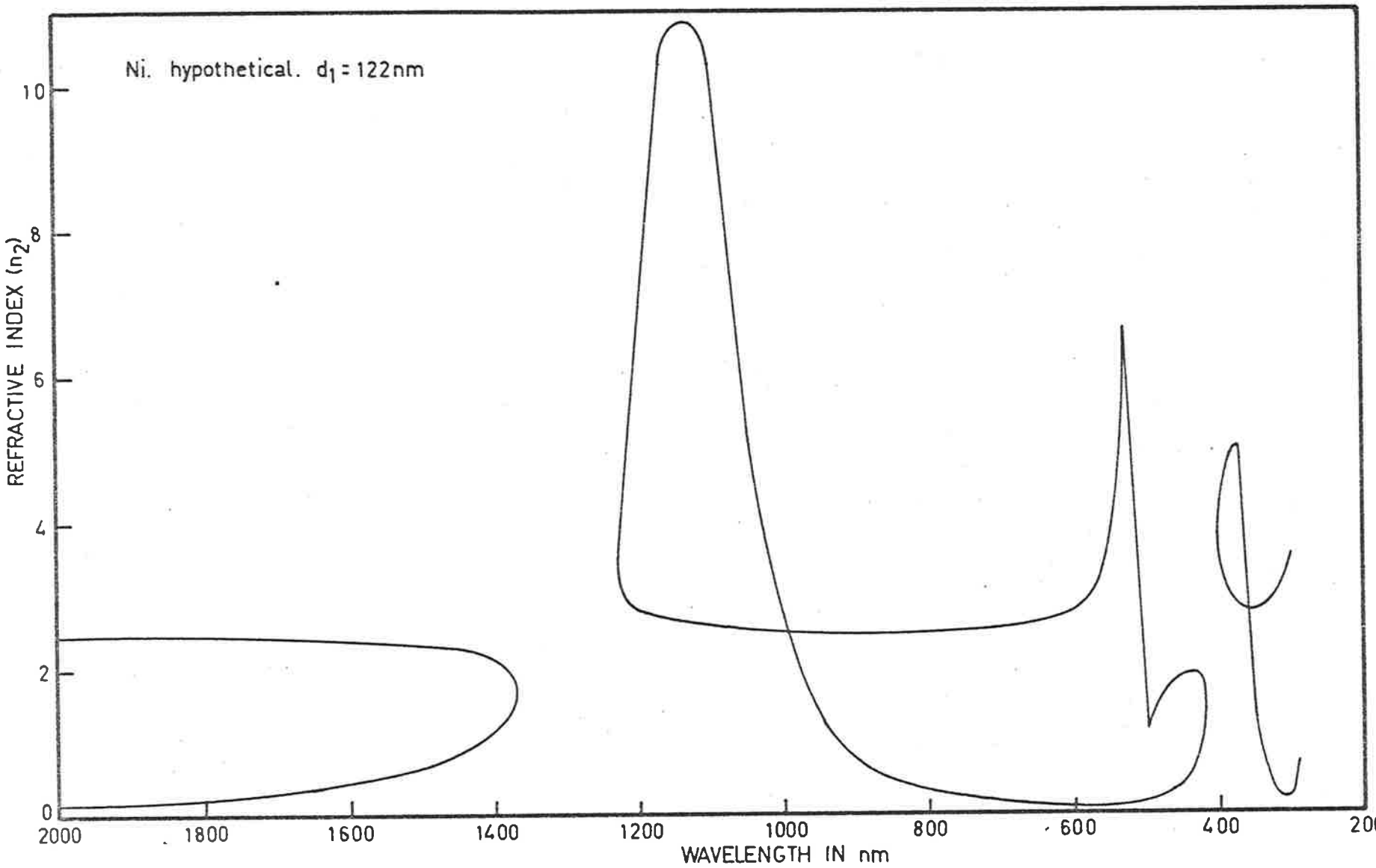
Ni. hypothetical. $d_1 = 122nm$
REFRACTIVE INDEX (n_2)
0
2
4
6
8
10
2000
1800
1600
1400
1200
1000
800
600
400
200
WAVELENGTH IN nm

Fig.5.9

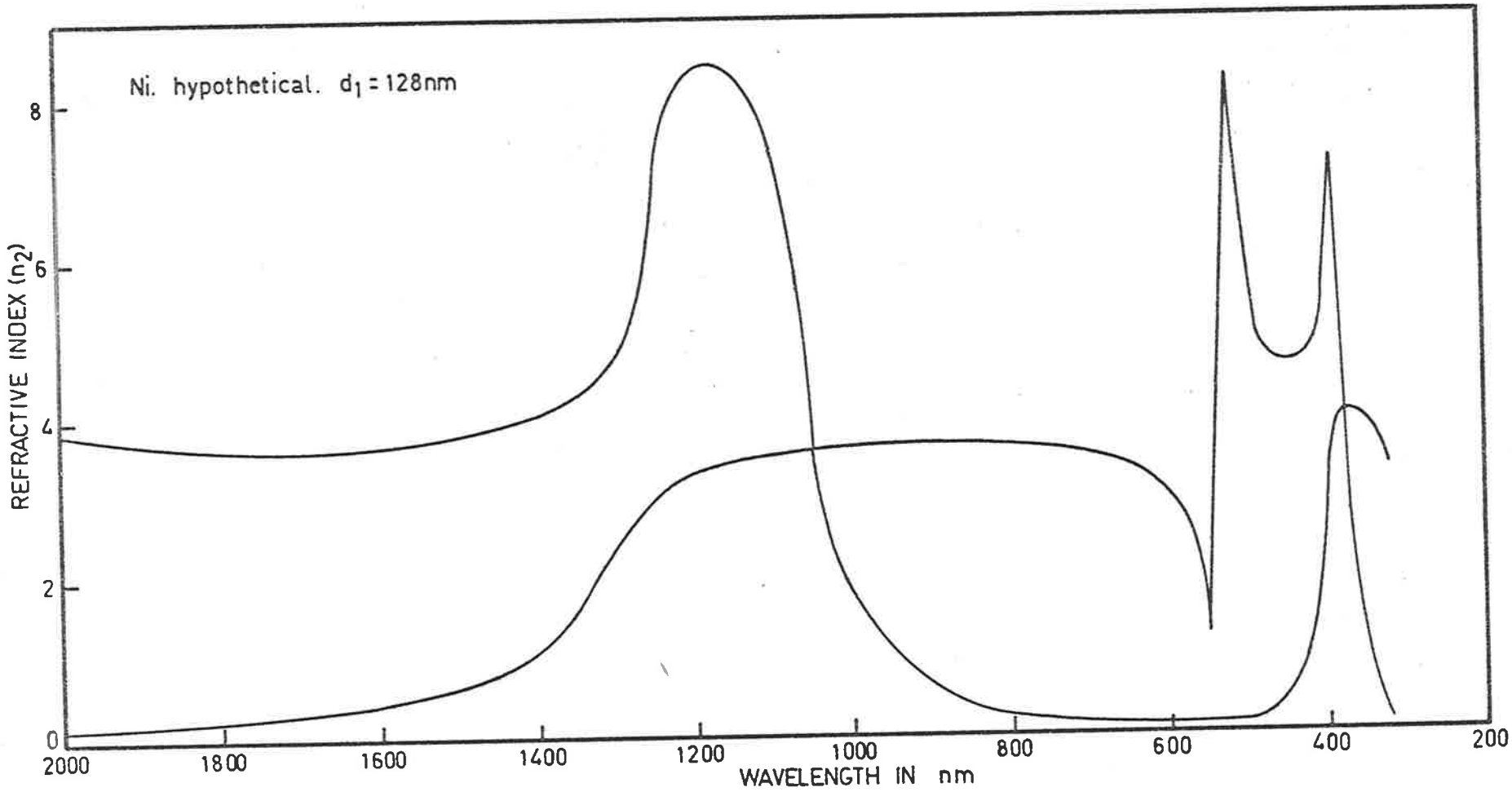
Ni. hypothetical. $d_1 = 128nm$
REFRACTIVE INDEX (n_2)
0
2
4
6
8
2000
1800
1600
1400
1200
1000
800
600
400
200
WAVELENGTH IN nm

Fig.5.10

Type I :

the correct value of R and R_1 increased or decreased by 2%, and

Type II :

the correct value of R_1 and R increased or decreased by 2% .

The results are shown in Figures (5.11 to 5.14). These systematic errors in R and R_1 , produce similar effects to those due to errors in thickness, breaking up the true dispersion curve into characteristic patterns. Clearly it is necessary to avoid systematic errors in R and R_1 if the correct value of film thickness is to be found by adjusting it until a continuous dispersion curve is obtained.

In practice the errors in R and R_1 are random errors of about $\pm$ 0.003 or considerably less than 1% except near the minima of R_1 , and the values of n_2 calculated from experimental data lie close to smooth curves which with a first rough estimate of film thickness, usually resemble those of Figures (5.9 and 5.10). The failure to obtain a continuous dispersion curve can then be attributed to errors in film thickness.

The random errors in R and R_1 will generally result in a few solutions being missing where the coefficients in the quadratic equation for n_2 happen to yield imaginary solutions only. This happens at wavelengths near the intersection of the R and R_1 curves and at the positions of minima of the R_1 curves. These regions can be shifted by repeating the measurements with a film of different thickness, so

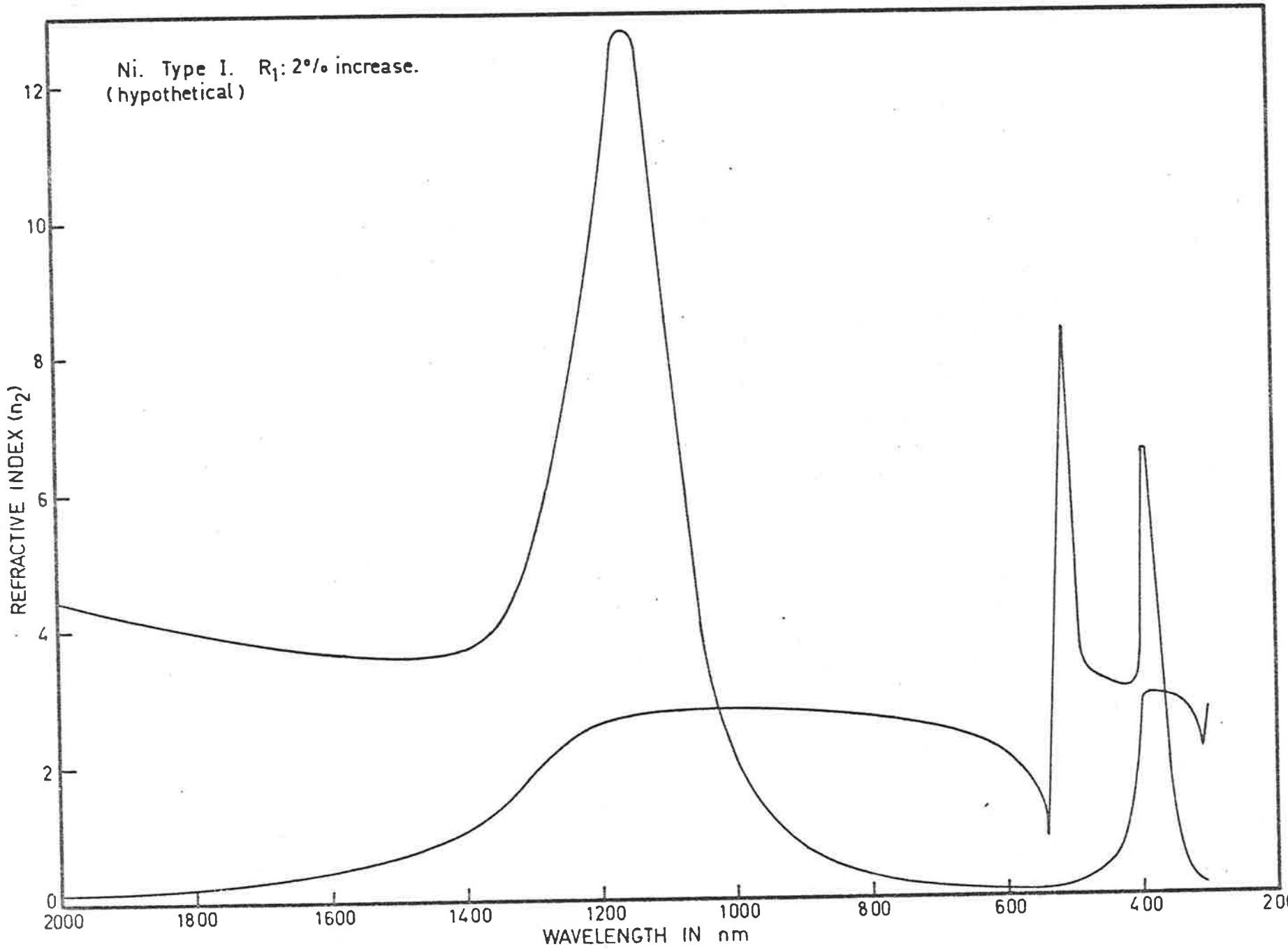
Ni. Type I. R_1: 2% increase.
(hypothetical)
REFRACTIVE INDEX (n_2)
0
2
4
6
8
10
12
2000
1800
1600
1400
1200
1000
800
600
400
200
WAVELENGTH IN nm

Fig. 5.11

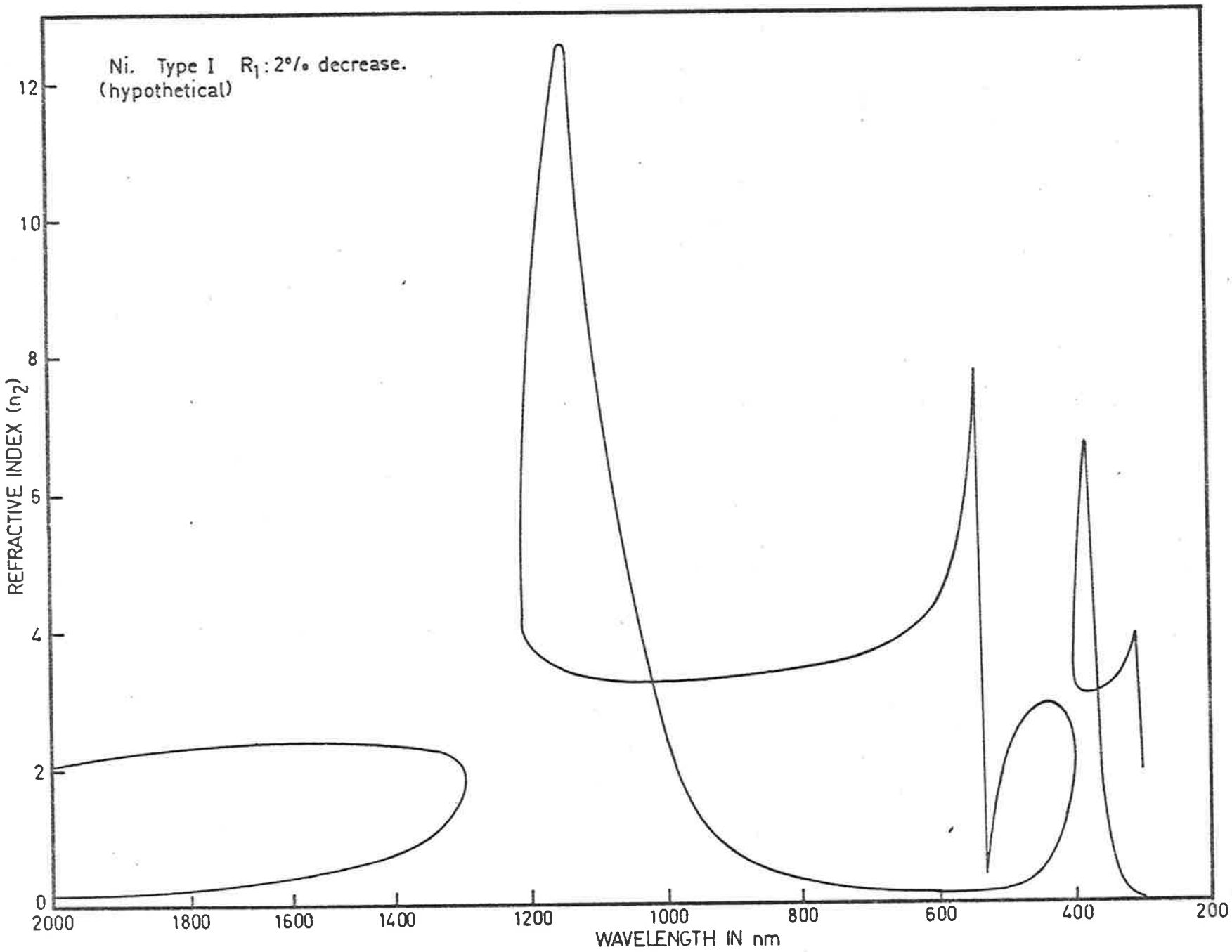
Ni. Type I R_1: 2% decrease.
(hypothetical)
REFRACTIVE INDEX (n_2)
0
2
4
6
8
10
12
2000
1800
1600
1400
1200
1000
800
600
400
200
WAVELENGTH IN nm

Fig. 5.12

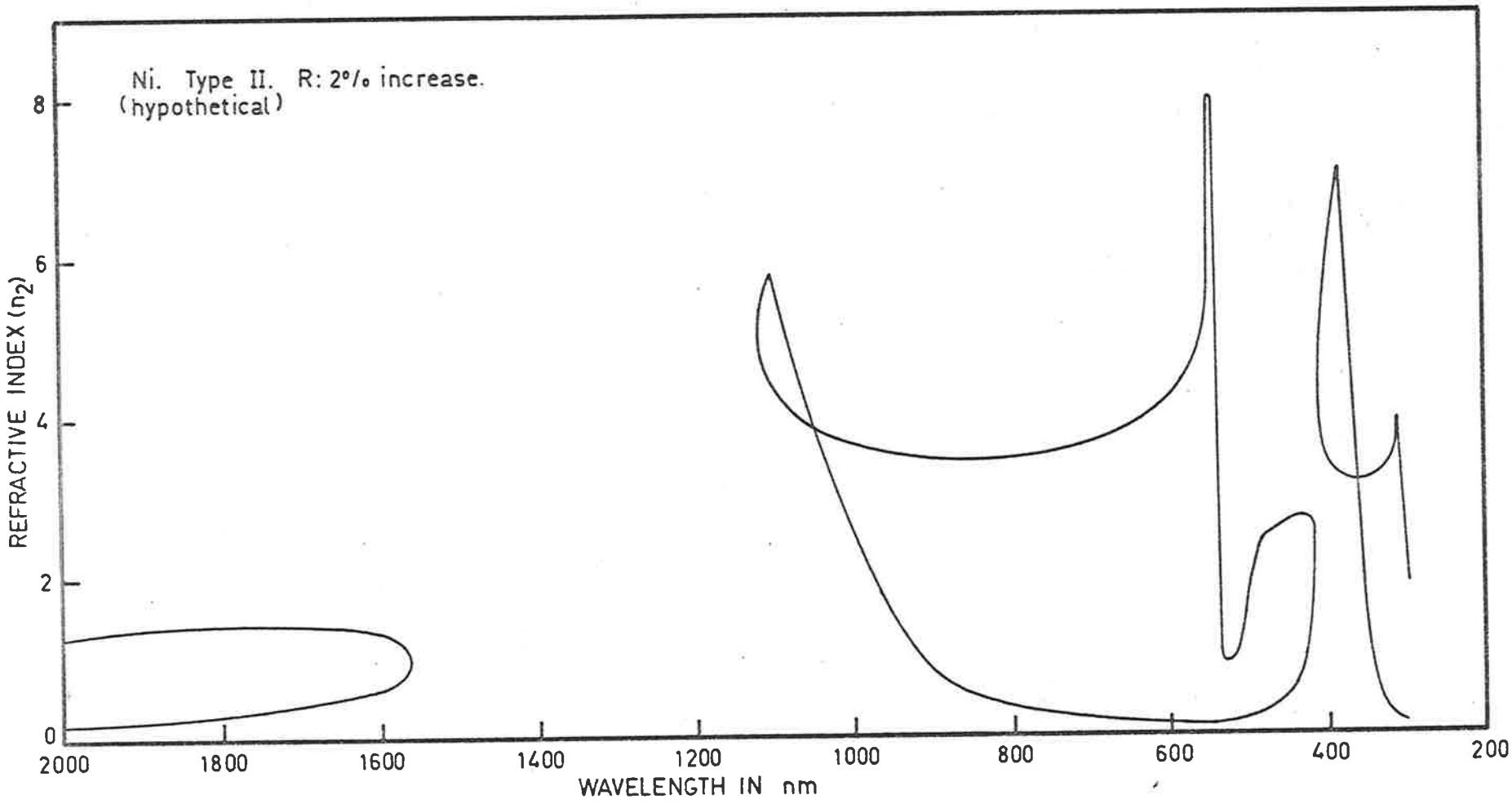
Ni. Type II. R: 2% increase.
(hypothetical)
REFRACTIVE INDEX (n_2)
0
2
4
6
8
2000
1800
1600
1400
1200
1000
800
600
400
200
WAVELENGTH IN nm

Fig.5.13

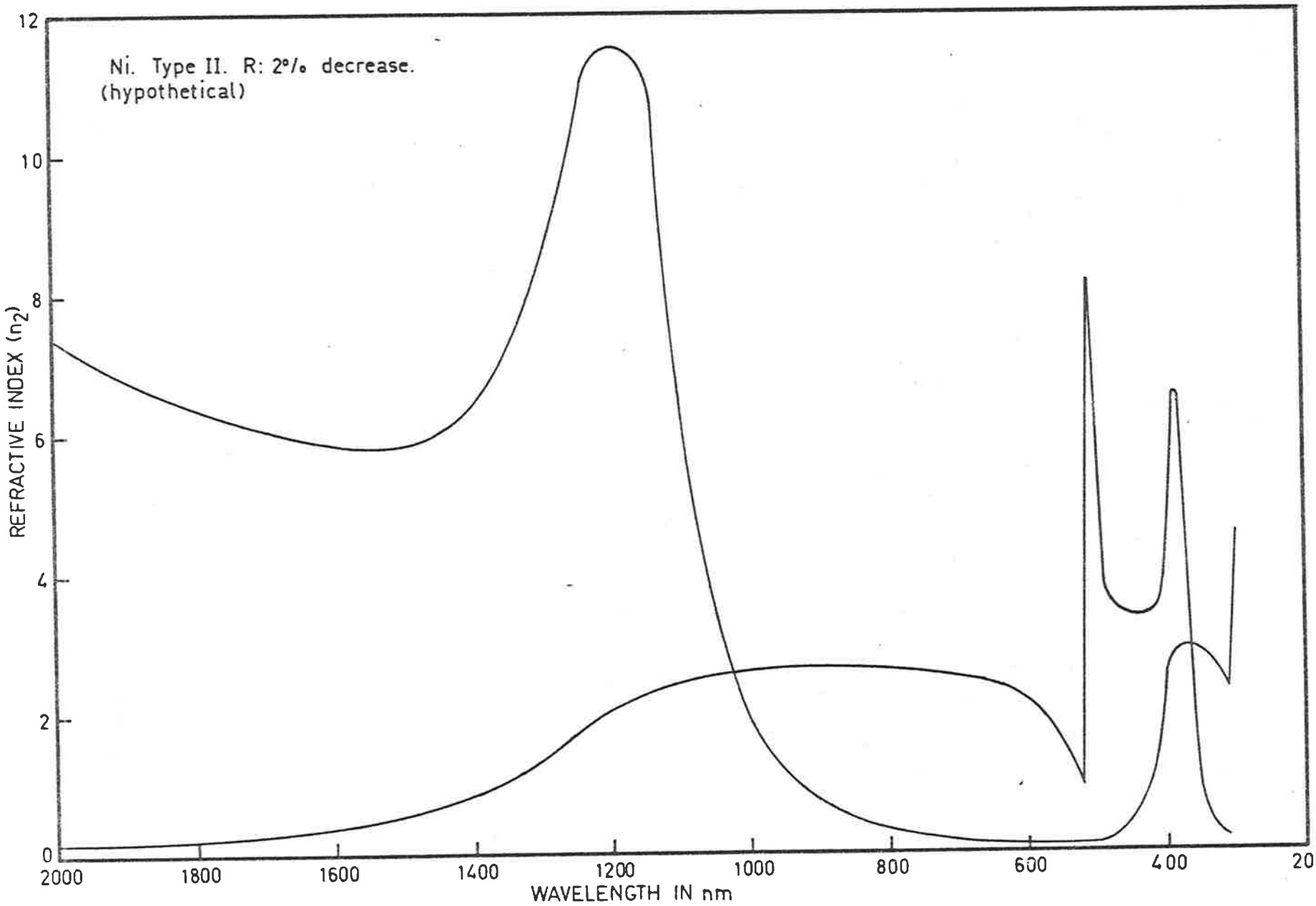
Ni. Type II. R: 2% decrease.
(hypothetical)
REFRACTIVE INDEX (n_2)
12
10
8
6
4
2
0
2000
1800
1600
1400
1200
1000
800
600
400
200
WAVELENGTH IN nm

Fig.5.14

that the doubtful part of the first dispersion curve can be covered by a reliable part of the second.

In the infrared region the reflectances tend towards unity and the quantities $\frac{1 + R}{1 - R}$ and $\frac{1 + R_1}{1 - R_1}$, become increasingly inaccurate. The method is therefore limited at the infrared end of the spectrum.

CHAPTER 6

DETERMINATION OF OPTICAL CONSTANTS OF Au

6.1 Introduction

The primary object of the work on the optical properties of metals which is to be described in the following chapters is to investigate the application of the method (Tomlin 1968), which involves the measurement of reflectances from the metal with and without a thin layer of Ta_2O_5 applied to its surface. This has been applied successfully to opaque films of Ge but in the case of metals the method must become increasingly inaccurate as $R \to 1.0$, because of the occurrence of the factor $\frac{1 + R}{1 - R}$ in the formulae from which n and k must be calculated. Measurements have been made on Ni, Co and Mo in the photon energy range from 0.62 to 4.0 eV and for Au from 1.7 to 4.2 eV. The results will be found to be in good agreement with other measurements and show the occurrence of features in dispersion, absorption and complex dielectric constant curves which may be related to the electron energy band structures of the different metals.

During the last decade theoretical band structures of Au have been derived. For example, Christensen and Seraphin (1971, Figure 6.10a) obtained the joint density of states in good agreement with Fermi surface and optical absorption data, although at high energies discrepancies occur.

In noble metals the d bands are submerged by about 2 to 4 eV below the Fermi surface whereas in transition metals the d bands intersect the Fermi level as shown in Figure (6.1a) for Co, Ni (transition metals) and Cu (noble metal) only. The difference in colour between Ag, Au and Cu arises from the position and properties of

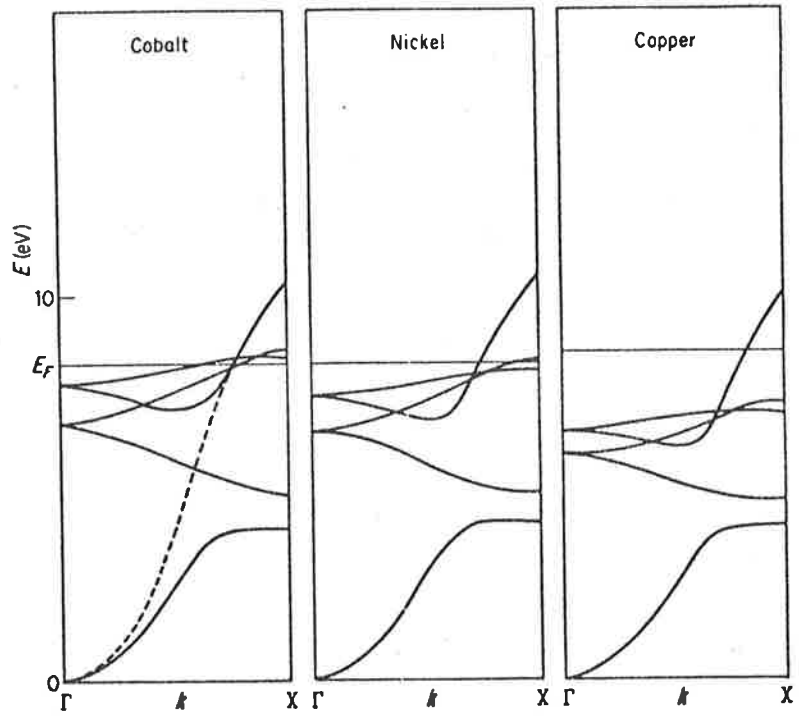

(a) Energy bands in f.c.c. Co, Ni and Cu for k along (1, 0, 0). These may be regarded crudely as made up of fairly flat d bands with an s band crossing them. If the d bands are neglected the s band would be as shown (dashed) in the first figure. The Fermi energy cuts the d bands for Co and Ni giving them a complicated Fermi surface. In Cu it cuts only the s band (after W. M. Lomer, 1971)

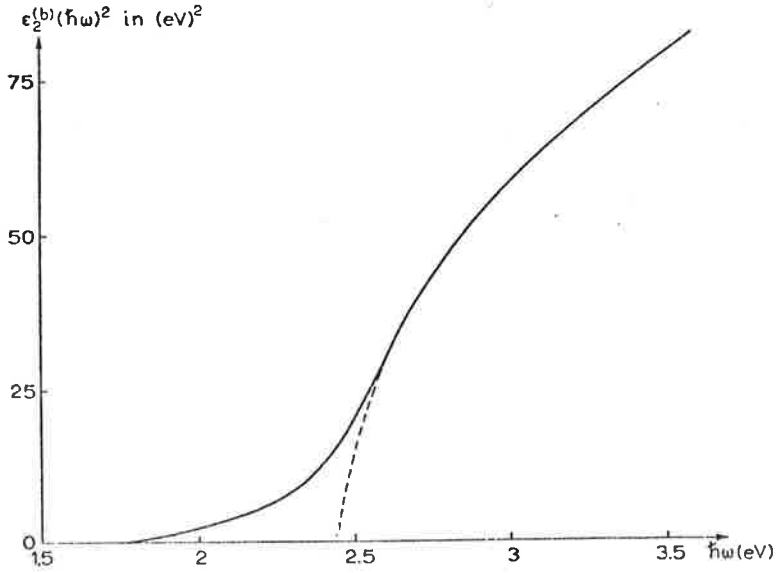

(b) $\varepsilon_2^{(b)}(\hbar\omega)^2$ versus photon energy for gold showing the parabolic behavior of the joint density of states in the vicinity of the absorption edge, located at 2.45 eV. The full curve below this energy has an exponential shape and its origin is not clear (after THÈYE [1970]). (From Abeles, 1972)

Fig.6·1

these d bands. For Au they give rise to an absorption edge at 2.45 eV and for Cu at 2.08 eV corresponding to the yellow and red colours of the metals respectively. But for Ag the absorption begins in the U.V. (around 3.87 eV), and for this reason it is possible to separate the intra and interband contribution to the dielectric constant in Ag which is not possible for Cu, Au and the transition metals. (see Chapter 7).

6.2 Sample preparation and structure of the films

Opaque films of Au were prepared in the D.R.C. laboratories by RF sputtering in the presence of dry argon. The evaporation rate and the pressure during sputtering were 0.625 nm/sec and 1.5m Torr respectively. Three different thicknesses of Ta_2O_5 of 71.5, 121.5 and 166.0 nm were sputtered on to the Au films which were prepared simultaneously.

Opaque films of Au did not show any surface structures when examined with the scanning electron microscope, but when the surface replicas of these films prepared according to the method described in Chapter 2, Section 2.8, were examined with the transmission electron microscope, it was observed that they had a roughness of the order of 3.0 to 3.5 nm (Figure 6.a).

6.3 Determination of the optical constants of Au

The optical constants of opaque Au films have been measured in the region 1.7 to 4.2 eV . The details of the method are given in Chapter 5, Section 5.2. The upper limit to the wavelength region is determined by the reflectivity tending to unity when the error in $\frac{1 + R}{1 - R}$ becomes too large.

The values of R and R_1 for three different thicknesses of

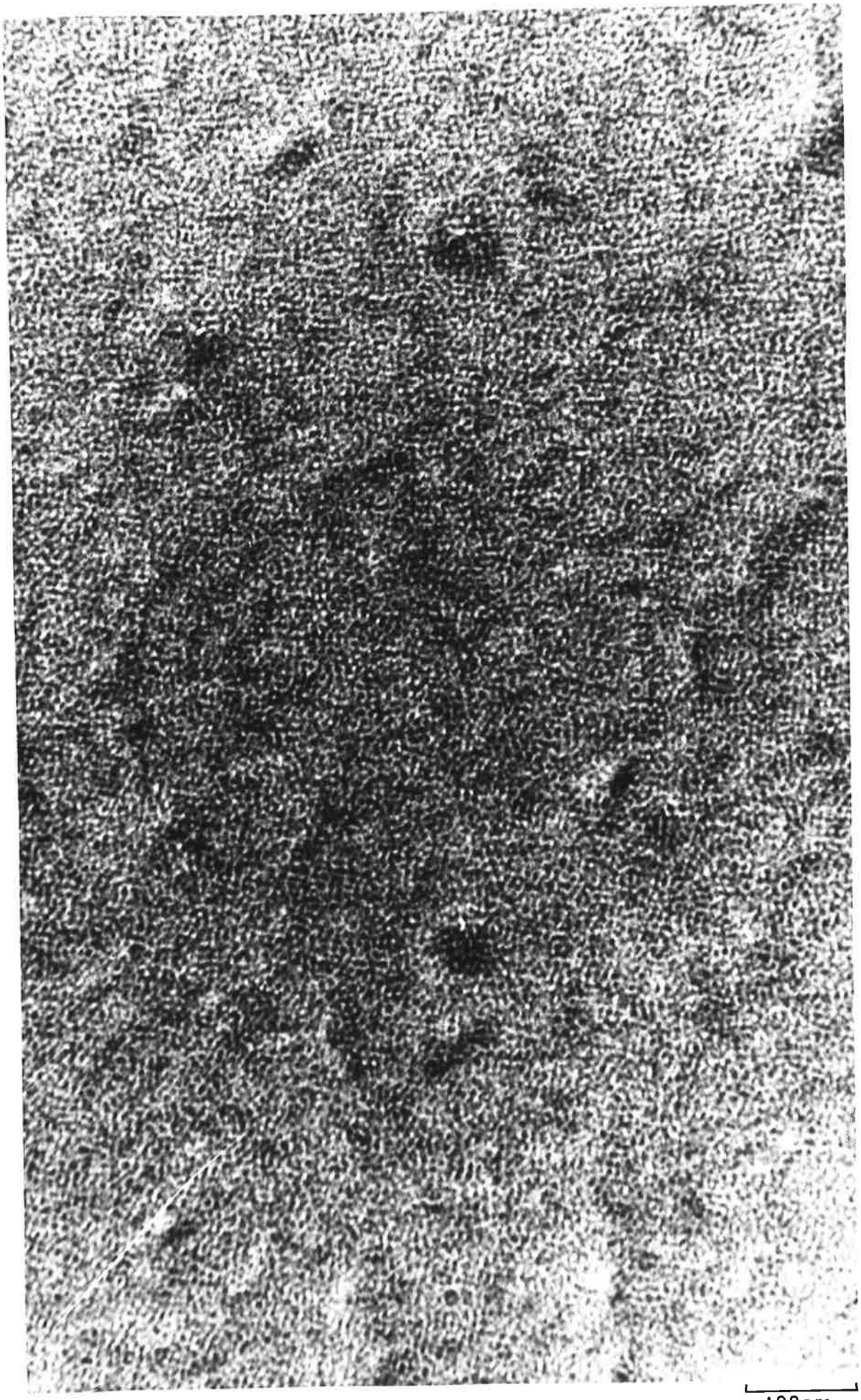

Fig.6-a

Ta_2O_5 (71.5, 121.5 and 166.0 nm) are shown in Figure (6.2).

The solution for refractive indices derived from measurements using a Ta_2O_5 film of 71.5 nm thickness are shown by curves (1) and (2) of Figure (6.3). It is not obvious from these two curves alone which curve represents the correct solutions, but from the known incorrect solutions for a Ta_2O_5 film of thickness 121.5 nm , indicated by curve (3), it is immediately clear that the curve (1) shows the correct solutions for thickness 71.5 nm, although the correct solutions for the other two thickness (121.5 and 166.0 nm) are more or less the same with small variations (see Figure 6.5). The position of the maxima of the wrong solutions may be varied by altering the thickness of the Ta_2O_5 film. It is possible to cover the whole wavelength region where one set of data leads to the large error bar by appropriate choice of film thicknesses and so obtain a dispersion curve with all points accurately determined. For this reason it was useful to coat the opaque gold films with at least three different thicknesses of Ta_2O_5 films. The correct solutions for these different layers are in good agreement as shown in Figures (6.3) to (6.6), because at any particular energy one set of solutions has large error bars and the others have not; the overall error varies from 1.5 to 3.5% except perhaps at the lowest photon energies where the error in $\frac{1 + R}{1 - R}$ becomes large, as $R \rightarrow 1.0$.

No ageing effects on reflectivity of the opaque Au films are observed when the measurements are taken within 10-15 days of the film preparation.

6.4 Results and discussion.

Figures (6.7) and (6.8) show a comparison of the author's results with other determinations by Heavens (1955), Johnson and Christy (1972), Joensen *et al* (1973), Venning (1975) and McMath *et al* (1977).

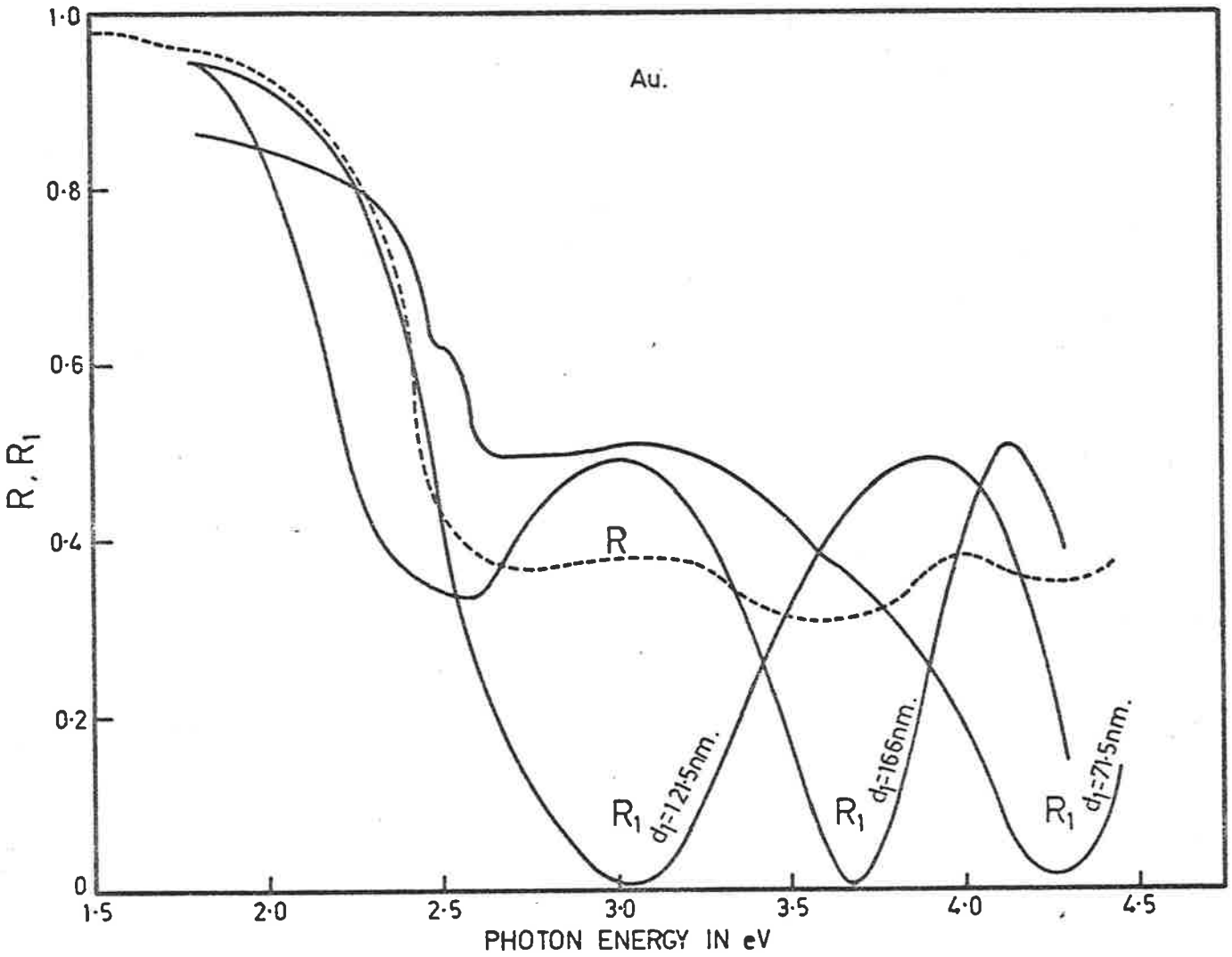
Au.
R
R_1 d_1=121·5nm.
R_1 d_1=166nm.
R_1 d_1=71·5nm.
R, R_1
PHOTON ENERGY IN eV
1·0
0·8
0·6
0·4
0·2
0
1·5
2·0
2·5
3·0
3·5
4·0
4·5

Fig.6.2

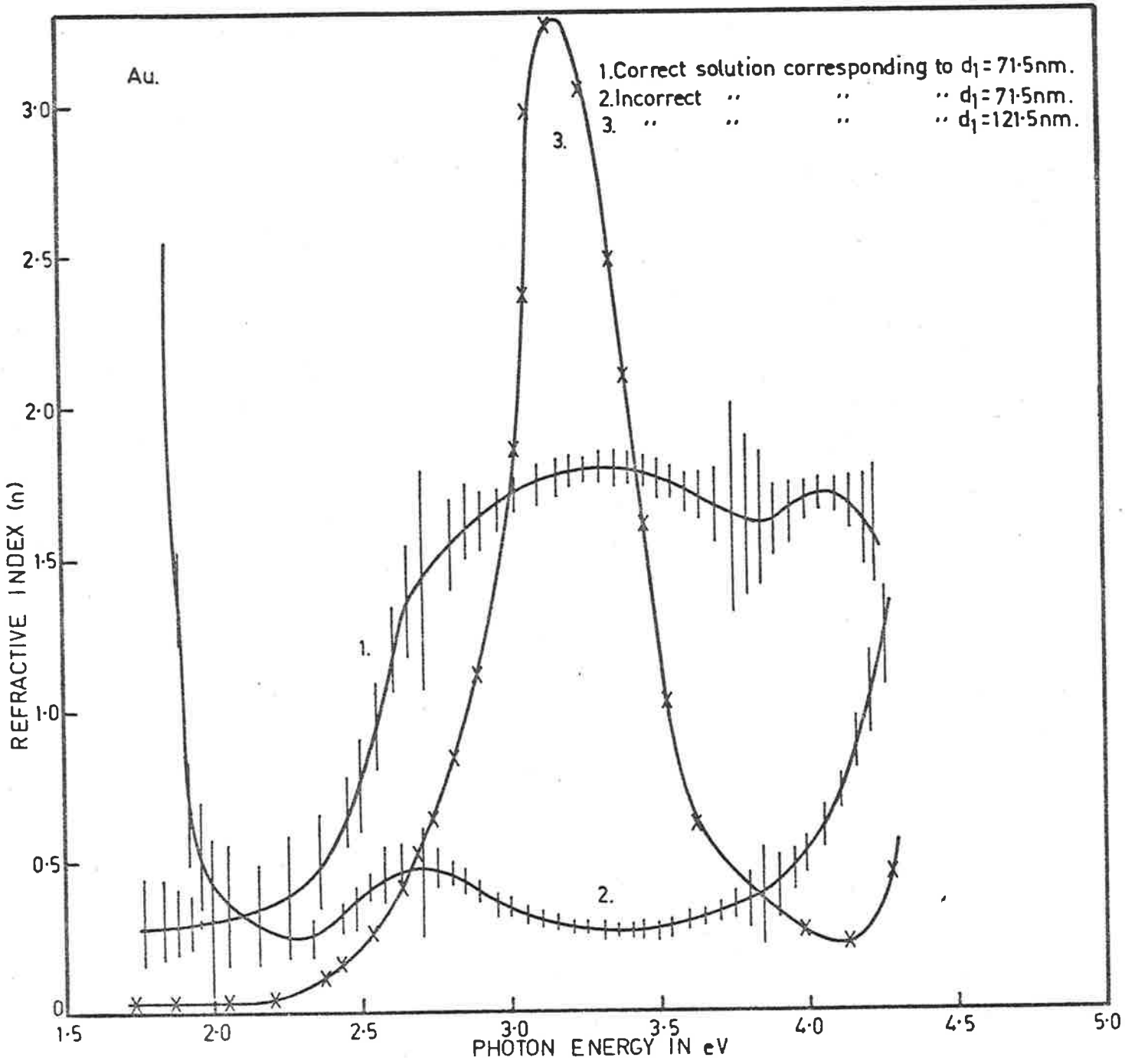
Au.
1.Correct solution corresponding to d_1 = 71·5nm.
2.Incorrect " " " d_1 = 71·5nm.
3. " " " d_1 = 121·5nm.
1.
2.
3.
REFRACTIVE INDEX (n)
PHOTON ENERGY IN eV
0
0·5
1·0
1·5
2·0
2·5
3·0
1·5
2·0
2·5
3·0
3·5
4·0
4·5
5·0

Fig.6.3

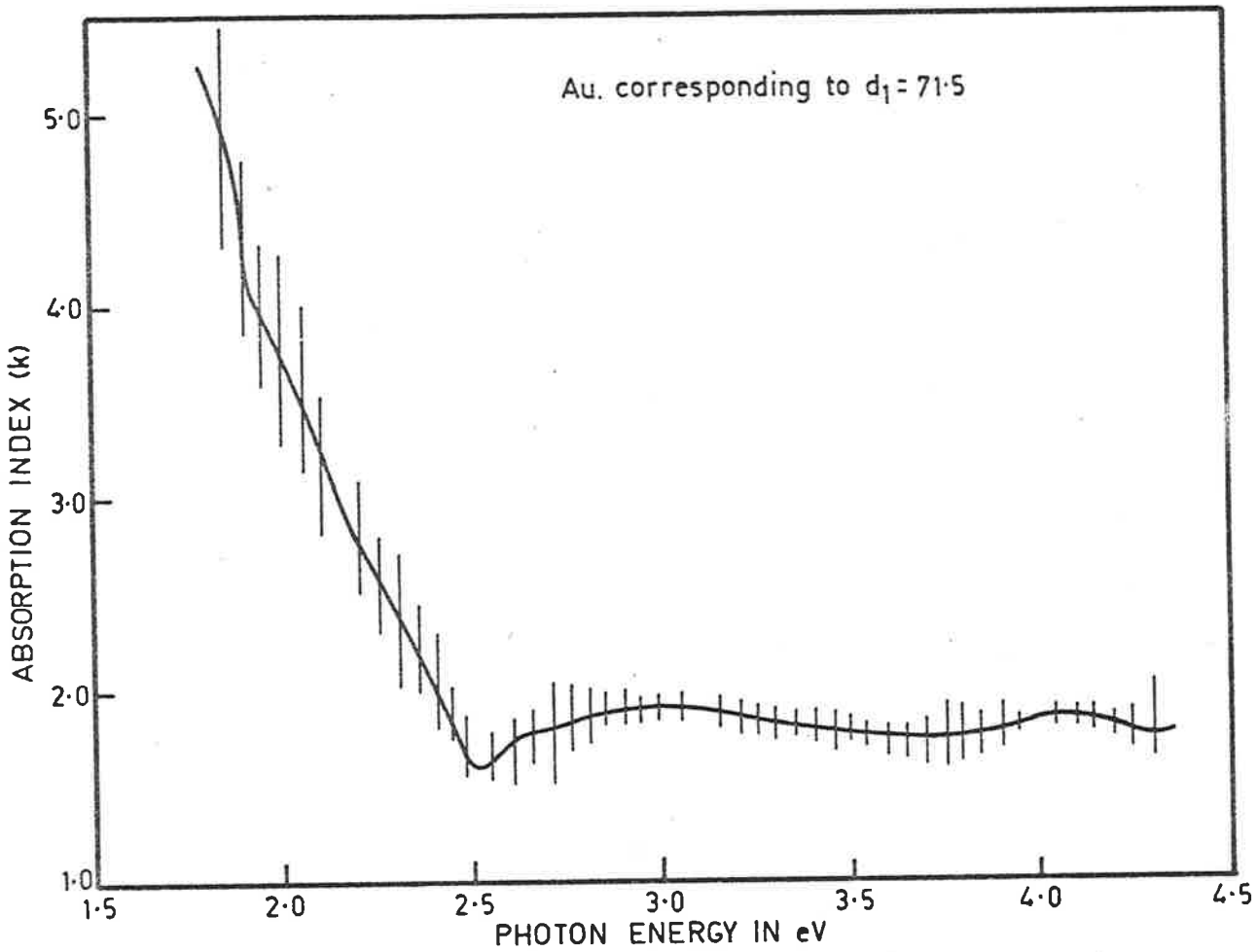
Au. corresponding to $d_1 = 71{\cdot}5$
ABSORPTION INDEX (k)
5·0
4·0
3·0
2·0
1·0
1·5
2·0
2·5
3·0
3·5
4·0
4·5
PHOTON ENERGY IN eV

Fig.6.4

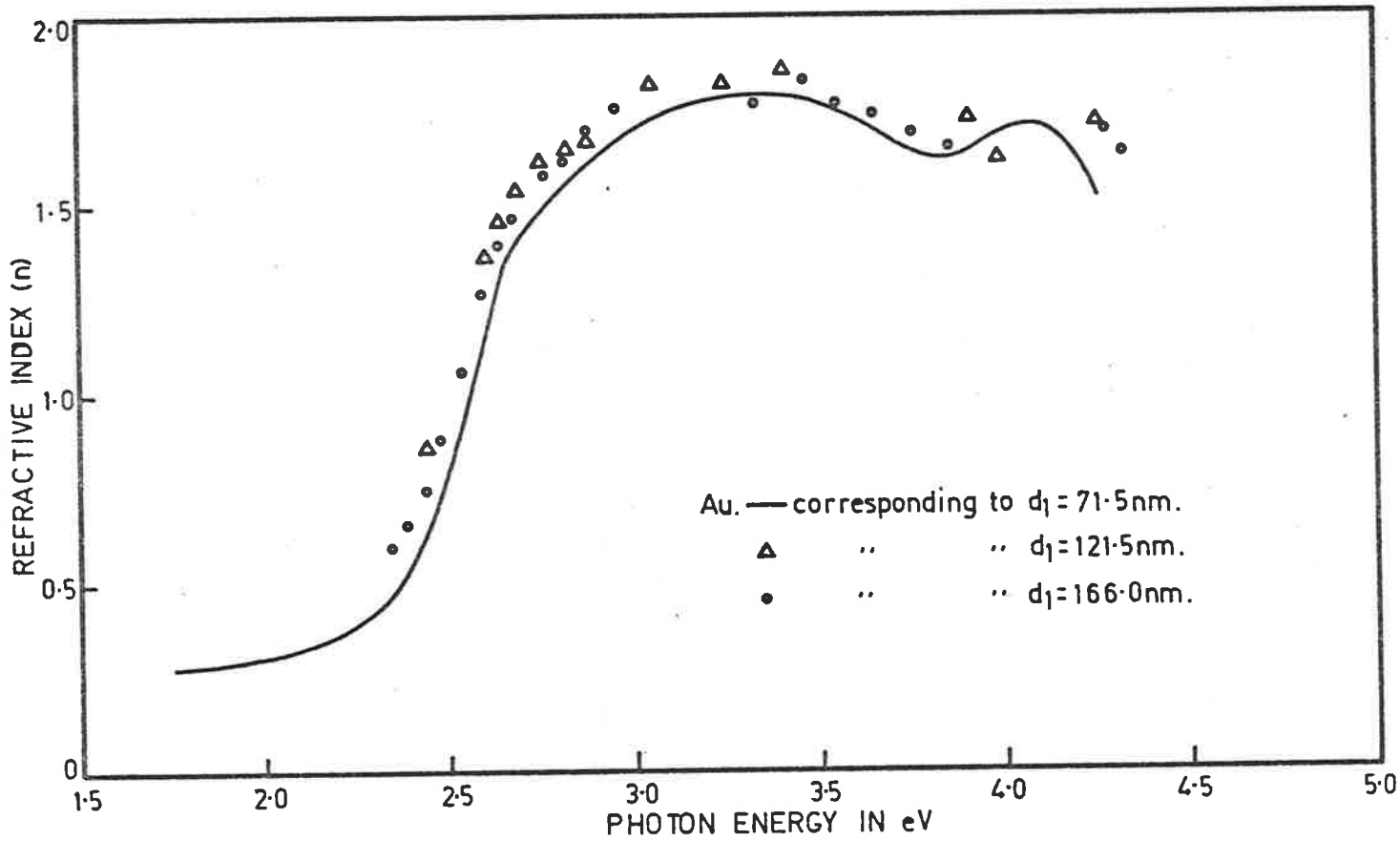
2·0
1·5
1·0
0·5
0
REFRACTIVE INDEX (n)
1·5
2·0
2·5
3·0
3·5
4·0
4·5
5·0
PHOTON ENERGY IN eV
Au. — corresponding to d_1 = 71·5nm.
△ " " d_1 = 121·5nm.
● " " d_1 = 166·0nm.

Fig.6.5

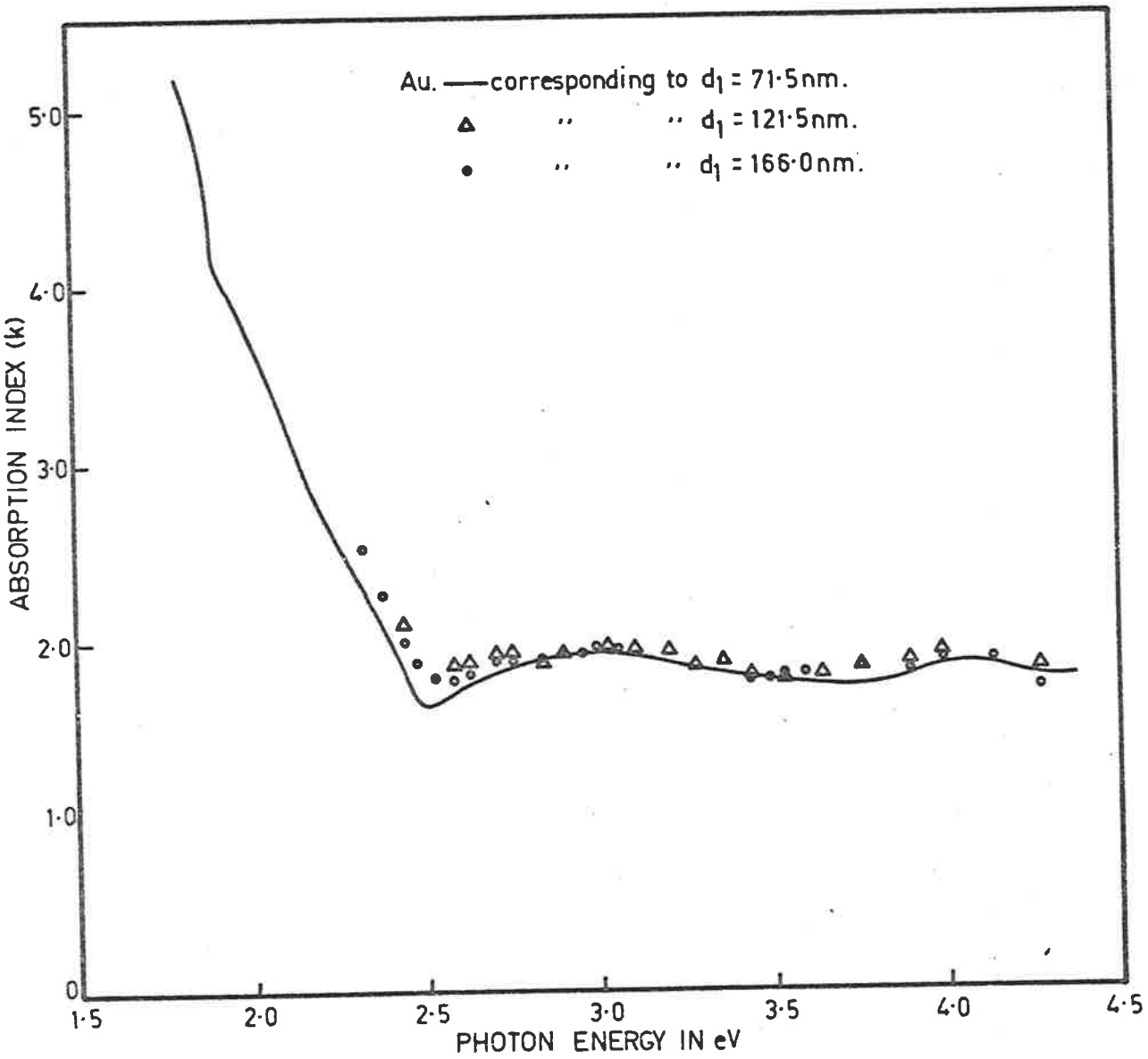
Au. —corresponding to d_1 = 71·5nm.
△ " " d_1 = 121·5nm.
● " " d_1 = 166·0nm.
ABSORPTION INDEX (k)
5·0
4·0
3·0
2·0
1·0
0
1·5
2·0
2·5
3·0
3·5
4·0
4·5
PHOTON ENERGY IN eV

Fig.6.6

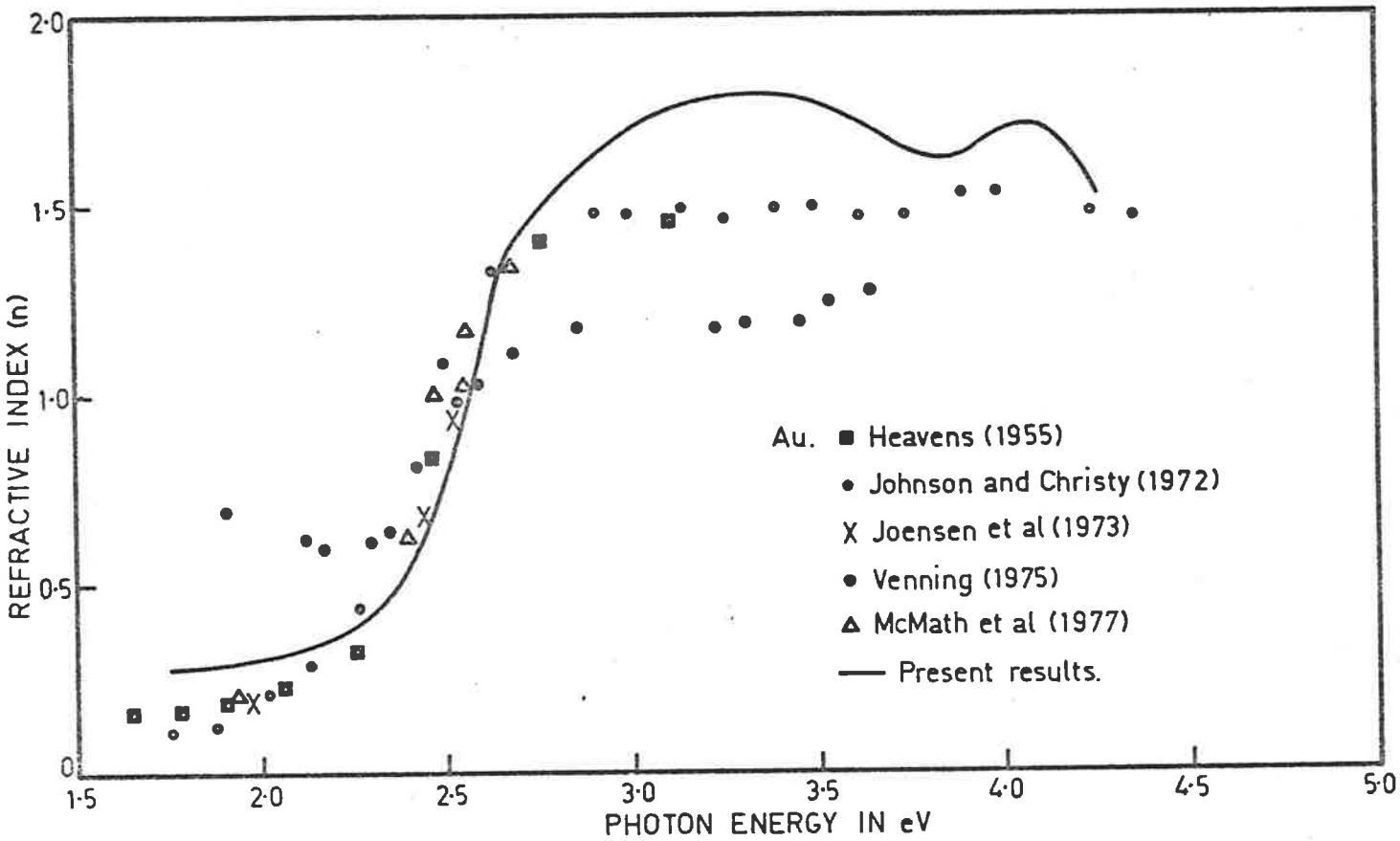
2·0
1·5
1·0
0·5
0
REFRACTIVE INDEX (n)
1·5
2·0
2·5
3·0
3·5
4·0
4·5
5·0
PHOTON ENERGY IN eV
Au. ■ Heavens (1955)
• Johnson and Christy (1972)
X Joensen et al (1973)
• Venning (1975)
△ McMath et al (1977)
—— Present results.

Fig. 6.7

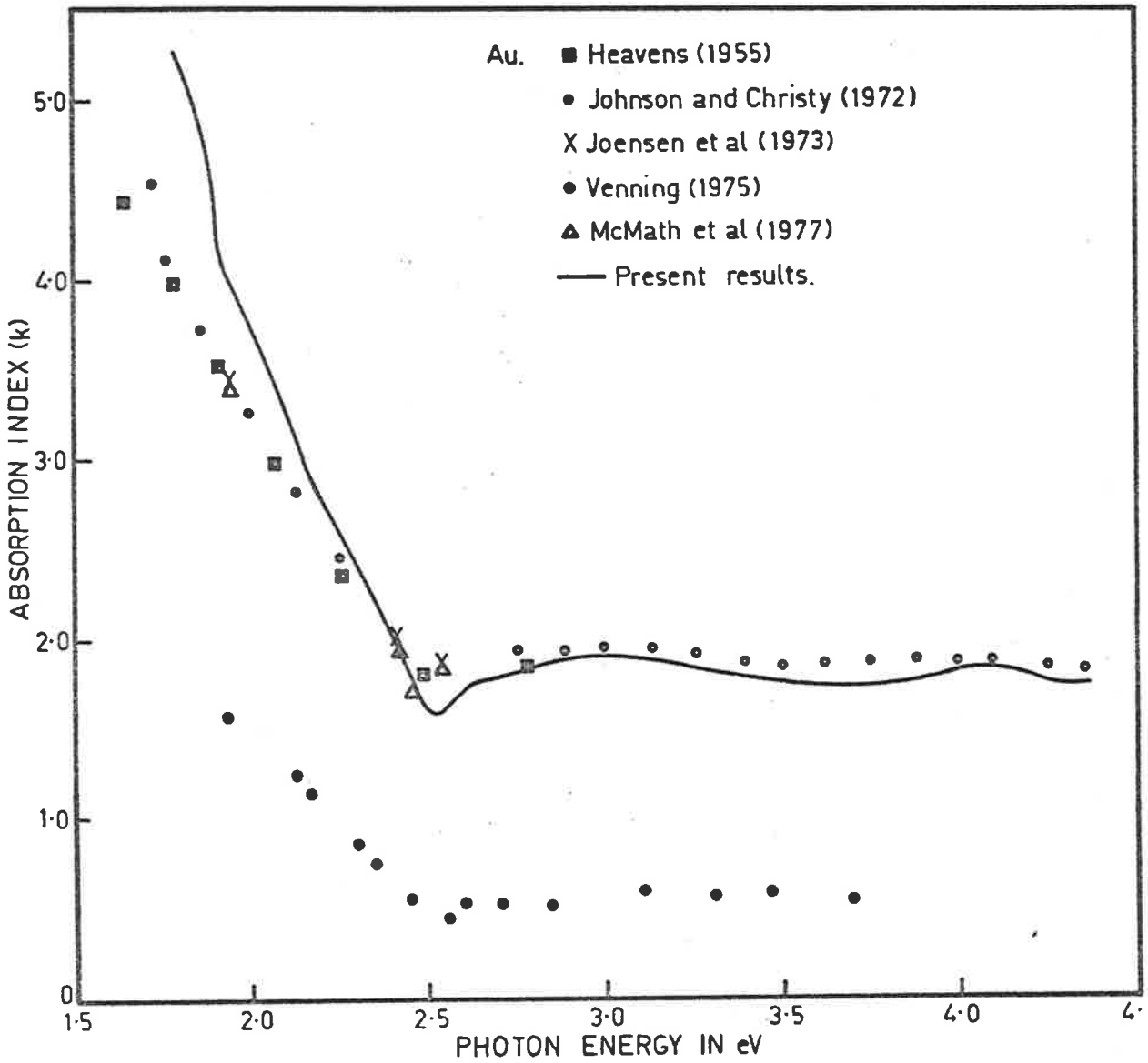
Au.
Heavens (1955)
Johnson and Christy (1972)
X Joensen et al (1973)
Venning (1975)
McMath et al (1977)
Present results.
ABSORPTION INDEX (k)
5·0
4·0
3·0
2·0
1·0
0
1·5
2·0
2·5
3·0
3·5
4·0
4·5
PHOTON ENERGY IN eV

Fig.6.8

Johnson and Christy made reflection and transmission measurements on thin films of Au of thickness 18.5 to 50.0 nm. Joensen *et al* (1973) also determined the optical constants of Au films with thicknesses in the range 17.0 to 180.0 nm using laser beams of wavelength 488.0, 514.5 and 632.8 nm. Venning (1975) determined the optical constants of two samples A and B of opaque Au film by an ellipsometer at an angle of incidence 67.8 and 70.0° respectively. The measurement on sample B was repeated 18 months later and a considerable change in optical constants was observed, specially below 450.0 nm . In Figures (6.7) and (6.8) the optical constants of the sample B are given for comparison with the present results. McMath *et al* (1977) determined the optical constants by measuring the transmittance and phase shift for a number of films of varying thickness 40 to 200 nm and gave the results for the thick film limit.

The present method leads to results in agreement with those other writers except perhaps those of Johnson and Christy (1972) whose results for rather thin films may be expected to differ from those for the thick opaque films used in this work.

In Figure (6.9) the real and imaginary parts of the complex dielectric constant calculated from the author's results are shown. The absorption curve and the $\varepsilon_2 = 2nk$ curve show the onset of absorption at about 2.5 eV. The extrapolation of the ε_2 curve as shown in Figure (6.9) makes the onset at 2.43 eV (2.45 eV, Theye 1970, Figure 6.1(b)). The sharp rise in ε_2 near 2.43 eV indicates that the transitions are probably from a very flat lower band to the Fermi surface. The first peak in ε_2 at 3.2 eV results from the transition from L_{32} to L_2' i.e. from the uppermost part of the d band to the bottom of the conduction band. The second peak in ε_2 at 4.0 eV

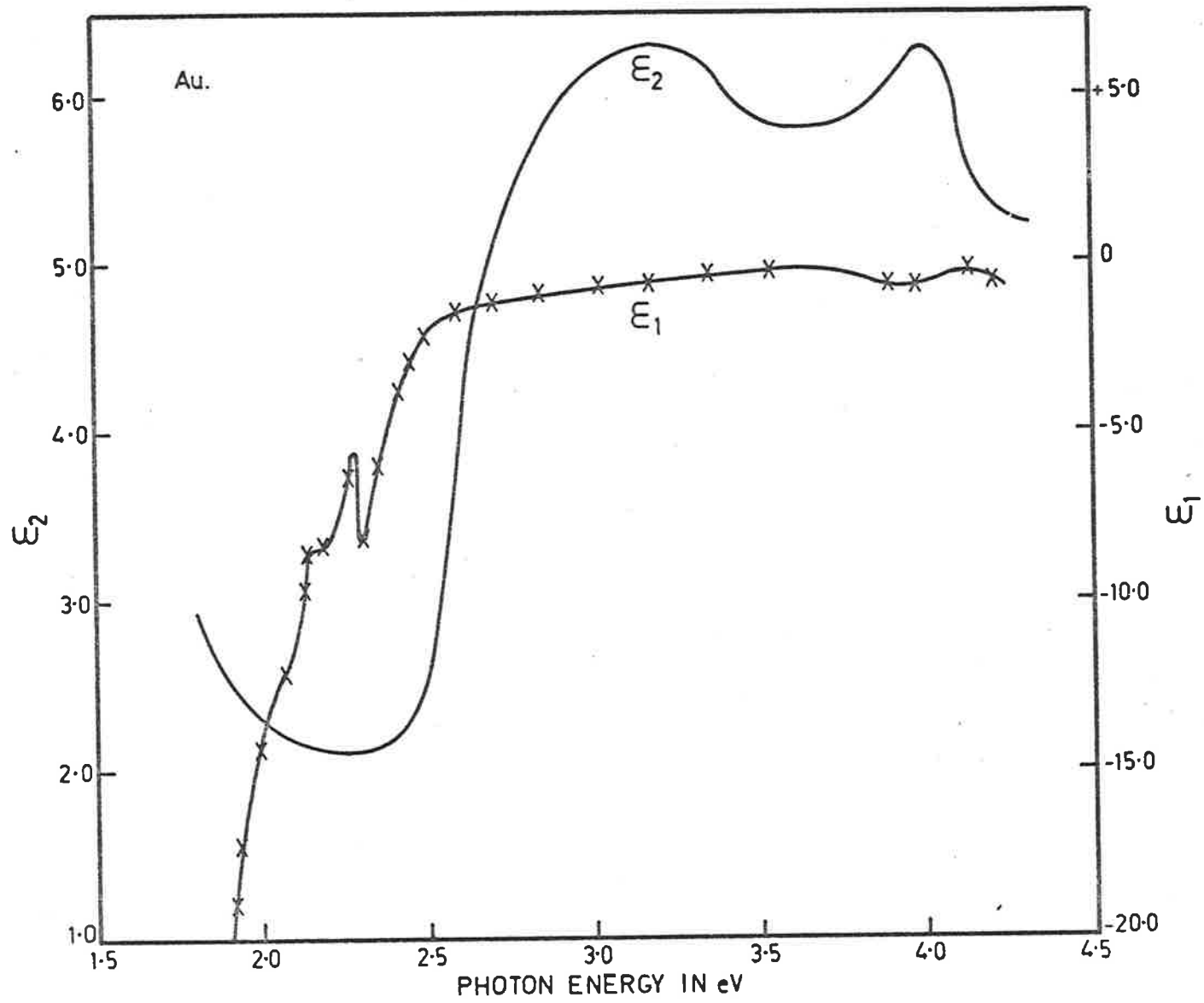
Au.
ε_2
ε_1
6·0
5·0
4·0
3·0
2·0
1·0
+5·0
0
-5·0
-10·0
-15·0
-20·0
1·5
2·0
2·5
3·0
3·5
4·0
4·5
PHOTON ENERGY IN eV

Fig.6.9

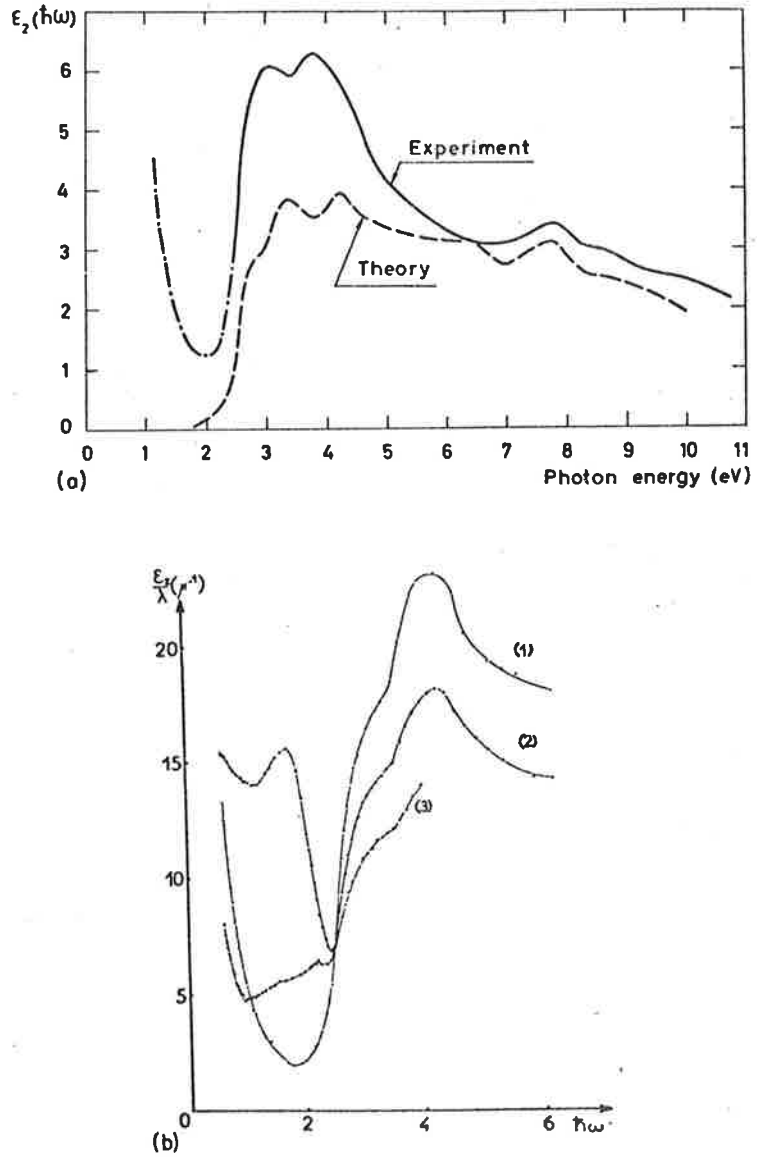

Fig. 6·10 (a) $\epsilon_2(\omega)$ as measured by Irani *et al.* (——) and by Theye (—•—•—). The dotted line is the joint density of states calculated from the band structure by Christensen and Seraphin. (b) Optical absorption in Au for three different films (1) well-crystallized, (2) nonannealed, and (3) island film. From M. L. Thèye, *Phys. Rev. B* **2**, 3060 (1970). (From Nilsson, 1974)

represents the contribution to the absorption from the conduction bands at L as for Cu . In most earlier work an onset of interband absorption was found around 2.5 eV followed by two peaks in ε_2 , one at 3.2 eV and the other at 4.0 eV . Present results also are in good agreement with Hodgson (1968) and with Pells and Shiga (1969) who performed polarimetric measurement in ultra-high vacuum on mechanically polished samples of Au . These two peaks are also clearly observed in the ε_2 curves of Irani *et al* (1971) who performed K-K analysis on evaporated annealed samples of Au and are very close to the theoretical prediction of Christensen and Seraphin (1971) as shown in Figure (6.10). These features correspond to the reflectances (Figure 6.2) at about 2.5 eV, 3.2 and 4.0 eV which indicate the presences of interband transitions at these regions.

The method of measuring the optical constants of Au which has been used in the range from 1.7 to 4.2 eV leads to results in satisfactory agreement with those of other workers, although it is clear that improvement in the accuracy of the reflectance measurement is needed to get more reliable results when the reflectances approach unity.

CHAPTER 7

DETERMINATION OF OPTICAL CONSTANTS OF TRANSITION METALS Ni, Co AND Mo

Though a great deal of work has been done on the optical properties of the transition metals, the determination of their band structures presents more serious theoretical and experimental problems than for normal metals because of the partially filled d and f shells. In the transition metals the Fermi level intersects the d bands (as shown in Figure (6.1a) of Chapter 6) and consequently there are most probably low lying interband transitions from the d bands above the Fermi level to relatively narrow low lying d bands below it. For this reason it is not always possible to achieve a separation of the intra and interband contributions to the dielectric constants of the transition metals.

Lenham and Treharne (1966) in determining the real and imaginary parts of the dielectric constants of transition metals in the region 0.35 to 12.0μ , found several absorption peaks in the infrared region from 0.1 to 2.4 eV. They also commented "It is possible to make a few tentative identifications of some, but by no means all, of the absorption features which are observed". Calculations of the joint density of states for metals also show a great number of fine structures but usually they are not all observed. It has been suggested that in practice some are washed out due to broadening mechanisms, such as electron-electron interactions. By using Tomlin's method (1972) a great number of absorption peaks are observed in the infrared region for transition metals. These will be discussed in detail in later sections of this chapter.

Among the transition metals Ni is the simplest prototype transition metal which has been studied extensively and for this reason the optical properties of Ni are discussed first and then Co and Mo .

7.1 Nickel

7.1.1 Introduction

The electronic band structure of Ni, which is ferromagnetic below 670° K has been of great interest during recent years. The band structure of Ni calculated by Hodges *et al* (1966) was later modified by Hanus *et al* (1968) in order to take into account the low energy structures at 0.25, 0.40 and 1.30 eV found in the temperature modulated reflectance of Ni (Figure 1.6, Chapter 1). Like other transition metals the Fermi level intersects the d bands and interband transitions set in at about 0.3 eV . This causes the reflectance to drop almost immediately from the limiting reflectance value of unity as E approaches zero, whereas in the case of Cu a broad shoulder up to 2.0 eV is observed. This is clear from comparison of the low energy reflectance curve of Ehrenreich and Philipp (1962) and Ehrenreich *et al* (1963) for Cu and Ni respectively as shown in Figure (7.10b). In the present investigation it was observed that the reflectivity of Ni (Figures 7.11, 7.12, 7.14A and 7.14B) fell off steadily, whereas the reflectivity of Au remained almost constant up to 2.0 eV and then fell gradually to 2.4 eV and after that sharply, owing to the absorption edge at 2.5 eV (see Figure 6.2 of Chapter 6). The optical properties of bulk polycrystalline Ni have been studied by Sasovskaya and Noskov (1971, 1972, Figures 7.19(a) and 7.19(b)). They found as many as fourteen peaks in the energy range 0.1 to 2.6 eV, Figure (7.19b) by using Beattie's (1955) polarimetric method. Almost all these structures have been observed independently in other experiments by Afanas'yeva *et al* (1966), Bolotin *et al* (1967), Krinchik *et al* (1968) and Krinchik and Gushchin (1969) and Stoll (1970). In the present investigation of Ni , almost all these peaks have been observed, but one feature which was observed in opaque sputtered Ni films was missing in the curves for opaque

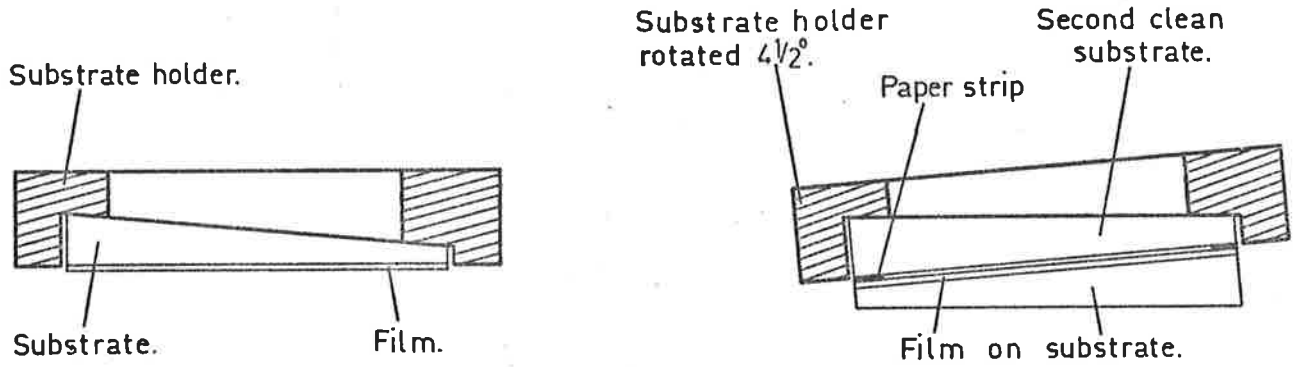

(a)

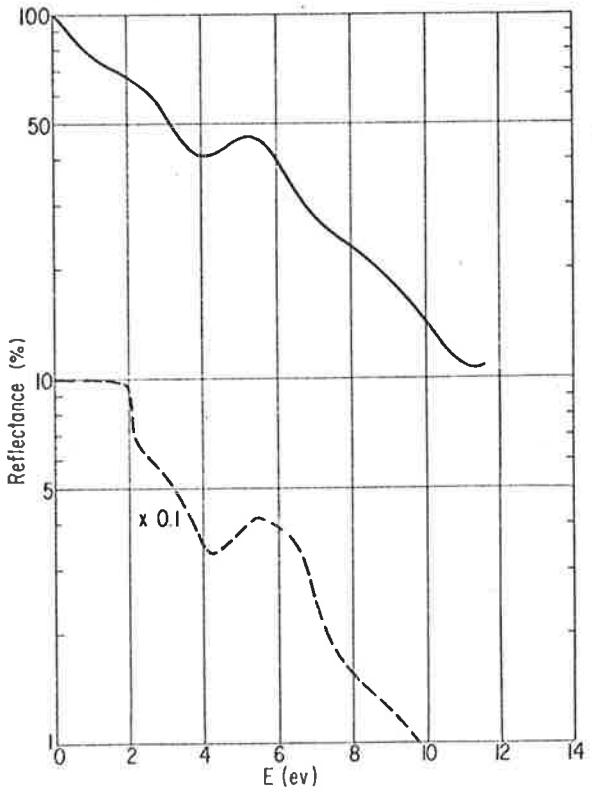

(b) Spectral dependence of the reflectance of Cu (lower curve) and Ni (upper curve). [Cu data from H. Ehrenreich and H. R. Philipp, *Phys. Rev.* **128**, 1622 (1962); Ni data from H. Ehrenreich, H. R. Philipp, and D. J. Olechna, *Phys. Rev.* **131**, 2469 (1963).]
(From Wooten, 1972)

Fig. 7·10

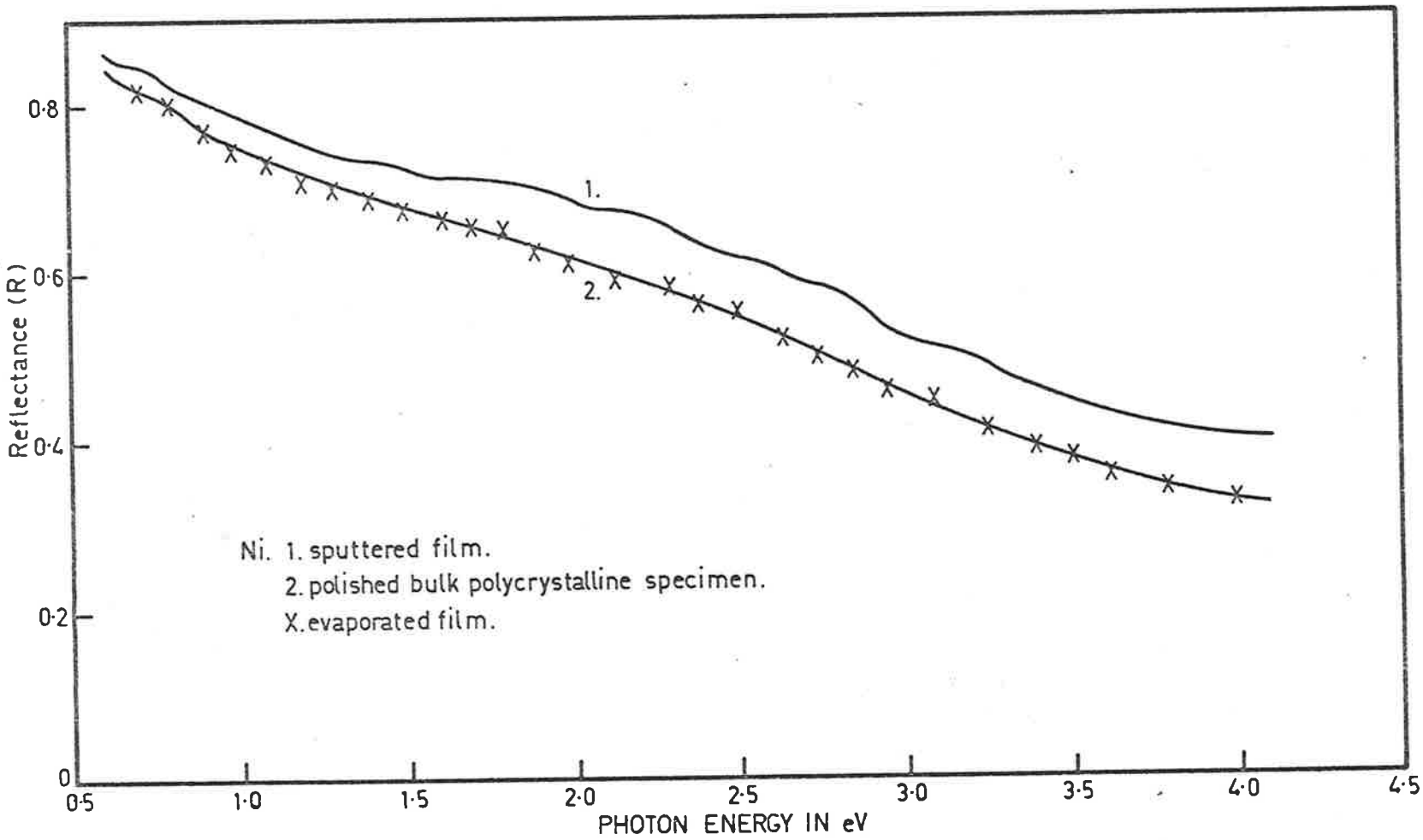
Reflectance (R)
0·8
0·6
0·4
0·2
0
1.
2.
Ni. 1. sputtered film.
2. polished bulk polycrystalline specimen.
X. evaporated film.
0·5
1·0
1·5
2·0
2·5
3·0
3·5
4·0
4·5
PHOTON ENERGY IN eV

Fig. 7.11

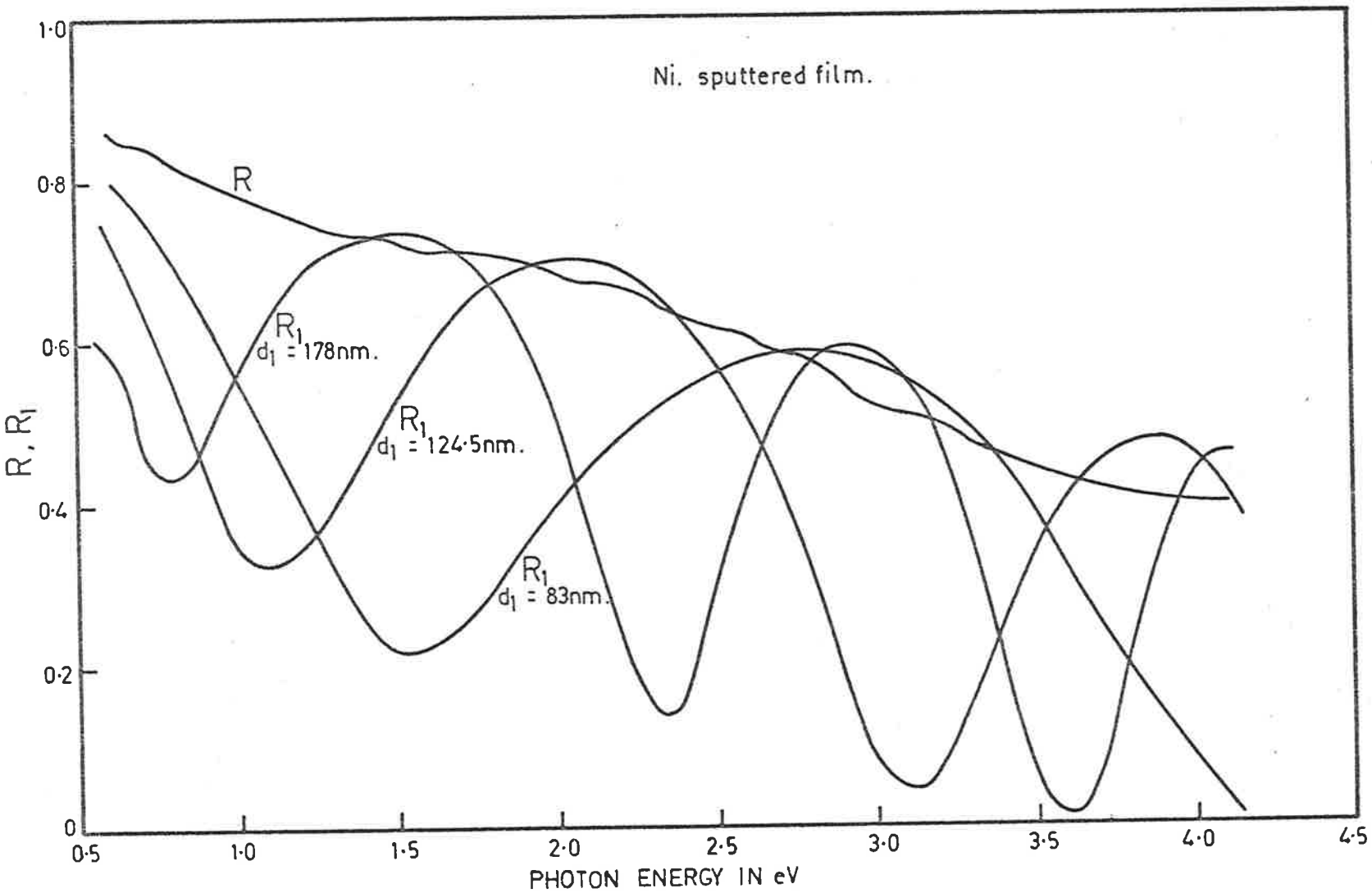
Ni. sputtered film.
R
R_1 d_1 = 178nm.
R_1 d_1 = 124·5nm.
R_1 d_1 = 83nm.
R, R_1
1·0
0·8
0·6
0·4
0·2
0
0·5
1·0
1·5
2·0
2·5
3·0
3·5
4·0
4·5
PHOTON ENERGY IN eV

Fig. 7.12

evaporated Ni films and for polished bulk specimens of Ni . These are shown in Figures (7.18A) and (7.18B) and will be discussed in detail in Section 7.14 of this Chapter. According to Ehrenreich (1966) low energy interband transitions in Ni are largely obscured by free carrier transitions, but they can be detected by using the Ferromagnetic Kerr effect (FKE) techniques. On the other hand Stoll (1970) who observed three structures around 2.25 eV, concluded that they appeared as a result of errors of measurement.

7.1.2 Sample Preparation and Structure of the films

Opaque Ni films were prepared by RF sputtering in the presence of dry argon at the rate of 0.33 nm/sec at a pressure of 1.5m Torr. Thin films of Ta_2O_5 were also prepared by RF sputtering in the presence of 90% extra dry argon and 10% O_2 (medical grade). The rate of evaporation was 0.125 to 0.167 nm/sec and the pressure was 1.5m Torr. The polycrystalline specimens of Ni (20 x 12 x 2 mm) were bought from Koch-Light Laboratories Limited, and were of 99.998% purity. All the polycrystalline specimens of transition metals e.g. Ni, Co, and Mo were polished to a mirror finish in D.R.C. Laboratories by mechanical polishing.

Polished specimens of Ni and opaque Ni films were first examined directly with the scanning electron microscope. No surface structure was detected suggesting that any such structure must be less than 7.0 to 7.5 nm . The scanning electron micrograph of a polycrystalline specimen of Ni is shown in Figure (7.1a). Replicas of the opaque Ni films when examined with the transmission electron microscope showed a roughness of about 2.0 nm .

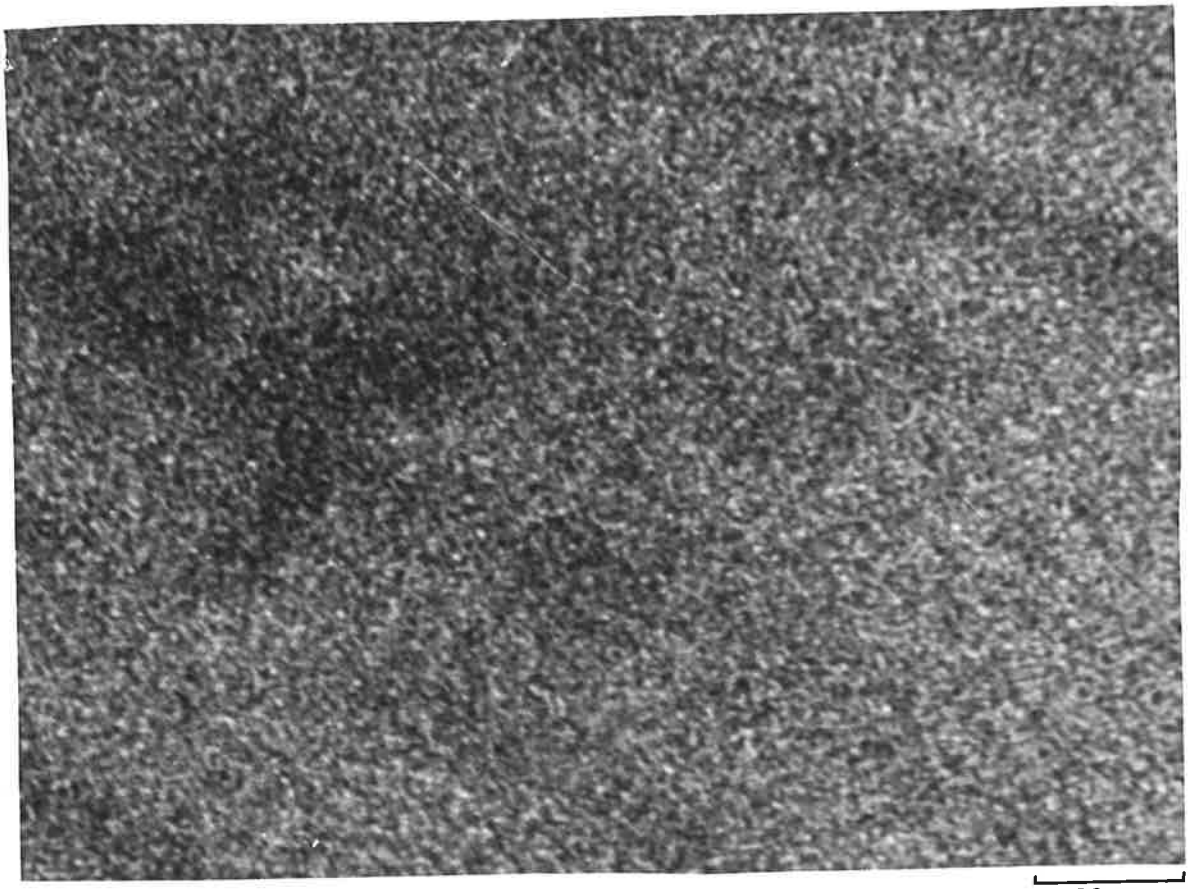

Fig. 7·1a

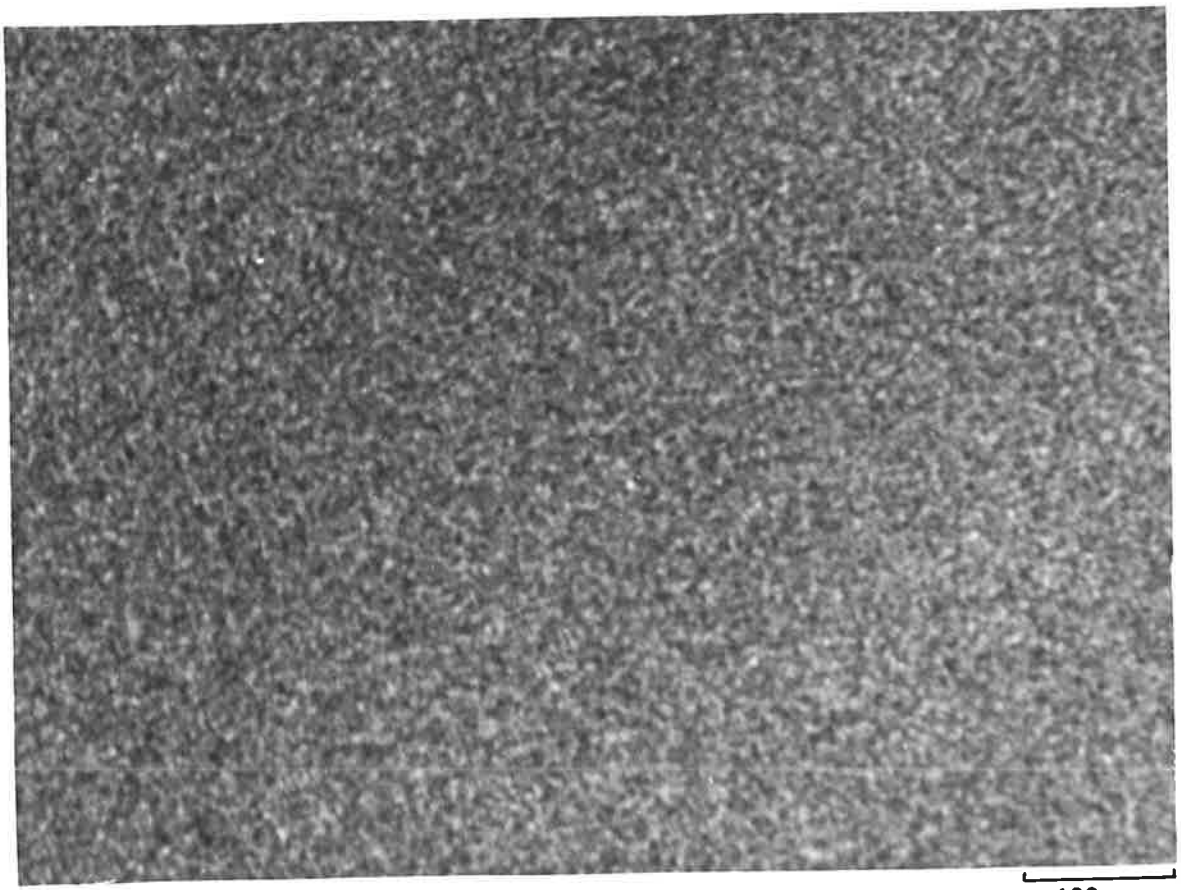

Fig. 7·1b

7.1.3 Determination of the Optical Constants of Ni

(a) Ni film prepared by sputtering

The values of the optical constants found by using a Ta_2O_5 film of thickness 83.0 nm are shown in Figures (7.13) and (7.16) with error bars. To take into account the surface roughness of the order of 2.0 nm , a double layer programme was used as mentioned in Chapter 5, Section (5.3). This showed that such a thin surface layer had little effect on the optical constants and proper continuity of the dispersion curve could be obtained by neglecting the surface roughness. Moreover the effect on the values of the optical constants due to this roughness was well within the variation between specimens.

The variation in reflectivity of Ni films with time, and when heated in the presence of oxygen to a temperature of about 1000°C are shown in Table 7.11. The reflectivity of the Ni films was reduced considerably in the visible and ultraviolet when heated in oxygen as might be expected, but the ageing effect on the reflectivity was much smaller and almost within the error limits of the experimental measurements, if the measurements were taken within three days. The values of reflectivities need to be measured as accurately as possible at wavelength or energy intervals as small as possible especially in the infrared region. In the present investigation the reflectivities R and R_1 were measured at least twice throughout the whole wavelength region. To avoid ageing effect the measurement of reflectivies were always done within three days of specimen preparation. Even so, the dispersion curve is not as smooth in the infrared as in the visible and ultraviolet. To minimise the errors in the optical constants, three different thicknesses of Ta_2O_5 films were deposited on the opaque Ni films. The observed values of the optical constants for three different

TABLE 7.11

THE OPAQUE Ni FILM WAS REMOVED FROM THE VACUUM CHAMBER 3 HOURS AFTER THE PREPARATION

Wavelength in nm.	Just after the opening of the vacuum chamber	After 3 hours	After 6 hours	After 1 day	After 3 days	After 7 days	After 14 days	Then heated in oxygen*
2000	0.832			0.832	0.830	0.832	0.831	0.829
1500	0.818			0.818	0.817	0.818	0.816	0.813
1600	0.800			0.800	0.798	0.800	0.800	0.798
1400	0.776			0.775	0.773	0.776	0.775	0.772
1200	0.743			0.744	0.743	0.744	0.744	0.742
1000	0.712	0.712	0.711	0.710	0.710	0.708	0.705	0.702
950	0.702	0.703	0.702	0.702	0.702	0.702	0.694	0.690
900	0.694	0.693	0.695	0.692	0.692	0.691	0.681	0.678
850	0.687	0.685	0.684	0.685	0.684	0.679	0.671	0.666
800	0.674	0.672	0.671	0.672	0.671	0.667	0.660	0.657
750	0.660	0.659	0.658	0.660	0.658	0.651	0.648	0.644
700	0.646	0.645	0.643	0.645	0.644	0.638	0.634	0.630

/continued...

TABLE 7.11 Continued...

Wavelength in nm.	Just after the opening of the vacuum chamber	After 3 hours	After 6 hours	After 1 day	After 3 days	After 7 days	After 14 days	Then heated in oxygen*
650	0.630	0.629	0.629	0.627	0.628	0.624	0.619	0.611
600	0.611	0.610	0.610	0.608	0.608	0.602	0.598	0.587
550	0.585	0.584	0.583	0.580	0.582	0.578	0.573	0.558
500	0.553	0.553	0.552	0.550	0.550	0.545	0.540	0.521
450	0.510	0.510	0.509	0.508	0.507	0.506	0.499	0.475
400							0.440	0.414
350							0.381	0.342
300							0.351	0.308
260							0.366	0.320
250							0.370	0.321

* For 15 to 18 minutes approximately at temperature 1000°C and pressure 0.1 Torr.

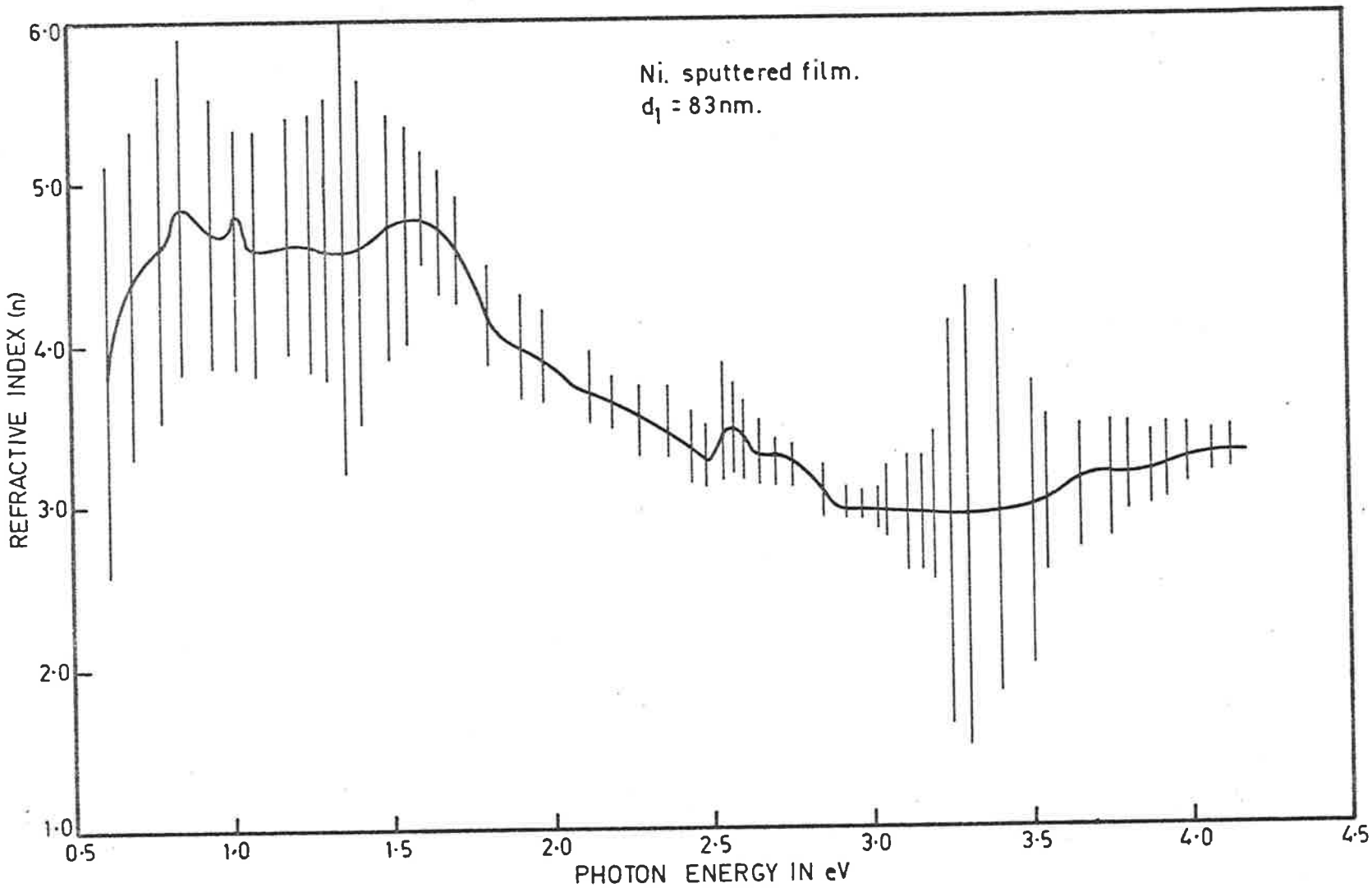
Ni. sputtered film.
d_1 = 83nm.
REFRACTIVE INDEX (n)
6·0
5·0
4·0
3·0
2·0
1·0
0·5
1·0
1·5
2·0
2·5
3·0
3·5
4·0
4·5
PHOTON ENERGY IN eV

Fig.7.13

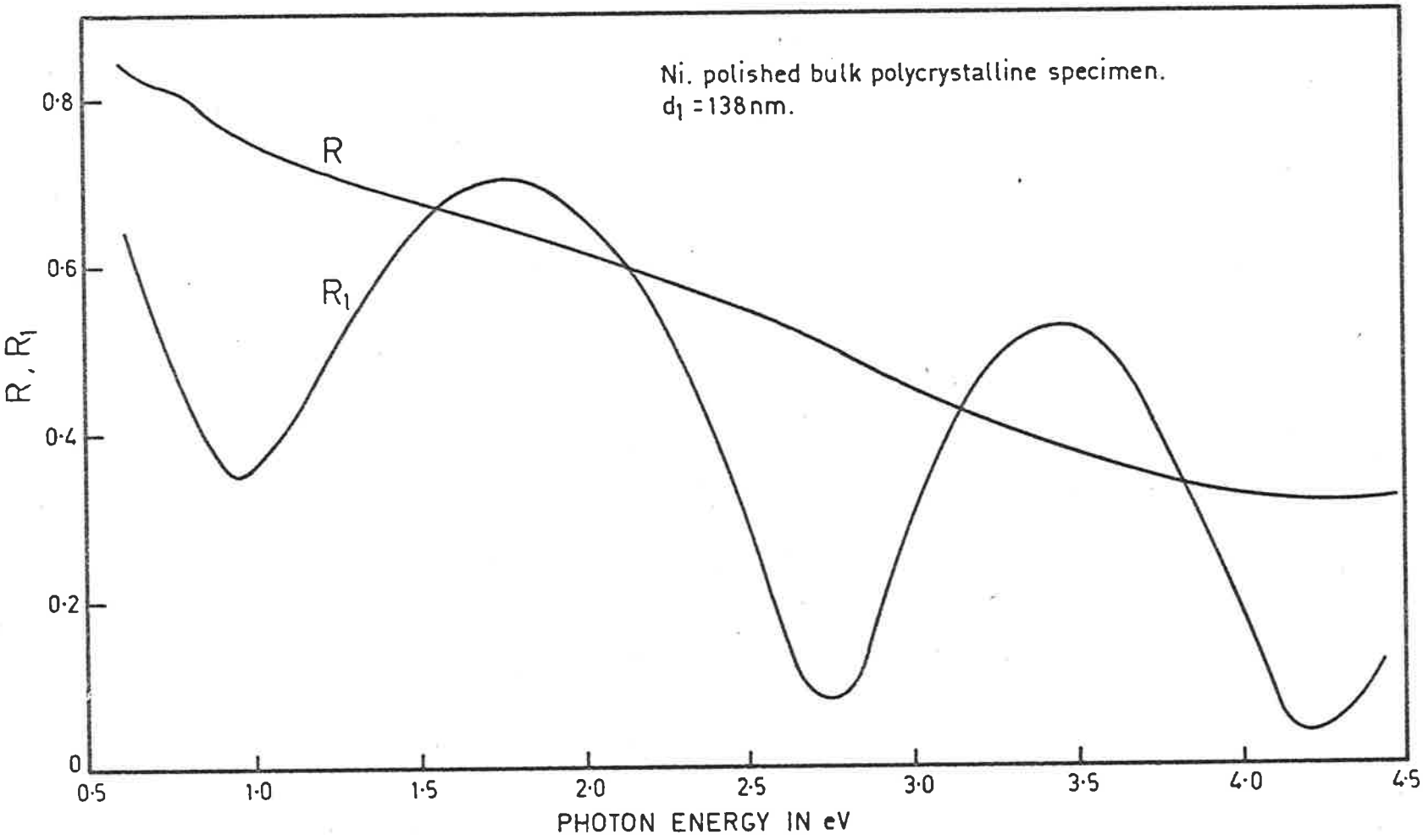
Ni. polished bulk polycrystalline specimen.
d_1 = 138 nm.
R
R_1
R, R_1
0·8
0·6
0·4
0·2
0
0·5
1·0
1·5
2·0
2·5
3·0
3·5
4·0
4·5
PHOTON ENERGY IN eV

Fig. 7.14A

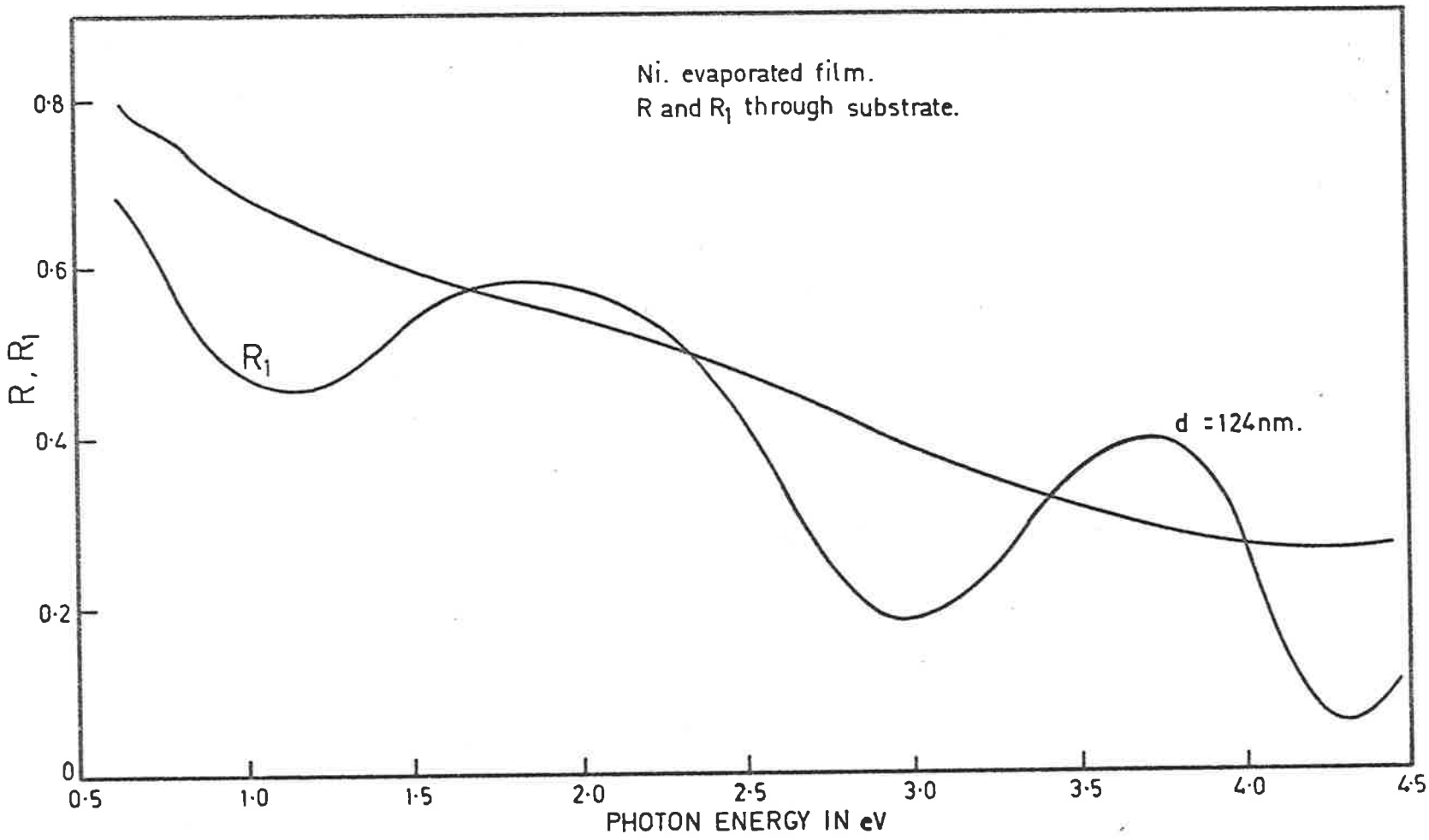
Ni. evaporated film.
R and R_1 through substrate.
R_1
d =124nm.
R, R_1
0·8
0·6
0·4
0·2
0
0·5
1·0
1·5
2·0
2·5
3·0
3·5
4·0
4·5
PHOTON ENERGY IN eV

Fig. 7.14B

thicknesses of Ta_2O_5 films varied from 2.0 to 4.5% throughout the whole energy range.

(b) Polished specimen of Ni

The reflectivity curve of this specimen together with that of an opaque sputtered Ni film is shown in Figure (7.11). The reflectivity of the opaque Ni film is much higher than that of the polished specimen and the values of the optical constants of the former were found to be higher than those of the latter. A similar situation arises in the case of Mo (see Section 7.3 of this Chapter).

The values of optical constants of this specimen are compared with those of other workers in Figures (7.17A) and (7.17B).

(c) Opaque Ni film with light incident through the quartz substrate

To minimise the ageing effects as well as the effect due to the formation of oxide layers, which usually affect metals films, they may be deposited onto a thin film of Ta_2O_5 prepared on the substrate and the measurements taken from the substrate side. For optical measurements the specimen was mounted in the specimen holder face downward on another cleaned quartz wedge separated by two thin strips of paper to prevent contact, as shown in Figure 7.10(a). To ensure the correct orientation of the film the substrate holder was rotated approximately $4\frac{1}{2}^{\circ}$ about the vertical so that the film plane remains in the same orientation, with respect to the beam, as it does when taking front surface measurements.

The values of reflectances (R) and (R_1) through the substrate side for an opaque Ni film prepared by electron beam evaporation and with a Ta_2O_5 film by 124.0 nm are shown in Figure (7.14B). The values of the optical constants are shown in Figures (7.15) and (7.16).

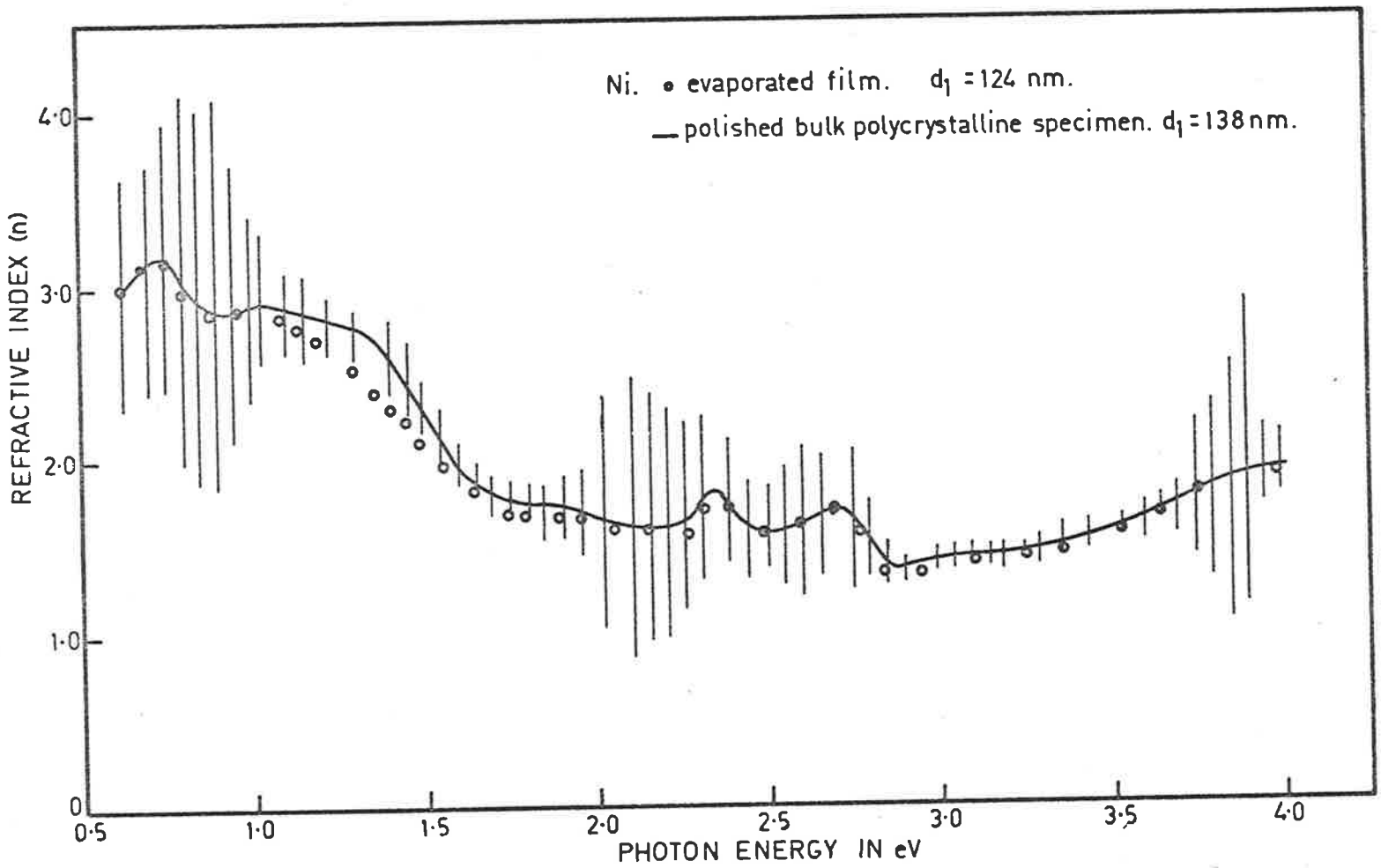
Ni. • evaporated film. d_1 = 124 nm.
— polished bulk polycrystalline specimen. d_1 = 138 nm.
REFRACTIVE INDEX (n)
4·0
3·0
2·0
1·0
0
0·5
1·0
1·5
2·0
2·5
3·0
3·5
4·0
PHOTON ENERGY IN eV

Fig. 7.15

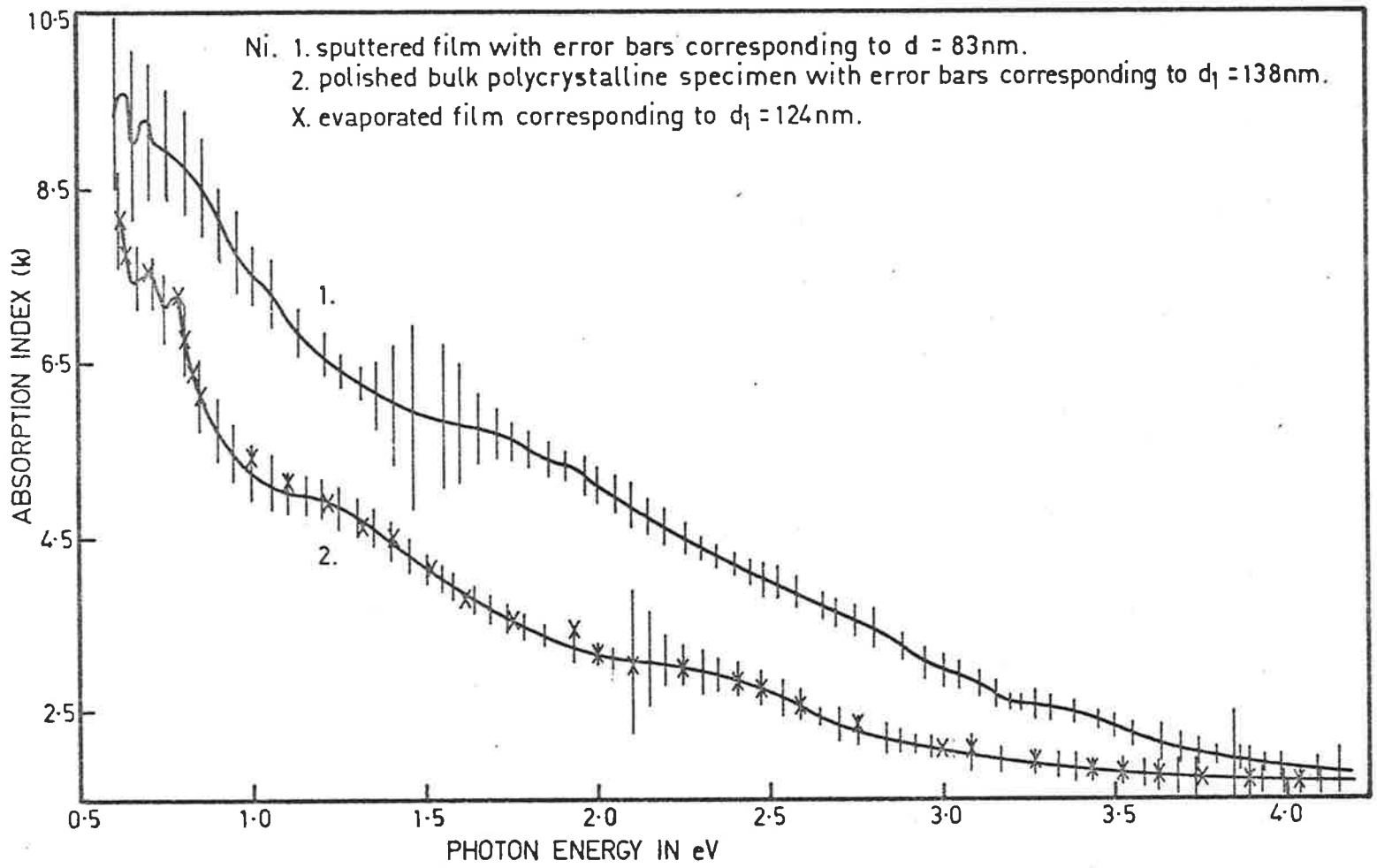
Ni. 1. sputtered film with error bars corresponding to d = 83nm.
2. polished bulk polycrystalline specimen with error bars corresponding to d_1 = 138nm.
X. evaporated film corresponding to d_1 = 124nm.
ABSORPTION INDEX (k)
10·5
8·5
6·5
4·5
2·5
1.
2.
0·5
1·0
1·5
2·0
2·5
3·0
3·5
4·0
PHOTON ENERGY IN eV

Fig. 7.16

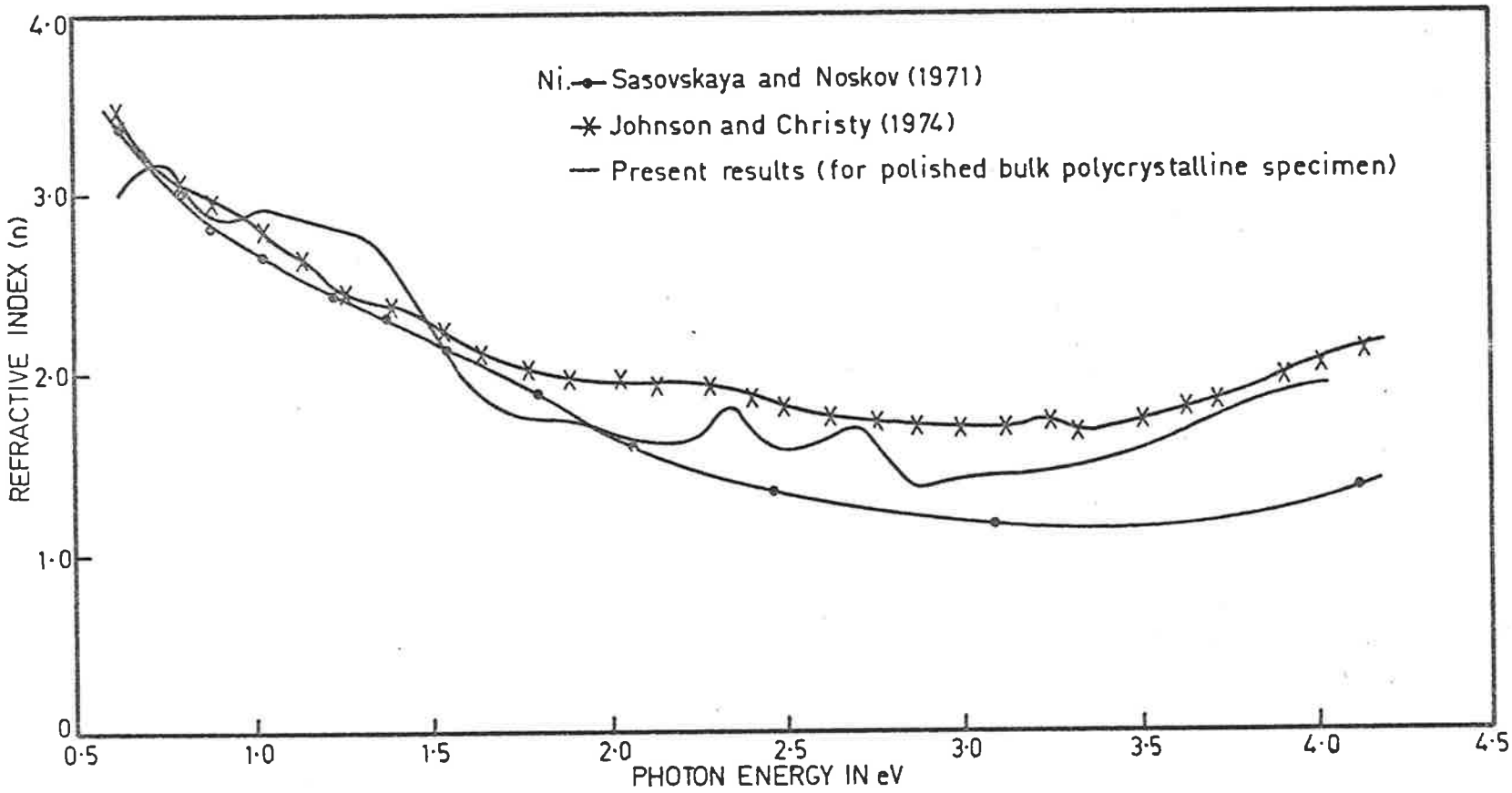
Ni.—●— Sasovskaya and Noskov (1971)
—✳— Johnson and Christy (1974)
— Present results (for polished bulk polycrystalline specimen)
REFRACTIVE INDEX (n)
PHOTON ENERGY IN eV
4·0
3·0
2·0
1·0
0
0·5
1·0
1·5
2·0
2·5
3·0
3·5
4·0
4·5

Fig. 7.17A

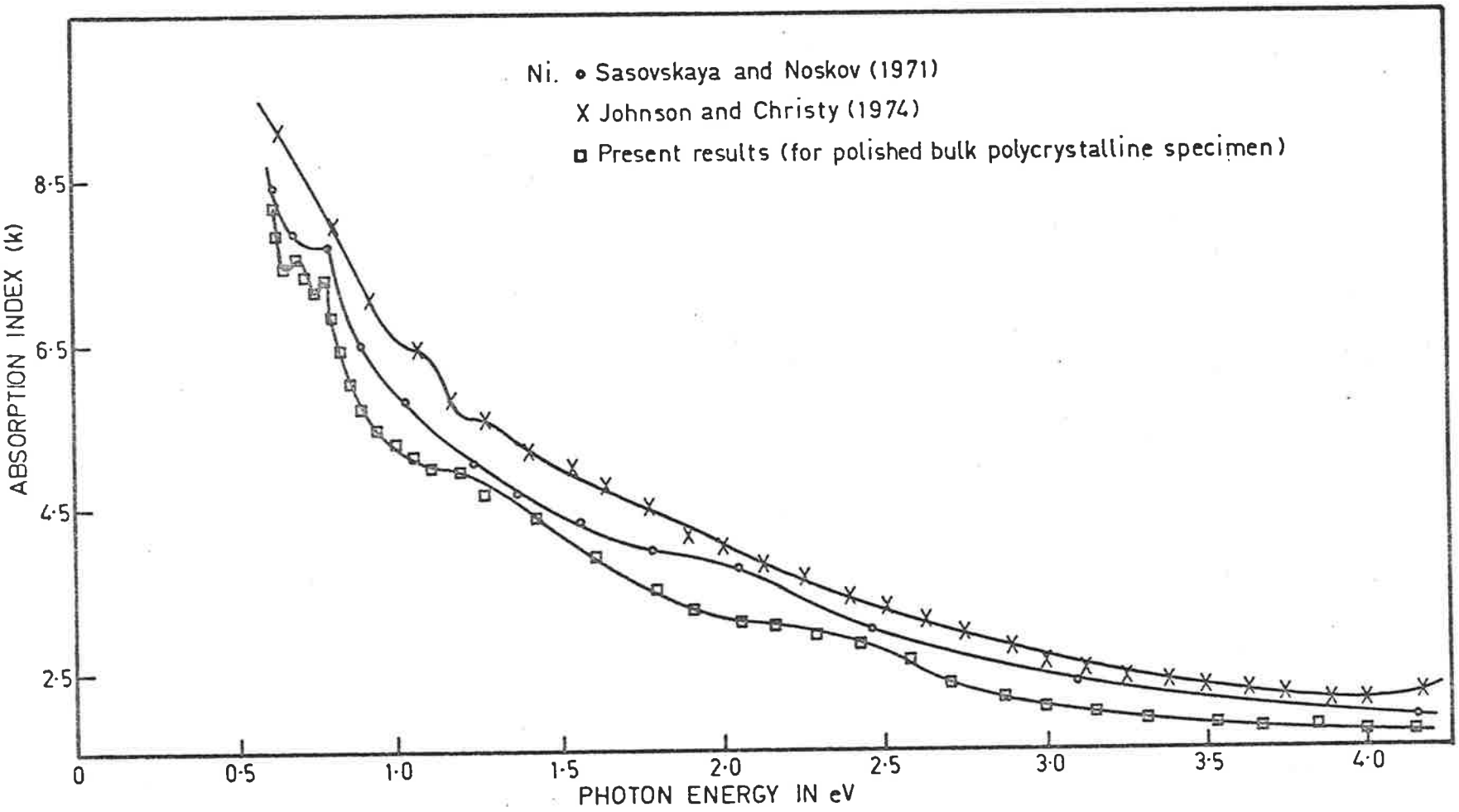
Ni. ∘ Sasovskaya and Noskov (1971)
X Johnson and Christy (1974)
□ Present results (for polished bulk polycrystalline specimen)
ABSORPTION INDEX (k)
8·5
6·5
4·5
2·5
0
0·5
1·0
1·5
2·0
2·5
3·0
3·5
4·0
PHOTON ENERGY IN eV

Fig. 7.17B

The reflectivity of this opaque specimen was also measured from the other side, i.e. with the light incident in air, and was found to be almost identical with that of the polished specimen referred to in Section (7.1.3b). Consequently, the two kinds of specimen were in very close agreement (Figures 7.11, 7.15 and 7.16). The real and imaginary parts of the dielectric constant of either specimen are as shown in Figure (7.18B).

7.1.4 Results and Discussion

The ε_2 curve for Ni films prepared by sputtering and by evaporation are shown in Figures (7.18A) and (7.18B). They show a number of maxima which, like those of the corresponding curves of Ge, can be attributed to interband transitions. The structures at 0.670 and 0.650 eV appear in ε_1 curves but are not shown in Figures (7.18A and 7.18B). The structure at 0.80 eV which is missing in ε_2 curves of bulk polycrystalline specimen of Ni and evaporated Ni films appears in the respective reflectance curves.

In Table (7.12) the energies at which peaks appear are set out. The first three entries refer to the author's own result and are very similar to those of Sasov'skaya and Noskov (1971, 1972), obtained by the procedure of Beattie (1955). Other authors find only a few peaks, but they are among those found in the present work. Thus Hanus *et al* (1968) using the method of thermo-modulated reflectances for Ni films find peaks at 0.25, 0.40 and 1.3 eV; Ehrenreich *et al* (1963) find peaks at 0.3 and 1.4 eV for electrically etched Ni by the K-K method; Stoll (1970), by the polarimetric method, finds structures at 2.25, 2.34, 2.17 and 2.45 eV for polycrystalline Ni .

Although there are some differences in our results for films prepared by sputtering and by electron beam evaporation, the latter were

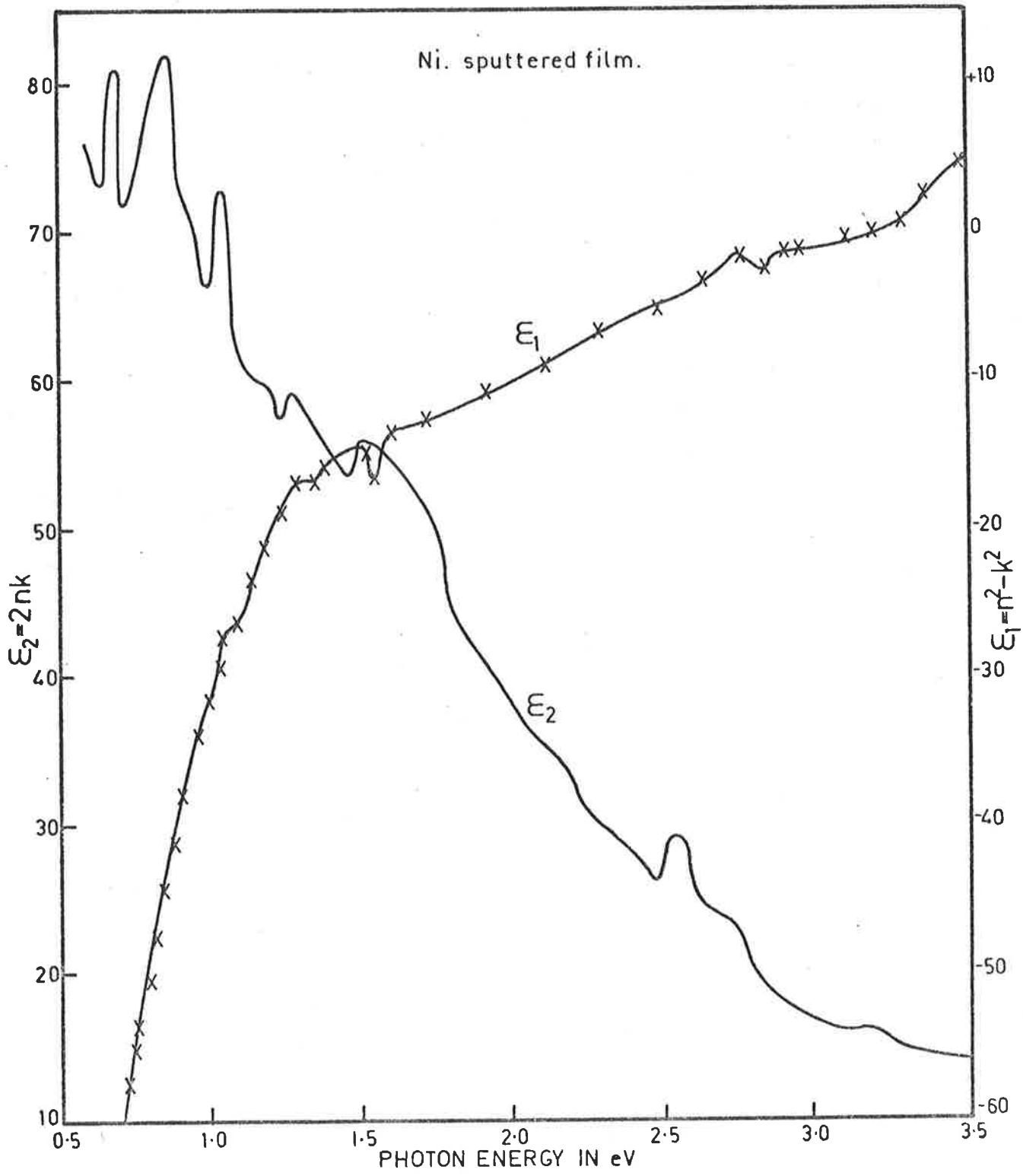
Ni. sputtered film.
80
70
60
50
40
30
20
10
+10
0
-10
-20
-30
-40
-50
-60
ε_1
ε_2
$\varepsilon_2=2nk$
$\varepsilon_1=n^2-k^2$
0·5
1·0
1·5
2·0
2·5
3·0
3·5
PHOTON ENERGY IN eV

Fig. 7·18A

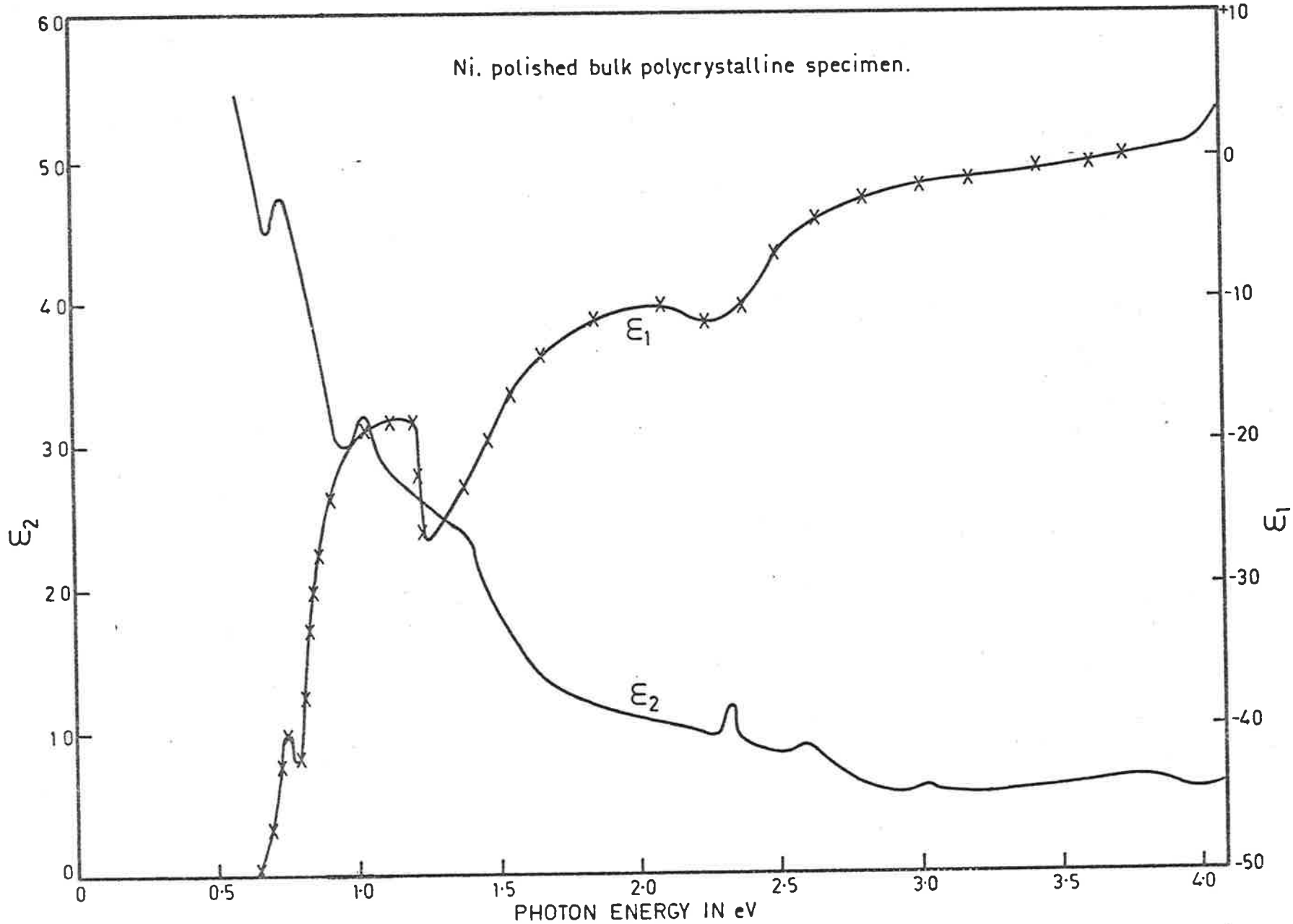
Ni. polished bulk polycrystalline specimen.
ε_1
ε_2
ε_2
ε_1
PHOTON ENERGY IN eV
0
0·5
1·0
1·5
2·0
2·5
3·0
3·5
4·0
60
50
40
30
20
10
0
+10
0
-10
-20
-30
-40
-50

Fig. 7.18B

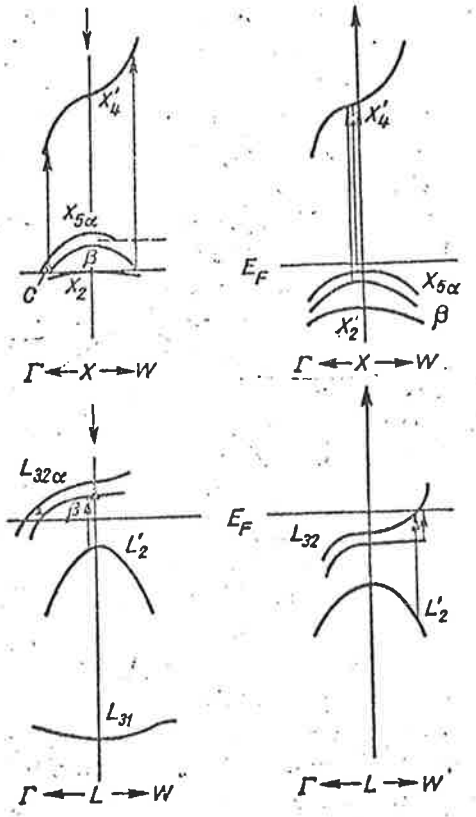

(a) Diagram showing arrangement of the energy levels near the high symmetry points L and X in the electron spectrum of ferromagnetic nickel.

(From Sasovskaya and Noskov, 1972)

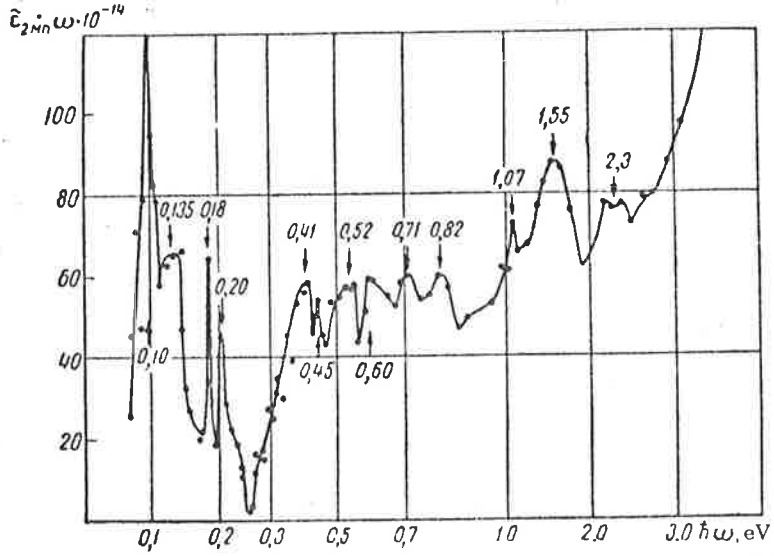

(b) Minimum fraction due to interband transitions in light conductivity of nickel.

(From Sasovskaya and Noskov, 1971)

Fig. 7·19

TABLE 7.12

	Type of Ni	Number of optical features in eV observed in Ni										
		1	2	3	4	5	6	7	8	9	10	11
†	Opaque Ni films prepared by D.R.C.S.	0.67	0.71	0.85	1.03	1.27	1.50	2.32 (WK)*	2.53	2.80 (WK)	3.21 (WK)	3.80 (WK)
†	Opaque Ni films prepared by evap.	0.65	0.75	0.80	1.03	1.22	1.40 (WK)	2.33	2.60		3.05	3.75 (WK)
†	Bulk polished poly-crystalline specimens of Ni	0.65	0.75	0.80	1.03	1.22	1.40 (WK)	2.33	2.60		3.05 (WK)	3.75 (WK)
	Poly-crystalline specimens of Ni (Sasovs'-kaya and Noskov 1971 and 1972)	0.60	0.71	0.82	1.05		1.55	2.3	2.6			
		and other features at 0.075, 0.095, 0.135, 0.18, 0.20, 0.41, 0.45 and 0.52 eV.										

† Present Results

/Continued....

TABLE 7.12 Continued....

Type of Ni	Number of optical features in eV observed in Ni										
	1	2	3	4	5	6	7	8	9	10	11
Ni films (Hanus *et al* 1967 and 1968)					1.3 other features at 0.25, 0.4 eV						
Electrically etched Ni (Ehrenreich *et al* 1963)					and others at 0.3 eV	1.4					
A disc of polycrystalline Ni (Stoll 1970)					others at 2.17, 2.25 and 2.45 eV		2.34				

$(WK)^{*}$ → weak.

very close to the results for polished bulk material, and include most of the features found by Sasovs'kaya and Noskov (1971, 1972) in the range of measurements 0.62 to 4.0 eV. The higher energy peak at 2.80 eV, has not been found by other workers, but a peak in this energy range has been found for Co by the writer.

Our main concern at present has been with the applicability of the method of measurement that has been used. The consistency of the results for opaque films and bulk material and the agreement with the results of Sasovs'kaya and Noskov (1971, 1972) shows that the method is sound in principle.

7.2 Cobalt

7.2.1 Introduction

According to theoretical predictions the densities of states for all 3d ferromagnetic materials (Fe, Co and Ni) are quite similar within about 3.5 eV of the Fermi surface (Spicer 1966, Figure 7.28). The energy spectrum of ferromagnetic metals is a combination of two band systems for electrons having spins oriented with and against the direction of spontaneous magnetization and hence behaves in a complicated way. The electronic structure of the ferromagnetic materials is not clearly understood yet despite a large number of excellent studies (Herring 1966, Afanas'yeva and Kirillova 1967, Yu and Spicer 1968, Yu *et al* 1968, Lomer 1971, Bolotin *et al* 1973), because of the lack of experimental information about the electronic structure away from the Fermi surface. A number of investigators (Kirillova and Charikov 1964, Lenham and Treherne 1966, Afanas'yeva and Kirillova 1967), have shown that interband transitions occur in Co beginning from quantum energies ~ 0.25 eV and that it has several optical features in the infrared region. Yu *et al* (1968) observed a series of structures at 3.2, 5.0 and 6.0 eV in the absorption coefficient while - Im(ε) is smooth and free of strong structure. Again photoemission investigations of Yu and Spicer (1968) showed three peaks in the density of states of cobalt at 0.3, 2.4 and 5.2 eV below the Fermi level. Afanas'yeva and Kirillova (1967, Figure 7.27) observed structures at 0.7, 0.85, 1.1 and 1.4 eV in the conductivity curve of polycrystalline specimens of cobalt. In the present work several absorption peaks were observed in polished specimens of Co which are almost identical with those of Ni . All these are discussed in detail in Section (7.2.4).

7.2.2 Sample preparation and structure of the films

Polycrystalline specimens of Co (25 x 24 x 2 mm) were bought from Koch-Light Laboratories Limited and were of 99.998% purity. All these specimens were mechanically polished and coated with Ta_2O_5 film by sputtering.

No surface roughness was observed when these specimens were examined with a scanning electron microscope (7.1b) which means that if there was any roughness it must be less than 7.0 to 7.5 nm.

7.2.3 Determination of the optical constants of Co

The reflectances R and R_1 for a polycrystalline specimen of Co before and after coating with a layer of Ta_2O_5 of thickness 129 nm are shown in Figure (7.2 1). The corresponding optical constants are shown in Figures (7.22 and 7.23). The same precautions as mentioned in case of Ni were adopted for the measurement of R and R_1. Figures (7.2 4) and (7.2 5) show a comparison with the result of Afanas'yeva and Kirillova (1967) and Bolotin *et al* (1973) who used Beattie's (1955) method for polycrystalline specimens of Co and of Johnson and Christy (1974) who used reflection and transmission measurements with thin films.

7.2.4 Results and discussion

The imaginary part of the dielectric constants (Figure 7.26) shows structures at 0.75, 0.85 , 1.2, 1.35, 2.22 and 3.2 eV like those of the corresponding curves of Ni . Some of these features may be attributed to the same transitions as those of Ni . The first four absorption features found by the author are very close to those of Afanas'yeva and Kirillova (1967), who found structures at 0.7, 0.85, 1.1 and 1.4 eV which are shown in Figure (7.27). The fifth absorption

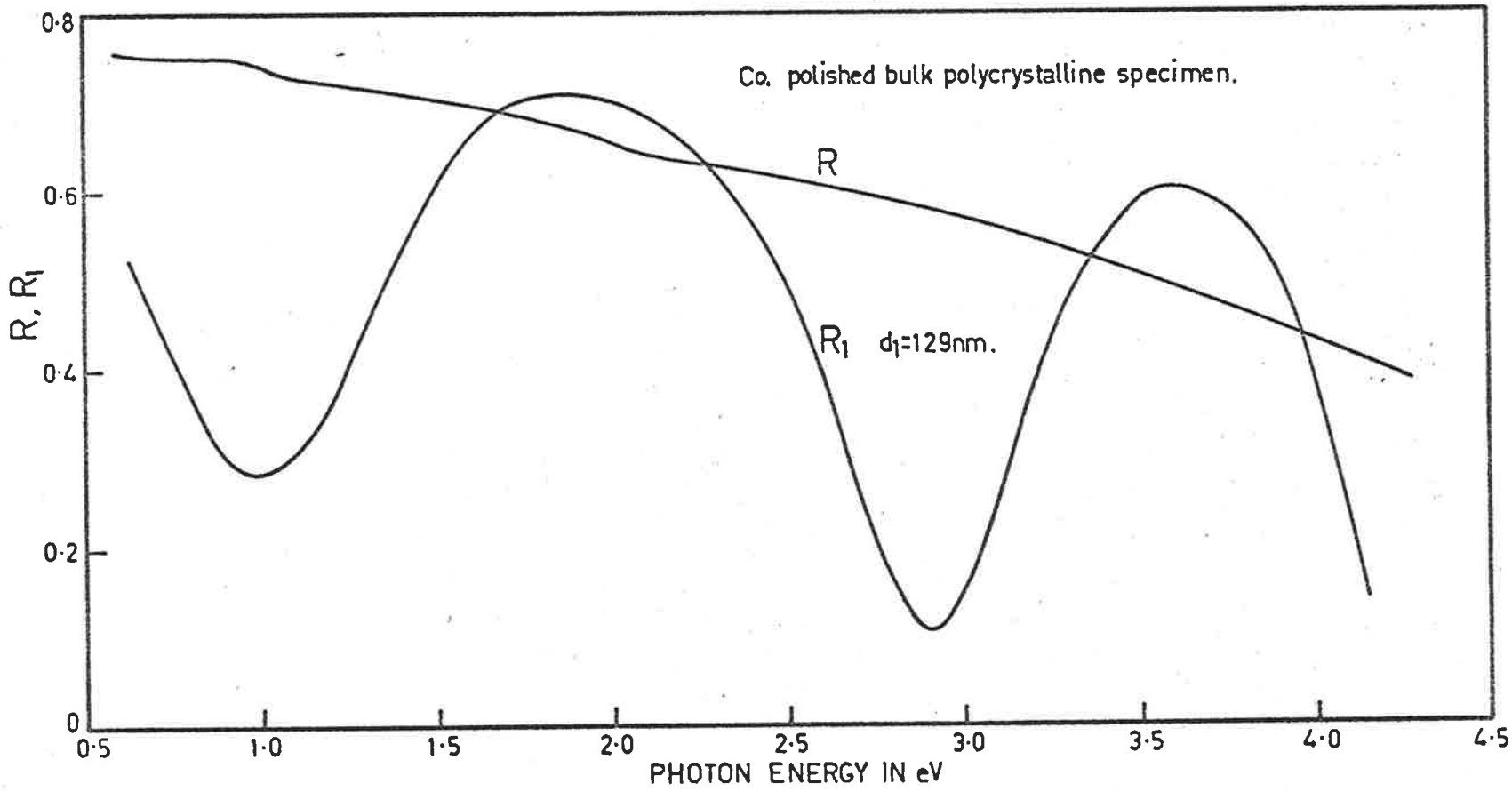
Co. polished bulk polycrystalline specimen.
R
R1 d1=129nm.
R, R1
0·8
0·6
0·4
0·2
0
0·5
1·0
1·5
2·0
2·5
3·0
3·5
4·0
4·5
PHOTON ENERGY IN eV

Fig. 7.21

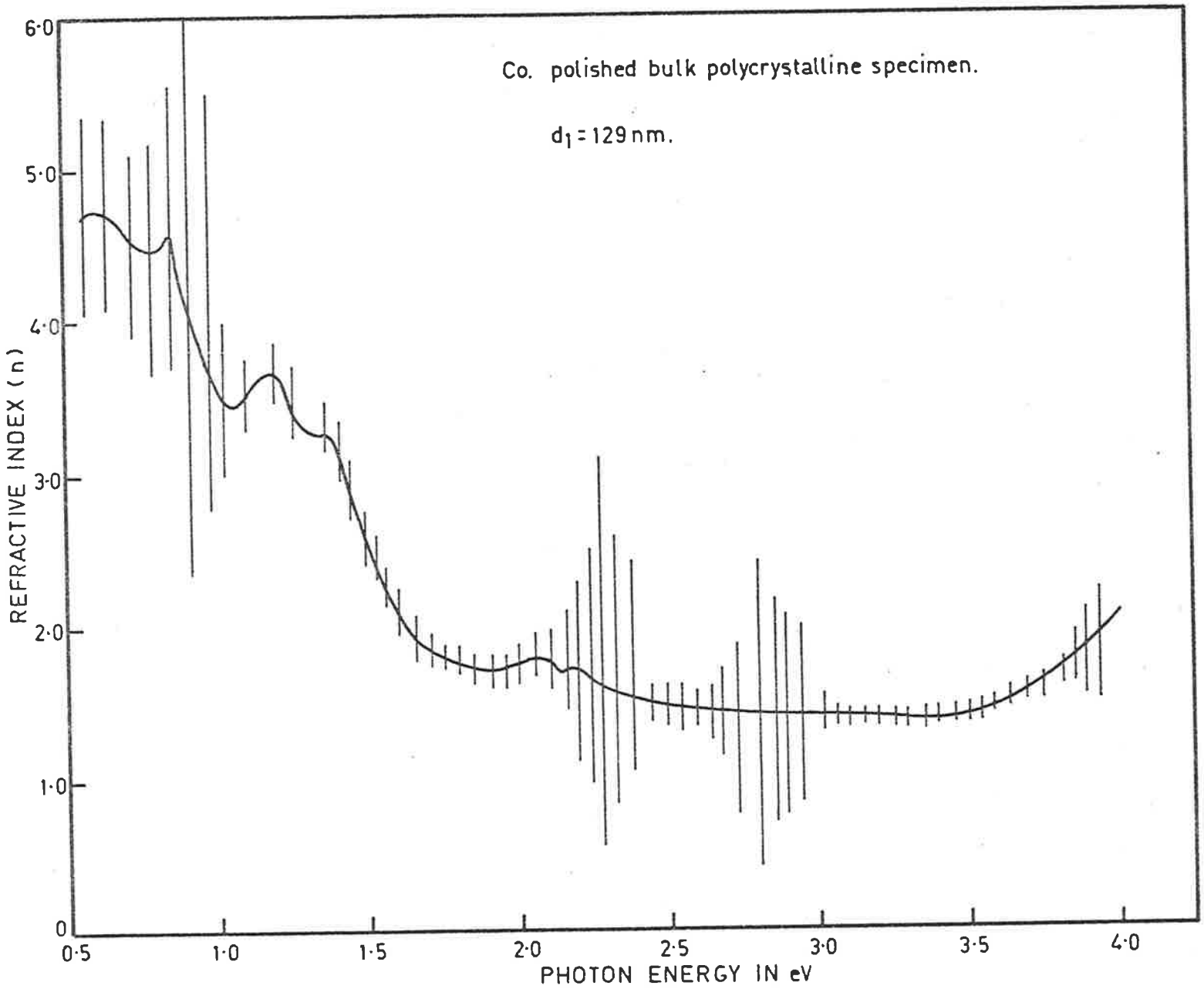
Co. polished bulk polycrystalline specimen.
d_1 = 129 nm.
REFRACTIVE INDEX (n)
6·0
5·0
4·0
3·0
2·0
1·0
0
0·5
1·0
1·5
2·0
2·5
3·0
3·5
4·0
PHOTON ENERGY IN eV

Fig. 7.22

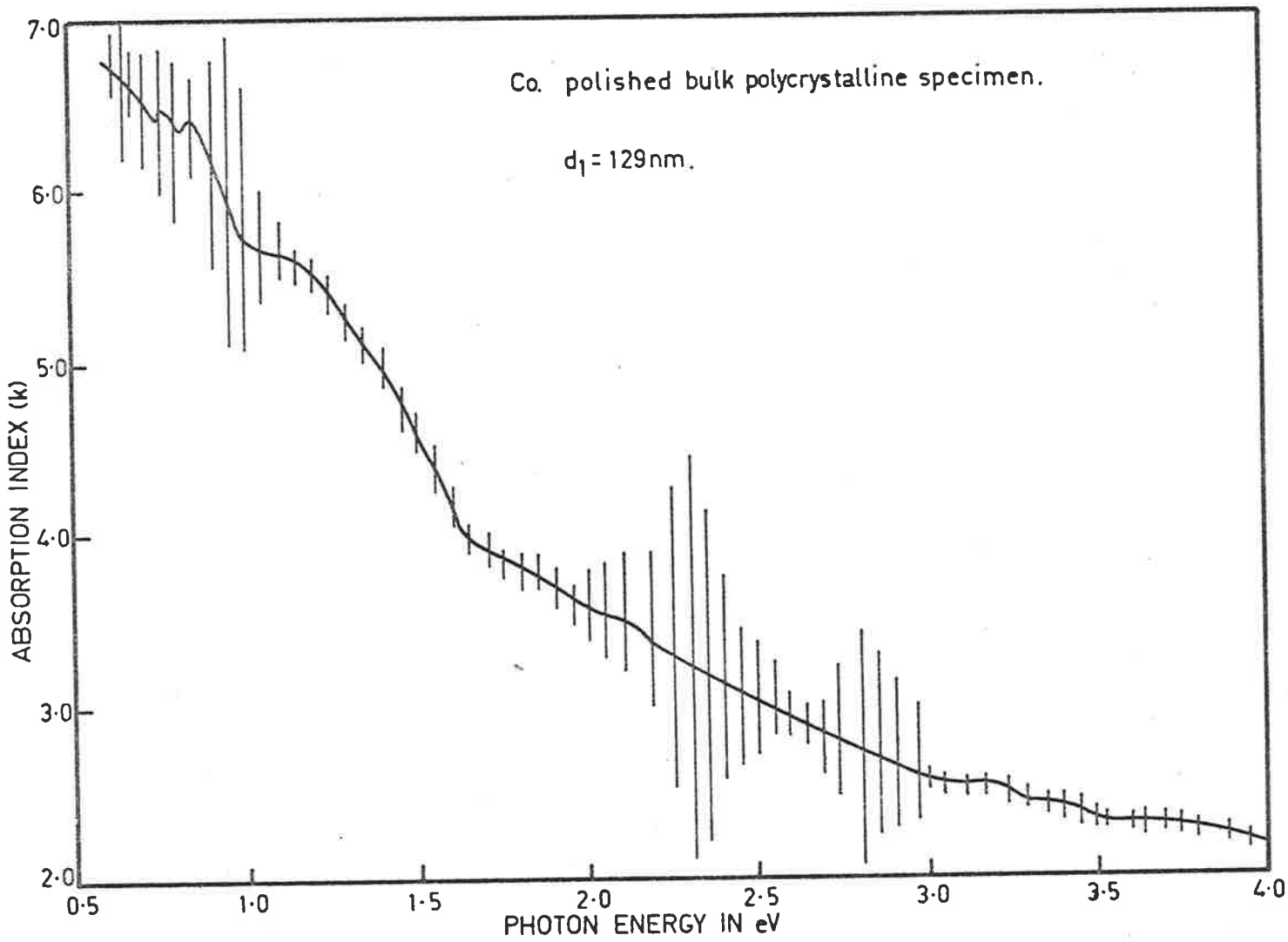
Co. polished bulk polycrystalline specimen.
d_1 = 129nm.
ABSORPTION INDEX (k)
7·0
6·0
5·0
4·0
3·0
2·0
0·5
1·0
1·5
2·0
2·5
3·0
3·5
4·0
PHOTON ENERGY IN eV

Fig. 7.23

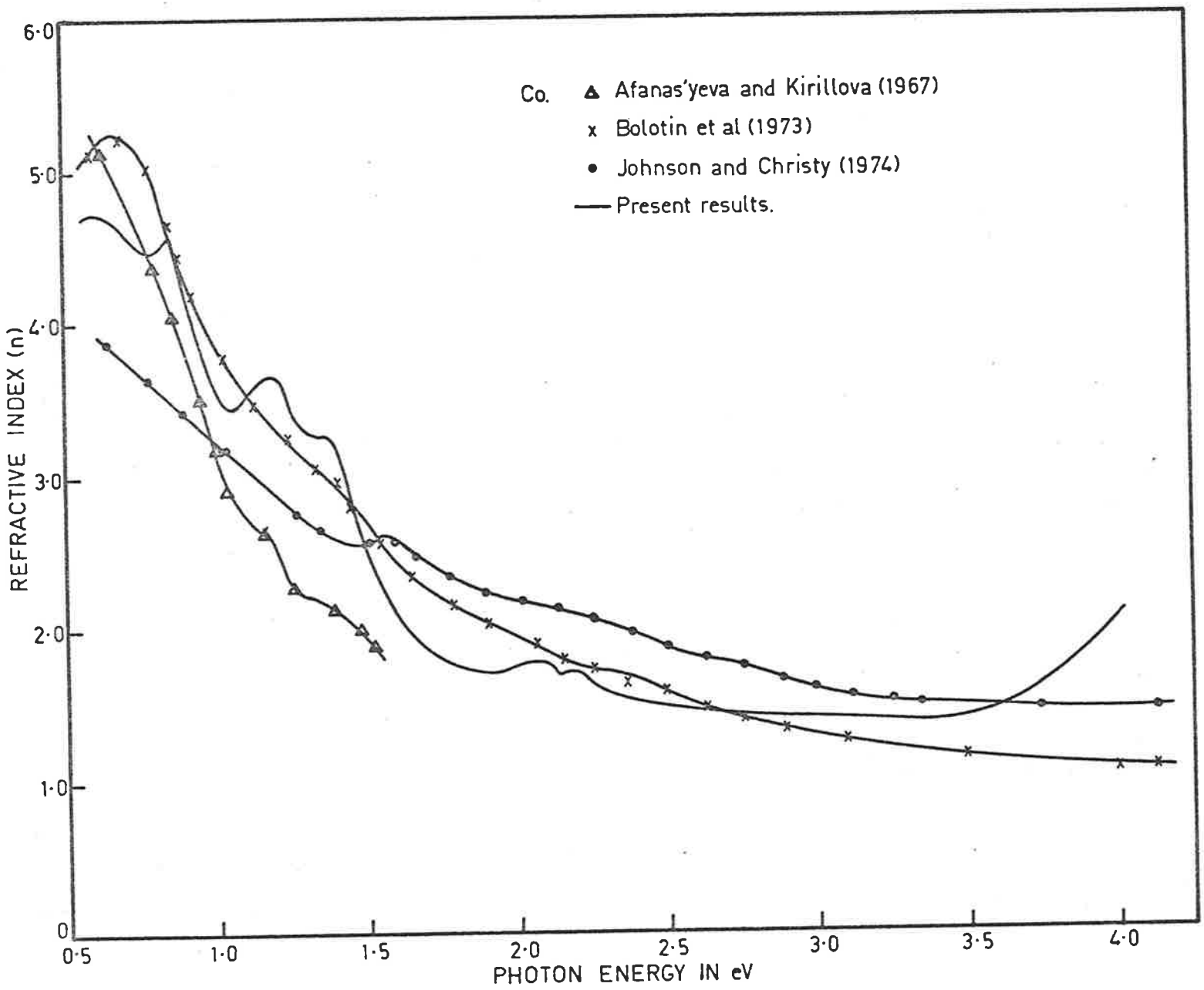
Co.
Afanas'yeva and Kirillova (1967)
Bolotin et al (1973)
Johnson and Christy (1974)
Present results.
REFRACTIVE INDEX (n)
PHOTON ENERGY IN eV
6·0
5·0
4·0
3·0
2·0
1·0
0
0·5
1·0
1·5
2·0
2·5
3·0
3·5
4·0

Fig. 7.24

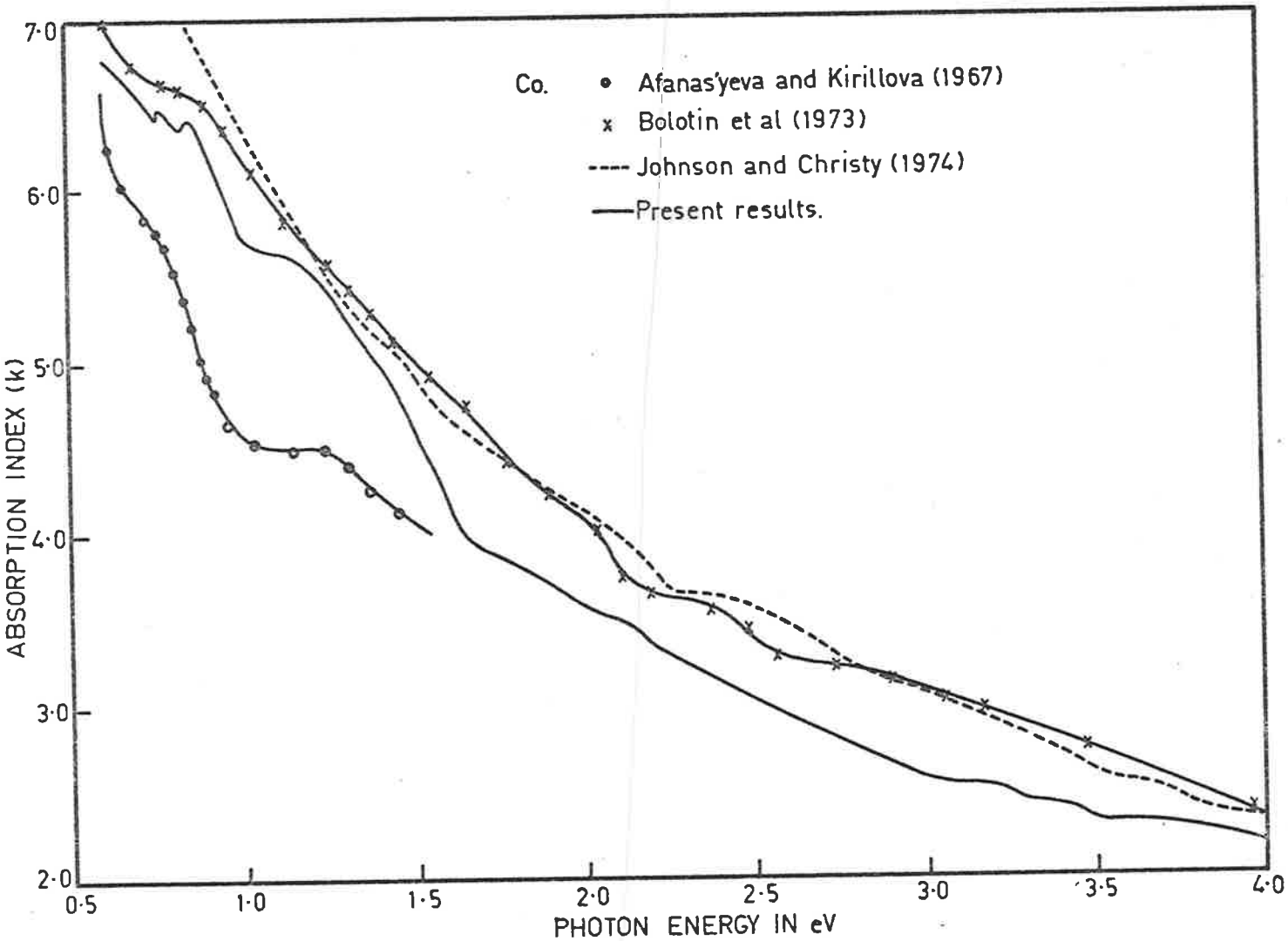
Co.
Afanas'yeva and Kirillova (1967)
Bolotin et al (1973)
Johnson and Christy (1974)
Present results.
ABSORPTION INDEX (k)
PHOTON ENERGY IN eV
7·0
6·0
5·0
4·0
3·0
2·0
0·5
1·0
1·5
2·0
2·5
3·0
3·5
4·0

Fig.7.25

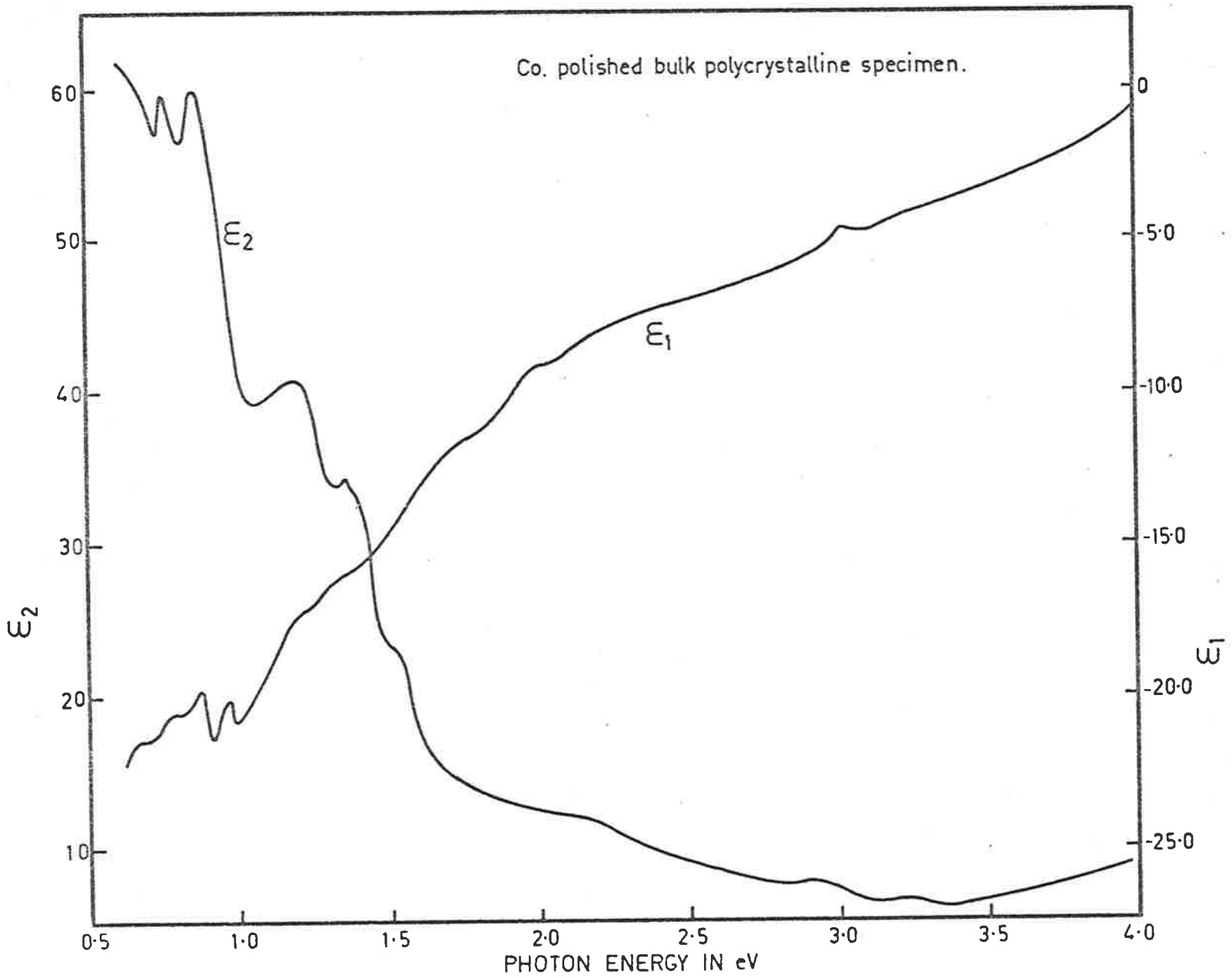
Co. polished bulk polycrystalline specimen.
ε_2
ε_1
60
50
40
30
20
10
0
-5·0
-10·0
-15·0
-20·0
-25·0
ε_2
ε_1
0·5
1·0
1·5
2·0
2·5
3·0
3·5
4·0
PHOTON ENERGY IN eV

Fig. 7.26

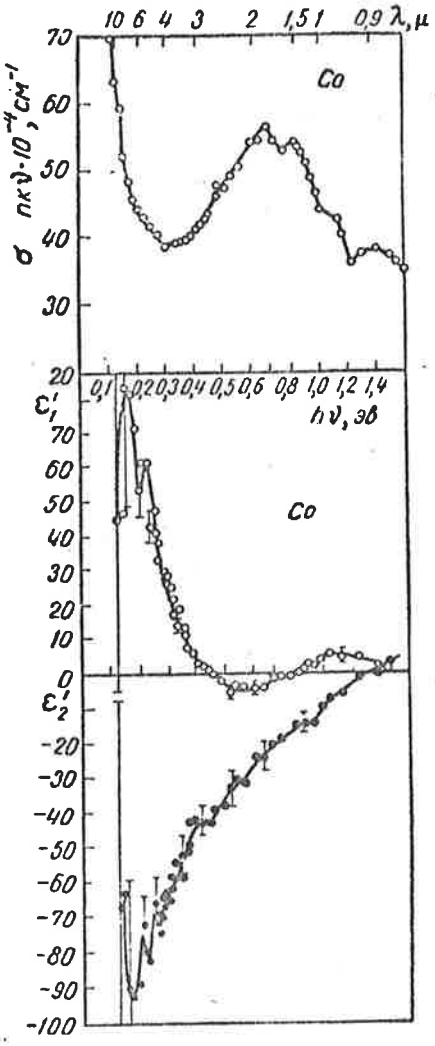

Fig. 7·27. Light conductivity $\sigma(\nu)$, the real part ε_1' and imaginary part ε_2' of the diagonal component ε_{xy} of the permittivity tensor of cobalt.
(From Afanas'yeva and Kirillova, 1967)

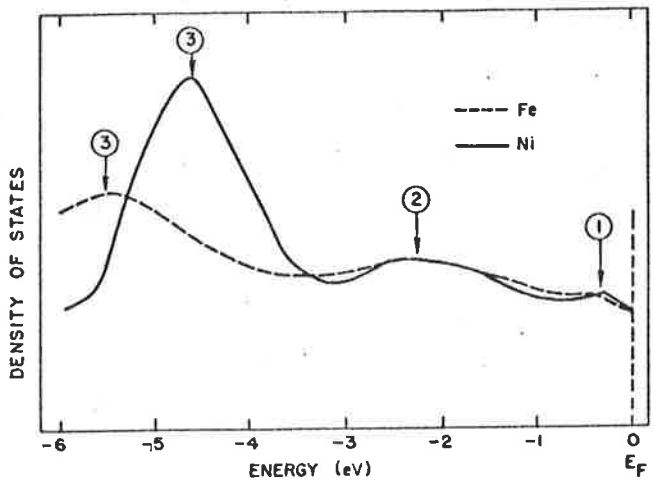

(a) Valence band density of states of Ni and Fe. The two higher energy maxima labeled (1) and (2) are very similar; however, the position and magnitude of the maximum labeled (3) are somewhat different for Ni and Fe. The curves have been normalized at 2.5 eV.

(From Spicer, 1966)

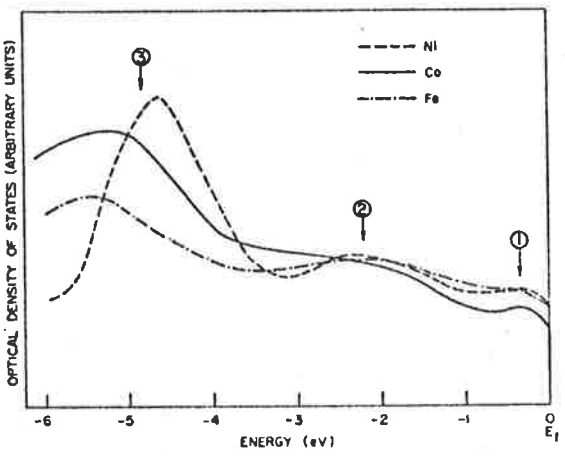

(b) Comparison of the optical densities of states of Ni, Co, and Fe.

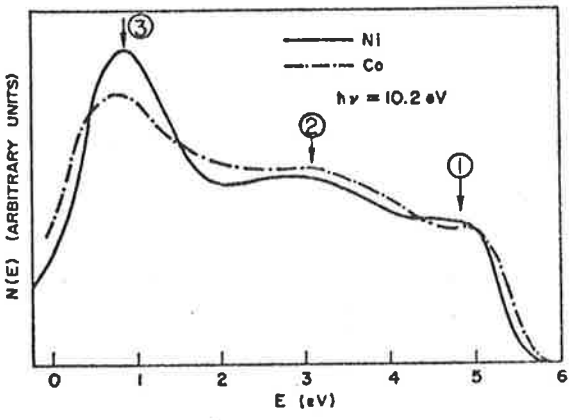

(c) Comparison of EDC's of Ni and Co at $h\nu = 10.2$ eV.

(From Yu and Spicer, 1968)

Fig. 7·28

feature is close to the spectral feature at 2.4 eV found by Yu and Spicer (1968) who determined the optical density of states (Figure 7.28 (b)) from photoemission and optical data. The sixth coincides with the peak at 3.2 eV found by Yu *et al* (1968) who determined the optical constants by using K-K relations.

The optical features of polished specimens of Ni are compared with those of polished specimens of Co in Table 7.21.

TABLE 7.21

Bulk polished polycrystalline specimen	Optical features of the ε_2 curve in eV							
Ni	0.65	0.75	0.80	1.03	1.22	1.40	2.33	3.05
Co		0.75	0.85	0.97 (ε_1)	1.20	1.35	2.22	3.20

Apparently all the optical structures which are observed in polished specimens of Ni occur also in polished specimens of Co up to an energy 3.5 eV , suggesting that Ni and Co have very similar band structures within about 3.5 eV of the Fermi surface (Spicer 1966, Yu and Spicer 1968).

7.3 Molybdenum

7.3.1 Introduction

As far as the author is aware no theoretical band structure of Mo is yet available, although theoretical calculations on band structure of Cu, Ni and other metals of the Cr-group such as W and Cr have been made. The optical conductivity curves of Nomerovannaya *et al* (1971) for Cr, Mo and W are shown in Figure 7.31(c). However the studies of Brandt and Rayne's (1963) of the de Haas-van Alphen effect in the Cr-group of transition elements indicate that the Lomer model (1962, 1964) gives an adequate description of the Fermi surface of Mo and W, apart from possible effects due to spin orbit splitting. The model is less satisfactory for Cr but this may be due to the occurrence of antiferromagnetic ordering at low temperatures. Kapitsa *et al* (1969) measured the optical properties of single crystal Mo using the K-K relations in the range 2 to 10 eV and compared their results with Ni as they had no calculations of theoretical model for band structure of Mo. They remarked that the $\varepsilon_2(h\nu)^2$ curve for Mo decreases sharply in the energy range $5 < h\nu < 8$ eV but did not comment on interband transitions; although their $\varepsilon_2(h\nu)^2$ and reflectivity curves show structures around 4.5 and 2.5 and 4.5 eV respectively. Kirillova *et al* (1971) made measurements on single crystal Mo using Beattie's (1955) polarimetric method and observed structures at 0.75, 0.98, 1.8 and 2.4 eV and some weak structures in the region 0.25 to 0.5 eV, Figures 7.31(a) and 7.31(b). Kress and Lapeyre (1970) and Kirillova *et al* (1967) however missed the

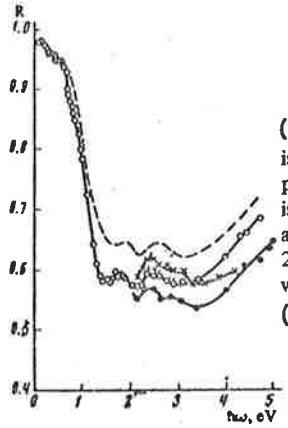

(a) Reflectivity of molybdenum is given by different workers. O–Mo(100), present paper, dashed–mechanically polished (MP) sample [1,2]: X–MP sample annealed in vacuum 10^{-7} mm Hg at T = 2200°K [3]; ●–MP sample annealed in vacuum [4].
(From Kirillova et al, 1971)

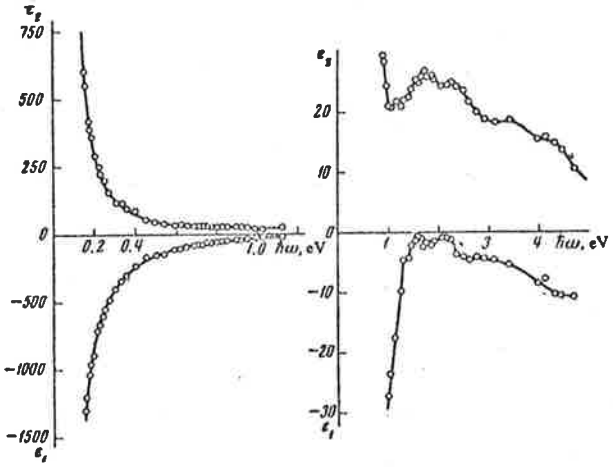

(b) Dispersion $\epsilon_1(\omega)$ and $\epsilon_2(\omega)$ of Mo(100).
(From Kirillova et al, 1971)

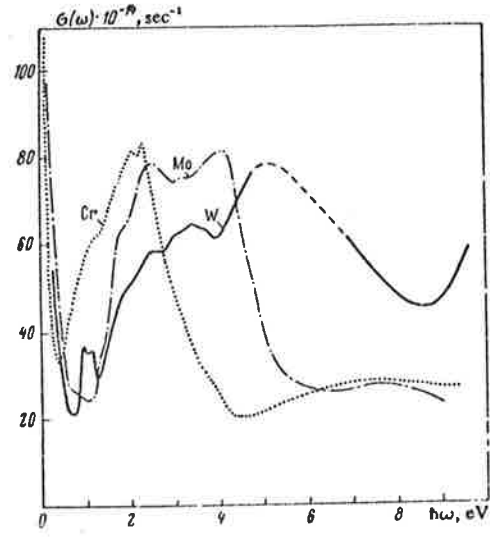

(c) The optical conductivity of Cr, Mo and W. From L. W. Nomerovannaya, M. M. Kirillova, and M. M. Noskov, *Sov. Phys.—JETP* 33, 405 (1971).
(From Nilsson, 1974)

Fig. 7·31

important structures at 1.8 eV but Kirillova *et al* (1967) observed two peaks at 2.3 and 4.0 eV, and a trough at 3.0 eV in the curves of optical conductivity and of ε_1, the real part of the permittivity. Recent studies by Weaver (1973) also revealed structures at 1.8, 2.35, and 4.1 eV in the ε_2 curves of electropolished single-crystal Mo. Udoyev *et al* (1971) gave an analysis of the optical spectra of the chromium subgroup and mentioned that the sharpest structural characteristics in the optical spectra are caused by direct transitions at critical points. The results of Mattheiss (1965) for W and Asano and Yamashita (1967) for Cr also demonstrate that there are many types of such transitions, a combination of which can give rise to observed spectra. All the absorption features mentioned above except one at 4.2 eV have been observed in the present studies of Mo together with some additional features in the infrared region.

7.3.2 Sample preparation and structure of the films

Opaque Mo films were prepared by sputtering and the pieces of Mo, A (27 dia. x 2 mm) and B(27 dia. x 1mm) were polished to a mirror finish mechanically. Ta_2O_5 films were sputtered on to these metal specimens.

No surface structure was revealed when the polished specimens and opaque films of Mo were examined with the scanning electron microscope (Figure 7.3a, for polished specimen), i.e. surface roughness must be less than 7.0 to 7.5 nm. The replicas of the opaque Mo films examined with the transmission electron microscope showed a roughness of the order of 2.5 to 3.0 nm (Figure 7.3b).

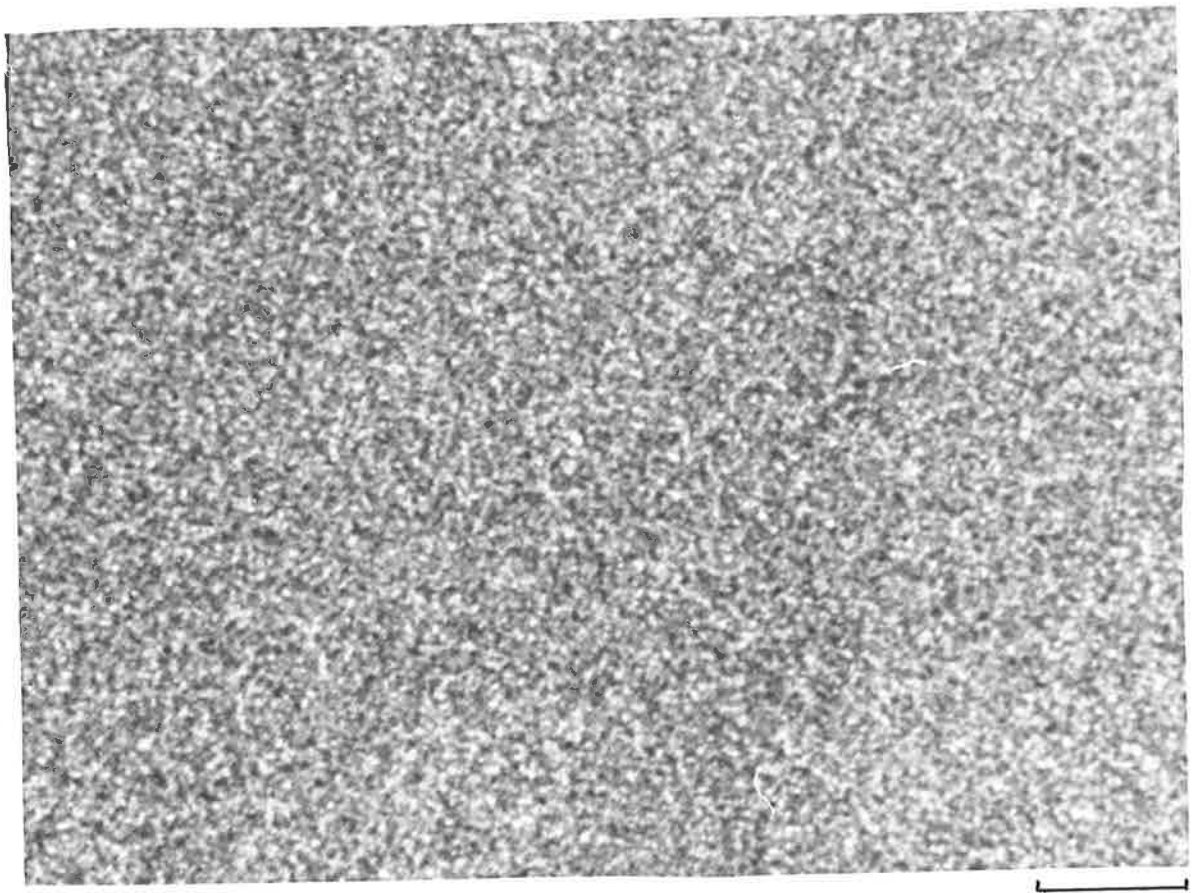

Fig. 7·3a

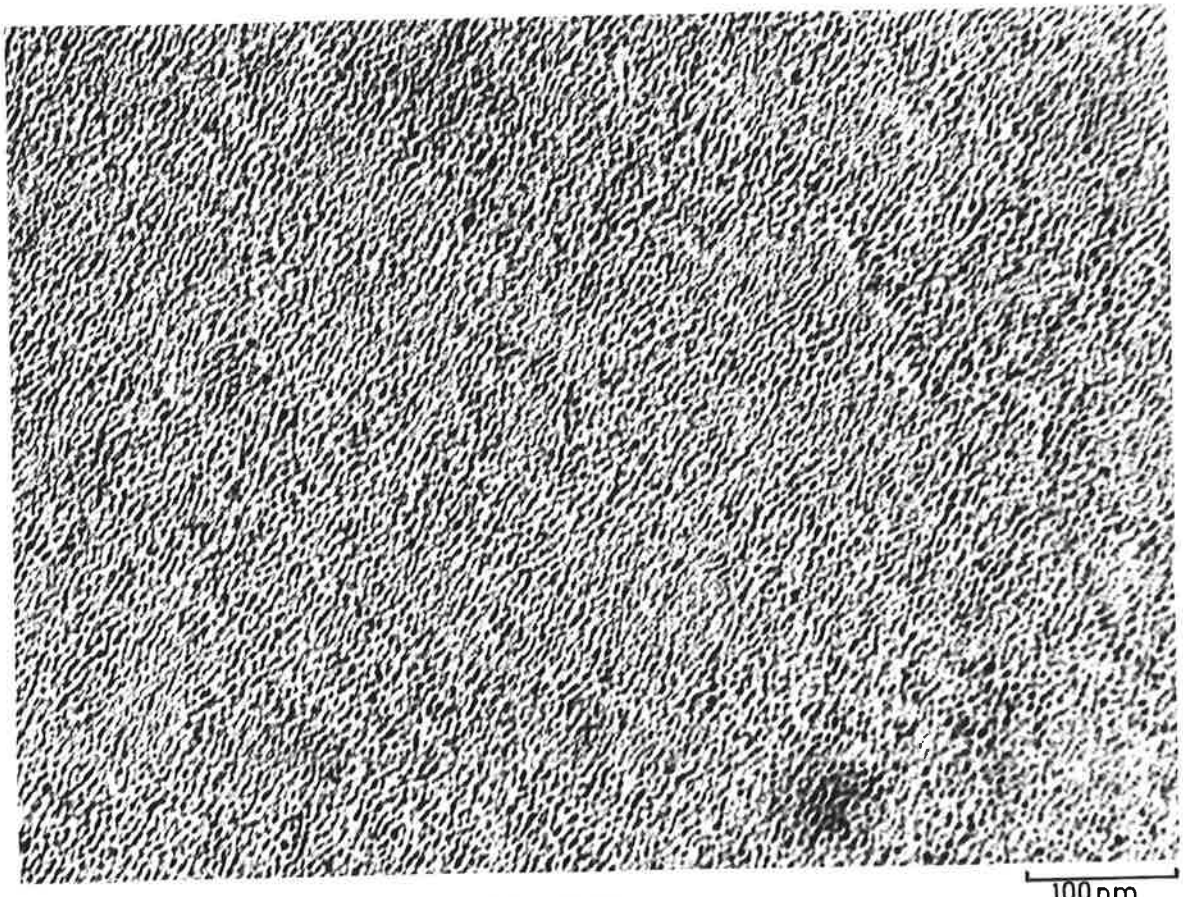

Fig. 7·3b

7.3.3. Determination of the optical constants of Mo

Two pieces of Mo (specimens A and B) polished in the same way had different values of reflectance (Figure 7.3 2) but the shapes of the reflectivity curves were almost identical and the reflectance and absorption index curves proved to be very similar. The optical constants of polycrystalline specimens A and B of Mo, with error bars, are shown in Figures (7.34, for Specimen A) and (7.36A,for Specimen B) corresponding to the reflectances shown in Figures (7.33A and 7.33B)respectively. The values of the optical constants of these two specimens of Mo are shown in Figure (7.36B).

The correct and incorrect solutions for the optical constants corresponding to the reflectances R and R_1 for Specimen A are shown in Figure (7.35). The incorrect solutions for the absorption index vary from positive to negative with sharp repeated maxima and minima whereas the correct solutions are everywhere positive and form a smoother curve. The behaviour of the wrong solutions for the refractive index curve are similar to the absorption index curve except that they never have negative values.

The values of the optical constants of the opaque sputtered Mo films, together with the reflectance curves, are shown in Figure (7.37).

The author's values of the optical constants of Mo (Specimen B) are compared with those of other workers in Figures (7.38A) and (7.38B). Generally the absorption index curves are in good agreement, but the refractive index curve of Kirillova *et al* (1971) for single crystal Mo shows some features in the infrared region which do not occur in the writer's curve for polycrystalline material.

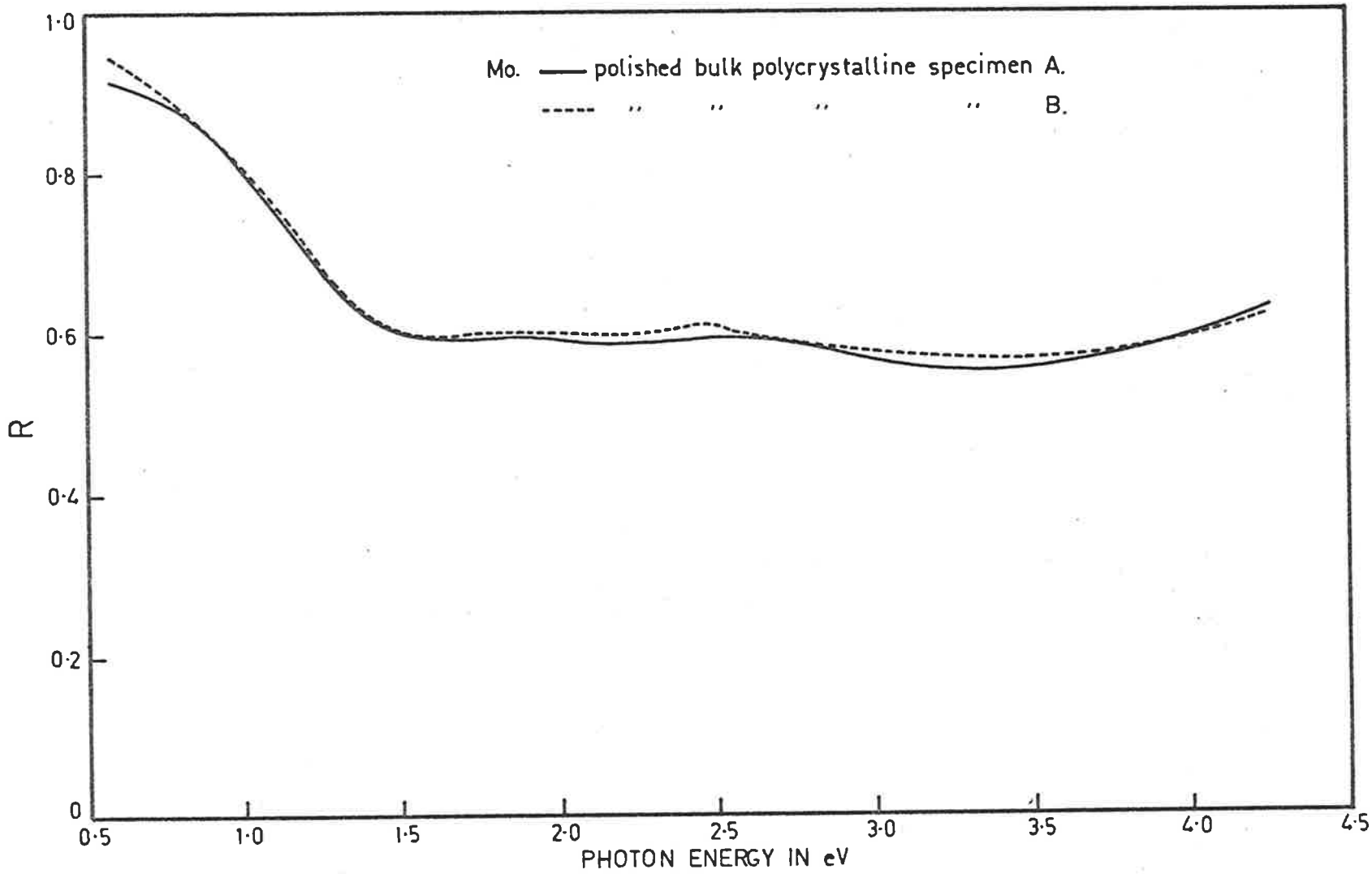
Mo. —— polished bulk polycrystalline specimen A.
----- " " " " B.
R
1·0
0·8
0·6
0·4
0·2
0
0·5
1·0
1·5
2·0
2·5
3·0
3·5
4·0
4·5
PHOTON ENERGY IN eV

Fig. 7.32

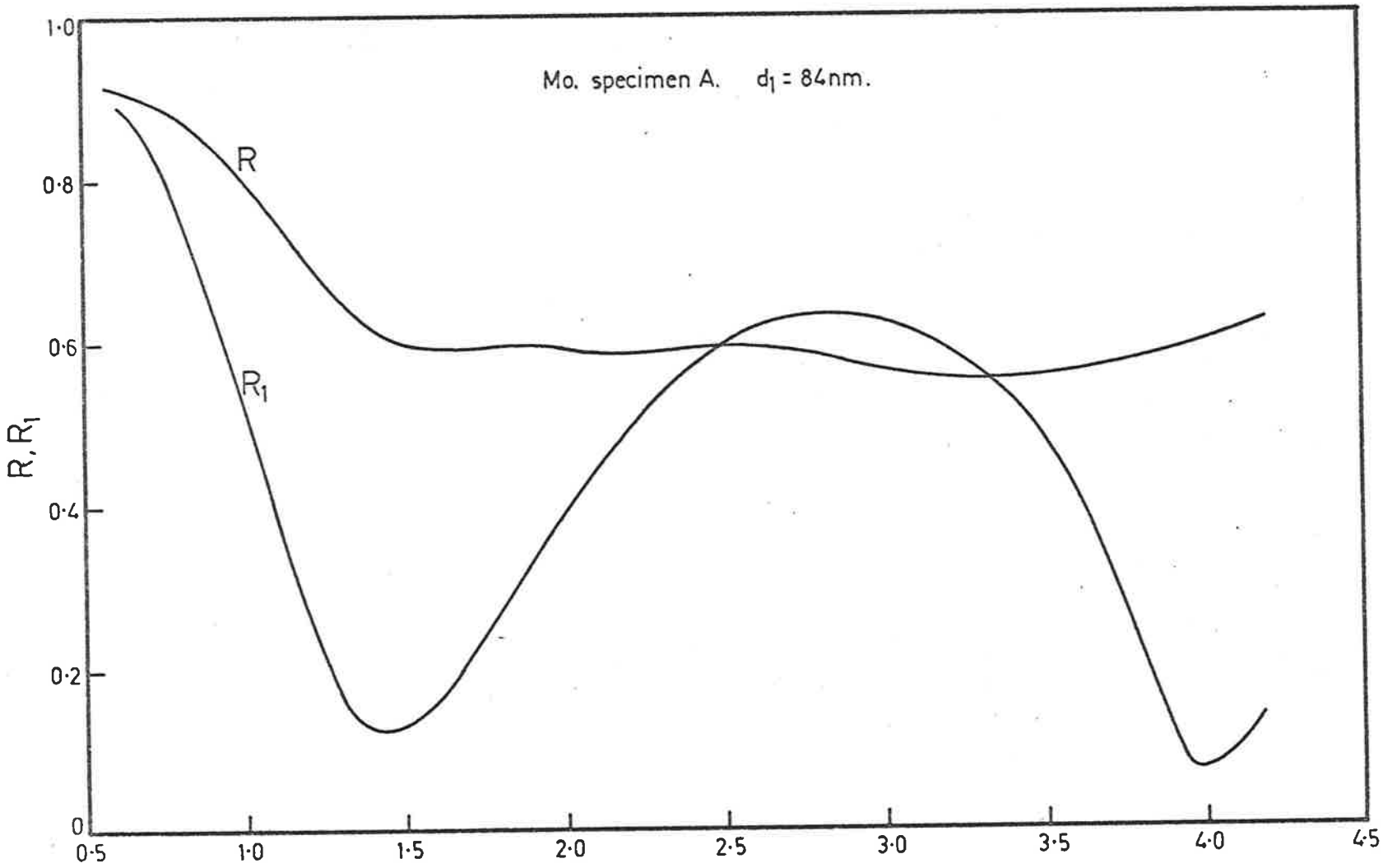
Mo. specimen A. d_1 = 84nm.
R
R_1
R, R_1
1·0
0·8
0·6
0·4
0·2
0
0·5
1·0
1·5
2·0
2·5
3·0
3·5
4·0
4·5

Fig. 7.33A

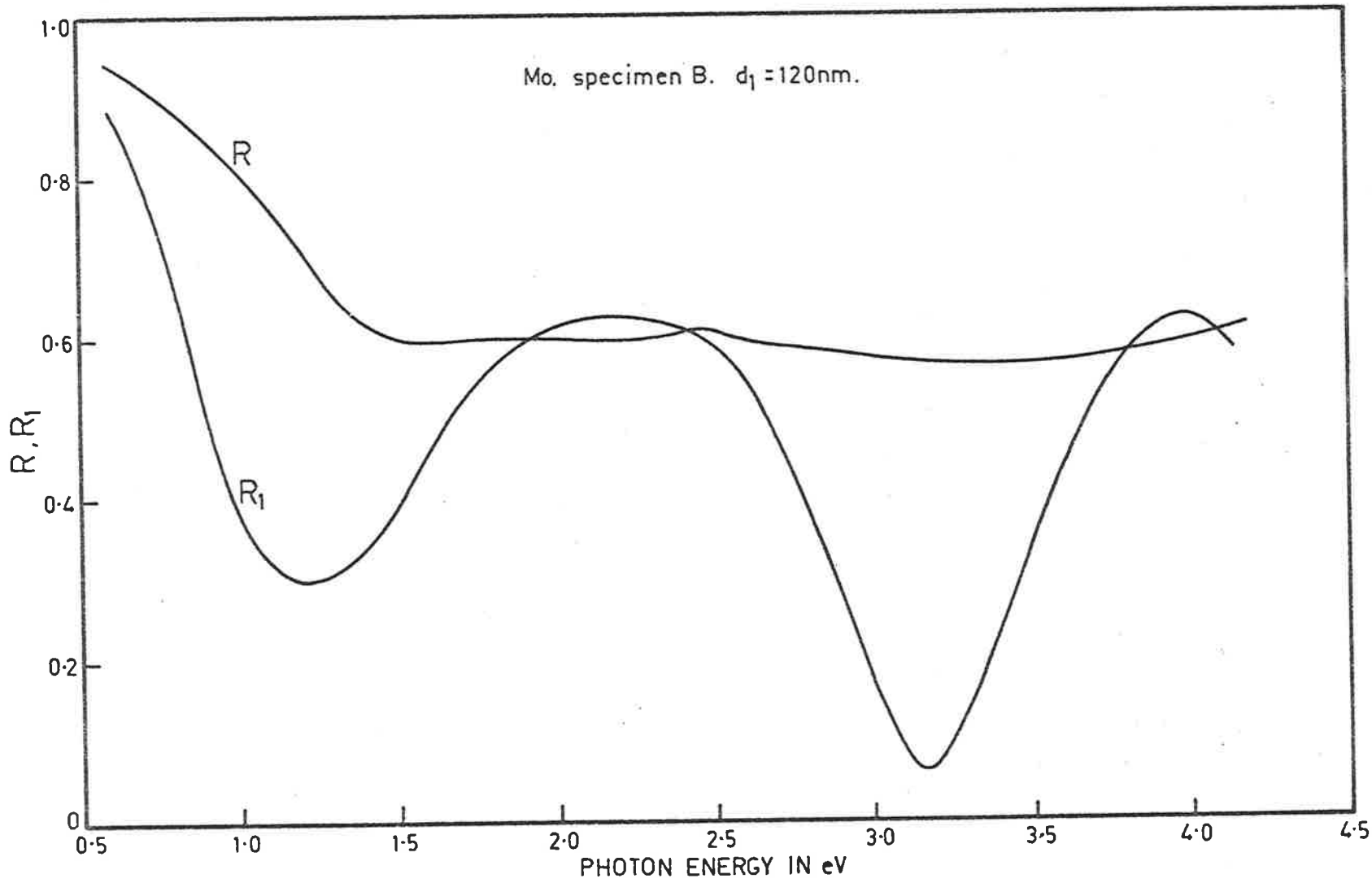
Mo. specimen B. d_1 = 120nm.
R
R_1
R, R_1
1·0
0·8
0·6
0·4
0·2
0
0·5
1·0
1·5
2·0
2·5
3·0
3·5
4·0
4·5
PHOTON ENERGY IN eV

Fig. 7.33B

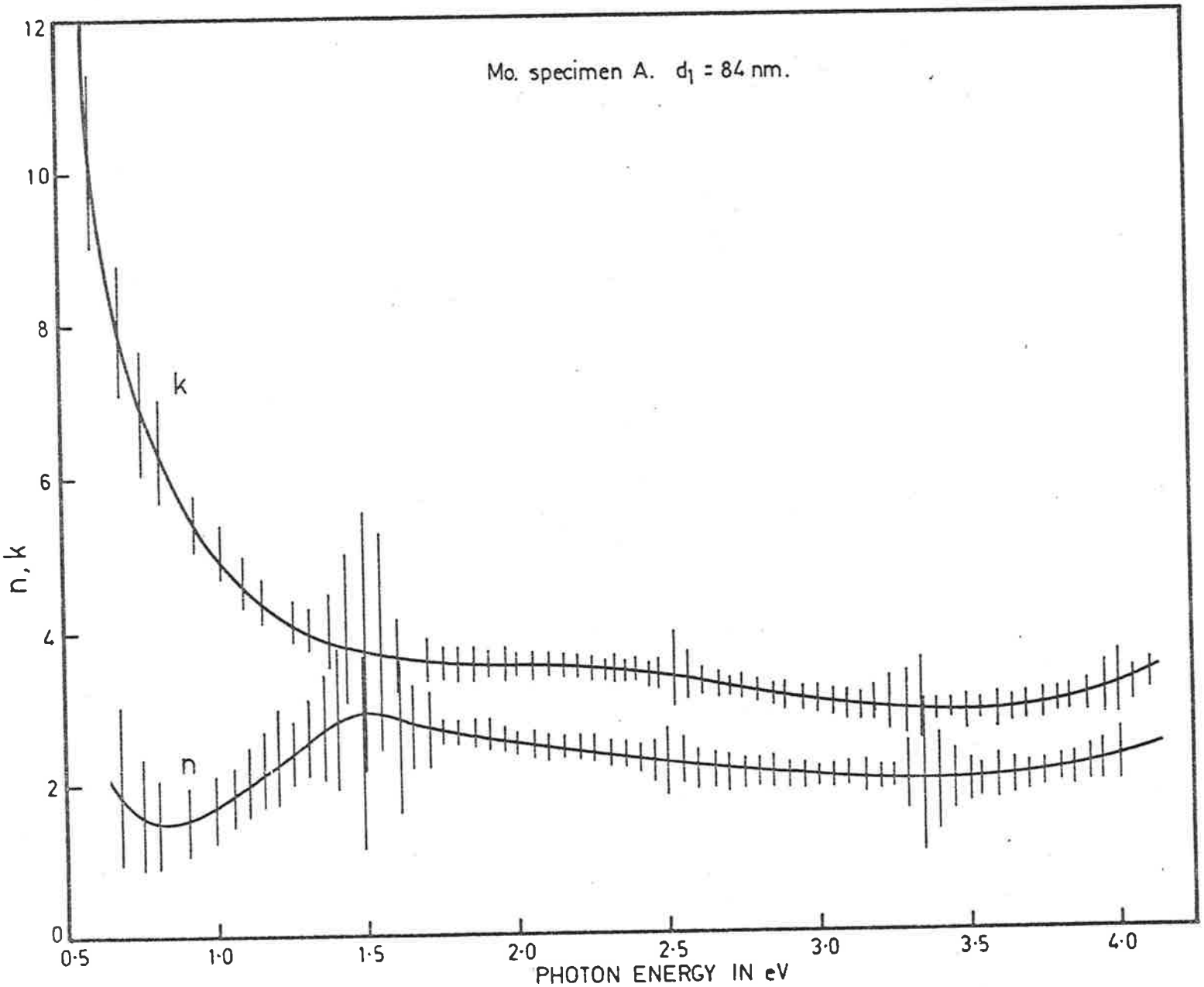
Mo. specimen A. d_1 = 84 nm.
n, k
k
n
PHOTON ENERGY IN eV
0
2
4
6
8
10
12
0·5
1·0
1·5
2·0
2·5
3·0
3·5
4·0

Fig. 7.34

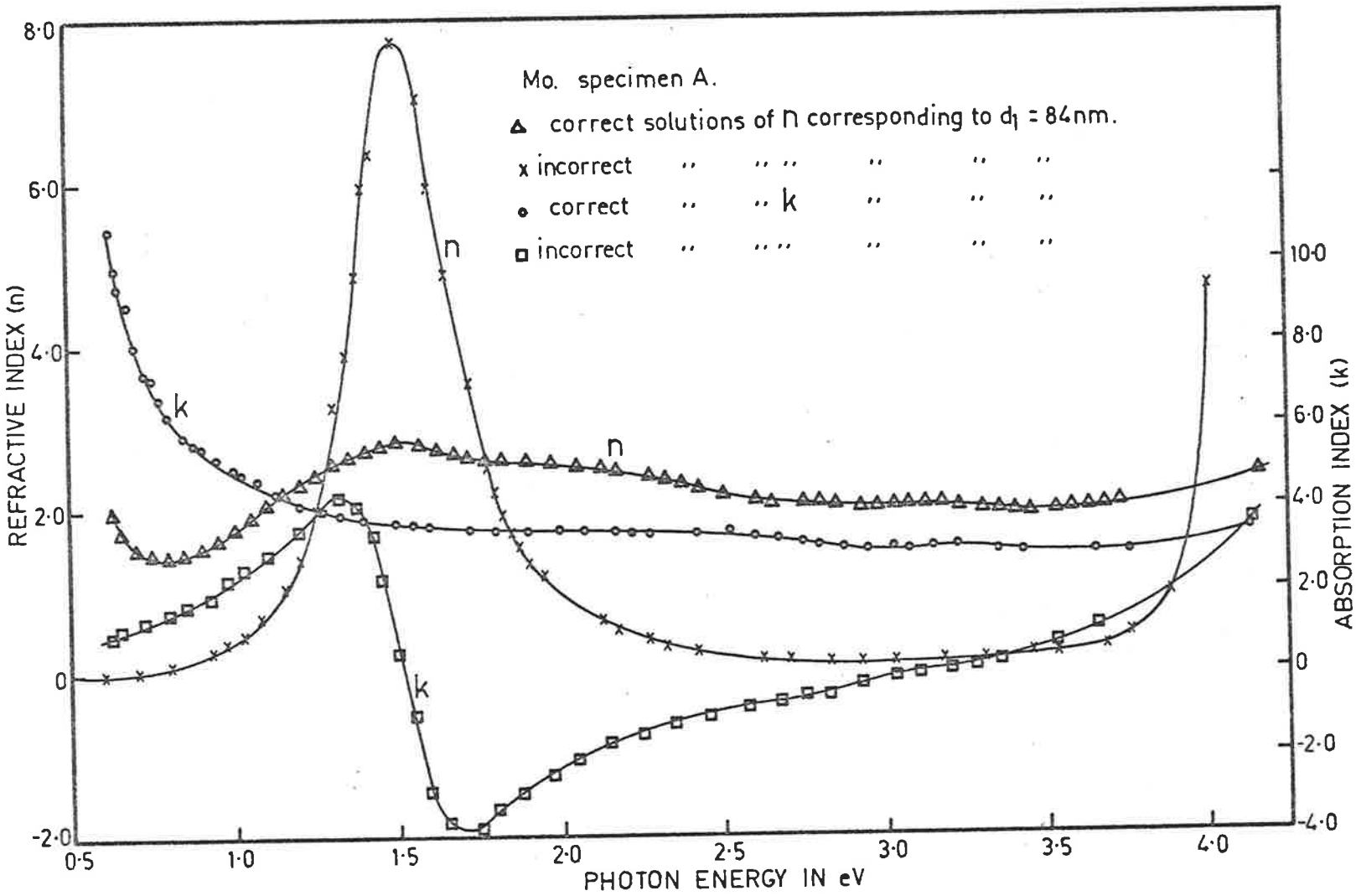
Mo. specimen A.
△ correct solutions of n corresponding to d_1 = 84nm.
x incorrect " " " " " "
o correct " " k " " "
□ incorrect " " " " " "
n
k
n
k
REFRACTIVE INDEX (n)
ABSORPTION INDEX (k)
PHOTON ENERGY IN eV
8·0
6·0
4·0
2·0
0
-2·0
10·0
8·0
6·0
4·0
2·0
0
-2·0
-4·0
0·5
1·0
1·5
2·0
2·5
3·0
3·5
4·0

Fig. 7·35

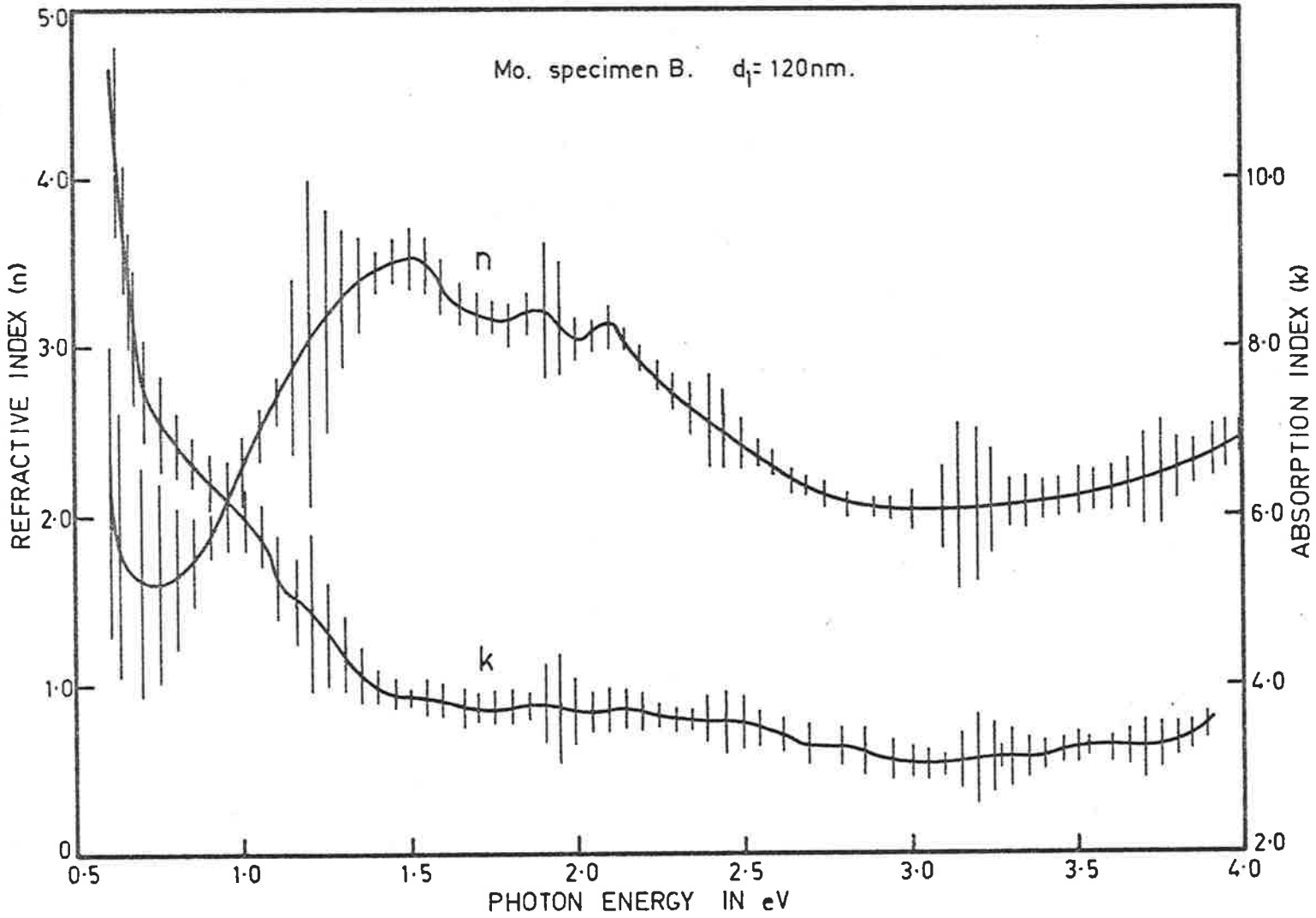
Mo. specimen B. d_1= 120nm.
REFRACTIVE INDEX (n)
ABSORPTION INDEX (k)
PHOTON ENERGY IN eV
n
k
5·0
4·0
3·0
2·0
1·0
0
10·0
8·0
6·0
4·0
2·0
0·5
1·0
1·5
2·0
2·5
3·0
3·5
4·0

Fig. 7.36A

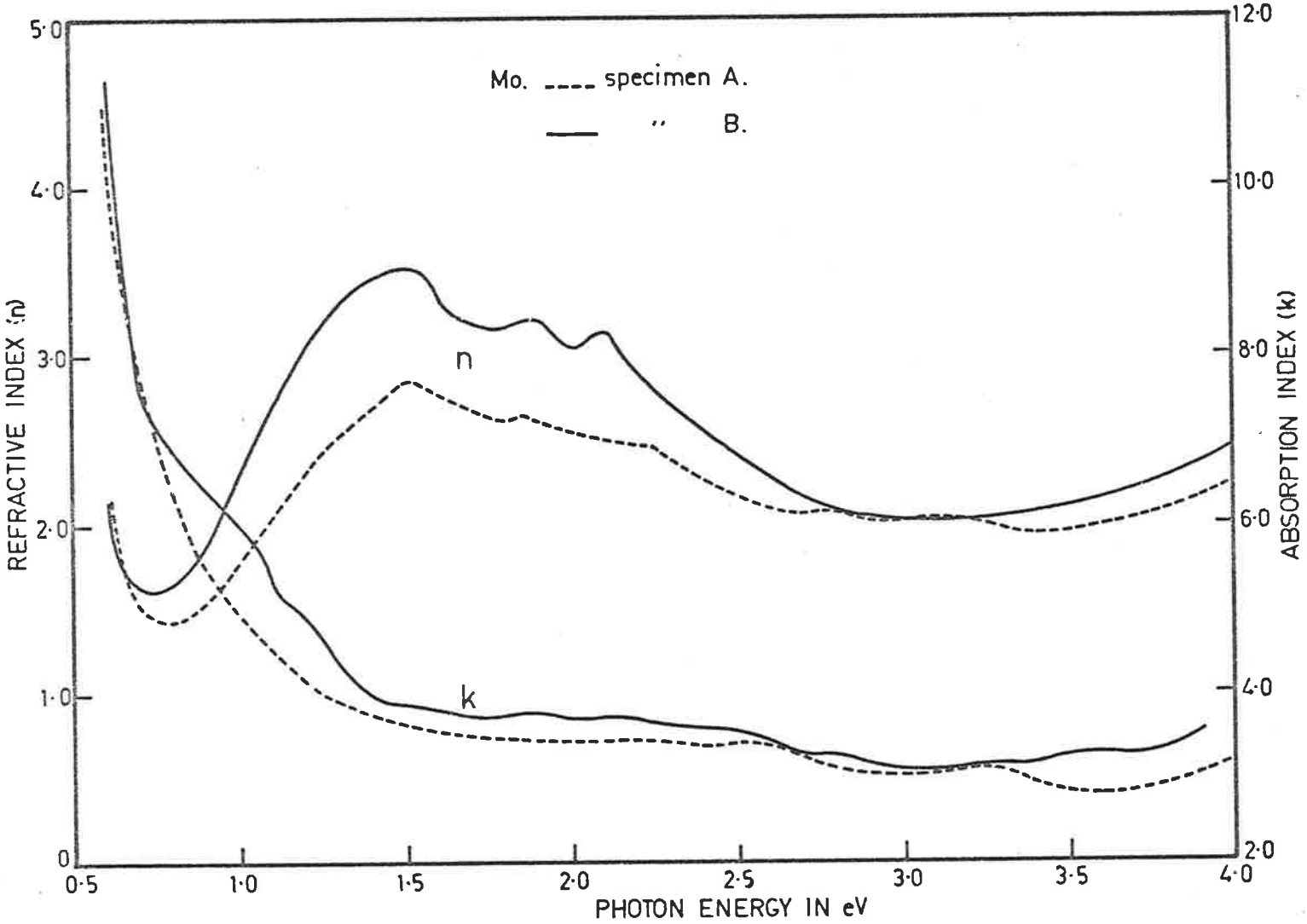
Mo. ---- specimen A.
—— " B.
n
k
REFRACTIVE INDEX (n)
ABSORPTION INDEX (k)
PHOTON ENERGY IN eV
5·0
4·0
3·0
2·0
1·0
0
12·0
10·0
8·0
6·0
4·0
2·0
0·5
1·0
1·5
2·0
2·5
3·0
3·5
4·0

Fig. 7·36B

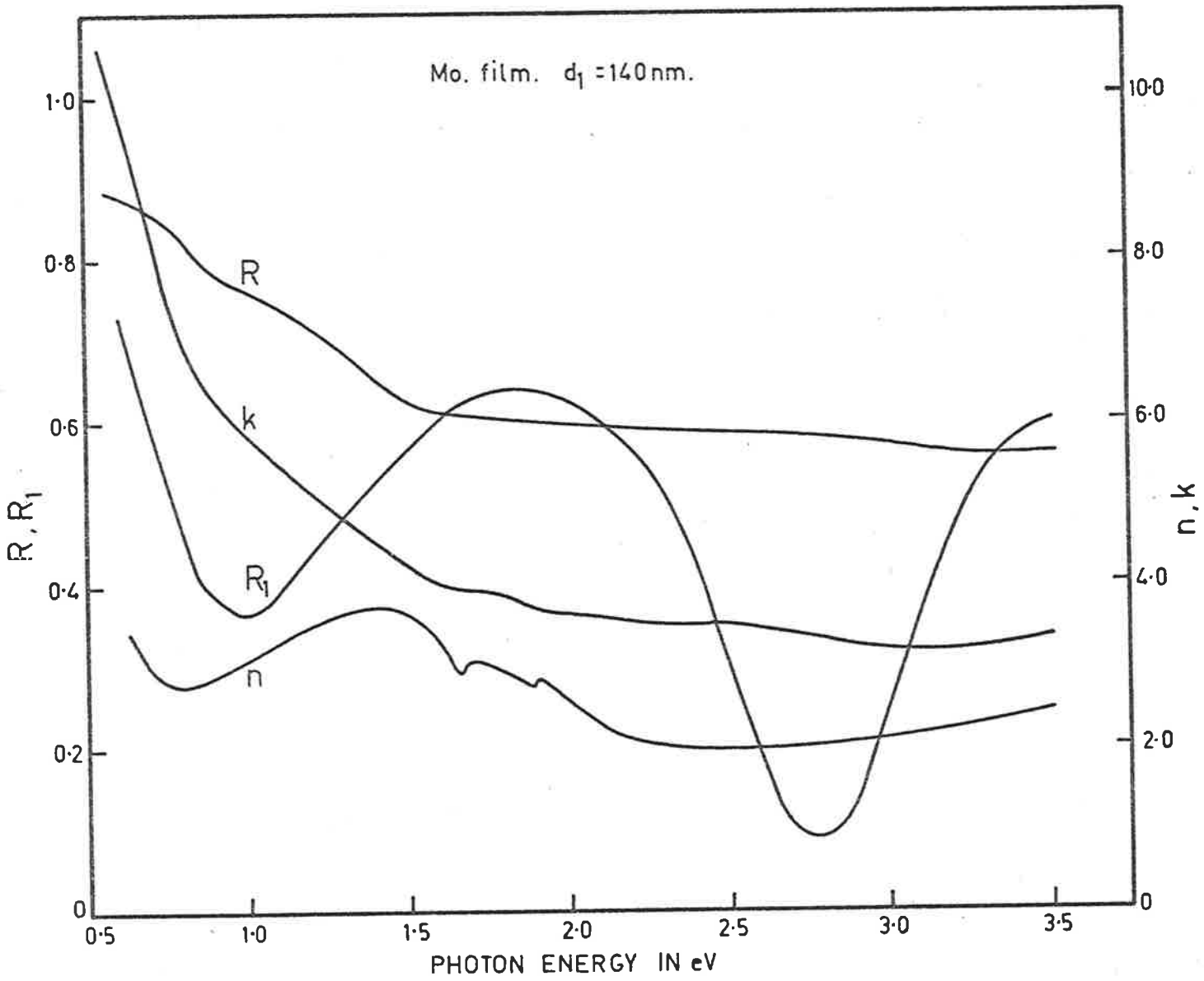
Mo. film. d_1 =140nm.
R
k
R_1
n
R, R_1
n, k
1·0
0·8
0·6
0·4
0·2
0
10·0
8·0
6·0
4·0
2·0
0
0·5
1·0
1·5
2·0
2·5
3·0
3·5
PHOTON ENERGY IN eV

Fig.7.37

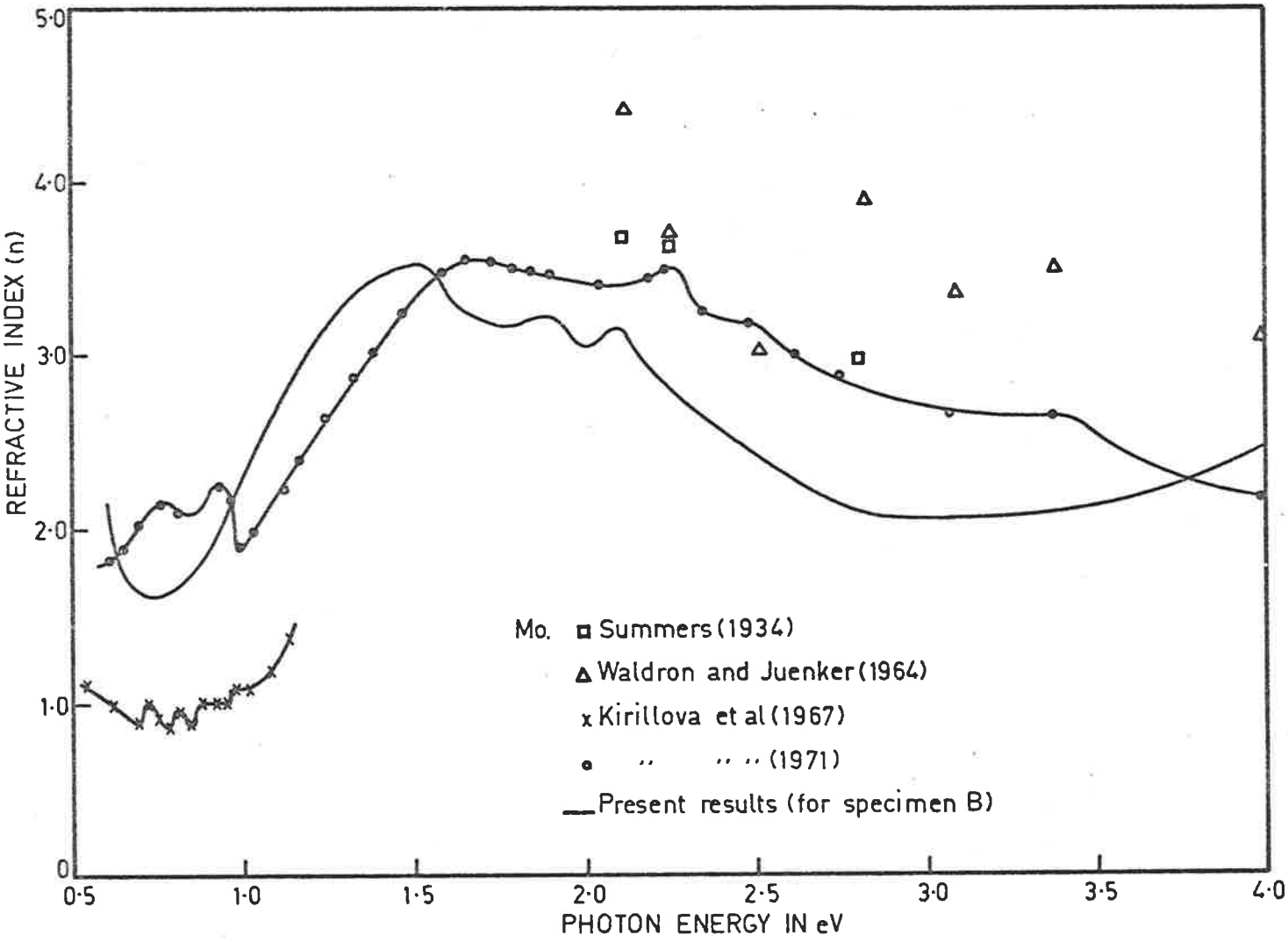
5·0
4·0
3·0
2·0
1·0
0
REFRACTIVE INDEX (n)
0·5
1·0
1·5
2·0
2·5
3·0
3·5
4·0
PHOTON ENERGY IN eV
Mo. □ Summers (1934)
△ Waldron and Juenker (1964)
x Kirillova et al (1967)
o " " " (1971)
— Present results (for specimen B)

Fig. 7·38A

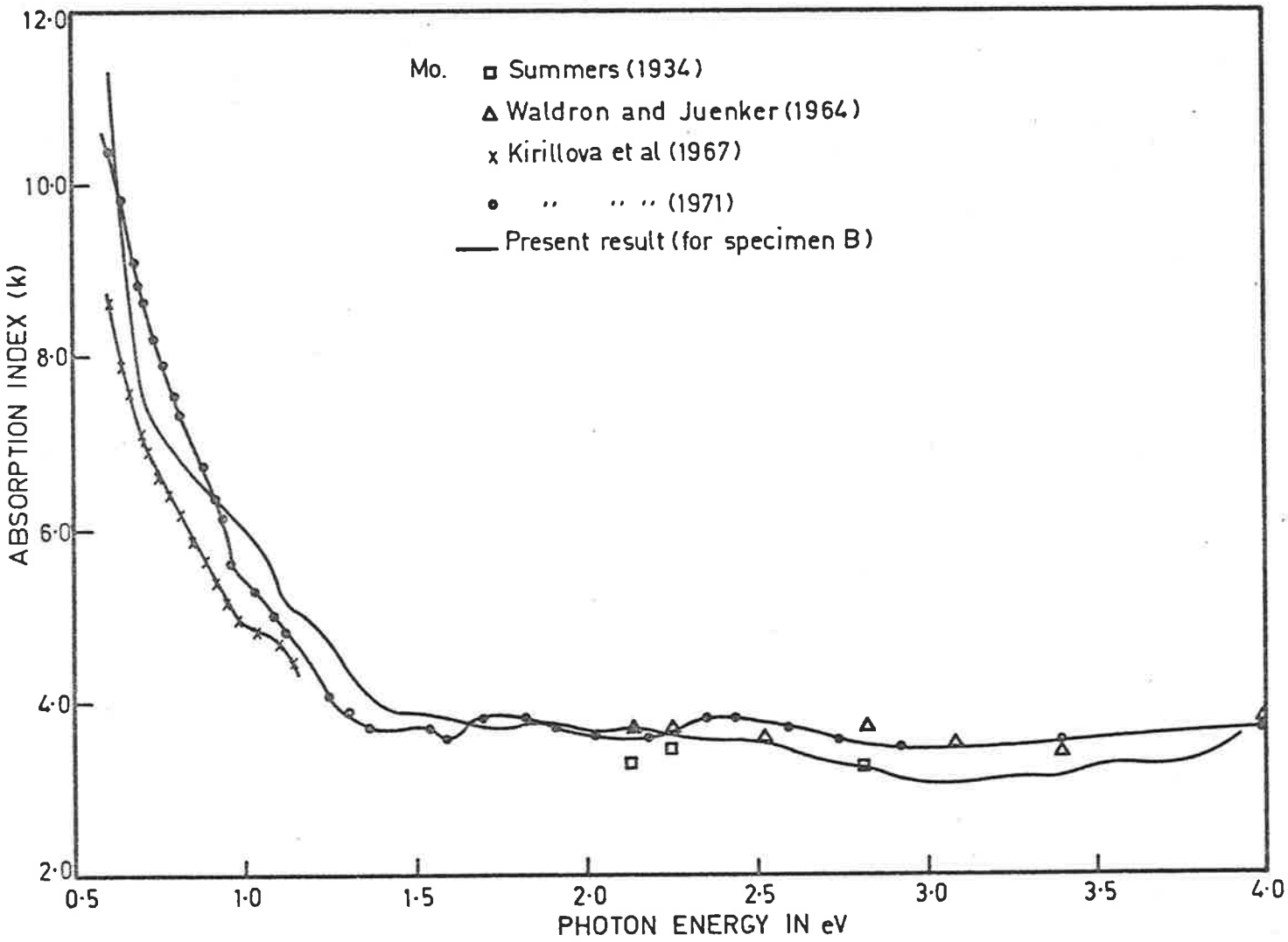
Mo.
Summers (1934)
Waldron and Juenker (1964)
x Kirillova et al (1967)
" " " (1971)
Present result (for specimen B)
ABSORPTION INDEX (k)
12·0
10·0
8·0
6·0
4·0
2·0
0·5
1·0
1·5
2·0
2·5
3·0
3·5
4·0
PHOTON ENERGY IN eV

Fig. 7.38B

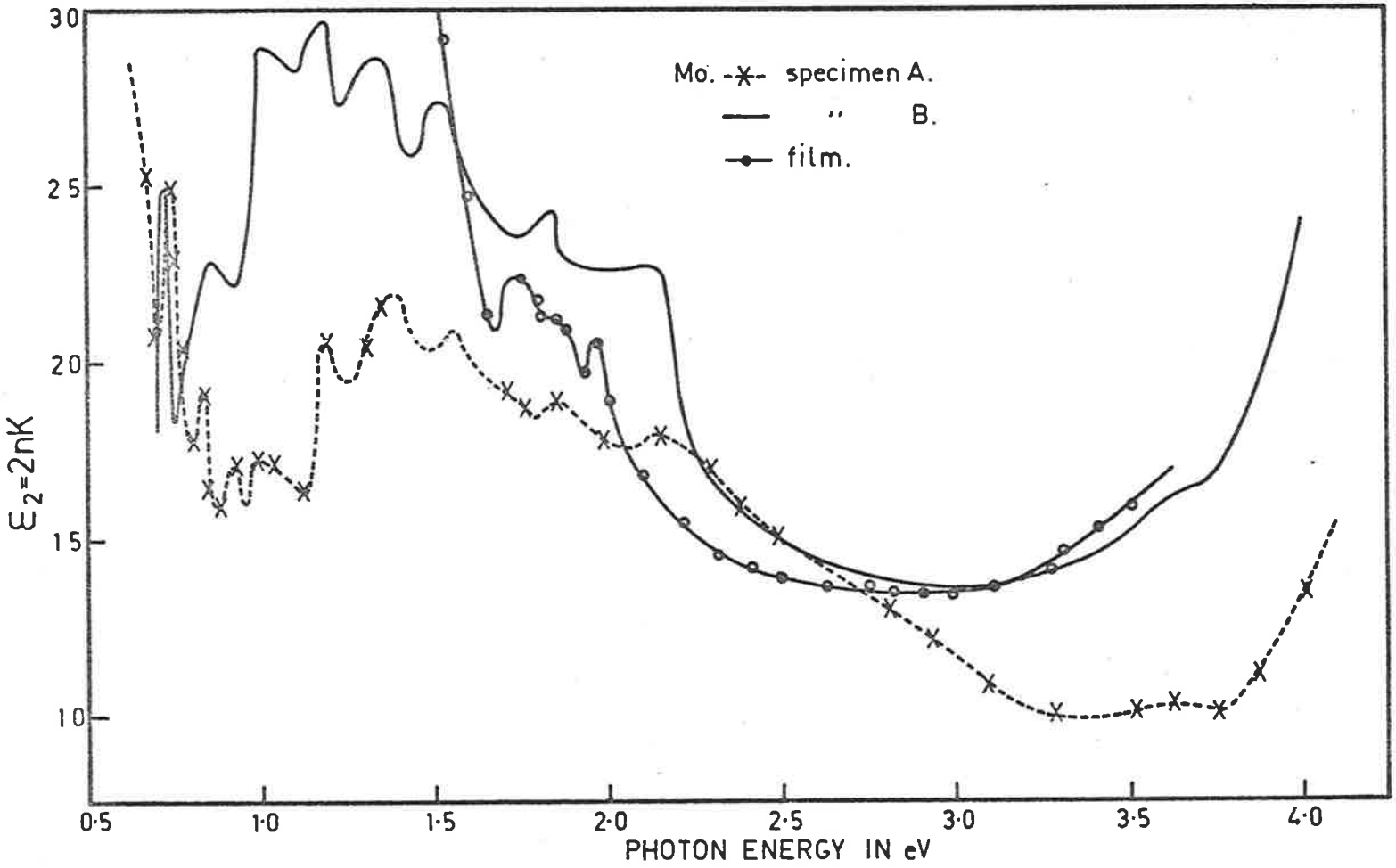
Mo. -x- specimen A.
" B.
film.
$\varepsilon_2=2nK$
30
25
20
15
10
0·5
1·0
1·5
2·0
2·5
3·0
3·5
4·0
PHOTON ENERGY IN eV

Fig. 7·39A

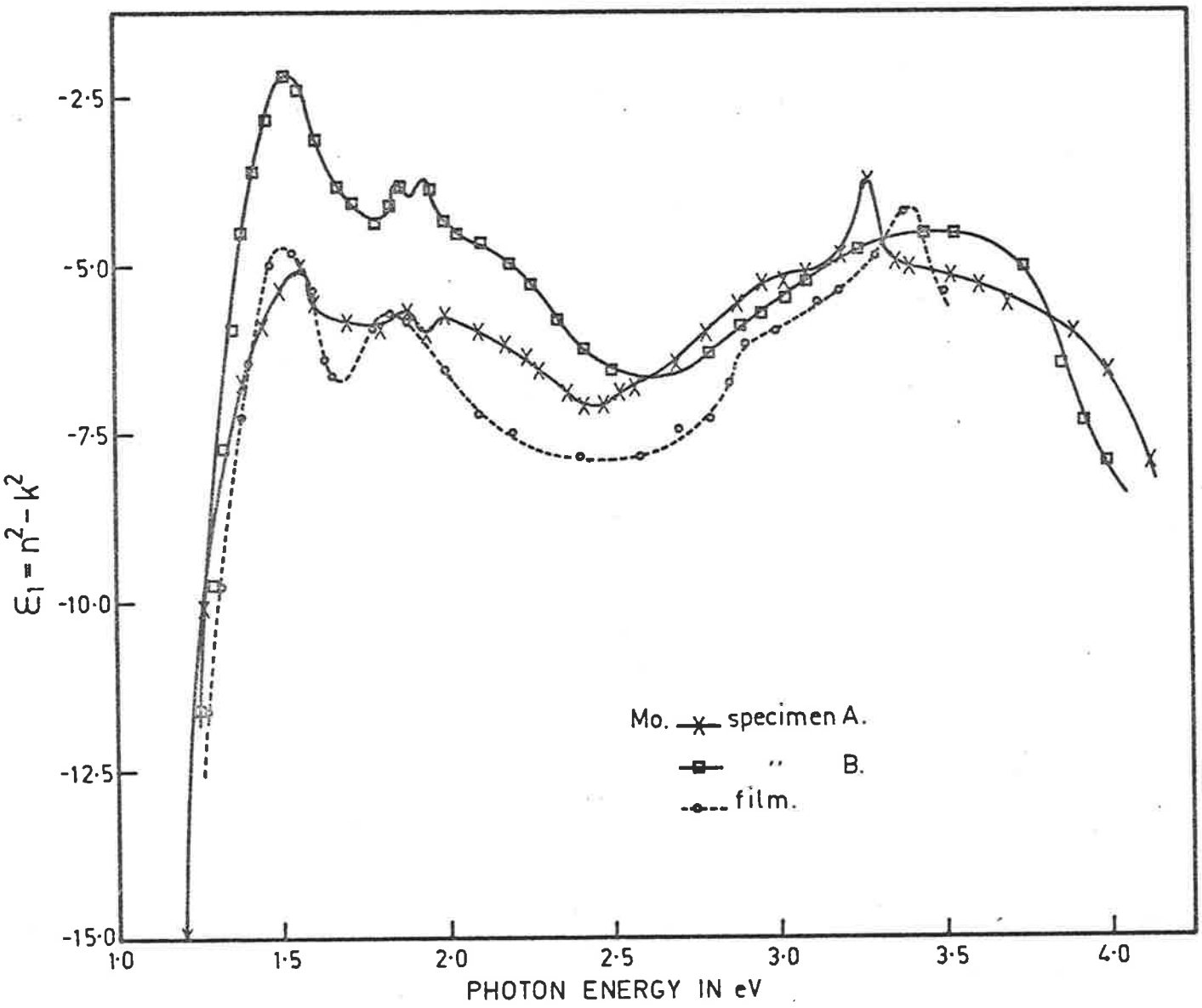
-2·5
-5·0
-7·5
-10·0
-12·5
-15·0
$\varepsilon_1 = n^2 - k^2$
1·0
1·5
2·0
2·5
3·0
3·5
4·0
PHOTON ENERGY IN eV
Mo. specimen A.
" B.
film.

Fig. 7.39B

7.3.4 Results and discussion

The imaginary part of the dielectric constant, ε_2 of polished specimens of molybdenum shows structures (Figure 7.39A) at 0.75, 0.85, 1.0, 1.2, 1.4, 1.55, 1.85, 2.15 eV and perhaps one around 3.6 eV. There is a wide trough around 3.0 eV as mentioned by Kirillova *et al* (1967). The structures at 0.75, 0.85, 1.85 and 2.15 eV are close to those of Kirillova *et al* (1971, Figure 7.31) for single-crystal Mo. Some of these spectral features are also close to those of Weaver (1973, Section 7.3.1) and the one at 2.15 eV is very close to the 2.2 eV structure of Kress and Lapeyre (1970) who measured reflectances and used the K-K relations. Opaque Mo films prepared by sputtering showed similar structures with small variations (Figures 7.39A and 7.39B), although there are differences which are due to the degree of crystalline perfection (see Section 7.3.2). The structures of polished specimens of Mo have some similarities with Ni (see Section 7.1), but it is not possible to provide any interpretation of all these spectral features since there are no theoretical band structures for Mo available.

7.4 Conclusions

From the results of measurements on polished specimens of Ni, Co and Mo and opaque films of Ni and Mo it appears that the method of determining optical constants by applying a thin film of Ta_2O_5 to the specimens is a satisfactory procedure for photon energies up to 4.0 eV. To extend this range to higher energies, the K-K method could be used together with direct measurements in the low energy range and the proposed improvements in the extrapolation procedures which has been discussed. The results of measurements of optical properties depend a good deal upon the nature of the specimens and methods of preparation, and there is room for further study of factors affecting the optical constants. Nevertheless the principal spectral features as shown, for example, in the ε_2 curves are closely similar for the different specimens used.

Because the method of measurement used involves the quantities $\frac{1 + R}{1 - R}$ and $\frac{1 + R_1}{1 - R_1}$, it becomes inaccurate at low photon energies where the reflectivities of the metals tend to unity. This will limit the longer wavelength range but considerable improvement in the accuracy of the apparatus is possible and the spectrophotometer will be rebuilt as a more reliable mechanical and optical system. The present manual operation of the equipment is very time consuming and automation of the spectrophotometer is contemplated. This would have the advantages of greatly reducing the time taken for any one set of measurements over the entire wavelength range and therefore make possible the study of many more specimens in a reasonable time.

ADDENDUM

Errors of measurement

The error bars shown in the figures of this thesis represent extreme systematic errors calculated as described by Denton *et al* (1972). In the case of a single layer on a substrate the extreme error was found to be given by

$$\Delta n_1 = \left| \frac{\partial n_1}{\partial \left(\frac{1+R_1}{T_1} \right)} \Delta \left(\frac{1+R_1}{T_1} \right) \right| + \left| \frac{\partial n_1}{\partial \left(\frac{1-R_1}{T_1} \right)} \Delta \left(\frac{1-R_1}{T_1} \right) \right|$$

$$+ \left| \frac{\partial n_1}{\partial d_1} \Delta d_1 \right| + \left| \frac{\partial n_1}{\partial n_2} \Delta n_2 \right| + \left| \frac{\partial n_1}{\partial k_2} \Delta k_2 \right| + \left| \frac{\partial n_1}{\partial \lambda} \Delta \lambda \right|$$

with a similar expression for Δk_1.

For a transparent substrate the term in Δk_2 does not occur and the one in $\Delta \lambda$ is negligible since the wavelength may be set more accurately than any of the other quantities may be measured.

Where the error calculated in this way becomes large this first order error formula is inadequate and overestimates the error (Denton *et al*), a conclusion supported by some direct numerical calculations of changes in n, due to changes in the other parameters.

These error bars show clearly the energy regions where large systematic errors could occur. By using films of different thicknesses these regions may be displaced so that accurate values corresponding to the smaller error bars may be obtained over the whole range. Then, bearing in mind that the errors in R and T are random errors rather than systematic, direct calculation of errors for possible combinations of signs of R and T suggest an overall accuracy of about 2% in n and k. The detailed points plotted in the graphs of $\sqrt{Enk}$ against E (Figs. 3.11 to 3.16) are consistent with such an estimate and lead to reliable estimates of energy gap parameters.

In the case of the measurements on metals similar considerations apply to the estimation of errors, except that as explained in the text the errors became large as $R \to 1$. In consequence one cannot have much confidence in attaching significance to apparent features of the curves for n, k, ε_1 and ε_2 at the longer wavelengths. For shorter wavelengths when R and R_1 are less than 0.6 or so, the errors are similar to those for the Ge films, and valid deductions may be drawn from features of the experimental curves.

It is again emphasised that the apparatus needs to be rebuilt to improve accuracy and to increase the ease of making large numbers of measurements to allow proper statistical treatment of errors.

APPENDIX A

OPTICAL PROPERTIES OF STEARIC ACID $(CH_3(CH_2)_{16}COOH)$

A-1 Introduction

For both practical and scientific reasons research workers (Jacobs *et al* 1954, Francis and Ellison 1959, Tweet 1963, Sperling and Ke 1966, Tomar and Srivastava 1972, 1973, Strickland 1973, Hong 1973, Natho 1973, Clint 1973, Agarwal and Ichijo 1977) have been studying insoluble monolayers for many years. Langmuir and Blodgett (1937) films are of potential importance in the current development of thin film technique. Because of their known and controllable thickness they can be used for making dielectric devices and interference filters. Monolayers are very useful for controlling evaporation and also an important factor for the synthesis of molecular aggregates of planned order.

It was thought worthwhile to apply the methods used for the study of the optical properties of thin films of semiconductors to films consisting of multilayers prepared by the Langmuir-Blodgett technique since these ordered structures might possibly show semiconducting properties. As this work has not proceeded very far only a brief account is given in this appendix.

A-2 Preparation of Mono and Multi-layers of stearic acid by the Langmuir and Blodgett technique

To prepare a monolayer a trough was filled to the brim with distilled water. A waxed silk thread (T) was attached by cleaned metal clips (P) to the edges of the trough as shown in Figure (A.1). All the experimental work relating to monolayers was done in a clean airconditioned

room to minimise airborne contamination. Just before spreading the film, the surface of the water was cleaned two or three times by sweeping a strip of glass (not shown in Figure A.1) over the surface to remove any floating material. Next , a known weight of stearic acid (0.034 gms) was dissolved in 10 ml of the volatile non-polar solvent benzene and 0.1 ml of this solution was delivered from a micropipette on to cleaned water surface near A in the trough. After allowing time for spreading the waxed thread was fastened to the edges of the trough by small clips (Q). Now a small drop of castor oil which exerts a pressure of 17 dynes/cm was placed near C .

In order to collect the films on only one side of the quartz wedges which were used as substrates, two of the wedges were placed back to back and the edges bound with tape. In this way two substrates with films could be prepared in one operation. A good estimate of thickness was made by considering the thickness of a monolayer of 2.3 nm following Blodgett (1935). To collect multilayers the quartz substrate was dipped into the water and withdrawn the required number of times near A . During the process of deposition of each monolayer the thread moves forward through an area equal to the total area of both the surfaces of the wedges. A mechanical device was made for lowering the substrate into the water and withdrawing it. The layers were deposited at a rate of 16 to 30 layers per minute. Depending on the age of the solution of stearic acid X or Y type films were formed which can be readily observed from the movement of the waxed thread. After collecting the multilayers of the desired thickness the substrate was dried and the wedges were separated.

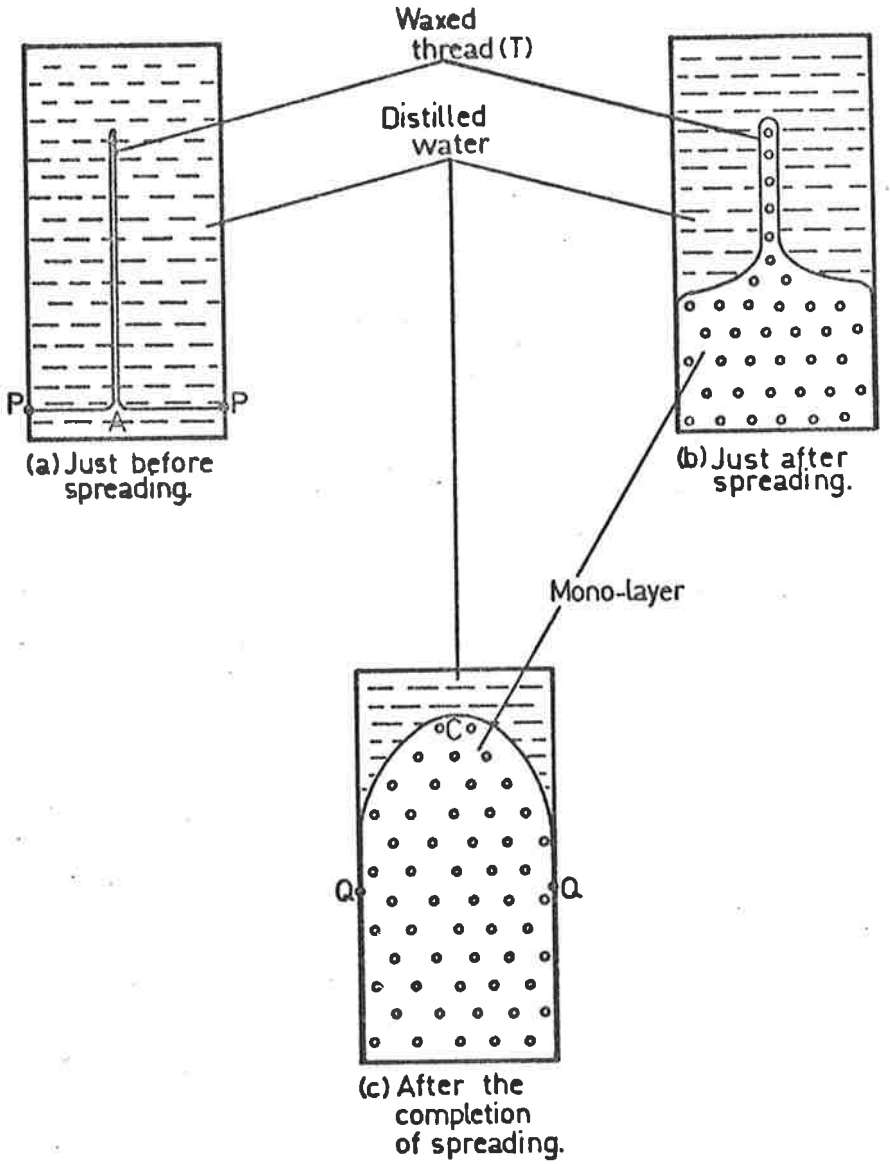

Fig.A.1. Positions of the waxed thread to mark the boundary of a monomolecular film.

A-3 Preparation of stearic acid films by evaporation

The deposition of thin films of stearic acid was carried out by evaporation in a vacuum following the method of Baker (1971). The apparatus used was essentially that described in Chapter 2, but as the melting point of stearic acid is $74^{\circ}C$ evaporation occurred at quite low temperatures. The evaporation rate was 0.021 nm/sec and the pressure during evaporation was 4×10^{-5} Torr.

A-4 The optical properties of stearic acid

Stearic acid films of thickness 100 to 400 nm were deposited on quartz by the Langmuir and Blodgett technique (1937) and the optical constants were determined by normal incidence reflectance and transmittance measurements. These films show no colours, and this is due to the very small difference in the refractive indices of the film and the substrate. The reflectance is very small and correspondingly the transmittance is high, since the films are transparent in the region 400 to 2000 nm. (Figures A.3 to A.6). At shorter wavelengths some absorption could be detected.

For non-absorbing films it may be shown by using the formulae for $\frac{1 + R}{T}$ and $\frac{1 - R}{T}$ that if $n_2 > n_1 > n_0$

$$R_{max} = \left(\frac{n_2 - n_0}{n_2 + n_0} \right)^2 \qquad \text{A-1}$$

$$R_{min} = \left(\frac{n_2^2 - n_0 n_1}{n_2^2 + n_0 n_1} \right)^2 \qquad \text{A-2}$$

where n_2 is the refractive index of the substrate

n_1 is the refractive index of the film

n_0 is the refractive index of the air.

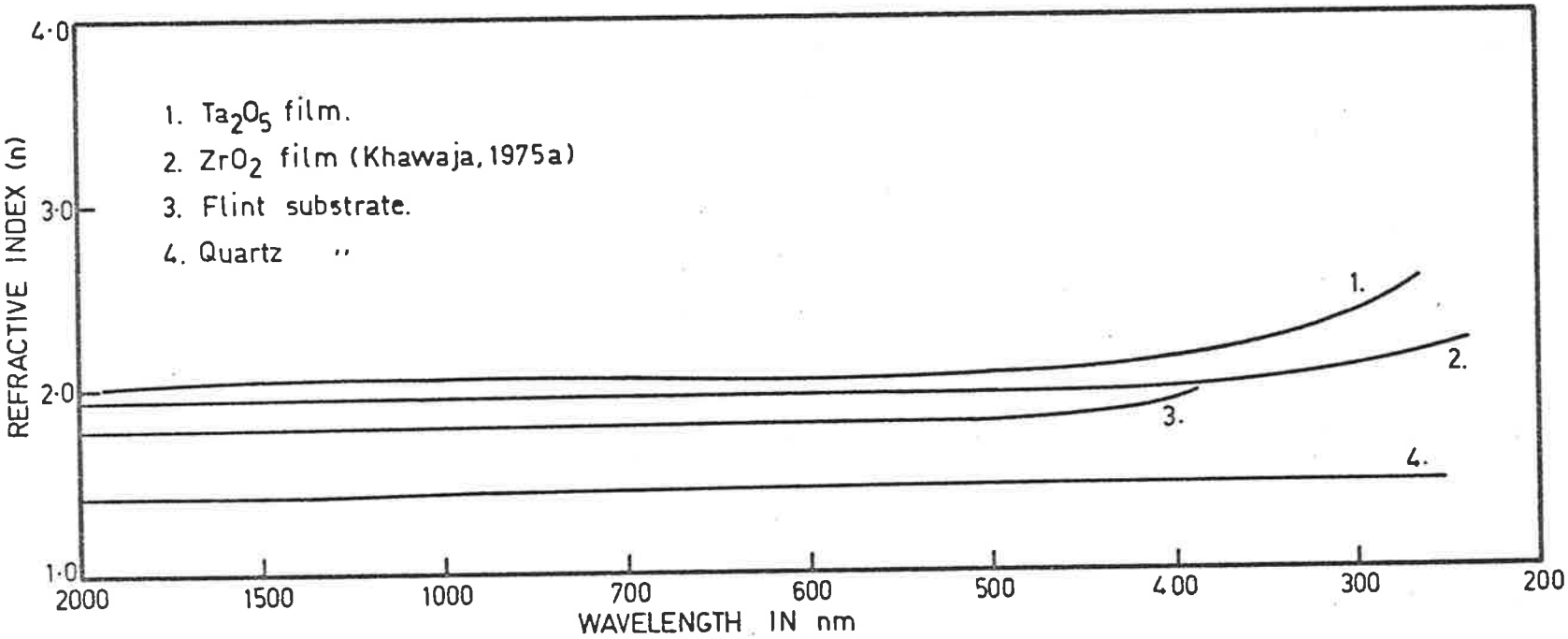
4·0
3·0
2·0
1·0
REFRACTIVE INDEX (n)
1. Ta_2O_5 film.
2. ZrO_2 film (Khawaja, 1975a)
3. Flint substrate.
4. Quartz ,,
1.
2.
3.
4.
2000
1500
1000
700
600
500
400
300
200
WAVELENGTH IN nm

Fig. A.2

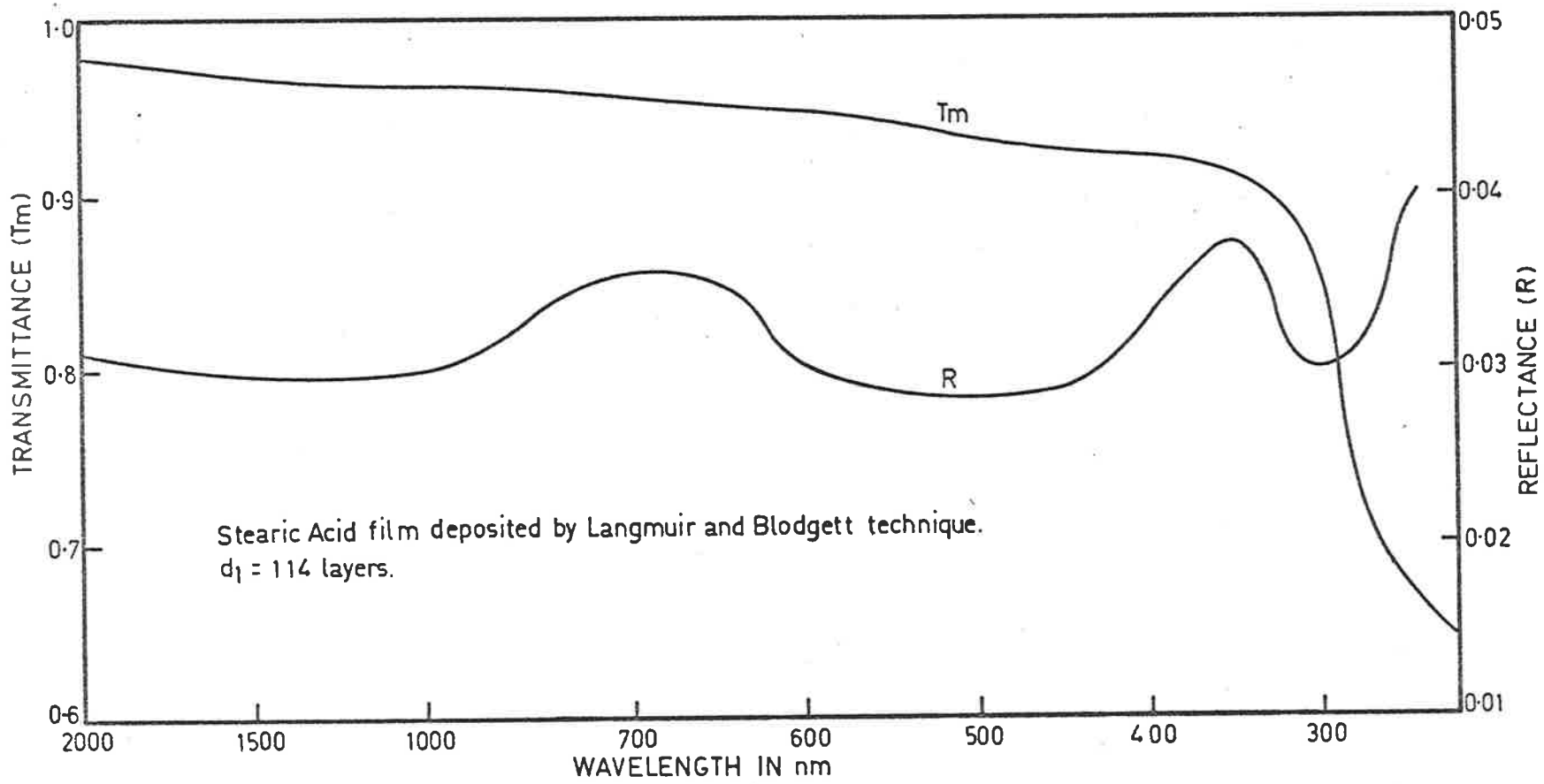
1·0
0·9
0·8
0·7
0·6
TRANSMITTANCE (Tm)
0·05
0·04
0·03
0·02
0·01
REFLECTANCE (R)
Tm
R
Stearic Acid film deposited by Langmuir and Blodgett technique.
d_1 = 114 layers.
2000
1500
1000
700
600
500
400
300
WAVELENGTH IN nm

Fig. A·3

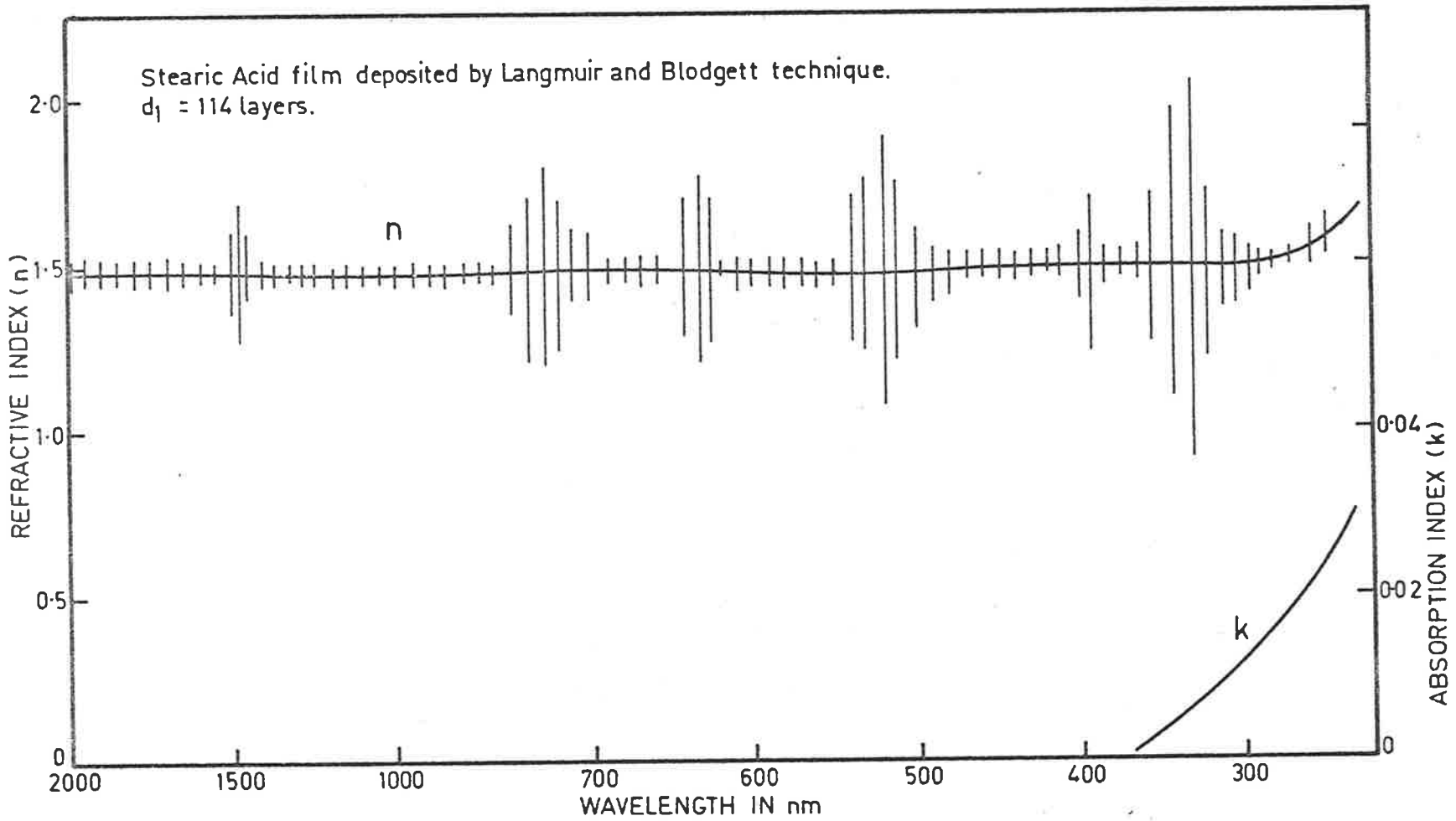
Stearic Acid film deposited by Langmuir and Blodgett technique.
d_1 = 114 layers.
n
k
REFRACTIVE INDEX (n)
ABSORPTION INDEX (k)
2·0
1·5
1·0
0·5
0
0·04
0·02
0
2000
1500
1000
700
600
500
400
300
WAVELENGTH IN nm

Fig. A·4

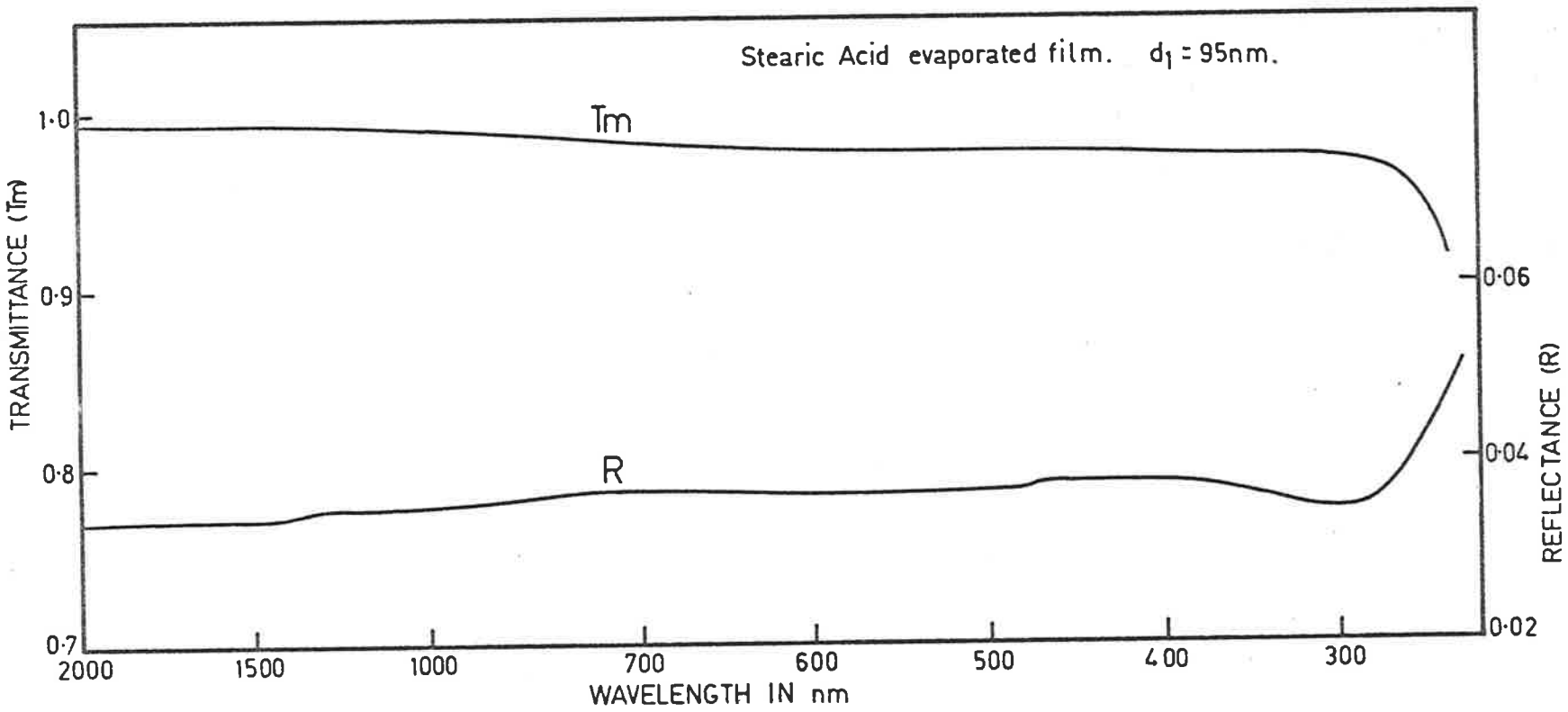
Stearic Acid evaporated film. d_1 = 95nm.
Tm
R
TRANSMITTANCE (Tm)
REFLECTANCE (R)
1·0
0·9
0·8
0·7
0·06
0·04
0·02
2000
1500
1000
700
600
500
400
300
WAVELENGTH IN nm

Fig. A.5

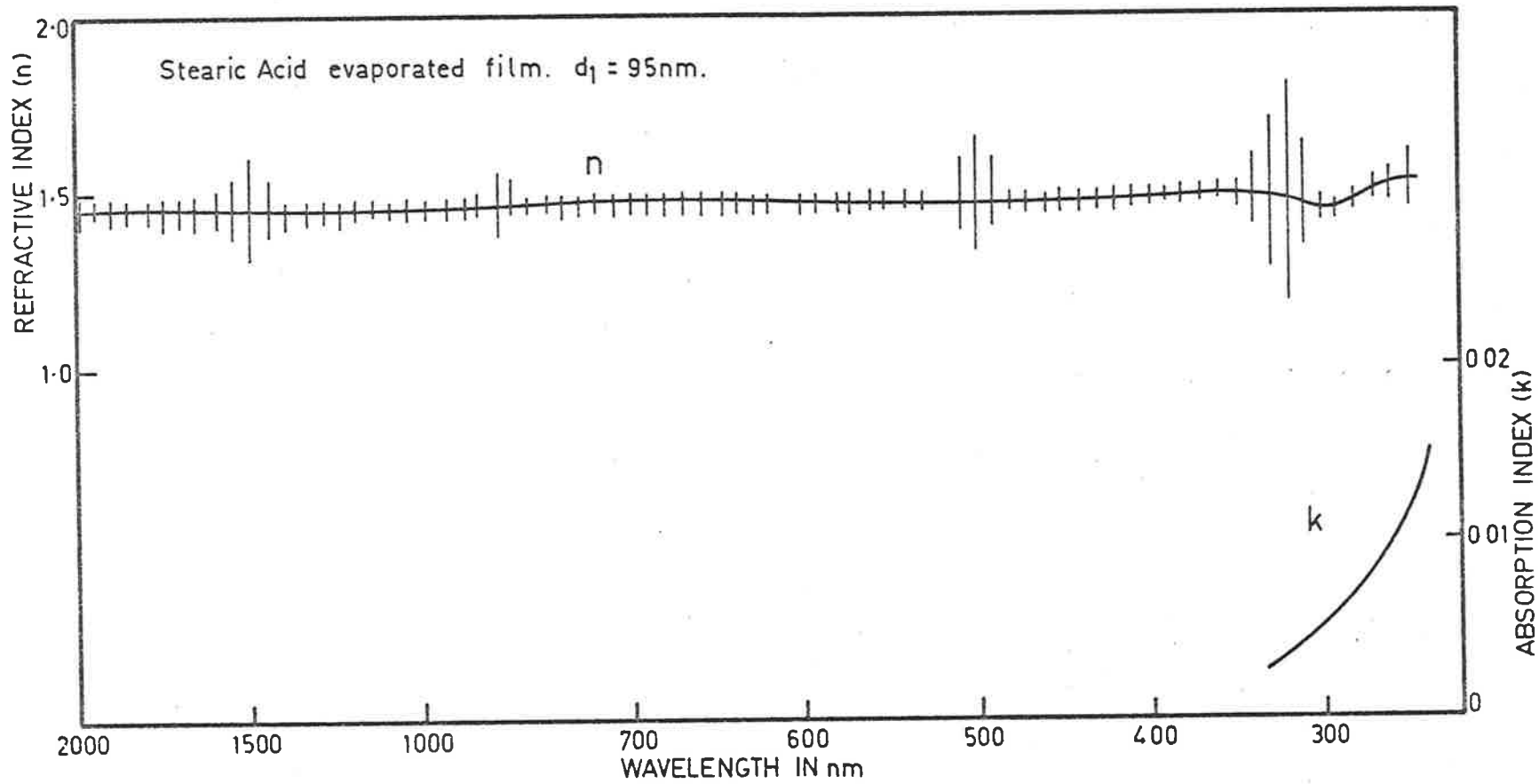
Stearic Acid evaporated film. d_1 = 95nm.
n
k
REFRACTIVE INDEX (n)
2·0
1·5
1·0
ABSORPTION INDEX (k)
0·02
0·01
0
2000
1500
1000
700
600
500
400
300
WAVELENGTH IN nm

Fig. A·6

For the accurate measurement of R it is desirable to have n_2, the refractive index of the substrate as large as possible. For this reason substrates of flint glass, and of evaporated layers of Ta_2O_5 or ZrO_2 on quartz were used. The dispersion curves of these materials are shown in Figure (A·2). Absorption in these materials in the U.V. limits the low wavelength limit of measurement.

A-5 Results

Measurements on multilayer films and evaporated films deposited on various substrates showed no detectable absorption in the range from 2000 to 400 nm . Typical dispersion curves are shown in Figures (A,4) and (A,6) corresponding to the reflectance and transmittance curves as shown in Figures (A,3) and (A,5) respectively. Beyond 400 nm absorption could be detected but was very small and it appears that any significant absorption in stearic acid occurs beyond the range of our apparatus. There is no significant difference in the optical properties of multilayer films and evaporated films.

APPENDIX B

SOME DETAILS OF KRAMERS-KRONIG CALCULATIONS

B-1 Solutions of equations for curve fitting by Least Squares method for two arbitrary parameters using extrapolation formula III.

It is necessary to consider the equations of the form

$$a_1 \sum_p I_{p1}^2 + a_2 \sum_p I_{p1} I_{p2} = \sum_p f_p I_{p1} \qquad \text{B-1}$$

and

$$a_1 \sum_p I_{p1} I_{p2} + a_2 \sum_p I_{p2}^2 = \sum_p f_p I_{p2} \qquad \text{B-2}$$

which give

$$a_1 = \frac{\sum_p f_p I_{p1} \sum_p I_{p2}^2 - \sum_p I_{p1} I_{p2} \sum_p f_p I_{p2}}{\sum_p I_{p1}^2 \sum_p I_{p2}^2 - \left(\sum_p I_{p1} I_{p2}\right)^2} \qquad \text{B-3}$$

and

$$a_2 = \frac{\sum_p f_p I_{p2} \sum_p I_{p1}^2 - \sum_p I_{p1} I_{p2} \sum_p f_p I_{p1}}{\sum_p I_{p1}^2 \sum_p I_{p2}^2 - \left(\sum_p I_{p1} I_{p2}\right)^2} \qquad \text{B-4}$$

where $I_{pn} = \frac{1}{\pi} \sum_{m=1}^{\infty} A_{mn} x_p^{2m-1}$ B-5

As explained in Chapter 4.

Now π^4 x denominator of equations (B-3) and (B-4)

$$= \sum_p \left(\sum_{m=1}^{\infty} A_{m1} x_p^{2m-1}\right)^2 \sum_p \left(\sum_{m=1}^{\infty} A_{m2} x_p^{2m-1}\right)^2 - \left(\sum_p \sum_{m=1}^{\infty} A_{m1} x_p^{2m-1} \sum_{m=1} A_{m2} x_p^{2m-1}\right)^2 \qquad \text{B-6}$$

where

$$\left(\sum_{m=1}^{\infty} A_{m1} x_p^{2m-1}\right)^2 = \left(A_{11} x_p + A_{21} x_p^3 + A_{31} x_p^5 + \text{---}\right)^2$$

$$= A_{11}^2 x_p^2 + 2 A_{11} A_{21} x_p^4 + (A_{21}^2 + 2 A_{11} A_{31}) x_p^6 + \text{----} \qquad \text{B-7}$$

and $$\left(\sum_{m=1}^{\infty} A_{m2}\, x_p^{2m-1}\right)^2 = (A_{12}\, x_p + A_{22}\, x_p^3 + A_{32}\, x_p^5 + \text{---})^2$$

$$= A_{12}^2\, x_p^2 + 2\, A_{12}\, A_{22}\, x_p^4$$

$$+ (A_{22}^2 + 2\, A_{12}\, A_{32})\, x_p^6 + \text{-----} \qquad \text{B-8}$$

and

$$\sum_{m=1}^{\infty} A_{m1}\, x_p^{2m-1} \sum_{m=1}^{\infty} A_{m2}\, x_p^{2m-1}$$

$$= (A_{11}\, x_p + A_{21}\, x_p^3 + A_{31}\, x_p^5 + \text{----})$$

$$x(A_{12}\, x_p + A_{22}\, x_p^3 + A_{32}\, x_p^5 + \text{----})$$

$$= A_{11}\, A_{12}\, x_p^2 + (A_{11}\, A_{22} + A_{12}\, A_{21})\, x_p^4$$

$$+ (A_{12}\, A_{31} + A_{21}\, A_{22} + A_{32}\, A_{11})\, x_p^6 + \text{----} \qquad \text{B-9}$$

Now putting the values of equations (B-7, B-8 and B-9) in equation (B-6), we get π^4 x denominator

$$= \sum_p (A_{11}^2\, x_p^2 + 2A_{11}\, A_{21}\, x_p^4 + (A_{21}^2 + 2A_{11}\, A_{31})\, x_p^6 + \text{----})$$

$$x \sum_p (A_{12}^2\, x_p^2 + 2A_{12}\, A_{22}\, x_p^4 + (A_{22}^2 + 2A_{12}\, A_{32})\, x_p^6 + \text{----})$$

$$- [\sum_p (A_{11}\, A_{12}\, x_p^2 + A_{11}\, A_{22} + A_{12}\, A_{21})\, x_p^4$$

$$+ (A_{12}\, A_{31} + A_{11}\, A_{32} + A_{21}\, A_{22})\, x_p^6 + \text{----})]^2 \qquad \text{B-10}$$

Now let us suppose

$$\sum_p x_p^2 = X_2\,, \quad \sum_p x_p^4 = X_4\,, \quad \sum_p x^6 = X_6 \text{ --- etc.}$$

$$\text{and } \sum_p f_p\, x_p^3 = F_3\,, \quad \sum_p f_p\, x_p^5 = F_5 \text{ --- etc.}$$

Now neglecting the $\sum_p x_p^8 = X_8$, $\sum_p x_p^{10} = X_{10}$ ---- etc.

and $\sum_p f_p x_p^7 = F_7$, $\sum_p f_p x_p^9 = F_9$ ---- etc, being very small.

Then π^4 x denominator after simplification

$$\simeq (A_{11} A_{22} - A_{12} A_{21})^2 (X_2X_6 - X_4^2)$$

and π^3 x numerator of equation (B-4)

$$\simeq A_{11} (A_{22} A_{11} - A_{21} A_{12}) (F_3X_2 - F_1X_4)$$

Therefore $$a_2 \simeq \frac{-\pi A_{11}}{(A_{21} A_{12} - A_{22} A_{11})} \frac{(F_3X_2 - F_1X_4)}{(X_2X_6 - X_4^2)} \qquad \text{B-11}$$

and $$a_1 \simeq \frac{\pi A_{12}}{(A_{21} A_{12} - A_{22} A_{11})} \frac{(F_3X_2 - F_1X_4)}{(X_2X_6 - X_4^2)} \qquad \text{B-12}$$

Now from the equations (B-11) and (B-12) it was observed that the values of a_1 and a_2 are of the order of x^{-3} (same as that of direct method as explained in Section (4.3.4) and the ratio of

$$\frac{a_2}{a_1} \simeq - \frac{A_{11}}{A_{12}} \simeq - 1.5 \qquad \text{B-13}$$

Similarly it can be proved that in the extrapolation formula I,

where $I_{pn} = - \frac{1}{\pi} \sum_{m=o}^{\infty} A_{mn} x_p^{2m+1}$.

The values of a_1 and a_2 are of the order of x^{-3} and the ratio of

$$\frac{a_2}{a_1} = - \frac{A_{01}}{A_{02}} \simeq - 1.5 \qquad \text{B-14}$$

From equations (B-13) and (B-14) it is seen that the ratio of the two consecutive arbitraty parameters, i.e. $\frac{a_2}{a_3}$, is the same if Least Squares method is used for all three extrapolation formulae I, II and III.

Some details of R's and θ's calculated by using extrapolation formulae I, II and III for different sets of arbitrary

parameters including the values of θ's of Tomlin *et al* (1976) and Philipp and Ehrenreich (1963), are given as follows in tabular form.

TABLE B-1

E in eV	R_I	R_{II}	R_{III}	$R_{Philipp}$
Extrapolated Reflectances for E_2 = 10 eV				
11	0.2710	0.2632	0.2716	0.2851
12	0.2250	0.2024	0.2244	0.2394
13	0.1836	0.1539	0.1865	0.2013
14	0.1524	0.1173	0.1561	0.1665
15	0.1273	0.0901	0.1312	0.1327
16	0.1071	0.0701	0.1110	0.1023
17	0.0907	0.0552	0.0945	0.0713
18	0.0772	0.0441	0.0809	0.0446
19	0.0662	0.0357	0.0696	0.0256
20	0.0571	0.0292	0.0601	0.0169
25	0.0294	0.0128	0.0310	0.0123
30	0.0168	0.0069	0.0174	0.0100
40	0.0068	0.0030	0.0067	0.0216
50	0.0033	0.0017	0.0031	0.0173
100	0.38×10^{-3}	0.54×10^{-3}	0.25×10^{-3}	0.43×10^{-2}
1000	0.25×10^{-6}	0.17×10^{-3}	0.31×10^{-7}	0.17×10^{-6}
E_2 = 15 eV				
16	0.1087	0.1073	0.1089	0.1023
17	0.0899	0.0860	0.0976	0.0713
18	0.0745	0.0687	0.0754	0.0446
19	0.0628	0.0550	0.0635	0.0256
20	0.0531	0.0442	0.0539	0.0169
25	0.0250	0.0166	0.0260	0.0123
30	0.0133	0.0075	0.0141	0.0103
40	0.0048	0.0024	0.0052	0.0216
50	0.0022	0.0011	0.0023	0.0173
100	0.17×10^{-3}	0.21×10^{-3}	0.18×10^{-3}	0.43×10^{-2}
1000	0.40×10^{-7}	0.36×10^{-4}	0.21×10^{-7}	0.17×10^{-6}

TABLE B-2

ANGLE IN RADIANS

BY LEAST SQUARES METHOD FOR E_2 = 10 eV

E in ev	θ_I a_0= 1.9952 a_1= 1.0791	θ_{II} a_1= 1.9952 a_2= 5.7151	θ_{III} a_1=- 2.0048 a_2=- 0.2597	θ_{exp}	$\theta_{Philipp}$
1.8	0.0292	0.0350	0.0353	0.0601	0.0130
2.0	0.0530	0.0600	0.0600	0.0984	0.0328
2.1	0.0835	0.0903	0.0906	0.1356	0.0609
2.2	0.1209	0.1281	0.1282	0.1586	0.1032
2.25	0.1360	0.1432	0.1436	0.1760	-
2.4	0.1790	0.1867	0.1871	0.1943	0.1557
2.6	0.2070	0.2156	0.2168	0.2061	0.1832
2.8	0.2180	0.2284	0.2274	0.2103	0.1911
3.0	0.2083	0.2183	0.2183	0.2196	0.1834
3.2	0.2148	0.2256	0.2257	0.2224	0.1879
3.4	0.2332	0.2449	0.2447	0.2283	0.2040
3.6	0.2500	0.2626	0.2621	0.2445	0.2190
3.8	0.2653	0.2787	0.2881	0.2733	0.2331
3.9	0.2738	0.2875	0.2870	-	0.2404
4.0	0.2934	0.2761	0.3025	0.3302	0.2451
4.1	0.2828	0.2976	0.2966	0.3295	0.2486
4.2	0.2956	0.3107	0.3097		0.2609
4.4	0.3661	0.3822	0.3810		0.3674
4.6	0.4672	0.4844	0.4826		0.4262
4.8	0.5251	0.5433	0.5438		0.4867
5.0	0.5732	0.5923	0.5894		0.5308

TABLE B-3

ANGLE IN RADIANS

BY LEAST SQUARES METHOD FOR E_2 = 15 eV

E in eV	θ I a_0= 3.0521 a_1= 0.5334	θ II a_1= 3.0521 a_2= 5.3690	θ III a_1 = -0.9480 a_2 = -0.2169	θ_{exp}	$\theta_{Philipp}$
1.8	0.0412	0.0360	0.0412	0.0601	0.0130
2.0	0.0678	0.0621	0.0679	0.0984	0.0328
2.1	0.0992	0.0931	0.0994	0.1356	0.0609
2.2	0.1369	0.1306	0.1370	0.1586	0.1032
2.25	0.1473	0.1408	0.1473	0.1760	-
2.4	0.1976	0.1853	0.1915	0.1943	0.1557
2.6	0.2260	0.2186	0.2260	0.2061	0.1832
2.8	0.2357	0.2277	0.2358	0.2103	0.1911
3.0	0.2301	0.2369	0.2222	0.2196	0.1834
3.2	0.2471	0.2290	0.2380	0.2224	0.1879
3.4	0.2636	0.2443	0.2479	0.2283	0.2040
3.6	0.2722	0.2596	0.2723	0.2445	0.2190
3.8	0.2930	0.2824	0.2932	0.2733	0.2331
3.9	0.3020	0.2922	0.3021	-	0.2404
4.0	0.3081	0.3021	0.3082	0.3302	0.2451
4.1	0.3120	0.3012	0.3128	0.3295	0.2486
4.2	0.3260	0.3143	0.3260		0.2609
4.4	0.3979	0.3857	0.3990		0.3674
4.6	0.5006	0.4879	0.5050		0.4262
4.8	0.5627	0.5489	0.5638		0.4867
5.0	0.6094	0.5956	0.6095		0.5308

TABLE B-4

ANGLE IN RADIANS

E in eV	θ_{exp}	Direct method for E_2 = 10 eV: θ_{III} (a_1 = - 2.0048, a_2 = - 0.7140)	Direct method for E_2 = 10 eV: θ_{III} (a_1 = - 2.0048, a_2 = - 509.6, a_3 = 681.6)	Least Squares Method for E_2 = 15 eV: θ_{III} (a_1 = - 0.9480, a_2 = - 1143.4, a_3 = 1526.5)
1.8	0.0601	0.0266	0.0601	0.0557
2.0	0.0984	0.0485	0.0974	0.0802
2.1	0.1356	0.0783	0.1148	0.1243
2.25	0.1760	0.1327	0.1669	0.1549
2.4	0.1943	0.1775	0.2088	0.1961
2.6	0.2061	0.2032	0.2344	0.2320
2.8	0.2103	0.2139	0.2418	0.2385
3.0	0.2196	0.2038	0.2332	0.2230
3.2	0.2224	0.2101	0.2272	0.2380
3.4	0.2283	0.2281	0.2377	0.2410
3.6	0.2445	0.2445	0.2445	0.2579
3.8	0.2733	0.2695	0.3389	0.2698
4.0	0.3302	0.3828	0.4559	0.2688

APPENDIX C

CONVERSION OF DOUBLE LAYER EQUATIONS TO SINGLE LAYER EQUATIONS WHEN $d_2 = 0$

The corrections of the complicated double layer equations may be checked by showing that they reduce to the single layer equations when $d_2 = 0$. The double layer equations are

$$\phi_1 - 2 n_0 \frac{1 + R_1}{1 - R_1} \phi_2 = 0 \qquad \text{C-1}$$

and

$$(n_0^2 + n_1^2) F_1 + (n_0^2 - n_1^2) F_2 - 8n_0n_1^2 \frac{(1 + R_2)}{(1 - R_2)} \phi_2 = 0 \qquad \text{C-2}$$

as explained in Section 5.3 of Chapter 5.

On putting $d_2 = 0$

$$\begin{aligned} \phi_1 &= (n_0^2 + n_2^2 + k_2^2)(n_2^2 + n_3^2 + k_2^2 + k_3^2) \\ &\quad + (n_0^2 - n_2^2 - k_2^2)(n_2^2 - n_3^2 + k_2^2 - k_3^2) \\ &= 2n_0^2(n_2^2 + k_2^2) + 2(n_2^2 + k_2^2)(n_3^2 + k_3^2) \\ &= 2(n_2^2 + k_2^2)(n_0^2 + n_3^2 + k_3^2) \end{aligned} \qquad \text{C-3}$$

$$\begin{aligned} \phi_2 &= 2n_2(n_2n_3 + k_2k_3) - 2k_2(n_2k_3 - n_3k_2) \\ &= 2n_3(n_2^2 + k_2^2) \end{aligned} \qquad \text{C-4}$$

$$F_1 = 4(n_2^2 + k_2^2)(n_1^2 + n_3^2 + k_3^2) \qquad \text{C-5}$$

and

$$F_2 = 4(n_2^2 + k_2^2)\{(n_1^2 - n_3^2 - k_3^2)\cos 2\gamma_1 + 2n_1k_3 \sin 2\gamma_1\} \qquad \text{C-6}$$

Putting the values of ϕ_1 , ϕ_2 , F_1 and F_2 in equations (C-1 and C-2), we get

$$\frac{(1 + R_1)}{(1 - R_1)} = \frac{n_0^2 + n_3^2 + k_3^2}{2n_3n_0}$$

$$\text{or} \quad R_1 = \frac{(n_3 - n_0)^2 + k_3^2}{(n_3 + n_0)^2 + k_3^2} \qquad \text{C-7}$$

and $$4n_0n_1^2n_3 \frac{(1 + R_2)}{(1 - R_2)} = (n_0^2 + n_1^2)(n_1^2 + n_3^2 + k_3^2)$$

$$+ (n_0^2 - n_1^2)\{(n_1^2 - n_3^2 - k_3^2)\cos 2\gamma_1$$

$$+ 2n_1k_3 \sin 2\gamma_1 \}$$

or $$\frac{(1 + R_2)}{(1 - R_2)} = \frac{1}{4n_0n_1^2n_3} [(n_0^2 + n_1^2)(n_1^2 + n_3^2 + k_3^2)$$

$$+ (n_0^2 - n_1^2)\{(n_1^2 - n_3^2 - k_3^2)\cos 2\gamma_1$$

$$+ 2n_1k_3 \sin 2\gamma_1 \}] \qquad \text{C-8}$$

The equations (C-7) and (C-8) which are free of n_2 and k_2 are equivalent to the single layer equations.

BIBLIOGRAPHY

Abeles F., 1972, "Optical Properties of Solids" (Abeles F., Ed.), North-Holland Publishing Co., Amsterdam, London.

Abeles F., 1971, in "Physics of Thin Films" (Francombe M.H. and Hoffman R.W., Eds.), Vol. 6, P. 151, Academic Press, New York and London.

Abeles F., 1958, J. de Physique Radium 19, 327.

Afanas'yeva L.A., Bolotin G.A. and Noskov M.M., 1966, Fiz. Metal. Metalloved. 22, 828.

Afanas'yeva L.A. and Kirillova M.M., 1967, Fiz. Metal. Metalloved. 23, 472.

Agarwal V.K. and Ichijo B., 1977, Electrocomp. Sci. Technol. 4, 29.

Asano S. and Yamashita J., 1967, Phys. Soc. Japan 23, 714.

Ashcroft N.W. and Strum K., 1971, Phys. Rev. B3, 1898.

Baker M.A., 1971, Thin Solid Films 8, R13.

Bassani F., 1957, Phys. Rev. 108, 263.

Batz B., 1966, Solid State Commun. 4, 241.

Bauer R.S. and Galeener F.L., 1972, Solid State Commun. 10, 1171.

Beattie J.R. and Conn G.K.T., 1955, Phil. Mag. 46, 989.

Blodgett K.B., 1935, J. Chem. Soc. 57, 1007.

Blodgett K.B. and Langmuir I., 1937, Phys. Rev. 51, 964.

Blum N.A. and Feldman C., 1976, J. Non-Cryst. Solids 22, 29.

Bolotin G.A., Kirrilova M.M., Nomerovannaya L.V. and Noskov M.M., 1967, Fiz. Metal. Metalloved. 23, 73.

Bolotin G.A., Noskov, M.M. and Sasovskaya I.I., 1973, Fiz. Metal. Metalloved. 35, 699.

Bradely D.E., 1965, in "Techniques for Electron Microscopy" (Kay D.H., Ed.), Second edition, P. 96, Scientic Publication, Oxford.

Brandt G.B. and Rayne J.A., 1963, Phys. Rev. 132, 1945.

Braunstein R., Moore A.R. and Herman F., 1958, Phys. Rev. 109, 695.

Brodsky M.H. and Title R., 1969, Phys. Rev. Lett. 23, 581.

Brodsky M.H., Weiser K. and Pettit G.D., 1970, Phys. Rev. B1, 2632.

Brust D., 1964, Phys. Rev. 134, A1337.

Brust D., Phillips J.C. and Bassani F., 1962, Phys. Rev. Lett. 9, 94.

Burge D.K. and Bennet H.E., 1964, J. Opt. Soc. Am. 54, 1428.

Butcher P.N., 1951, Proc. Phys. Soc., London A64, 765.

Cardona M. and Sommers H.S. (Jr), 1961, Phys. Rev. 122, 1382.

Christensen N.E. and Seraphin B.O., 1971, Phys. Rev. B4, 3321.

Clark A.H., 1967, Phys. Rev. 154, 750.

Clint J.H., 1973, J. Colloid Interface Sci. 43, 132.

Connell G.A.N. and Paul W., 1972, J. Non-Cryst. Solids 8-10, 215.

Dash W.C. and Newman R., 1955, Phys. Rev. 99, 1151.

Davis E.A., 1973, in "Electronic and Structural properties of Amorphous Semiconductors" (Le Comber P.G. and Mort J., Eds.), Academic Press, London and New York.

Davis E.A. and Shaw R.F., 1970, J. Non-Cryst. Solids 2, 406.

Denton R.E., 1972, Ph.D. Thesis, Adelaide University.

Denton R.E., Campbell R.D. and Tomlin S.G., 1972, J. Phys. D : Appl. Phys. 5, 852.

Denton R.E. and Tomlin S.G., 1972, Aust. J. Phys. 25, 743.

Donovan T.M., Ashley E.J. and Spicer W.E., 1970, Phys. Lett. 32A, 85.

Ehrenreich H. 1966, in "Optical properties and Electronic Structure of Metals and Alloys"(Abeles F.,Ed.), North Holland Publishing Company - Amsterdam.

Ehrenreich H. and Philipp H.R., 1962, Phys. Rev. 128, 1622.

Ehrenreich H., Philipp H.R. and Olechna D.J., 1963, Phys. Rev. 131, 2469.

Ehrenreich H., Philipp H.R. and Segall B., 1963, Phys. Rev. 132, 1918.

Fischer J.E., 1971, Phys. Rev. Lett. 27, 1131.

Fischer J.E. and Donovan T.M., 1972, J. Non-Cryst. Solids 8-10, 202.

Fochs P.D., 1950, J. Opt. Soc. Am. 40, 623.

Francis S.A. and Ellison A.H., 1959, J. Opt. Soc. Am. 49, 131.

Ghosh A.K., 1966, Solid State Commun. 4, 565.

Golovashkin A.I., Kopeliovich A.I. and Motulevich G.P., 1968, Sov. Phys. JETP 26, 1161.

Halder N.C., Montante J.M. and Swartz W.E. (Jr), 1977, Phys. Stat. Sol. (a) 39, 213.

Hanus J., Feinleib J. and Scouler W.J., 1967, Phys. Rev. Lett. 19, 16.

Hanus J., Feinleib, J. and Scouler W.J., 1968, J. Appl. Phys. 39, 1272.

Hartman R.E., 1954, J. Opt. Soc. Am. 44, 192.

Heavens O.S.,1955, "Optical properties of Thin Solid Films", Butterworths Scientific Publications, London.

Herring C., 1966, "Magneitism" Vol. IV (Rado G.T. and Suhl H., Eds.), Academic Press, New York and London.

Hodges L., Ehrenreich H. and Lang, N.D., 1966, Phys. Rev. 152, 505.

Hodgson J.N., 1968, J. Phys. Chem. Solids 29, 2175.

Hong E.P., 1973, J. Colloid Interface Sci. 43, 66.

Humphreys-Owen S.P.F., 1961, Proc. Phys. Soc. London 77, 949.

Irani G.B., Huen T. and Wooten F., 1971, J. Opt. Soc. Am. 61, 128.

Jacobs E.E., Holt A.S. and Rabinowitch E., 1954, J. Chem. Phys. 22, 142.

Jahuda F.C., 1957, Phys. Rev. 107, 1261.

Joensen P., Irwin J.C., Cochran J.F. and Curzon A.E., 1973, J. Opt. Soc. Am. 63, 1556.

Jarrett D.N. and Ward L., 1976, J. Phys. D. 9, 1515

Johnson P.B. and Christy R.W., 1972, Phys. Rev. B6, 4370.

Johnson P.B. and Christy R.W., 1974, Phys. Rev. 9, 5056.

Juenker D.W., LeBlanc L.J. and Martin C.R., 1968, J. Opt. Soc. Am. 58, 164.

Kapitsa M.L., Odoyev Yu. P. and Shirokikh E.I., 1969, Fiz. Tverd. Tela.: Sov. Phys. Solid State 11, 814.

Khawaja E.E., 1975a, Ph.D. Thesis, Adelaide University.

Khawaja E.E. and Tomlin S.G., 1975, J. Phys. D : Appl. Phys. 8, 581.

Khawaja E.E. and Tomlin S.G., 1975, Thin Solid Films 30, 361.

Kirillova M.M., Bolotin G.A. and Mayevskiy V.M., 1967, Fiz. Metal. Metalloved. 24, 95.

Kirillova M.M. and Charikov B.A., 1964, Optika i Specktroskopiia 17, 254.

Kirillova M.M., Nomerovannaya L.V., Bolotin, G.A., Mayevskiy V.M., Noskov M.M. and Bolotina M.S., 1968 , Fiz. Metal. Metalloved. 25, 459.

Kirillova M.M., Nomerovannaya L.V., and Noskov M.M., 1971, Sov. Phys. JETP 33, 1210.

Kittel C., 1976, "Introduction to Solid State Physics", 5th Edition, John Wiley and Sons, Inc., New York/London/Sydney/Toronto.

Kohn W. 1966, in "Optical properties and Electronic Structure of Metals and Alloys" (Abeles F., Ed.) , North-Holland Publishing Company - Amsterdam.

Kress K.A. and Lapeyre G.J., 1970, J. Opt. Soc. Am. 60, 1681.

Krinchik G.S. and Gushchin V.S., 1969, Sov. Phys. JETP 29, 984.

Krinchik G.S., Gushchin V.S. and Ganshina E.A., 1968, JETP Lett. 8, 31. (quoted from Nilsson 1974).

Lenham A.P. and Treherne D.M., 1966, in "Optical properties and Electronic Structure of Metals and Alloys" (Abeles F., Ed.), North-Holland Publishing Company - Amsterdam.

Lomer W.M., 1962, Proc. Phys. Soc. London 80, 489 : 1964, 84, 327.

Lomer W.M. 1971, Progress in Material Sci. 14, 117.

MacFarlane G.G., McLean T.P., Quarrington J.E. and Roberts V., 1957, Phys. Rev. 108, 1377.

Male J., 1950, J. de Physique Radium 11, 332.

Mattheiss L.F., 1965, Phys. Rev. 139, A1893.

McMath T.A., Hewko R.A.D., Singh O.,Curzon A.E. and Irwin J.C., 1977, J. Opt. Soc. Am. 67, 630.

Moss S.C. and Alder D., 1973, Comments on Solid State Physics 5, 47.

Mott N.F. and Davis E.A., 1971, "Electronic Processes in Non-Crystalline Materials", Oxford, Clarendon Press.

Motulevich G.P., 1969, Sov. Phys. USP. 12, 80.

Murmann H., 1933, Z. Physik, 80, 161 : 1936, Z. Physik, 101, 643.

Natho M.H., 1973, Thin Solid Films 16, 215.

Nilsson P.O., 1974, in "Solid State Physics", Vol. 29, (Ehrenreich H., Seitz F. and Turnbull D., Eds.), Academic Press. New York and London.

Nomerovannaya L.V., Kirillova M.M. and Noskov M.M., 1971, Sov. Phys. JETP 33, 405.

Pankove J.I., 1971, "Optical processes in Semiconductors", Prentice-Hall, Inc., Englewood Cliffs, New Jersey.

Pells G.P. and Shiga M., 1969, J. Phys. C : Solid State Phys. 2, 1835.

Philipp H.R. and Enrenreich H., 1963, Phys. Rev. 129, 1550.

Philipp H.R. and Taft E.A., 1959, Phys. Rev. 113, 1002.

Piller H., Seraphin B.O., Markel K. and Fischer J.E., 1969, Phys. Rev. Lett. 23, 775.

Polk D.E., 1971, J. Non-Cryst. Solids 5, 365.

Potter R.F., 1966, Phys. Rev. 150, 562.

Robinson T.S., 1952, Proc. Phys. Soc. London B 65, 910.

Roessler D.M., 1965, Brit. J. Appl. Phys. 16, 1119 : 16, 1359.

Rudee M.L., 1972, Thin Solid Films 12, 207.

Sak J., 1972, J. Phys. C : Solid State Phys. (GB) 5, 1335.

Sasovskaya I.I. and Noskov M.M., 1971, Fiz. Metal. Metalloved. 32, 723. ; 1972, Fiz. Metal. Metalloved. 33, 86.

Schopper H., 1951, Z. Physik 130, 565. : 1952, Z. Physik 131, 215.

Schulz L.G., 1954, J. Opt. Soc. Am. 44, 357 : 44, 540.

Seraphin B.O. and Hess R.B., 1965, Phys. Rev. Lett. 14, 138.

Smith R.A., 1961, "Wave Mechanics of Crystalline Solids", Chapman and Hall, London.

Sperling W. and Ke B., 1966, Photochem. PhotoBiol. 5, 857.

Spicer W.E., 1966, in "Optical properties and Electronic Structure of metals and alloys" (Abele F., Ed.), North-Holland Publishing Company - Amsterdam.

Spicer W.E. and Donovan T.M., 1970, J. Non-Cryst. Solids 2, 66.

Spicer W.E., Donovan T.M., and Fischer J.E., 1972, J. Non-Cryst. Solids 8-10, 122.

Stern F., 1963, in "Solid State Physics" (Seitz F. and Turnbull D., Eds.), Vol. 15, p. 299, Academic Press. New York and London.

Stoll M.P., 1970 , Solid State Commun. 8, 1207.

Strickland F.G.W., 1973, J. Colloid Interface Sci. 42, 96.

Summers R.D., 1934, J. Opt. Soc. Am. 24, 261.

Tauc J., 1969, in "Optical properties of Solids" (Nudelman S. and Mitra S.S., Eds.), Plenum Press, New York.

Tauc J., 1962, in "Proceedings of the 6th International Semiconductor Conference", Exeter, England.

Tauc J. and Menthe A., 1972, J. Non-Cryst. Solids 8-10, 569.

Theye M.L., 1970, Phys. Rev. B2, 3060.

Theye M.L., 1971, Mat. Res. Bull. 6, 103.

Thutupalli G.K.M., 1976, Ph.D Thesis, Adelaide University.

Thutupalli G.K.M. and Tomlin S.G., 1976, J. Phys. D : Appl. Phys. 9, 1639.

Tomar M.S. and Srivastava V.K., 1972, Thin Solid Films 12, S29.

Tomar M.S. and Srivastava V.K., 1973, Thin Solid Films 15, 207.

Tomlin S.G., 1968, Brit. J. Appl. Phys. : J. Phys. D. 1, 1667.

Tomlin S.G., 1972, Thin Solid Films 13, 265.

Tomlin S.G., 1972, J. Phys. D : Appl. Phys. 5, 847.

Tomlin S.G., Khawaja E.E., Thutupalli G.K.M., 1976, J. Phys. C : Solid State Phys. 9, 4335.

Tweet A.G., 1963, Rev. Sci. Instr. 34, 1412.

Udoyev Yu. P., Koz'yakova N.S. and Kapitsa M.L., 1971, Fiz. Metal. Metalloved. 31, 439.

Vasicek A., 1947 , J. Opt. Soc. Am. 37, 145 : 37, 979.

Venning J.R., 1975, W.R.E. Technical Note - 1373 (AP).

Vincent-Geisse J., Nguyen Tan Tai and Pinan-Lucarre J.P., 1967, J. de Physique, Tome 28, 26.

Vincent-Geisse J., 1964 , J. de Physique, Tome 25, 291.

Waldron J.P. and Juenker D.W., 1964, J. Opt. Soc. Am. 54, 204.

Weaver J.H., 1973, Ph.D. Thesis, Iowa State University, Ames. (quoted from Nilsson 1974).

Wilson A.H., 1936, "The Theory of Metals", p. 133, New York.

Wooten F., 1972, "Optical properties of Solids", Academic Press , New York and London.

Yu A. Y.-C., Donovan T.M. and Spicer W.E., 1968, Phys. Rev. 167, 670.

Yu A. Y.-C. and Spicer W.E., 1968, Phys. Rev. 167, 674.

Zornberg E.I., 1970, Phys. Rev. B1, 244.

Zwerdling S. and Lax B., 1956, Phys. Rev. 106, 51.